VOLUME 79 JUNE 19, 1975 NUMBER 13

JPCHAx

# THE JOURNAL OF PHYSICAL CHEMISTRY

PUBLISHED BIWEEKLY BY THE AMERICAN CHEMICAL SOCIETY

THE JOURNAL OF

# PHYSICAL CHEMISTRY



 Published biweekly by the American Chemical Society at 20th and Northampton Sts., Easton, Pa. 18042. Second-class postage paid at Washington, D.C., and at additional mailing offices.

All manuscripts should be sent to *The Journal of Physical Chemistry*, Department of Chemistry, University of Minnesota, Minneapolis, Minn. 55455.

*Additions and Corrections* are published once yearly in the final issue. See Volume 78, Number 26 for the proper form.

*Extensive or unusual alterations in an article after it has been set in type are made at the author's expense,* and it is understood that by requesting such alterations the author agrees to defray the cost thereof.

The American Chemical Society and the Editor of *The Journal of Physical Chemistry* assume no responsibility for the statements and opinions advanced by contributors.

Correspondence regarding accepted copy, proofs, and reprints should be directed to Editorial Processing Department, American Chemical Society, 20th and Northampton Sts., Easton, Pa. 18042. Department Head: CHARLES R. BERTSCH. Associate Department Head: MARIANNE C. BROGAN. Assistant Editor: CELIA B. MCFARLAND. Editorial Assistant: JOSEPH E. YURVATI.

Advertising Office: Centcom, Ltd., 50 W. State St., Westport, Conn. 06880.

**Business and Subscription Information**

Send all new and renewal subscriptions *with payment* to Office of the Controller, 1155 16th Street, N.W., Washington, D.C. 20036. Subscriptions should be renewed promptly to avoid a break in your series. All correspondence and telephone calls regarding changes of address, claims for missing issues, subscription service, the status of records, and accounts should be directed to Manager, Membership and Subscription Services, American Chemical Society, P.O. Box 3337, Columbus, Ohio 43210. Telephone (614) 421-7230. For microfiche service, contact ACS Journals Department, 1155 16th St. N.W., Washington, D.C. 20036. Telephone (202) 872-4444.

On changes of address, include both old and new addresses with ZIP code numbers, accompanied by mailing label from a recent issue. Allow four weeks for change to become effective.

Claims for missing numbers will not be allowed (1) if loss was due to failure of notice of change in address to be received before the date specified, (2) if received more than sixty days from date of issue plus time normally required for postal delivery of journal and claim, or (3) if the reason for the claim is "issue missing from files."

Subscription rates (hard copy or microfiche) in 1975: $20.00 for 1 year to ACS members; $80.00 to nonmembers. Extra postage $4.50 in Canada and PUAS, $5.00 other foreign. Supplementary material (on microfiche only) available on subscription basis, 1975 rates: $15.00 in U.S., $19.00 in Canada and PUAS, $20.00 elsewhere. All microfiche airmailed to non-U.S. addresses; air freight rates for hard-copy subscriptions available on request.

Single copies for current year: $4.00. Rates for back issues from Volume 56 to date are available from the Special Issues Sales Department, 1155 Sixteenth St., N.W., Washington, D.C. 20036.

Subscriptions to this and the other ACS periodical publications are available on microfilm. For information on microfilm write Special Issues Sales Department at the address above.

**Notice to Authors last printed in the issue of January 16, 1975**

THE JOURNAL OF

# PHYSICAL CHEMISTRY

*Volume 79, Number 13 June 19, 1975*

JPCHAx 79(13) 1233–1326 (1975)

ISSN 0022-3654

## COMMUNICATIONS TO THE EDITOR



■ Supplementary material for this paper is available separately, in photocopy or microfiche form. Ordering information is given in the paper.

* In papers with more than one author, the asterisk indicates the name of the author to whom inquiries about the paper should be addressed.

## AUTHOR INDEX

THE JOURNAL OF
PHYSICAL CHEMISTRY



VOLUME 79, NUMBER 13 JUNE 19, 1975

# A Determination by Resonance Radiation Flash Photolysis of the Absolute Reaction Rates of Excited Cadmium($5^3P_{0,1}$) Atoms with Several Gases

**W. H. Breckenridge,*[1] T. W. Broadbent, and D. S. Moore**

*Department of Chemistry, University of Utah, Salt Lake City, Utah 84112* *(Received November 25, 1974)*

*Publication costs assisted by the Petroleum Research Fund*

Reaction rate constants for the quenching and/or chemical reaction of equilibrated Cd($5^3P_{0,1}$) atoms with several molecules have been determined. The excited atoms were generated by 3261-Å resonance radiation flash photolysis of cadmium vapor in excess bath gas at 280°, and monitored by kinetic absorption spectroscopy. Absolute quenching cross sections calculated from the rate constants were compared to those obtained by other workers for the quenching of Hg($6^3P_1$) and Hg($6^3P_0$) atoms. The rate of collisional spin–orbit relaxation of Cd($^3P_1$) to Cd($^3P_0$) by He has been estimated, and lower limits for spin–orbit relaxation by Ar, $N_2$, and $CH_4$ have been determined.

## Introduction

The quenching and chemical reactivity of Hg($^3P_1$) has been studied thoroughly,[2a] in large part due to ease of excitation at room temperature and the resultant importance of Hg photosensitization as a convenient indirect source of electronically excited molecules and transient species. In the last 10 years, the direct techniques of modern gas kinetics have provided substantial quantitative knowledge of the primary interaction of Hg($^3P_1$) with diatomic and polyatomic molecules.[2b–8] In order to obtain a *general* understanding of the factors which influence the dissipation of chemically interesting amounts of electronic energy in the collision of an excited metal atom with a molecule, however, comparable studies must be undertaken of excited states of other metals such as Cd, Zn, and Mg. Magnesium excited states have apparently not been studied, there has been almost no work on the excited states of zinc, and only very recently have a few modern studies of the quenching of excited cadmium atoms appeared.[9–14] We are engaged in a comprehensive investigation of the quenching and reactivity of the first $^3P_J$ and $^1P_1$ excited states of Cd, Zn, and Mg atoms, using pulsed excitation techniques with detection by kinetic absorbtion spectroscopy. Reported here is an investigation, by resonance-radiation flash photolysis,[2b,9] of the quenching by several gases of equilibrated Cd($^3P_{0,1}$) at 280°. A preliminary account of some of these measurements has appeared elsewhere.[15]

## Experimental Section

Schematic diagrams of the experimental apparatus and the firing circuit are shown in Figures 1 and 2. The resonance-radiation flash lamp and reaction vessel are situated inside a thermostatted oven which can be heated to 320° with temperature control of ±2°. Fans with external motors mounted at opposite corners inside the furnace ensure uniform temperature throughout. The 70-cm long flash lamp is constructed from two quartz tubes, internal diameter 3.0 and 5.4 cm, which are sealed together at the ends. Eighteen pairs of opposing electrodes (⅛-in. tungsten rod in 10-mm i.d. quartz tubes) are sealed onto the outer cylinder at 4-cm intervals. The resonance lamp is powered by a 1.0-μF capacitor at 20 kV and fired with a spark gap. Each electrode pair is connected to a plate distributor at the spark gap by means of one meter of low-inductance coaxial cable in order to ensure a uniform discharge along the lamp. When the lamp is filled with 2 Torr of helium and the vapor pressure of cadmium at the temperature of operation, intense pulses of 2288- and 3261-Å cadmium resonance radiation of approximately 40 μsec duration can be generated with no observable background continuum. The 2288-Å emission was eliminated in the experiments reported here by jacketing the reaction vessel with a Corex D glass cylinder. Both the maximum intensity and total photon output of the 3261-Å pulses were quite reproducible from experiment to experiment (especially over the course

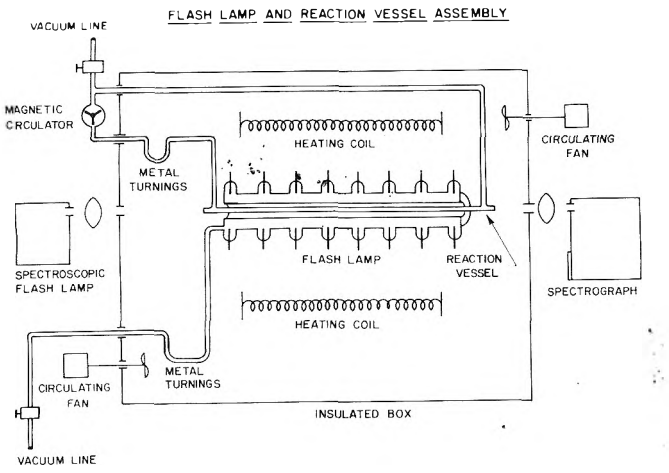


**Figure 1.** Schematic diagram of flash lamp and reaction vessel assembly.

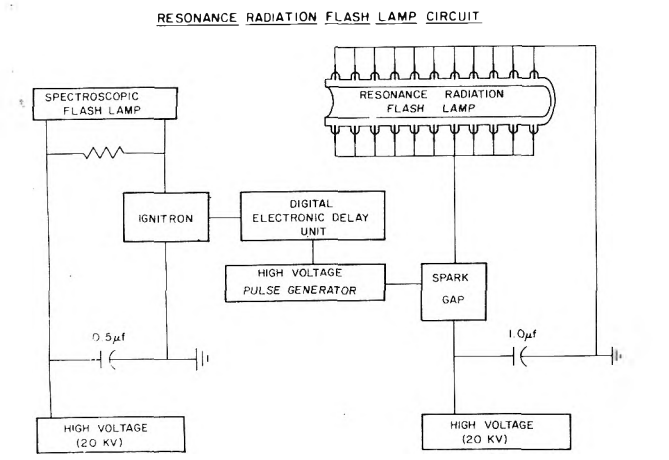


**Figure 2.** Resonance radiation flash lamp circuit.

of day-long experiments necessary for one measurement of the quenching cross section for a gas).

The 3261-Å radiation is absorbed by Cd vapor in a 5.0-mm i.d., 75-cm long quartz reaction vessel mounted coaxially inside the hollow lamp. Suprasil quartz windows are sealed onto the ends of the reaction vessel. Gas mixtures are saturated with Cd vapor and circulated continuously through the reaction vessel by means of a magnetically operated all-glass pump. Under normal circulation conditions with 400 Torr of "buffer" gas, the diffusion rate for cadmium vapor is smaller than the bulk flow rate through the reaction vessel, thus ensuring that the pressure of cadmium vapor is uniform along the reaction vessel length and equal to the cadmium vapor pressure at the temperature of the cadmium saturator.

The spectroscopic continuum source is an ignitron-fired, krypton-filled capillary discharge lamp which can be triggered at any preset interval from 1 μsec to 1 sec after the beginning of the resonance lamp pulse, using a digital electronic delay unit. The spectroscopic flash has a duration at half-height of 8 μsec. Spectra were taken with a Jarrel-Ash 0.75-m grating spectrograph using Kodak 103a0 plates sensitized when necessary with sodium salicylate.

Relative concentrations of CdH, $Cd(^3P_0)$, and $Cd(^3P_1)$ were determined by plate photometry of absorption bands at 2483, 3404, and 3466 Å, respectively, using a Joyce-Loebl Mark III CS recording microdensitometer. The following empirically modified form of the Beer–Lambert law was adopted to relate plate optical density to relative concentration:

$$OD = a(bc)^{\alpha}$$

where OD is the change in the optical density of the spectroscopic continuum on the photographic plate at the absorption maximum, $a$ is a constant, $b$ is the absorption path length, $c$ is the concentration of the species of interest, and $\alpha$ is a constant less than one. The value of $\alpha$ for each absorption was determined by reduction of the path length $b$ by factors of 0.8, 0.6, 0.4, and 0.2. This was done by blanking off successive fifths of the reaction vessel using flexible stainless steel cylinders. For the CdH absorption, $\alpha = 0.95 \pm 0.07$, and it was assumed that the Beer–Lambert law was followed for this diffuse absorption ($\alpha = 1$). For both the $Cd(^3P_0)$ and $Cd(^3P_1)$ absorptions, $\alpha = 0.55 \pm 0.10$, over the concentration range utilized in the quenching studies. Care was taken during all the experiments, especially those involving high concentrations of absorbing species, to ensure that the optical density measured was always in the linear region of photographic plate response.

Gas pressures were measured using a Wallace and Tiernan differential pressure gauge. Low pressures of quenching gases were measured into the reaction vessel circulation system using calibrated expansion volumes. Larger pressures of buffer gas were then added directly to the quencher gas. The circulator system was found to achieve mixing within 10 min (as determined by monitoring apparent quenching as a function of time after addition of the buffer gas). Mercury vapor from the vacuum system was isolated from both the lamp and the reaction vessel by intervening traps packed tightly with glass wool and kept continuously at −78°. The effectiveness of this trapping procedure has been demonstrated previously.[16] Also, the presence of very small pressures of mercury can be detected by absorption of the 2537-Å line over the 75-cm path length of the reaction vessel. Similarly, mercury in the photolysis lamp would result in detectable emission at 2537 Å. No trace of 2537-Å absorption or emission was ever detected. Only in the case of benzene was it necessary to let the reaction-vessel trap warm to −25° to obtain sufficient pressures of benzene.

Ethylene, propylene, ethane, propane (all Matheson Research Grade), and benzene (Mallinckrodt, Spectrochemical Grade) were freeze–pumped several times. Methane (Phillips Research Grade), $D_2$ (Bio-Rad, 99.65% D), and HD (Merck Sharp and Dohme, >98% D) were used without further purification. Hydrogen (Matheson Prep Grade) and helium (Matheson Ultra High Purity) were passed through a trap packed with 5A molecular sieves at −196°. Argon (Matheson Ultra High Purity), nitrogen (Matheson Prep. Grade), and carbon monoxide (Matheson Research Grade) were passed through a glass-wool-packed trap at −196°. Sulfur hexafluoride (Matheson Instrument Grade), carbon dioxide (Coleman Instrument Grade), and ammonia (Matheson Anhydrous Grade) were distilled from −78 to −196°, and freeze–pumped several times. Nitric oxide (Matheson) was passed through a trap containing baked silica gel at −78°.

## Results

The quenching of $Cd(^3P_0)$ and $Cd(^3P_1)$ can be discussed in terms of the set of reactions

| | | |
|---|---|---|
| | $Cd(^1S_0) + h\nu \longrightarrow Cd(^3P_1)$ | |
| | $Cd(^3P_1) \longrightarrow Cd(^1S_0) + h\nu$ | $k_r$ |
| (d) | $Cd(^3P_1) + M \longrightarrow Cd(^3P_0) + M$ | $k_d$ |
| (−d) | $Cd(^3P_0) + M \longrightarrow Cd(^3P_1) + M$ | $k_{-d}$ |
| (1) | $Cd(^3P_1) + Q \longrightarrow$ quenching | $k_1$ |
| (0) | $Cd(^3P_0) + Q \longrightarrow$ quenching | $k_0$ |
| ($1_H$) | $Cd(^3P_1) + H_2 \longrightarrow CdH + H$ | $k_{1_H}$ |
| ($0_H$) | $Cd(^3P_0) + H_2 \longrightarrow CdH + H$ | $k_{0_H}$ |

The natural radiative lifetime of $Cd(^3P_1)$ (2.3 $\mu$sec)[17] is relatively short compared to the length of the 3261-Å resonance radiation excitation flash (~40 $\mu$sec). Under conditions of large excess M, for M = Ar, $CH_4$, and $N_2$, the ratio of concentrations of $Cd(^3P_0)$ and $Cd(^3P_1)$ is approximately constant and the intensity–time profile of the concentrations of the two excited states essentially parallels that of the 3261-Å excitation pulse. This implies that a steady state is established rapidly, and that equations derived from the steady-state assumption are valid in this system. By assuming that steady-state concentrations exist for $Cd(^3P_0)$ and $Cd(^3P_1)$ at any chosen analysis interval during the excitation flash, the following equations can be derived:

$$\frac{[Cd(^3P_1)]_{Q=0}}{[Cd(^3P_1)]} = 1 + \left\{k_0[Q]\left(\frac{k_d[M]}{k_{-d}[M] + k_0[Q]}\right) + k_1[Q]\right\}/k_r \quad (A)$$

$$\frac{[Cd(^3P_0)]_{Q=0}}{[Cd(^3P_0)]} = 1 + \frac{k_0[Q]}{k_{-d}[M]} + \left\{k_0[Q]\left[\left(k_d + \frac{k_1[Q]}{[M]}\right)\Big/k_{-d}\right] + k_1[Q]\right\}/k_r \quad (B)$$

If it can be further assumed that at large [M] the equilibration reactions d and −d are always rapid compared to reactions 0 and 1 (i.e., that $Cd(^3P_0)$ and $Cd(^3P_1)$ are equilibrated under the experimental quenching conditions), the above equations simplify to

$$\frac{[Cd(^3P_1)]_{Q=0}}{[Cd(^3P_1)]} = 1 + \left\{\left(\frac{k_d}{k_{-d}}k_0 + k_1\right)[Q]\right\}/k_r \quad (C)$$

$$\frac{[Cd(^3P_0)]_{Q=0}}{[Cd(^3P_0)]} = 1 + \left\{\left(\frac{k_d}{k_{-d}}k_0 + k_1\right)[Q]\right\}/k_r \quad (D)$$

Inspection shows that these equations are similar to the classical Stern–Volmer expression for fluorescence quenching, except that the normal quenching rate constant is replaced by an "effective" quenching rate constant ($k_dk_0/k_{-d} + k_1$). A statistical mechanical calculation yields $k_d/k_{-d} = 1.37$ at 280°. Knowing $k_r$, the effective quenching rate constant at 280° ($1.37k_0 + k_1$) can be determined by plotting [Q] vs. $1/[Cd(^3P_1)]$ or $1/[Cd(^3P_0)]$. Delay times are chosen near the maximum of the excitation flash intensity.

The following expansion is informative:

$$\left(\frac{k_d}{k_{-d}}k_0 + k_1\right)/k_r = \left\{\left(\frac{k_d}{k_d + k_{-d}}\right)k_0 + \left(\frac{k_{-d}}{k_d + k_{-d}}\right)k_1\right\}\Big/\left(\frac{k_{-d}}{k_d + k_{-d}}\right)k_r \quad (E)$$

Because of the population of nonradiating $Cd(^3P_0)$, the apparent first-order lifetime of $Cd(^3P_1)$ due to fluorescence decay only is increased, and $k_r$ is therefore multiplied by a factor equal to the equilibrium fractional population of $Cd(^3P_1)$. However the quenching rate constant for $Cd(^3P_1)$, $k_1$, is multiplied by the same factor, and the quenching rate constant for $Cd(^3P_0)$, $k_0$, is multiplied by the fractional population of $Cd(^3P_0)$.

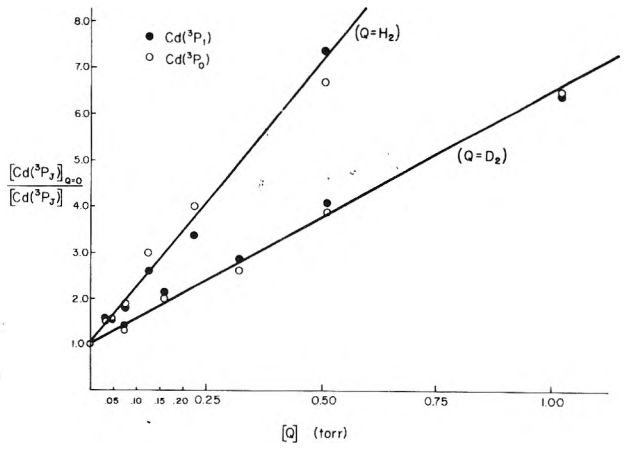


**Figure 3.** Variation of $Cd(^3P_0)$ and $Cd(^3P_1)$ concentrations with pressure of added $H_2$ and $D_2$; 400 Torr of Ar, 280°; delay time, 10 $\mu$sec.

Reactions $0_H$ and $1_H$ represent the rapid reaction of $Cd(^3P_J)$ with $H_2$ to form CdH, which can be easily detected in absorption via several bands in the ultraviolet. Because CdH is fairly long lived under our conditions (approximate half-life of 150 $\mu$sec), we are able to use the CdH concentration (at a time near the end of the excitation flash) as a product "marker" for $Cd(^3P_J)$ reactions.[18] Again assuming steady-state conditions for $Cd(^3P_J)$ and collisional equilibration of $Cd(^3P_0)$ and $Cd(^3P_1)$ by buffer gas M, the following equation obtains. If [Q] = $[H_2]$

$$\frac{[CdH]_\infty}{[CdH]} = 1 + k_r/\left(\frac{k_d}{k_{-d}}k_0 + k_1\right)[H_2] \quad (F)$$

where $[CdH]_\infty$ is the extrapolated maximum value of [CdH] when 1/[CdH] is plotted vs. $1/[H_2]$. Note that it is possible that reactions $0_H$ and $1_H$ represent only a constant fraction of the total quenching by Q = $H_2$ in reactions 1 and 0, respectively, if physical quenching by $H_2$ occurs at a competitive rate.[19] A plot of $[CdH]_\infty/[CdH]$ vs. $1/[H_2]$ allows calculation of the "effective" overall quenching rate constant, ($k_dk_0/k_{-d} + k_1$), for $H_2$.

Typical plots (Q = $H_2$, Q = $D_2$) which illustrate that eq C and D are valid are shown in Figure 3. Similar plots were obtained for other quenching gases. Equation F was found to be valid for quenching by $H_2$, HD, or $D_2$. The plots for Q = $H_2$ and Q = $D_2$ are shown in Figure 4.

It was necessary to conduct experiments at 280° in order to obtain sufficient concentrations of $Cd(^3P_J)$ for accurate measurements. Unfortunately, for vapor pressures of cadmium at temperatures above 240° the lengthening of the effective radiative lifetime of $Cd(^3P_1)$ due to radiation "imprisonment" is no longer completely negligible. Thus the factor by which the "natural" $k_r$ should be reduced for the conditions of our quenching measurements must be determined. Michael and Yeh,[20] Yang,[21] Hong and Mains,[6] and Thomas and Gwinn[22] have made experimental measurements of the imprisonment lifetime of $Hg(^3P_1)$ under comparable conditions of low opacity. Samson's "equivalent opacity" theory[23] will fit all the data adequately when the thickness $l$ of Samson's "infinite slab" geometry is set

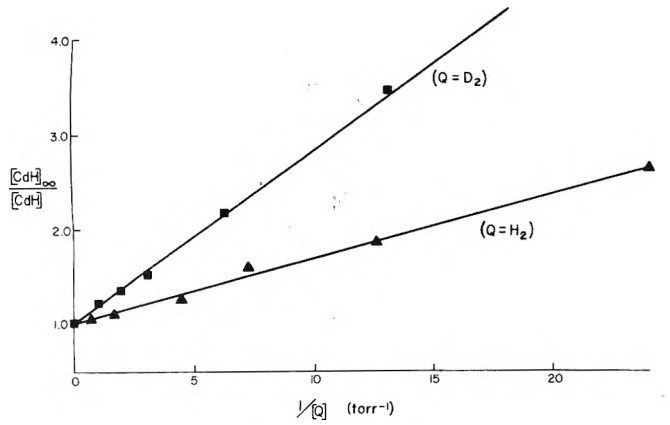


**Figure 4.** Variation of CdH (CdD) concentration with pressure of added $H_2$ ($D_2$); 400 Torr of Ar, 280°; delay time, 50 μsec. $[CdH]_\infty$ is the extrapolated value of [CdH] as $[H_2]$ approaches infinity.

equal to the radius of a cylindrical reaction vessel.[20] The apparent equivalence, with regard to radiation imprisonment at low opacities, of an infinite slab of thickness $l$ to an infinite cylinder with radius $l$ has recently been given theoretical justification.[24] Milne's early "diffusion" theory of resonance radiation imprisonment[20,23] led to an expression for the ratio of the "imprisonment" radiative lifetime, $\tau$, to the "natural" lifetime, $\tau_0$:

$$\tau/\tau_0 = 1 + \left(\frac{kl}{\lambda}\right)^2 \qquad \text{(G)}$$

where $k$ is the absorption coefficient at the line center (a narrow band of radiation is presumed to be scattered without frequency change), $l$ is the thickness of the infinite slab, and λ is the root between 0 and $\pi/2$ of the equation:

$$\tan(X) = kl/X \qquad \text{(H)}$$

Samson modified Milne's theory so that an "equivalent" opacity $\overline{kl}$ is used instead of $kl$, to allow for the fact that the scattered (imprisoned) radiation has a frequency distribution which depends on the absorption line shape. The equivalent opacity can be defined in general terms by

$$\exp(-\overline{kl}) = \frac{\int_{-\infty}^{+\infty} F(w)\ \exp[-k_0 l F(w)]\,dw}{\int_{-\infty}^{+\infty} F(w)\,dw} \qquad \text{(I)}$$

where $w = [2(\nu - \nu_0)/\Delta\nu_D](\ln 2)^{1/2}$, and $\nu_0$ is the frequency at the center of the line, $\Delta\nu_D$ is the width of a Doppler-broadened line,[25] $k_0$ is the absorption coefficient at the center of a Doppler-broadened line,[25] and $F(w)$ is the absorption line-shape function. For the experiments on $Hg(^3P_1)$ imprisonment lifetimes, the line shapes were determined entirely by Doppler broadening (i.e., $F(w) = e^{-w^2}$). For reasons discussed below, our experiments were conducted in 100–400 Torr of bath gas, where both Doppler and Lorentz (collision) broadening influence the absorption line shape, $F(w)$. We have evaluated $F(w)$ by assuming classical Lorentz broadening for these low-pressure conditions (no asymmetry or frequency shift) and using the method of Reiche as outlined by Mitchell and Zemansky to calculate the Voigt profile.[26] Lorentz broadening cross sections for He, Ar, $N_2$, and $CH_4$ were chosen to be 22, 70, 62, and 43 Å$^2$, respectively, from experimental measurements.[27]

Because of isotopic and hyperfine splitting, the 3261-Å absorption cannot be considered a single broadened absorption, however. Although the isotopic composition of cadmium is somewhat similar to that of mercury (where the 2537-Å line has traditionally been considered, as an approximation, to consist of five lines of equal intensity),[20,25] the splittings are smaller, so that some isotopic components are not completely resolved even under conditions of Doppler broadening at 280°.[28] There are two odd isotopes of Cd (~25% total) which do produce essentially resolved nuclear-spin hyperfine lines of low intensity on either side of the main absorption, which consists of closely bunched even-isotope lines. The absorption line shape was calculated graphically by summation of weighted profiles for each isotopic and hyperfine line, to obtain an overall $F(w)$.[28,29] Under Doppler-broadened conditions at 280° ([Cd] = 1.9 × $10^{-2}$ Torr,[30] $l$ = 0.25 cm) the 3261-Å line profile is found to consist of three components in the approximate ratio of 2:7:1, with each component substantially broader than the normal Doppler width[25] of 0.048 cm$^{-1}$; the maximum opacity was calculated to be $k_{max}l$ = 1.30. With Voigt profile conditions at 400 Torr of Ar, $k_{max}l$ = 0.33. Equation I was solved by numerical integration for each pressure condition. The equivalent opacity thus obtained was used to determine $\tau/\tau_0$ in eq G. The results are shown in Table I. Because most of our measurements have been performed at 400 Torr, a radiation imprisonment correction of approximately 20% is required at 280°.[31]

Quenching experiments were conducted with 400 Torr of buffer gas (Ar, $CH_4$, $N_2$) present in order to (i) maximize

**TABLE I: Calculated Imprisonment Ratios for $Cd(^3P_1)$ Under Various Conditions (See Text for Details)**

| Conditions[a] | [Cd], Torr | $\tau/\tau_0$[b] |
|---|---|---|
| 400 Torr Ar, 260° | $7.8 \times 10^{-3}$ | 1.09 |
| 400 Torr Ar, 270° | $12 \times 10^{-3}$ | 1.14 |
| 400 Torr Ar, 280° | $19 \times 10^{-3}$ | 1.21 |
| 400 Torr Ar, 290° | $29 \times 10^{-2}$ | 1.39 |
| 400 Torr Ar, 300° | $44 \times 10^{-2}$ | 1.63 |
| 400 Torr Ar, 310° | $67 \times 10^{-2}$ | 2.00 |
| 400 Torr Ar, 320° | $99 \times 10^{-2}$ | 2.81 |
| 100 Torr Ar, 280° | $19 \times 10^{-3}$ | 1.47 |
| 400 Torr He, 280° | $19 \times 10^{-3}$ | 1.23 |
| 400 Torr $N_2$, 280° | $19 \times 10^{-3}$ | 1.18 |
| 400 Torr $CH_4$, 280° | $19 \times 10^{-3}$ | 1.22 |
| Doppler broadening only, 280° | $19 \times 10^{-3}$ | 2.05 |

[a] $l$ = 0.25 cm (radius of vessel). [b] $\tau$ is the "imprisonment" lifetime, $\tau_0$ is the natural radiative lifetime.

**TABLE II: Comparison of Apparent $Cd(^3P_1)$ Quenching Half-Pressures for $H_2$ in the Presence of Other Gases (Using CdH as "Marker")**

| Gas | Pressure, Torr | $P_{1/2}(H_2)$, Torr |
|---|---|---|
| Ar | 100 | 0.061 ± 0.008 |
| Ar (2% $N_2$) | 400 | 0.065 ± 0.010 |
| Ar | 400 | 0.069 ± 0.008 |
| $CH_4$ | 400 | (0.080 ± 0.020)[a] |
| $N_2$ | 400 | 0.31 ± 0.04 |

[a] Corrected for a small amount of CdH produced in the reaction: $Cd(^3P_1) + CH_4 \rightarrow CH_3 + CdH$.

**TABLE III: Quenching Half-Pressures of Cd($^3P_J$) for $H_2$, HD, and $D_2$ (280°, Torr)**

| Gases | Method of determination: CdH (CdD) formation | Cd($^3P_1$) quenching | Cd($^3P_0$) quenching |
|---|---|---|---|
| $H_2$ (400 Torr Ar) | 0.067 ± 0.012 | 0.080 ± 0.015 | 0.070 ± 0.015 |
| $H_2$ (8 Torr $N_2$, 392 Torr Ar)[a] | 0.061 ± 0.010 | 0.070 ± 0.014 | 0.076 ± 0.014 |
| HD (400 Torr Ar) | 0.075 ± 0.010 | 0.078 ± 0.015 | 0.080 ± 0.015 |
| HD (8 Torr $N_2$, 392 Torr Ar)[a] | 0.088 ± 0.012 | 0.086 ± 0.015 | 0.075 ± 0.015 |
| $D_2$ (400 Torr Ar) | 0.150 ± 0.030 | 0.20 ± 0.05 | 0.21 ± 0.05 |
| $D_2$ (8 Torr $N_2$, 392 Torr Ar)[a] | 0.176 ± 0.020 | 0.155 ± 0.030 | 0.168 ± 0.030 |

[a] Values at 8 Torr of $N_2$, 392 Torr of Ar have been corrected for a small amount of quenching by $N_2$ (7%).

the likelihood of rapid Cd($^3P_0$), Cd($^3P_1$) equilibration, (ii) minimize any changes in absorption line broadening, and thus total light absorbed, when much smaller pressures of quenching gas are added, and (iii) prevent any possible temperature rise when large amounts of Cd($^3P_J$) electronic energy are dissipated in small pressures of quencher gas. To measure absolute rates for Cd($^3P_J$) deactivation, it is necessary to show that the addition of 400 Torr of at least one buffer gas is insufficient to increase the apparent value of $k_r$ via a parallel quenching reaction. Shown in Table II are values of the Cd($^3P_J$) quenching half-pressure for hydrogen, $P_{1/2}(H_2)$, obtained under various conditions. (Quenching half-pressure is the pressure of added quencher necessary to decrease [Cd($^3P_1$)] or [Cd($^3P_0$)] by one-half, or to create [CdH] equal to ½[CdH]$_\infty$.) These values were determined using the plots discussed above. According to the imprisonment calculations in Table I, decreasing the pressure of argon from 400 to 100 Torr should result in a decrease in $P_{1/2}(H_2)$ of approximately 20%. The observed decrease is less than this, but is consistent within our experimental error, and the conclusion can certainly be made that quenching of Cd($^3P_J$) by 400 Torr of Ar is negligible. There is appreciable quenching by 400 Torr of $N_2$, but 400 Torr of $CH_4$ quenches Cd($^3P_J$) only very slightly. Production of CdH was just detectable with 400 Torr of pure $CH_4$ at 280°.

Table III contains a summary of values of $P_{1/2}$ obtained for the isotopic hydrogens. These results clearly support our assumptions of steady-state conditions and rapid Cd($^3P_0$), Cd($^3P_1$) equilibration. The satisfactory agreement between the CdH formation and the Cd($^3P_1$), Cd($^3P_0$) quenching measurements is also consistent with the assumed conditions and provides additional confirmation of the validity of the procedure for determining the Beer-Lambert ($\alpha$) factors for the absorptions. The experiments with 2% $N_2$ in Ar were conducted to double check our assumptions about true equilibration of the Cd($^3P_1$) and Cd($^3P_0$) states. Nitrogen gas is very efficient in deactivating Cd($^3P_1$) to Cd($^3P_0$).[32,33]

Using the methods discussed, absolute rates of quenching of equilibrated Cd($^3P_0$,$^3P_1$) by several gases have been determined and are listed in Table IV. The natural radiative lifetime of Cd($^3P_1$) was taken to be $2.3 \times 10^{-6}$ sec,[17] resulting in $k_r = 4.4 \times 10^5$ sec$^{-1}$. An "effective" $k_r$ was calculated for each imprisonment condition using Table I. The quenching rates for all gases except those for which upper limits are listed were measured in 400 Torr of 2% $N_2$ in Ar to assure equilibration of Cd($^3P_1$) and Cd($^3P_0$). The apparent quenching rates in these cases were corrected for a small amount of net quenching by $N_2$ (~7%). The quenching rate for nitrogen was calculated from the apparent $P_{1/2}$ for hydrogen in 400 Torr of nitrogen, using CdH as a marker.

In order to make sure that the radiation imprisonment treatment was not producing serious errors, the quenching rate for nitric oxide was measured at 260°, where the concentrations of Cd($^3P_J$) are sufficiently low that quenching measurements of Cd($^3P_0$) only could be made with the available absorption signal-to-noise. At 260°, the rate of quenching by equilibrated Cd($^3P_{1,0}$) is equal to $1.44k_0 + k_1$, and was determined to be $(2.3 \pm 0.4) \times 10^{11}$ $M^{-1}$ sec$^{-1}$ using the imprisonment ratio of 1.09 at 260° shown in Table I. This is to be compared with the value of $1.37k_0 + k_1$, obtained at 280°, of $(2.4 \pm 0.3) \times 10^{11}$ $M^{-1}$ sec$^{-1}$, where the imprisonment ratio is 1.21. Because no marked temperature dependence is expected for such a rapid quenching reaction, it can be concluded that the radiation imprisonment treatment employed in this study is not grossly incorrect. A 20° change in temperature in this range results in a 2.5-fold increase in [Cd]. Only at very low $\tau/\tau_0$ valves could such a large increase in [Cd] result in the observed change in $\tau/\tau_0$ of ~10%. (See the higher temperature calculations in Table II, and Figure 5 in ref 20.) Taking error limits into consideration, the experiment proves that $\tau/\tau_0$ cannot be greater than about 1.40 at 280° with 400 Torr of argon.

The lower limit quoted for the rate of quenching by $SO_2$ is the result of an unusual but apparently reproducible phenomenon. When $SO_2$ was added to the reaction vessel by expansion as usual for low pressures of quenching gas (with 2% $N_2$–Ar added subsequently and mixing allowed in the circulating system for 15–20 min), *no* quenching was observed until the apparent addition of at least 0.13 Torr of $SO_2$, whereupon quenching increased quite rapidly with the apparent pressure of added $SO_2$, with 80% quenching at about 0.20–0.25 Torr. There was *no trace* of the strong absorptions by $SO_2$ in the 2000-Å region until apparent pressures of $SO_2$ *greater* than 0.13 Torr had been added, and absorption by several of the strong bands of $SO_2$ had completely whitened the photographic plate by 0.20 Torr of $SO_2$. These observations are consistent with some kind of saturable up-take of $SO_2$, probably on the surface of the hot cadmium metal. If it is assumed that the observed quenching can be due only to $SO_2$ at the maximum apparent pressure added, the lower limit shown in the table is

TABLE IV: Quenching of $Cd(^3P_J)$ by Various Gases

| Gas | 280° | | 25° | |
|---|---|---|---|---|
| | $(1.37k_0 + k_1)$, $M^{-1}$ sec$^{-1}$ [c] | $1.37\sigma^2_{Cd(^3P_0)} + \sigma^2_{Cd(^3P_1)}$, Å$^2$ | $\sigma^2_{Hg(^3P_1)}$, Å$^2$ [a] | $\sigma^2_{Hg(^3P_0)}$, Å$^2$ |
| $C_6H_6$ | $(6.6 \pm 1.8) \times 10^{11}$ | 68 | (48,[38] 50[2a])[b] | |
| $C_3H_6$ | $(6.9 \pm 1.1) \times 10^{11}$ | 59 | (40,[2a] 48[3])[b] | |
| $C_2H_4$ | $(6.0 \pm 1.0) \times 10^{11}$ | 44 | 32–40[2,3] | 26[2b] |
| $SO_2$ | $>4 \times 10^{11}$ | >60 | | |
| NO | $(2.40 \pm 0.30) \times 10^{11}$ | 18 | 26–31[2,3] | 16.2,[2b] 12.9,[7] 8.0[36] |
| $CO_2$ | $(1.40 \pm 0.20) \times 10^{11}$ | 12 | 3.0,[2,37] 3.3[2b,37,39] | 0.033,[2b] 0.035[36] |
| $H_2$ | $(1.79 \pm 0.22) \times 10^{11}$ | 3.9 | 11.1,[2b,3] 10.0[2b,6] | 1.0,[2b] 1.65,[7] 2.1[36] |
| HD | $(1.48 \pm 0.20) \times 10^{11}$ | 3.9 | 12.2,[3,21] 10.9[6] | |
| $D_2$ | $(7.1 \pm 1.1) \times 10^{10}$ | 2.0 | 10.7[3,21] | 0.9,[2b,37] 2.9[36] |
| $SF_6$ | $(1.9 \pm 0.4) \times 10^{10}$ | 2.3 | | |
| CO | $(2.37 \pm 0.40) \times 10^{10}$ | 1.7 | <0.7[2,37] | 0.66,[2b] 0.21,[36] 2.49[7] |
| $NH_3$ | $(7.4 \pm 1.4) \times 10^8$ | 0.044 | <1.2[2,37] | 0.019[2b,7] |
| $N_2$ | $(1.03 \pm 0.20) \times 10^8$ | 0.0076 | <0.01[8] | $<2 \times 10^{-6}$ [8] |
| $CH_4$ | $<2 \times 10^7$ | <0.0012 | ~0.06[2] | $3 \times 10^{-5}$,[2b] $1 \times 10^{-4}$ [36] |
| $C_2H_6$ | $<1.5 \times 10^7$ | <0.0011 | ~0.05[2,37] | 0.0057,[2b] 0.028[7] |
| $C_3H_8$ | $<1.5 \times 10^7$ | <0.0013 | ~1.6[2,37] | 0.033[2b] |
| Ar | $<1 \times 10^7$ | <0.0008 | (<0.006[40])[b] | |
| He | $<1 \times 10^7$ | <0.0003 | | |

[a] These cross sections have been obtained by multiplying the measured $Hg(^3P_1)$ quenching cross section by $(1 - f)$, where $f$ represents the fraction of quenching collisions with that molecule which produce $Hg(^3P_0)$. Thus, these cross sections represent the sum of all cross sections of quenching processes which do not produce $Hg(^3P_0)$. [b] Fractional $Hg(^3P_0)$ yields have not been determined in these cases. [c] The uncertainties listed are estimates based on the scatter of the data. Until the theoretical treatment used to correct for radiation imprisonment is subjected to a rigorous experimental test, the rate constant values should be considered to have a total uncertainty of ±25%.

obtained. Attempts to measure quenching by oxygen failed because of the rapid reaction of $O_2$ with cadmium at 280°, even at low pressures.

Two more sets of experiments were performed to check further the consistency of our interpretation of this kinetic system. In the first, ethylene pressure was varied from 0 to 2 Torr in mixtures of 2 Torr of $H_2$–400 Torr of $N_2$. Nitrogen was used as bath gas because rapid $Cd(^3P_1)$, $Cd(^3P_0)$ equilibration is essential for these measurements, which involve relatively high pressures of the efficient quenchers $H_2$ and $C_2H_4$. Under the conditions of the experiments, 87% of the $Cd(^3P_J)$ was reacting with $H_2$ when no $C_2H_4$ was present. As the ethylene pressure was increased, the CdH yield decreased due to competitive quenching of $Cd(^3P_J)$ by $C_2H_4$. A plot of 1/[CdH] vs. $[C_2H_4]$ yielded a straight line, as would be expected for direct competitive quenching, and from the slope-to-intercept ratio the following quantity was calculated:

$$(1.37k_0 + k_1)_{C_2H_4}/(1.37k_0 + k_1)_{H_2} = 3.7 \pm 0.4$$

This can be compared to a value of 3.4 ± 0.5 determined from the quenching rates listed in Table IV.

In the second set of experiments, the apparent $P_{1/2}$ for deuterium in 400 Torr of nitrogen was measured, using CdD as a marker, and was found to be 0.72 Torr of $D_2$. By comparing this result with the equivalent $P_{1/2}$ for hydrogen in 400 Torr of nitrogen (0.31 Torr $H_2$) the following ratio can be calculated:

$$(1.37k_0 + k_1)_{D_2}/(1.37k_0 + k_1)_{H_2} = 0.43 \pm 0.05$$

This compares to the ratio of 0.40 ± 0.05 calculated from the rates in Table IV. It should be noted that in both sets of experiments just described, the steady-state concentrations of $Cd(^3P_1)$ and $Cd(^3P_0)$ are lower by factors of 4–100 than in the direct $Cd(^3P_J)$ quenching experiments.

Also shown in Table IV are the corresponding effective quenching cross sections for equilibrated $Cd(^3P_1,^3P_0)$, calculated using the simple collision theory expression:

$$\sigma_Q^2 = k_c\left[8\pi RT\left(\frac{M_{Cd} + M_Q}{M_{Cd}M_Q}\right)\right]^{-1/2}$$

where $M_{Cd}$ and $M_Q$ are the atomic and molecular weights of cadmium and the quencher molecule, respectively. The cross section, by long-standing convention,[25] is therefore designated as the square of the "effective" radius of the collision complex. The reader should be wary when comparing cross sections of quenching of excited atoms, because many authors have adopted the perhaps more logical convention whereby the designated cross section is greater by a factor of $\pi$. (See, for example, ref 8, 10, and 35.) Included in Table IV for comparison are values of cross sections for quenching of $Hg(^3P_1)$ and $Hg(^3P_0)$. The $Hg(^3P_1)$ cross sections listed are the sums of all quenching processes *except* quenching to $Hg(^3P_0)$, which are obviously the most useful values to compare with equilibrated $Cd(^3P_1,^3P_0)$ cross sections.

From the observation of equilibration of $Cd(^3P_1)$ and $Cd(^3P_0)$ in a time interval short compared to the radiative lifetime of $Cd(^3P_1)$, a lower limit for deactivation of $Cd(^3P_1)$ to $Cd(^3P_0)$ can be calculated for several gases. The "radiative" lifetime of $Cd(^3P_1)$ under conditions of 400 Torr of buffer gas at 280°, from Table I, is approximately 2.8 μsec. The half-time for conversion of $Cd(^3P_1)$ to $Cd(^3P_0)$ must therefore be less than 2.8 μsec, and a lower limit for the rate constant $k_d$ for deactivation of $Cd(^3P_1)$ to $Cd(^3P_0)$ for Ar, $N_2$, and $CH_4$ can be calculated: $k_d > 2 \times 10^7$ $M^{-1}$ sec$^{-1}$.

Only in experiments with 400 Torr of pure helium were major variations observed in the ratio of concentrations of $Cd(^3P_0)$ to $Cd(^3P_1)$. The concentration of $Cd(^3P_1)$ essentially followed the 3261-Å flash intensity as a function of

**TABLE V: Comparison of Cd($^3P_1$) Quenching Cross Sections**

| Ref | Temp, °C | Cross-section measured | Cross sections, Å$^2$ $C_6H_6$ | $C_3H_6$ | $C_2H_4$ | $H_2$ | $D_2$ | $NH_3$ |
|---|---|---|---|---|---|---|---|---|
| This work | 280 | $1.37\sigma_{Cd(^3P_0)} + \sigma_{Cd(^3P_1)}$ | 68 | 59 | 44 | 3.9 | 2.0 | 0.044 |
| 42 | 213 | $\sigma_{Cd(^3P_1)}$ (?) | 30[a] | 31[a] | 27[a] | 3.8[c] | 2.0[a] | 0.045[a,b] (0.056) |
| 10 | 285 | $\sigma_{Cd(^3P_1)}$ (?) | | | | | | 0.049 |
| 14 | 27 | $0.81\sigma_{Cd(^3P_0)} + 0.19\sigma_{Cd(^3P_1)}$ | < 0.0007 | | 0.064 | 0.0014 | | |
| 14 | 280 | $0.81\sigma_{Cd(^3P_0)} + 0.19\sigma_{Cd(^3P_1)}$ | | | 0.30[c] | 0.070[c] | | |
| 14 | 280 | $4.26\sigma_{Cd(^3P_0)} + \sigma_{Cd(^3P_1)}$ | | | 1.58[c] | 0.37[c] | | |

[a] Adjusted to a natural lifetime of $2.3 \times 10^{-6}$ sec for Cd($^3P_1$). [b] Calculated using only the data below 6 Torr of $NH_3$. Curvature in the Stern–Volmer plot above 8 Torr of $NH_3$ may have been due to effect of pressure broadening. Value quoted by Steacie and LeRoy is shown in parentheses. [c] Calculated using the Arrhenius parameters estimated in ref 14.

time, but the Cd($^3P_0$) concentration was appreciably lower than normal at the beginning of the flash, built up during the flash, then decayed beyond the flash termination. From the assumption that the post-flash decay is due to reaction −d with $M$ = He, followed by fluorescence of Cd($^3P_1$), the following rate constant can be estimated: $k_{-d}$ (M = He) = $(4.5 \pm 2.0) \times 10^6\ M^{-1}\ \text{sec}^{-1}$. Thus, by the principal of microscopic reversibility (shown to be valid by Krause and coworkers[8] for the case of Hg($^3P_1$), Hg($^3P_0$) interconversion by $N_2$)

$$k_d(\text{M} = \text{He}) = (6 \pm 3) \times 10^6\ M^{-1}\ \text{sec}^{-1}$$

## Discussion

It is interesting and informative to compare our results with those obtained in other studies. A method of monitoring *both* Cd($^3P_0$) and Cd($^3P_1$) is required for definitive measurements of quenching rates in this reaction system, where the difference in energy between the two excited sublevels (~1.5 kcal/mol) is comparable to $kT$ (1.1 kcal/mol at 280°), so that collisional repopulation of the resonance $^3P_1$ level can often occur at a rate comparable to net quenching to the ground state. Thus classical Stern–Volmer Cd($^3P_1$) fluorescence quenching measurements such as those of Lipson and Mitchell,[41] and Steacie and LeRoy,[42] cannot be interpreted correctly unless the extent of Cd($^3P_1$), Cd($^3P_0$) interconversion in the presence of quencher *only* is known. The results of Lipson and Mitchell[41] are probably not reliable in any case. Their quartz fluorescence cell was apparently illuminated directly with a lamp which emitted both 2288- ($^1S_0 \rightarrow {}^1P_1$) and 3261-Å ($^1S_0 \rightarrow {}^3P_1$) radiation. It has been shown recently[9] that several gases, including $H_2$, are quite efficient in quenching Cd($^1P_1$) to Cd($^3P_J$), and such a process could of course lead to large errors in measurements of apparent Cd($^3P_1$) fluorescence quenching.

Shown in Table V is a comparison of our cross-section values with those measured in the careful work of Steacie and LeRoy.[42] The apparent cross sections for $H_2$, $D_2$, and $NH_3$ are consistent with our measured values within experimental error. Such agreement is expected for two limiting cases for the Stern–Volmer conditions. (i) Quenching of Cd($^3P_0$) occurs at a negligible rate compared to quenching of Cd($^3P_1$) (i.e., in equation A, for M = Q, because $k_d/k_{-d} \approx 1.5$, if $k_0 \ll k_1$ the right half of the equation will always reduce to $1 + k_1[Q]/k_r$, the correct Stern–Volmer form). (ii) Cd($^3P_0$) and Cd($^3P_1$) are equilibrated by the quenching species Q much more rapidly than net deactivation to the ground state can occur.

Case i is a reasonable possibility for the isotopic hydrogens, for which the reaction of Cd($^3P_1$) to form CdH (or CdD) is slightly endothermic so that even an activation energy difference of 1.5 kcal/mol (the $^3P_0 - {}^3P_1$ energy difference) would cause the reaction of Cd($^3P_0$) with a certain isotopic hydrogen to occur at a rate less than 20% that of Cd($^3P_1$). In the analogous quenching of Hg($^3P_J$), hydrogen quenches Hg($^3P_1$) about ten times as rapidly as Hg($^3P_0$), even though the chemical reaction channels to form (HgH + H) or Hg + 2H are exothermic in both cases.[2,6]

Case ii seems more likely for $NH_3$, which should be a relatively efficient "M" in reactions d and −d. *Net* quenching is inefficient, so that Stern–Volmer measurements are carried out at 1–25 Torr of $NH_3$ pressure. The value of $k_d$ for Hg($^3P_1$) with M = $NH_3$ has been determined to be $\sim 3 \times 10^{10}\ M^{-1}\ \text{sec}^{-1}$ from the overall quenching rate and the fact that the fraction of quenching collisions which produce Hg($^3P_0$) is at least 0.65.[1,2,37] Also, the rate constant for spin–orbit quenching by the isoelectronic hydride $CH_4$ of Cs($6^2P_{3/2}$) to Cs($6^2P_{1/2}$), where the multiplet energy difference is 554 $\text{cm}^{-1}$ compared to 542 $\text{cm}^{-1}$ for Cd($^3P_{0,1}$), is $\sim 2 \times 10^{11}\ M^{-1}\ \text{sec}^{-1}$.[43] These rate constants can be compared to the value of only $7 \times 10^8\ M^{-1}\ \text{sec}^{-1}$ shown in Table IV for net quenching of equilibrated Cd($^3P_{0,1}$). The recent phase-shift study of Morten et al.[10] of quenching of Cd($^3P_1$) by $NH_3$ (with no buffer gas present) has also yielded an apparent cross section which is in good agreement with our value and that of Steacie and LeRoy.

Our cross sections for the efficient quenchers $C_6H_6$, $C_2H_4$, and $C_3H_6$ are consistently larger than those of Steacie and LeRoy by a factor of about 2. Net quenching by these molecules takes place at essentially every gas-kinetic encounter, so that it is reasonable to assume that in the Steacie–LeRoy experiments there was essentially no formation of Cd($^3P_0$). It has been shown that the quenching of Hg($^3P_1$) by $C_2H_4$ does *not* produce Hg($^3P_0$) (less than 10% of the quenching collisions could produce Hg($^3P_0$)).[2] Thus for these particular molecules it is likely that the apparent quenching rate measured by Steacie and LeRoy corresponds to net quenching of Cd($^3P_1$) only. Quenching of Hg($^3P_0$) by $C_2H_4$ occurs at a rate ~60% that of Hg($^3P_1$) by $C_2H_4$.[2,3] Because the $^3P_0$–$^3P_1$ splitting is much less for cadmium than for mercury (5 vs. 1.5 kcal/mol), quenching by $C_2H_4$ of Cd($^3P_0$) and Cd($^3P_1$) should also occur at similar rates. It is therefore quite reasonable that the "effective" cross sections ($1.37\sigma^2_{Cd(^3P_0)} + \sigma^2_{Cd(^3P_1)}$) obtained in this study for $C_2H_4$, $C_3H_6$, and $C_6H_6$ should be approximately twice those obtained by Steacie and LeRoy, if $\sigma^2_{Cd(^3P_0)}$ is slightly less than $\sigma^2_{Cd(^3P_1)}$.

Relative cross sections for apparent $Cd(^3P_1)$ quenching for several alkenes and acetylenes have been determined by Sato et al. at 270° using butene-2 cis–trans isomerization as a rate probe.[44] Quenching rates for 15 different alkenes, dienes, and acetylenes all fell within a 30% range, which is difficult to interpret except as collision-limited quenching, with large cross sections similar to those obtained in this study and by Steacie and LeRoy for simple alkenes.

The only other experiments in which the quenching of apparently equilibrated $Cd(^3P_{0,1})$ has been studied are those reported in two communications by Strausz and coworkers,[13,14] who used a conventional Norrish-Porter continuum flash lamp to dissociate $(CH_3)_2Cd$ near room temperature in order to create (in addition to methyl radicals) very high nonequilibrium amounts of cadmium vapor. The $Cd(^1P_1)$ state, populated by absorption of the continuum flash radiation at 2288 Å, was deactivated by excess $CH_4$ bath gas to form $Cd(^3P_J)$. Their measured cross sections at room temperature for $C_6H_6$, $C_2H_4$, and $H_2$ are three to five orders of magnitude lower than our values or those of Steacie and LeRoy (see Table V), and can only be rationalized if $Cd(^3P_J)$ quenching rates are strongly temperature dependent. A study of the temperature dependence of $Cd(^3P_J)$ quenching by one gas, $C_2H_4$, was carried out over an 80° range near room temperature, and there was an apparent increase in rate of a factor of about 2, with 25% standard error.[14] By assuming Arrhenius behavior and extrapolating their quenching rates for $C_2H_4$ to 275°, these authors utilized the relative $Cd(^3P_J)$ quenching rates determined indirectly by Tsunashima et al.[44] to estimate activation energies for other quenchers based on two temperatures, 27 and 275°. The values calculated at 280° with these estimated Arrhenius parameters are shown in Table V. There is obviously still a large discrepancy. Even assuming that $\sigma^2_{Cd(^3P_1)}$ is always much larger than $\sigma^2_{Cd(^3P_0)}$ (see the last row of Table V), which certainly does not appear to be reasonable for $C_2H_4$, the Strausz et al. extrapolated cross sections are still a factor of 10 lower than our values or those of Steacie and LeRoy for $C_2H_4$ and $H_2$. We are therefore forced to conclude that either the quenching of $Cd(^3P_J)$ by these particular gases has an unusual non-Arrhenius temperature dependence, or that the results of Strausz et al. are in error. Based on the fact that at 280° the quenching cross section for $H_2$ is within a factor of 3 of the hard-sphere collision cross section, and that the quenching cross section for $C_2H_4$ is even greater than the hard-sphere cross section, we believe that an activation energy of less than 1 kcal/mol for quenching by $C_2H_4$, and less than 2 kcal/mol for quenching by $H_2$ is likely, and that the Arrhenius *A* factor for either gas is comparable to the calculated hard-sphere collision rate constant. Further direct measurements would obviously be desirable, and we are currently developing a method for studying $Cd(^3P_J)$ quenching over a wide range of intermediate temperatures.

The patterns of quenching efficiency observed in this study for $Cd(^3P_{0,1})$ are roughly similar to those which have been established for *net* quenching or reaction of $Hg(^3P_1)$ and/or $Hg(^3P_0)$, as shown in Table IV. Benzene, the alkenes, and NO quench very efficiently, while the isotopic hydrogens, $CO_2$, and CO are moderately good quenchers, and $N_2$, $NH_3$, and the alkanes are relatively ineffective in the quenching process.

The quenching cross sections for the isotopic hydrogens are smaller for $Cd(^3P_{0,1})$ than for $Hg(^3P_1)$, and the cross sections for quenching by $CH_4$, $C_2H_6$, and $C_3H_8$ are much smaller for $Cd(^3P_{0,1})$ than for $Hg(^3P_1)$. These trends are to be expected if the main product channel in both cases is chemical reaction, to form HgH + H and/or Hg + 2H in the mercury case, CdH + H in the cadmium case. Reaction of $Hg(^3P_1)$ with $H_2$ or alkanes to form HgH is at least 18 kcal/mol exothermic, while reaction to form ground-state $Hg(^1S_0)$ + H is at least 9 kcal/mol exothermic.[45,46] Reaction of $Cd(^3P_1)$ with hydrogen to form CdH is 0.1 kcal/mol endothermic, and the reaction with propane to form CdH and the isopropyl radical is only 8 kcal/mol exothermic.[45,26] Reactions of $Cd(^3P_1)$ with $H_2$ or the alkanes to form $Cd(^1S_0)$ + H are all substantially endothermic.[46] It is quite reasonable, therefore, to expect greater energy barriers for the $Cd(^3P_1)$–$H_2$ and $Cd(^3P_1)$–alkane reactions than the $Hg(^3P_1)$–$H_2$ and $Hg(^3P_1)$–alkane reactions. Production of CdH and CdD from the reactions of normal and deuterium-labeled hydrogens and alkanes, and the mechanism of quenching of $Cd(^3P_{0,1})$ by these species, will be discussed in a subsequent paper.[47]

The large quenching cross sections for $C_6H_6$, $C_2H_4$, and $C_3H_6$ can be explained by efficient spin-allowed transfer of electronic energy from $Cd(^3P_{0,1})$ to form electronically excited triplet states of the molecules. The $\tilde{a}^3B_{1u}$ state of benzene lies approximately 84 kcal/mol above ground-state $C_6H_6$,[48] so that exothermic, near-resonant electronic energy transfer can occur from either $Cd(^3P_1)$ or $Cd(^3P_0)$, which contain 87.6 and 86.1 kcal/mol electronic energy, respectively. A study by Hunziker of the effect of benzene on the $Cd(^3P_1)$-photosensitized isomerization of butene-2 has provided indirect evidence for production of $C_6H_6$ ($\tilde{a}^3B_{1u}$) in the quenching process.[49] The quenching of $Hg(^3P_0)$ (107.6 kcal/mol electronic energy) by $C_6H_6$ has been shown to produce $C_6H_6$ ($\tilde{a}^3B_{1u}$), identified directly by kinetic modulation absorption spectroscopy.[50]

In contrast to the benzene case, a Franck–Condon-like transfer of electronic energy to produce vibrationally excited triplet states of ethylene or propylene requires approximately 100–110 kcal/mol,[51] considerably in excess of the 87.6 kcal/mol available from $Cd(^3P_1)$. However, the minimum potentials of the nonplanar excited triplet states of the alkenes are known to lie 60–80 kcal above the ground states,[51] and the large cross sections observed for quenching of $Cd(^3P_J)$ by these species would seem to imply that a complex between $Cd(^3P_{0,1})$ and an alkene double bond forms which is sufficiently long-lived to allow C–C bond twisting for curve crossing with little or no potential barrier to form $Cd(^1S_0)$ and triplet alkene. The formation of such a complex would be entirely consistent with the proposals of Strausz, Gunning, and coworkers that $Hg(^3P_J)$ and $Cd(^3P_J)$ are electrophilic reactants.[14,52] Hunziker has observed $Cd(^3P_1)$-photosensitized cis–trans isomerization of ethylene-$d_2$ and interpreted the results in terms of $C_2H_4$ ($^3B_{1u}$) produced *via* a $Cd(^3P_1)$–$C_2H_4$ complex.[11] Cis–trans isomerization in the quenching of $Cd(^3P_1)$ by propylene-*1,3,3,3-d*$_4$ has also been observed.[53]

The efficient quenching of $Cd(^3P_{0,1})$ by $SO_2$ and $CO_2$ could also involve formation of excited triplet states of the molecules as product channels. Production of $SO_2(^3B_1)$ in the quenching of $Cd(^3P_{0,1})$ by $SO_2$ would be 12–14 kcal/mol exothermic.[54] Recent theoretical calculations have indicated that the lowest bound triplet state of $CO_2$ (the bent $^3B_2$ state) may in fact lie approximately 85 kcal/mol above ground-state $CO_2$,[55] and thus could be excited by $Cd(^3P_{0,1})$ in a nonvertical manner similar to that proposed for ethylene. If this is the case, however, it is difficult to understand

why the quenching by $CO_2$ of $Hg(^3P_0)$ occurs with such a low cross section (see Table IV), because $Hg(^3P_0)$ has 20.0 kcal/mol more electronic energy than $Cd(^3P_1)$. For this reason, we checked the unlikely possibility that the large cross section determined for $Cd(^3P_{0,1})$ quenching by $CO_2$ was due to an impurity. To explain the large quenching rate constant observed, an impurity level greater than 10% would be required; mass spectrometric analysis of the purified $CO_2$ showed no impurities (<0.1%).

Early evidence has often been interpreted to indicate that $NO(a^4\Pi_i)$ is formed in the quenching of $Hg(^3P_1)$ by NO.[56] Polanyi and coworkers[57] have since shown directly that vibrationally excited ground-state NO is formed in the quenching process, but production and deactivation of $NO(a^4\Pi_i)$ could not definitely be ruled out. Excitation to $NO(a^4\Pi_i)$ in the deactivation of $Cd(^3P_{0,1})$ by NO is at least 15 kcal/mol endothermic.[56] Because the quenching cross section determined here for $Cd(^3P_{0,1})$ quenching by NO is of similar magnitude to the cross section for quenching of $Hg(^3P_0)$ and $Hg(^3P_1)$ by NO, it is obvious that the presence of an energy-transfer channel leading to $NO(a^4\Pi_i)$ is not necessary to explain the large NO quenching cross sections for $Hg(^3P_0)$ and $Hg(^3P_1)$.

At least one product channel in the quenching of $Cd(^3P_{0,1})$ by $NH_3$ has been shown to involve the formation and fluorescence of a $Cd(^3P_J)$–$NH_3$ complex,[58] similar to the $Hg(^3P_0)$–$NH_3$ case.[59]

Quenching of $Hg(^3P_0)$ by CO produces vibrationally excited CO in reasonable yield.[60] Because the net quenching cross section determined here of $Cd(^3P_{0,1})$ by CO is of the same order as that of $Hg(^3P_0)$–CO quenching, a similar reaction path may be involved.

A major exit channel in the quenching of $Cd(^3P_{0,1})$ by $SF_6$ is the production of CdF:

$$Cd(^3P_{0,1}) + SF_6 \longrightarrow SF_5 + CdF$$

The CdF was identified in absorption via the known bands in the 2800–2900-Å region[48] and a new band at ~2125 Å.[61] As the $SF_6$ pressure was increased in 400 Torr of 2% $N_2$–Ar, the increase in the CdF absorptions was roughly consistent with the decrease in $Cd(^3P_{0,1})$ concentrations. In an auxiliary experiment, increasing pressure of $H_2$ were added to 100 Torr of $SF_6$; the increase in CdH and the decrease in CdF (the diffuse band was assumed to follow the Beer–Lambert law) yielded values of the ratio of quenching cross sections for $H_2$ and $SF_6$ which were consistent with the cross sections shown in Table IV. The concentration of $Cd(^3P_{0,1})$ was 100 times less in this experiment so that CdF cannot be produced in a secondary absorption process. The quenching of $Hg(^3P_1)$ or $Hg(^3P_0)$ by $SF_6$ has apparently never been studied.

Deactivation of both $Cd(^3P_{0,1})$ and $Hg(^3P_{0,1})$ by the inert gases appears to be extremely inefficient. The upper limit for the cross section of quenching of $Hg(^3P_1)$ by Ar in Table IV was calculated from the data of Callear and Wood,[40] who observed an apparent lifetime for $Hg(^3P_1)$ fluorescence of $2.0 \times 10^{-7}$ sec in a 0.50-cm diameter tube containing $6 \times 10^{-3}$ Torr of Hg vapor and 500 Torr of Ar, as compared to the natural radiative lifetime of $1.14 \times 10^{-7}$ sec. We have calculated the imprisonment lifetime for $Hg(^3P_1)$ under these conditions using the same "equivalent opacity" method for Doppler and Lorentz broadening as outlined in the Results section, and find $\tau/\tau_0 = 1.9$. Thus, $\tau = 2.2 \times 10^{-7}$ sec and deactivation of $Hg(^3P_1)$ must therefore be essentially negligible at 500 Torr of Ar. Allowing for 20% error, the upper limit for the Ar quenching rate constant is calculated to be $5 \times 10^7\ M^{-1}\ sec^{-1}$ and for the cross section, 0.006 Å$^2$. The actual cross section may be substantially smaller than this, because Deech et al.[39] using a direct, time-resolved method have determined an upper limit for the $Hg(^3P_1)$ quenching cross section by the more polarizable Xe atom as 0.0006 Å$^2$. Freeman et al.[62] have reported a cross section of 0.0003 Å$^2$ for the deactivation of $Hg(^3P_0)$ by Xe, determined by the phase-shift method. The estimates of Gunning et al.[63] of similar cross sections of 0.1–0.3 Å$^2$ for quenching of $Hg(^3P_1)$ by He, Ne, Ar, Kr, and Xe appear to be in error.[62]

The value for the rate constant $k_d$ for deactivation of $Cd(^3P_1)$ to $Cd(^3P_0)$ for M = He, $6 \times 10^6\ M^{-1}\ sec^{-1}$, corresponds to a cross section for spin–orbit deactivation by helium of $\sim 2 \times 10^{-4}$ Å$^2$. Gallagher[64] has measured the cross section for spin–orbit deactivation of $Cs(6^2P_{3/2})$ to $Cs(6^2P_{1/2})$ by helium as a function of temperature, where as pointed out above the energy difference is nearly the same as the $Cd(^3P_1)$–$Cd(^3P_0)$ energy gap. It is interesting to note that at 280°, the cross section was determined[64] to be $\sim 8 \times 10^{-4}$ Å$^2$, which is certainly of the same order of magnitude.

NOTE ADDED IN PROOF: Sato and coworkers[65] have just reported a study which corroborates several of our conclusions. In particular, equilibration of $Cd(^3P_0, {}^3P_1)$ by $N_2$ was shown to be very rapid, and the relative rates of net quenching at 250° of equilibrated $Cd(^3P_0, {}^3P_1)$ by $N_2$, CO, and $CO_2$, determined in excess Ar, are in excellent agreement with our own rates. Calculation of absolute quenching cross sections from the Sato data using the above treatment of radiation imprisonment yields values for $N_2$, CO, and $CO_2$ of 0.012, 1.8, and 11 Å$^2$, respectively, compared with our determinations of 0.008, 1.7, and 12 Å$^2$.

*Acknowledgments.* Acknowledgment is made to the donors of the Petroleum Research Fund, administered by the American Chemical Society, for partial support of this research. Acknowledgment of financial assistance is also made to the Research Corporation and to the University of Utah Research Fund. The authors wish to thank Drs. Phillips and Freeman for communicating results prior to publication.

## References and Notes

(1) Camille and Henry Dreyfus Teacher-Scholar.
(2) (a) R. J. Cvetanovic, *Prog. React. Kinet.*, **2**, 39 (1964); (b) A. Callear and J. McGurk, *J. Chem. Soc., Faraday Trans. 2*, **69**, 97 (1973).
(3) J. V. Michael and G. N. Suess, *J. Phys. Chem.*, **78**, 482 (1974).
(4) C. Burton and H. E. Hunziker, *J. Chem. Phys.*, **57**, 339 (1972), and earlier references.
(5) H. Heydtmann, J. Polanyi, and R. Taguchi, *Aopl. Opt.*, **10**, 1755 (1971), and earlier references.
(6) J. Hong and G. Mains, *J. Photochem.*, **1**, 463 (1972–1973).
(7) C. Freeman, M. McEwan R. Claridge, and L. Phillips, *Trans. Faraday Soc.*, **67**, 2004 (1971).
(8) J. Pitre, K. Hammond, and L. Krause, *Phys. Rev. A*, **6**, 2101 (1972).
(9) W. Breckenridge and A. Callear, *Trans. Faraday Soc.*, **67**, 2009 (1971).
(10) P. Morten, C. Freeman, R. Claridge, and L. F. Phillips, *J. Photochem.*, **3**, 285 (1974).
(11) H. Hunziker, *J. Chem. Phys.*, **50**, 1288 (1969).
(12) S. Sato, C. Takahashi, and S. Tsunashima, *Bull. Chem. Soc. Jpn.*, **43**, 1319 (1970).
(13) P. Young, G. Greig, and O. Strausz, *J. Am. Chem. Soc.*, **92**, 413 (1970).
(14) P. Young, E. Hardwidge, S. Tsunashima, G. Greig, and O. Strausz, *J. Am. Chem. Soc.*, **96**, 1946 (1974).
(15) W. H. Breckenridge and T. W. Broadbent, *Chem. Phys. Lett.*, **29**, 421 (1974).
(16) W. H. Breckenridge and H. Taube, *J. Chem. Phys.*, **53**, 1750 (1970).
(17) A. R. Schafer, *J. Quant. Spectrosc. Radiat. Transfer*, **11**, 197 (1971). An average of 12 reported lifetimes of $Cd(^3P_1)$ was chosen. The range was from $2.05 \times 10^{-6}$ to $2.50 \times 10^{-6}$ sec.
(18) I. W. M. Smith, *Trans. Faraday Soc.*, **64**, 378 (1968).

(19) P. Lee, H. Broida, W. Braun, and J. Herron, *J. Photochem.*, **2**, 165 (1973–1974). These authors have found a "significant" population of vibrationally excited $H_2$ produced in the deactivation of $Hg(^3P_1)$ by $H_2$. Quantum yield work (A. Callear and P. Wood, *J. Chem. Soc., Faraday Trans. 2*, **68**, 302 (1972)), has indicated, however, that this product channel is of minor importance compared to formation of HgH + H and Hg + 2H.
(20) J. Michael and C. Yeh, *J. Chem. Phys.*, **53**, 59 (1970).
(21) K. Yang, *J. Am. Chem. Soc.*, **87**, 5294 (1965).
(22) L. Thomas and W. Gwinn, *J. Am. Chem. Soc.*, **70**, 2643 (1948).
(23) E. W. Samson, *Phys. Rev.*, **40**, 940 (1932); E. A. Milne, *J. London Math. Soc.*, **1**, 1 (1926).
(24) W. H. Breckenridge, R. P. Blickensderfer, and J. Simons, to be submitted for publication.
(25) A. Mitchell and M. Zemansky, "Resonance Radiation and Excited Atoms", MacMillan, New York, N.Y., 1934.
(26) Reference 25, pp 160–163.
(27) Reference 25, p 171.
(28) R. Hull and H. Stroke, *J. Opt. Soc. Am.*, **53**, 1147 (1963); P. Brix and A. Steudel, *Z. Phys.*, **128**, 260 (1950).
(29) Landolt-Bornstein, "Zahlenwerte und Funktionen", Vol. 1, No. 5, Springer-Verlag, Berlin, 1952.
(30) R. Hultgren, R. L. Orr, P. D. Anderson, and K. K. Kelley, "Selected Values of Thermodynamic Properties of Metals", Wiley, New York, N.Y., 1963.
(31) Note that the imprisonment corrections with complete treatment of isotopic and hyperfine structure differ slightly from our preliminary report,[15] where an approximate method was utilized.
(32) The early work of Bender[33] is consistent with a value of $k_d$ for M = $N_2$ of greater than $5 \times 10^{10}\ M^{-1}\ sec^{-1}$. The corresponding rate constant for deactivation of $Hg(^3P_1)$ to $Hg(^3P_0)$ by $N_2$ has been measured by Krause and coworkers to be $2 \times 10^9\ M^{-1}\ sec^{-1}$.[8] There is considerable evidence that for similar metals the rate of multiplet interconversion is inversely related to the energy-level separation.[34] The $^3P_0 - {}^3P_1$ separation is only 542 $cm^{-1}$ for cadmium compared to 1767 $cm^{-1}$ for mercury, so that $k_d$ (M = $N_2$) should be considerably larger than $2 \times 10^9\ M^{-1}\ sec^{-1}$.
(33) P. Bender, *Phys. Rev.*, **36**, 1535 (1930).
(34) L. Krause, "Collisional Transfer Between Fine-Structure Levels," in "The Physics of Electronic and Atomic Collisions", T. Govers and F. Detteer, Ed., North-Holland Publishing Co., Amsterdam, 1972.
(35) L. G. Piper, J. E. Velazco, and D. W. Setser, *J. Chem. Phys.*, **59**, 3323 (1973).
(36) H. Horiguchi and S. Tsuchiya, *Bull. Chem. Soc. Jpn.*, **44**, 3221 (1971).
(37) A. Vikis, G. Torrie, and D. J. LeRoy, *Can. J. Chem.*, **50**, 176 (1972).
(38) G. Mains and M. Trachtman, *J. Phys. Chem.*, **76**, 2665 (1972).
(39) J. Deech, J. Pitre, and L. Krause, *Can. J. Phys.*, **49**, 1976 (1971).
(40) A. B. Callear and P. Wood, *Trans. Faraday, Soc.*, **67**, 2862 (1971).
(41) H. C. Lipson and A. C. G. Mitchell, *Phys. Rev.*, **48**, 625 (1935).
(42) E. W. R. Steacie and D. J. LeRoy, *J. Chem. Phys.*, **11**, 164 (1943).
(43) D. A. McGillis and L. Krause, *Can. J. Phys.*, **47**, 473 (1969).
(44) S. Tsunashima, S. Satoh, and S. Sato, *Bull. Chem. Soc. Jpn.*, **42**, 329 (1969).
(45) D. Golden and S. Benson, *Chem. Rev.*, **69**, 125 (1969).
(46) A. Gaydon, "Dissociation Energies and Spectra of Diatomic Molecules", Chapman and Hall, London, 1968.
(47) W. H. Breckenridge, T. W. Broadbent, and D. S. Moore, to be submitted for publication.
(48) G. Herzberg, "Spectra of Diatomic Molecules", Van Nostrand-Reinhold, New York, N.Y., 1950.
(49) H. Hunziker, *J. Chem. Phys.*, **50**, 1294 (1969).
(50) C. Burton and H. Hunziker, *Chem. Phys. Lett.*, **6**, 352 (1970).
(51) A. J. Merer and R. S. Mulliken, *Chem. Rev.*, **69**, 639 (1969).
(52) H. Gunning and O. Strausz, *Adv. Photochem.*, **1**, 209 (1963).
(53) S. Tsunashima, S. Satoh, and S. Sato, *Bull. Chem. Soc. Jpn.*, **43**, 2389 (1970).
(54) J. Vikesland and S. Strickler, *J. Chem. Phys.*, **60**, 660 (1974).
(55) N. Winter, C. Bender, and W. Goddard, III, *Chem. Phys. Lett.*, **20**, 489 (1973).
(56) J. Heicklen and N. Cohen, *Adv. Photochem.*, **5**, 157 (1968).
(57) G. Karl, P. Kruus, J. Polanyi, and I. Smith, *J. Chem. Phys.*, **46**, 244 (1967).
(58) P. Morten, C. Freeman, M. McEwan, R. Claridge, and L. Phillips, *Chem. Phys. Lett.*, **16**, 148 (1972).
(59) A. Callear, J. Connor, and J. Koskikallio, *J. Chem. Soc., Faraday Trans. 2*, **70**, 1542 (1974), and references therein.
(60) Y. Fushiki and S. Tsuchiya, *Chem. Phys. Lett.*, **22**, 47 (1973).
(61) W. H. Breckenridge, T. W. Broadbent, J. FitzPatrick, and D. S. Moore, to be submitted for publication.
(62) C. Freeman, M. McEwan, R. Claridge, and L. Phillips, *Chem. Phys. Lett.*, **6**, 482 (1970).
(63) H. Gunning, S. Penzes, H. Sandhu, and O. Strausz, *J. Am. Chem. Soc.*, **91**, 7684 (1969).
(64) A. Gallagher, *Phys. Rev.*, **172**, 88 (1968).
(65) S. Yamamoto, M. Takaoka, S. Tsunashima, and S. Sato, *Bull. Chem. Soc. Jpn.*, **48**, 130 (1975).

# Kinetics of the Thermal Isomerization of *trans*-1,2-Dichloro-3,3-difluorocyclopropane

**J. C. Ferrero, E. A. R. de Staricco, and E. H. Staricco***

*Departamento de Fisicoquímica, Facultad de Ciencias Químicas, Universidad Nacional de Córdoba, Córdoba, Argentina*
*(Received July 15, 1974; Revised Manuscript Received December 2, 1974)*

The thermal reaction of *trans*-1,2-dichloro-3,3-difluorocyclopropane has been studied from 192.8 to 242.7°. The reaction is first order, homogeneous, and proceeds by two pathways to yield *trans*-1,3-dichloro-3,3-difluoropropene and *cis*-1,2-dichloro-3,3-difluorocyclopropane. The overall and the individual rate constants were calculated as $\log k_t(sec^{-1}) = (14.34 \pm 0.23) - (42{,}635 \pm 310)/RT$, $\log k_{trans\text{-propene}} = (14.06 \pm 0.25) - (42{,}236 \pm 230)/RT$, and $\log k_{cis\text{-cyclopropane}} = (14.20 \pm 0.74) - (43{,}818 \pm 790)/RT$. The geometrical isomerization is interpreted on the basis of a diradical mechanism while for the structural isomerization a concerted process with chlorine migration is suggested. The influence of both chlorine and fluorine substitution on the activation energies is discussed mainly in terms of an increased ring strain. The synthesis of the reactant and the identification of the reactant and products is also reported.

## Introduction

Hydrocarbon cyclopropanes undergo both structural and geometrical isomerizations. These reactions have been the subject of many kinetic studies,[1] and most of the results are in agreement with the diradical mechanism predictions, both qualitatively and quantitatively.[2] However a similar understanding for the reactions of halogenated cyclopropanes has not been achieved, mainly due to the relatively few kinetic studies reported and to the substantial influence that the nature of the substituent halogen has on the reaction products and the Arrhenius parameters. Thus, the reactions of polyfluorocyclopropanes[3] are characterized by lower activation energies than cyclopropane and the elimination of difluorocarbene, with the exception of perfluoro-

vinylcyclopropane which isomerizes to perfluorocyclopentene.[3b] The low activation energy has been attributed to an increase in the ring strain by fluorine substitution.[2,3b] Chemically activated 1,1,2,2-tetrafluorocyclopropane also undergoes difluorocarbene elimination instead of the usual cyclopropane-type isomerization reactions.[4] In contrast with such behavior, chlorinated cyclopropanes react in the gas phase to give only structural isomerizations products through chlorine migration.[5] It was also found that chlorine migration from a CHCl group is preferred over that from a $CCl_2$ group.[6] The absence of geometrical isomerization together with the activation energy values suggested a concerted process rather than a diradical mechanism.[5,6]

We believe that a cyclopropane having both a *gem*-difluorocarbene group and chlorine substitution may provide a route to the comparison of the difluorocarbene elimination process with that of chlorine migration. Eventually, such a compound is the *trans*-1,2-dichloro-3,3-difluorocyclopropane. Since we were unable to find a description of this compound in the literature we have proceeded to its synthesis and characterization.

## Experimental Section

*Kinetic Apparatus and Procedure.* The reaction was studied using a standard high-vacuum system, the kinetic section being provided with Teflon-glass stopcocks in order to avoid absorption. The cylindrical reaction vessel (90 ml) was enclosed in a horizontal furnace whose temperature was controlled to better than ±0.3° by a Lauda Electronic regulator Type PTR 50. The temperature fluctuation along the reaction vessel was ±0.5°. The temperature was measured with a chromel–alumel thermocouple calibrated against a standarized platinum–rhodium thermocouple. Pressure measurements were made with a Hg manometer using a Bodenstein-type quartz spiral as a null instrument, with a sensitivity such that a pressure change of at least 0.2 mm could be detected. The dead space was smaller than 1% and ignored in calculations.

To eliminate a possible initial irreproducibility in the kinetic results the reaction vessel was conditioned by heating the reactant during 24 hr at 300°. Before any kinetic run the reactant was degassed and the system evacuated to $10^{-4}$ mm.

At the end of a run the entire content of the reaction vessel was transferred to a gas chromatograph sample loop. Quantitative analysis were made with a Varian Aerograph Model 202 gas chromatograph equipped with a Gow-Mac gas density detector and using a 30 ft by ⅛ in. column packed with 30% Halocarbon Oil on Chromosorb P (30–60 mesh) at 45°. The reactant and the products were all well separated and had near-gaussian shapes. The areas of the peaks were calculated by triangulation. Some runs were also analyzed on dinonylphthalate and Silicone QF-1 columns.

*Spectral Analysis.* The structure of the reactant and products were established by infrared and nuclear magnetic resonance spectroscopy. Infrared spectra were recorded on a Beckman IR-8 instrument calibrated with polystyrene, using a 10-cm gas cell with NaCl windows. Nuclear magnetic resonance spectra were made with a Varian T-60 spectrometer operating at 60.0 MHz for $^1H$ and 45.6 MHz for $^{19}F$, and using tetramethylsilane and trichlorofluoromethane as standards for the determination of the chemical shifts. Chemical shifts are reported downfield to TMS and upfield to $CCl_3F$.

*Materials.* *trans*-1,2-Dichloro-3,3-difluorocyclopropane was prepared by the reaction of difluorocarbene (from hexafluoropropene epoxide[7]) with *trans*-dichloroethylene, according to a general method.[8] *trans*-Dichloroethylene (0.13 mol) and hexafluoropropene epoxide (0.18 mol) were charged in vacuo into a 200-ml stainless-steel bomb and heated at 197° for 7 hr. The bomb was then cooled to −100°, opened, and the volatile compounds were pumped-off, and the remaining fraction was purified by preparative glpc on a Halocarbon Oil column to yield 40% of the *trans*-cyclopropane. The molecular weight, determined by gas density, was 146.5. The infrared spectrum shows the following absorptions ($\nu_{max}$): 3058, 1295, 1235, 1183, 990, 785, and 653 $cm^{-1}$. The band around 1450 $cm^{-1}$ has been attributed to cyclopropanes containing a $CF_2$ group.[9]

Both the $^1H$ and $^{19}F$ nuclear magnetic resonance spectra show a triplet centered at 3.50 ppm for $^1H$ and 142.5 ppm for $^{19}F$ and spaced by $J_{HF}$ = 4.96 Hz, confirming the assigned structure.

*Product Analysis.* The reaction products were recovered at the gas chromatograph outlet during the glpc analysis of the reaction mixture. After sufficient amounts of each product were collected they were identified by spectral analysis, as described below.

The retention time for the reactant and the products relative to the *trans*-dichloroethylene, on the Halocarbon Oil column, were *trans*-propene, 1.52; *trans*-cyclopropane, 1.90; and *cis*-cyclopropane, 2.98.

*trans-1,3-Dichloro-3,3-difluoropropene.* The main feature of the infrared spectrum is the presence of an absorption at 1650 $cm^{-1}$. The complete spectrum shows the following absorptions ($\nu_{max}$): 3125, 1650, 1234, 1115, 1052, 980, 926, 862, 819, and 746 $cm^{-1}$.

The $^1H$ nuclear magnetic resonance spectrum consists of two vinylic absorptions at 6.42 ppm (dt, $J_{HH}$ = 13.7 Hz, $J_{HF}$ = 8.4 Hz) and 7.10 ppm (dd, $J_{HH}$ = 13.7 Hz, $J_{HF}$ = 1.6 Hz). The $^{19}F$ nuclear magnetic resonance spectrum presents an absorption at 52.8 ppm (dd, $J_{FH}$ = 8.4 Hz, $J_{FH}$ = 1.6 Hz). All of these data are in agreement with the 1,3-dichloro-3,3-difluoropropene structure. The trans configuration was assigned according to the infrared absorption at 1650 $cm^{-1}$ and the coupling constant values.

*cis-1,2-Dichloro-3,3-difluorocyclopropane.* This compound was isolated by glpc as described above, and also synthesized in small amounts by the same procedure as the trans isomer but starting with *cis*-dichloroethylene. The infrared spectrum also shows the characteristic band at 1450 $cm^{-1}$ and the following absorptions ($\nu_{max}$): 3077, 1450, 1300, 1247, 1175, 1004, 855, 747, and 658 $cm^{-1}$.

The $^1H$ nuclear magnetic resonance spectrum shows a doublet centered at 3.66 ppm ($J_{HFcis}$ = 11.8 Hz) which with high resolution is a double doublet ($J_{HFtrans}$ = 3.9 Hz). The $^{19}F$ nuclear magnetic resonance spectra consists of an absorption at 130.7 ppm (dt, $J_{FF}$ = 164.7 Hz, $J_{FHcis}$ = 11.8 Hz) and another at 151.5 ppm (d, $J_{FF}$ = 164.7 Hz). The chemical shifts and the coupling constants are as expected, in agreement with the values reported for similar compounds.[8]

## Results

The thermal reaction of *trans*-1,2-dichloro-3,3-difluorocyclopropane was studied in the temperature range of 192.8–242.7° and with initial reactant pressures of 19–22 mm. The reaction products are *trans*-1,3-dichloro-3,3-difluoropropene and *cis*-1,2-dichloro-3,3-difluorocyclopro-

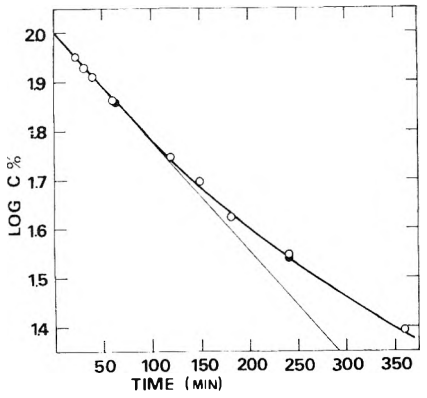


**Figure 1.** Plot of log percent reactant vs. time for runs at 232.7°: (●) runs with 500 mm of added inert gas.

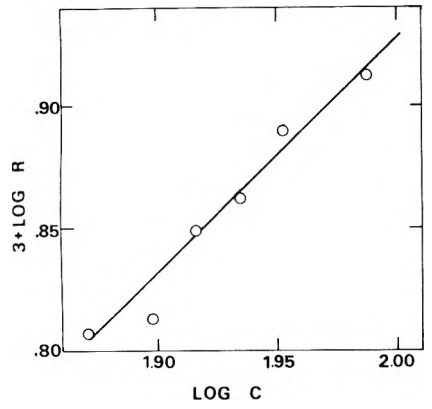


**Figure 2.** Plot of log rate against log concentration for runs at 232.7°.

pane, together with a minor, unidentified product, which was 6% at 232.7° and 75% reaction, and negligible under the conditions the reaction was studied.

Intensive search was made for 1,2-dichloroethylene and $C_2F_4$ but they were not found, neither by infrared spectroscopy nor by glpc, although by the later method amounts lower than 0.5% could be detected. Furthermore, there were no pressure changes during the reaction, confirming that only isomerization reactions were involved. Also, neither *cis*-propene nor other propenes were found as important products. The possibility of *cis*-propene superimposed with the reactant or another product can be ruled out as the chromatographic analysis was performed on different columns. Further, as mentioned in the Experimental Section, both reactant and products were collected and analyzed by infrared and nuclear magnetic resonance spectroscopy.

First-order plots for the reactant loss were good straight lines up to 30% decomposition, but an increasing departure from the first-order behavior was observed at higher conversions (Figure 1). This deviation cannot be attributed to a fall-off from the first-order kinetics since the addition of 500 mm of 1,2-dichloro-1,1,2,2-tetrafluoroethane as an inert gas did not return the plot to linearity but the conversion remained the same. To confirm the order of the overall reaction the rate of disappearence of the reactant was calculated from the smoothed curve of a concentration vs. time plot. These values, in a log $R$ against log $C$ plot, yielded a straight line with a slope of $n = 1.0$ up to 30% decomposition (Figure 2).

As far as the overall reaction is first order, a plot of per-

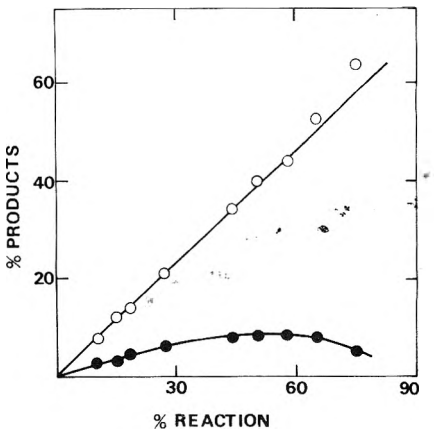


**Figure 3.** Product distribution for runs at 232.7°: (O) *trans*-1,3-dichloro-3,3-difluoropropene; (●)*cis*-1,2-dichloro-3,3-difluorocyclopropane.

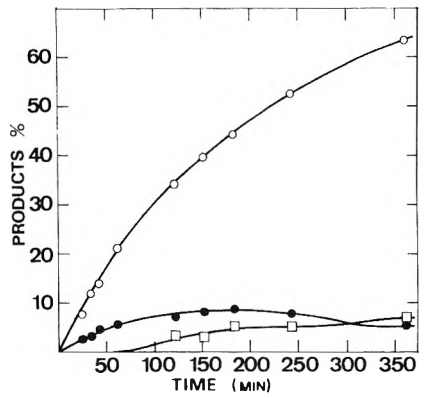


**Figure 4.** Appearance curves for (O) *trans*-1,3-dichloro-3,3-difluoropropene, (●) *cis*-1,2-dichloro-3,3-difluorocyclopropane, and (□) unidentified product, for runs at 232.7°.

cent products against percent reaction should be linear if the individual reactions were also first order, with a slope equal to $k_i/k_t$. In Figure 3 it can be seen that a straight line is obtained for *trans*-propene but *cis*-cyclopropane shows a pronounced curvature above 30% reaction. Further, analysis of the appearance curves of the products (Figure 4) shows that while *trans*-propene increases steadily, the curve for *cis*-cyclopropane has a maximum. All of these facts clearly indicate that the complication in the first-order kinetics is due to subsequent reactions of *cis*-cyclopropane. A possible explanation is that, as in other well-known reactions, the geometrical isomerization is reversible. Also, the unidentified product seems to be a consequence of a further reaction of *cis*-cyclopropane although the experimental data show a wide scattering due to its low concentration.

To avoid the above complications the reaction was studied to no more than 30% decomposition.

In conclusion, the reactions taking place under the above conditions are

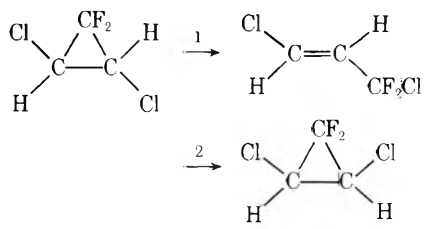

**TABLE I: First-Order Rate Constants for *trans*-1,2-Dichloro-3,3-difluorocyclopropane Decomposition[d]**

| Temp, °C | $10^5 k_t$, sec$^{-1}$ | $10^5 k_1$, sec$^{-1}$ | $10^5 k_2$, sec$^{-1}$ |
|---|---|---|---|
| 242.7 | 18.732 | 14.477 | 4.255 |
| 232.7 | 8.524 | 6.588 | 1.936 |
| 232.7[a] | 7.956 | 5.806 | 2.150 |
| 232.7[b] | 9.226 | 6.946 | 2.280 |
| 222.6 | 3.592 | 2.839 | 0.753 |
| 222.6[a] | 3.250 | 2.624 | 0.626 |
| 222.6[c] | 3.453 | 2.692 | 0.761 |
| 212.7 | 1.405 | 1.117 | 0.288 |
| 212.7[b] | 1.465 | 1.117 | 0.348 |
| 212.7[c] | 1.431 | 1.095 | 0.336 |
| 202.7 | 0.592 | 0.464 | 0.128 |
| 192.8 | 0.219 | 0.176 | 0.043 |

[a] Runs in the packed vessel. [b] 500 mm of added inert gas. [c] 30 mm of added cyclohexene. [d] From the experimental data it can be concluded that the reaction is first order, homogeneous, and molecular.

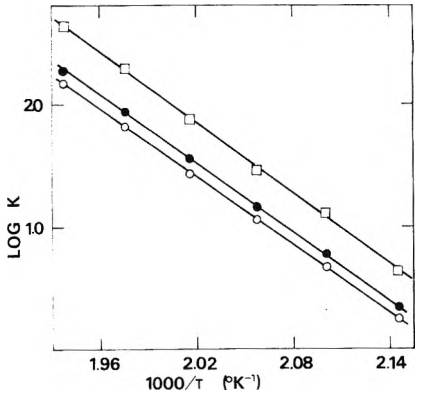


**Figure 5.** Variation of log $k$ with $1/T$: (●) 6 + log $k_t$, (○) 6 + log $k_1$, and (□) 7 + log $k_2$.

At each temperature that the reaction was studied the first-order rate constant for the reactant loss ($k_t$) was obtained from a plot of log $C$ against time. Also, at each temperature the product ratio was measured at low percentage reaction. From these ratio and the overall rate constant the individual rate constants, $k_1$ and $k_2$, were calculated.

Arrhenius plots gave good straight lines (Figure 5) from which the Arrhenius parameters were evaluated by the least-squares method, hence: $k_t = 10^{(14.34\pm0.23)} \exp(42{,}635 \pm 310/RT)$ sec$^{-1}$; $k_1 = 10^{(14.06\pm0.25)} \exp(42{,}236 \pm 230/RT)$ sec$^{-1}$; $k_2 = 10^{(14.20\pm0.74)} \exp(43{,}818 \pm 790/RT)$ sec$^{-1}$; where the error limits are standard deviations and, so, give a measurement of the precision on a statistical basis. The probable errors should certainly be higher and the accuracy limits in the activation energy can be estimated to be around 1.2 kcal mol$^{-1}$.

A series of runs was carried out in a packed vessel with a surface:volume ratio 5 times larger than the unpacked vessel. The rate constants were the same within experimental error and are shown in Table I.

To test for the presence of free radicals in the system, some runs were carried out in the presence of 30 mm of cyclohexene, substance known to be effective chain suppressors. The results are shown in Table I. As the rate constants are essentially independent of the presence of inhibitor it may reasonably be concluded that the reaction does not proceed by a chain mechanism.

As mentioned above, runs with added inert gas (500 mm) do not show any important change in the rate constant values, indicating that the reaction is in the first-order region (Table I).

## Discussion

Perhaps the most important findings of this work are the total absence of difluorocarbene elimination from the reactant and the fact that both, geometrical and structural isomerization reactions occur, together with the rather low activation energies required for these reactions. According to other reactions of fluorinated cyclopropanes, difluorocarbene elimination would be expected,[3] though qualitative studies have shown that when chlorine is present in the molecule some isomerization also occur.[10]

The geometrical isomerization is typical of those reactions supposed to take place through a diradical intermediate. Moreover, such a mechanism has been used to explain most of the small ring compounds reactions.[2,11] In the present case there are two possible diradicals, obtained through either $\alpha$ or $\beta$ (C–C) split.

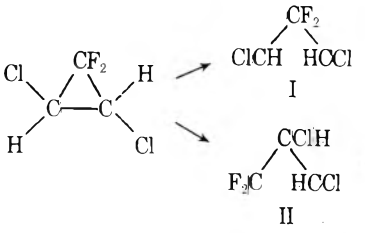


Isomerization of I to a propene requires a fluorine atom migration, which would be a highly unlikely process due to the C–F bond strength. As a consequence, diradical I has no simple alternative except to return to a cyclopropane. This pathway would certainly be able to account for *cis*-cyclopropane formation. Diradical II can undergo ring closing to cyclopropane and also isomerization to propene involving a chlorine migration. The preference of this latter process over hydrogen migration can be rationalized as being due to the relatively weak C–Cl bond in comparison with the C–H bond. Furthermore, hydrogen migration cannot account for the observed products.

According to the diradical mechanism, the activation energy for hydrogen migration and the activation energy for the $C_3$ ring closing have been calculated as 10.8 and 9.3 kcal mol$^{-1}$, respectively.[11] As chlorine migrates undoubtly faster than hydrogen, the reaction path leading to diradical II would be the rate-determining step in the structural isomerization process, as has been suggested.[11]

However, an analysis of the reaction products provides evidence against a diradical mechanism for the structural isomerization process. On the basis of a diradical intermediate the appearance of *cis*-propene and of $F_2CCHCHCl_2$ in addition to *trans*-propene must be expected. The fact that only *trans*-propene is produced can be understood in terms of a concerted process involving a chlorine atom migration simultaneously with an outward rotation of the CHCl and $CF_2$ groups. Such a disrotatory process is in agreement with the Woodward–Hoffman selection rules.[12]

According to the above considerations, if the structural isomerization takes place through a concerted process, then the geometrical isomerization must necessarily occur in a two-stage process involving diradical I.

The activation energy for the isomerization to *cis*-1,2-dichloro-3,3-difluorocyclopropane is 20.4 kcal $mol^{-1}$ lower than that of cyclopropane. The decrease can be attributed to an increase in the ring strain. It has been suggested that the replacement of hydrogen for a more electronegative atom causes a rehybridization that would increase the $\pi$ character and the strain of the cyclopropyl ring.[3b,14] O'Neal and Benson have also suggested that this increase is of about 5 kcal $mol^{-1}$ per fluorine and 3 kcal $mol^{-1}$ per chlorine substitution.[11] Thus, an additional strain energy of 16 kcal $mol^{-1}$ over that of cyclopropane would be expected.

It is generally considered that the presence of a chlorine atom will stabilize a radical. Quantitative information about this point can be obtained by comparison of the C–H bond dissociation energy between compounds of the type RCHCl–H and $RCH_2$–H. While a value of 98.0 kcal $mol^{-1}$ is usually accepted for the latter,[11] a value of 96 ± 2 kcal $mol^{-1}$ has been reported for the former.[13] This yields a stabilization energy of about 2 kcal $mol^{-1}$ for chlorine substitution in a radical center. As a consequence, diradical I would have a stabilization energy of about 4 kcal $mol^{-1}$. This value plus 16 kcal $mol^{-1}$ of strain energy would cause a lowering in the activation energy of about 20 kcal $mol^{-1}$, in agreement with the experimental result. We conclude that within the uncertainty in the thermodynamics, the pathway leading to *cis*-1,2-dichloro-3,3-difluorocyclopropane seems to be properly suited to a mechanism involving diradical I.

The isomerization to propene seems to be concerted and, if so, an increase in the strain energy will be the main cause of the decrease in the activation energy but not the only factor to be considered. An important contribution may come from a polarization in the transition state. The migration of a high electronegative atom, such as chlorine, would produce a change in the molecule's polarity, with the migrating chlorine having a partial negative charge and so migrating to the more positive center, that is, the carbon atom in the $CF_2$ group. Such a transition state will enhance the rate of chlorine migration and so will prevent the difluorocarbene elimination.

The activation entropies can be calculated from eq 1 as

$$A = ekT/h \exp(\Delta S^{\ddagger}/R) \quad (1)$$

$\Delta S^{\ddagger}$(*trans*-propene) = 2.8 Gibbs $mol^{-1}$ and $\Delta S^{\ddagger}$(*cis*-cyclopropane) = 3.5 Gibbs $mol^{-1}$. The former value appears to be consistent with a concerted process. The activation entropy for the geometrical isomerization seems to be rather low for a diradical mechanism but an important consideration may be the decreased symmetry in the reaction path together with a higher barrier to the internal rotations in comparison with the diradical from cyclopropane.

*Acknowledgment.* The authors wish to express their appreciation to the Consejo Nacional de Investigaciones Científicas y Técnicas (R. Argentina) for financial support (Grant No. 1880b).

## References and Notes

(1) (a) T. S. Chambers and G. B. Kistiakowsky, *J. Am. Chem. Soc.*, **56**, 399 (1934); (b) E. W. Schlag and B. S. Rabinovitch, *ibid.*, **82**, 5986 (1960); H. M. Frey, *Adv. Phys. Org. Chem.*, **4**, 147 (1966).
(2) H. E. O'Neal and S. W. Benson, *J. Phys. Chem.*, **72**, 1866 (1968).
(3) (a) F. F. Herbert, J. A. Kerr, and A. F. Trotman-Dickenson, *J. Chem. Soc.*, 3655 (1964); (b) R. A. Mitsch and E. W. Neuvar, *J. Phys. Chem.*, **70**, 546 (1966).
(4) N. C. Craig, Tai-na Hu, and P. H. Martyn, *J. Phys. Chem.*, **72**, 2234 (1968).
(5) (a) K. A. Holbrook and K. A. W. Parry, *J. Chem. Soc. B*, 1019 (1970); (b) R. P. Clifford and K. A. Holbrook, *J. Chem. Soc., Perkin Trans. 2*, 1972 (1972).
(6) J. C. Ferrero, J. J. Cosa, and E. H. Staricco, *J. Chem. Soc., Perkin Trans. 2*, 2382 (1972).
(7) D. Sianesi, A. Pasetti, and F. Tarli, *J. Org. Chem.*, **31**, 2312 (1966).
(8) P. B. Sargeant, *J. Org. Chem.*, **35**, 678 (1970).
(9) R. A. Mitsch, *J. Heterocyclic Chem.*, **1**, 271 (1964).
(10) J. M. Birchall, R. N. Haszeldine, and D. W. Rpberts, *J. Chem. Soc., Perkin Trans. 2*, 1071 (1973).
(11) S. W. Benson and H. E. O'Neal, *Natl. Stand. Ref. Data Ser., Natl. Bur. Stand.*, **No. 21** (1970).
(12) R. B. Woodward and R. Hoffman, *Angew. Chem., Intl. Ed. Engl.*, **8**, 781 (1969).
(13) Z. B. Alfassi, D. M. Golden, and S. W. Benson, *Int. J. Chem. Kinet.*, **5**, 155 (1973).
(14) H. A. Bent, *Chem. Rev.*, **61**, 275 (1961).

# Thermodynamic and Kinetic Model of Sequential Nucleoside Base Aggregation in Aqueous Solution

**Frank Garland*[1] and Sherril D. Christian**

*Department of Chemistry, The University of Oklahoma, Norman, Oklahoma 73069* *(Received August 7, 1974; Revised Manuscript Received January 2, 1975)*

*Publication costs assisted by the National Science Foundation*

The thermodynamics and kinetics of the self-association of several nucleoside bases are described by a model which involves the stepwise addition of free base molecules to "stacks" of varying size. Existing molal osmotic coefficient data are used to calculate association equilibrium constants on the basis of the model. The analysis is also performed allowing the association equilibrium constant for the first step to vary independently of the general stepwise constant, with the result that cooperativity is found to be significant for the more strongly associated bases, purine and 6-methylpurine, but is negligible in the case of the weakly associated bases, uridine, 5-bromouridine, and cytidine. The model was also tested by applying it to previously published ultrasonic absorption spectra of 6-methylpurine covering the frequency range 7–450 MHz. Analysis of the absorption data in terms of the kinetic model is described, and yields $k_d = 2.0 \times 10^8$ sec$^{-1}$ as the rate constant for the dissociation of a single base molecule from a stack. Evaluation of the amplitudes of the relaxation curves leads to a sequential volume change of $|4.5|$ ml/mol of stack formed. The assumptions and implications of the models are discussed.

Numerous thermodynamic reports dealing with the molecular interactions which maintain the secondary structure of nucleic acids have appeared in recent years. Work by Ts'o and others on the monomeric units of nucleic acids in aqueous solution indicate that (a) mononucleosides associate in "stacks" made up of the essentially planar base moiety, and (b) the stacks are held together primarily by so-called "hydrophobic" interactions rather than by hydrogen bonding.[2] The stacking process has been described by a model which assumes that the free-energy change as well as the enthalpy change for the addition of a single base molecule to a stack is independent of the size of the stack. For some nucleoside bases, however, particularly those which associate to a higher degree, it appears that this model overestimates the degree of association at higher base concentrations. Attempts to correct for this overestimation include placing an artificial limit on the size of the stack,[3,4] and introducing activity coefficients for the aggregates which results in a sequence of decreasing association equilibrium constants.[5] In one case, that of $N^6$,$N^9$-dimethyladenine, the dimerization equilibrium constant, $K_2$, was allowed to vary independently of the equal sequential constant, $K$, with the result that $K_2 > K$.[6]

Kinetic investigations of the aggregation of nucleoside bases are quite rare, consisting essentially of ultrasonic absorption studies of $N^6$,$N^9$-dimethyladenine[6] and 6-methylpurine.[7] The relaxation curves observed are *somewhat* broader than would be predicted on the basis of a single relaxation time, thus indicating the presence of more than one equilibrium reaction step. The sequential, equal $K$ (SEK) model described above is not consistent with these kinetic results since this model predicts relaxation curves much broader than a single relaxation time curve. The fact that the curves almost fit a single relaxation time and the observation that the SEK model does not provide a suitable basis for a kinetic mechanism have led to the postulation of a two-state model to describe the sound spectra.[6] A somewhat similar situation exists for the hydrogen bond association of alcohols and amides in nonpolar solvents.[8,9]

We have reinterpreted existing thermodynamic data on nucleoside–base aggregation in aqueous solution using a modified sequential $K$ model. In addition we have tested the model by fitting it to previously published kinetic data.[7]

## Thermodynamics

The equilibrium constant for forming an aggregate consisting of $i$ mononucleoside molecules from an $(i - 1)$ monomer–aggregate and a monomer is

$$K_i = \exp(-\Delta G_i/RT)$$

In the SEK model it is argued that (a) the entropy change of all such reactions is constant and (b) the enthalpy change is independent of the value of $i$, i.e.

$$\Delta H_2 = \Delta H_3 = \ldots = \Delta H_i = \ldots = \Delta H$$

so that for each of the stepwise reactions the equilibrium constant is given by

$$K = \exp(-\Delta H/RT) \times \text{constant}$$

Since the base molecules in the various stacks can reversibly exchange with one another, it seems more reasonable to argue that there should be a varying entropy change, given by

$$\Delta S_i = R\Delta \ln \Omega_i + \text{constant}$$

where $\Omega_i$ is the number of ways of distributing indistinguishable solute monomers among the aggregates. For the particular reaction considered above

$$\Delta S_i = R\left[\ln \frac{1}{i!} - \ln \frac{1}{(i-1)!} - \ln 1\right] + \text{constant}$$

or

$$\Delta S_i = -R \ln i + \text{constant}$$

The sequential entropy change thus decreases monotonically from the value for the formation of dimers to quite large negative values for large aggregates approaching minus infinity as $i$ approaches infinity. The equilibrium

**TABLE I: One-Constant Fits of the Equilibrium Data**

| | SEK model[a] | | AK model[b] | | |
|---|---|---|---|---|---|
| | $K$, $M^{-1}$ | RMSD, $M^c$ | $K$, $M^{-1}$ | RMSD, $M^c$ | Previous results, $M^{-1}$ |
| Purine | 2.03 ±0.03 | 0.011 | 6.13 ± 0.18 | 0.015 | 2.1[d] |
| 6-Methylpurine | 5.86 ±0.12 | 0.015 | 21.4 ± 0.9 | 0.021 | 6.7[e] |
| Uridine | 0.614 ± 0.009 | 0.007 | 1.42 ± 0.03 | 0.010 | 0.67[f] |
| 5-Bromouridine | 1.54 ± 0.02 | 0.009 | 3.76 ± 0.11 | 0.016 | $K_2$ = 1.0[g]<br>$K$ = 2.9 |
| Cytidine | 0.852 ± 0.013 | 0.007 | 1.99 ± 0.06 | 0.011 | 0.87[e] |

[a] Fitted using eq 4 and 6. [b] Fitted using eq 3 and 5. [c] RMSD is the minimum in the root mean square deviation in $C_F$, obtained by a non-linear least-squares fitting procedure (see refs 11 and 12). [d] From ref 2; according to the authors this value apparently overestimates the degree of aggregation at higher purine concentrations. [e] From ref 3; apparently only aggregates up to pentamers were considered in computing this result. [f] From ref 2. [g] From ref 3; only aggregates up to tetramers were considered in computing this result.

constant for the formation of $(i)$-mers from $(i-1)$-mers is therefore given by

$$K_i = \exp(-\ln i)\exp(-\Delta H/RT) \times \text{constant}$$

or

$$K_i = K/i \tag{1}$$

where $K$ is defined as above. Note that the argument introduced here does not affect assumption b above; i.e., we still assume that the enthalpy change for adding a monomer to a stack is independent of the size of the stack. A similar argument has been used to modify the BET adsorption isotherm.[10] We shall also assume that the volume change for adding a monomer to a stack is independent of the size of the stack.

The model suggested by eq 1 is evaluated using molal osmotic coefficient data previously published.[3,4] Assuming an ideal mixture of aggregates, one has

$$\begin{aligned} 2N_1 &\rightleftharpoons N_2 \qquad K_2 = \bar{C}_2/\bar{C}_1^2 \\ N_2 + N_1 &\rightleftharpoons N_3 \qquad K_3 = \bar{C}_3/\bar{C}_2\bar{C}_1 \\ &\vdots \\ N_{i-1} + N_1 &\rightleftharpoons N_i \qquad K_i = \bar{C}_i/\bar{C}_{i-1}\bar{C}_1 \\ &\vdots \end{aligned} \tag{2}$$

where $\bar{C}_i$ is the equilibrium concentration of $(i)$-mer (designated by $N_i$). $K_i$ is the equilibrium constant for the formation of $(i)$-mer from $(i-1)$-mer; the relationship among the various $K_i$ is expressed by eq 1 so that, as in the case of the SEK model, only one independent variable is required to calculate the distribution of nucleoside base among the various aggregates. No artificial restriction is made as to the maximum size of aggregate formed.

The formal concentration of solute, $C_F$, is given by

$$C_F = \bar{C}_1 + 2\bar{C}_2 + \ldots + i\bar{C}_i + \ldots$$

Introducing eq 1 and 2

$$C_F = \bar{C}_1 + \frac{2K}{2!}\bar{C}_1^2 + \ldots + \frac{iK^{i-1}}{i!}\bar{C}_1^i + \ldots$$

This series converges for all values of $K\bar{C}_1$, giving

$$C_F = \bar{C}_1 \exp(K\bar{C}_1) \tag{3}$$

This result contrasts with that obtained in the SEK case, where the comparable series reduces to

$$C_F = \bar{C}_1/(1 - K\bar{C}_1)^2 \tag{4}$$

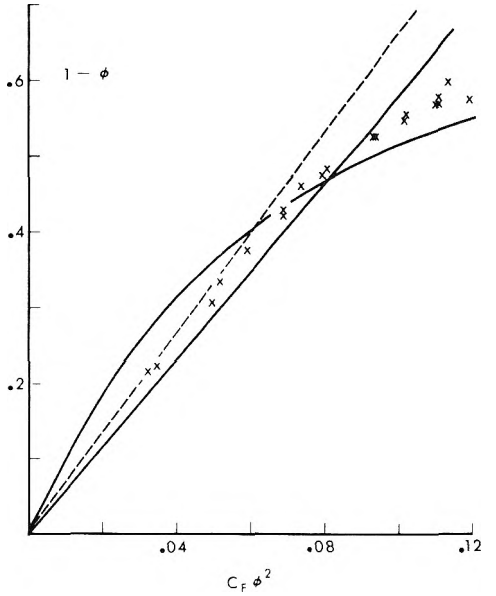


**Figure 1.** Best one-equilibrium constant fits of osmotic coefficient data of 6-methylpurine in water at 25°. The solid straight line is calculated according to SEK model (eq 4 and 6); the curve is calculated according to AK model (eq 3 and 5). The dashed line gives previous result.

with the restriction $K\bar{C}_1 < 1$. Similarly, the total concentration of aggregates is given by

$$C_A = C_F\phi = \bar{C}_1 + \bar{C}_2 + \ldots + \bar{C}_i + \ldots$$

which sums to

$$C_A = \frac{1}{K}\left[\exp(K\bar{C}_1) - 1\right] \tag{5}$$

for all $K\bar{C}_1$. $\phi$ is the molal osmotic coefficient. The comparable SEK sum is

$$C_A = \frac{\bar{C}_1}{1 - K\bar{C}_1} \qquad K\bar{C}_1 < 1 \tag{6}$$

The results obtained by fitting osmotic coefficient data[3,4] to the above equations using a non-linear least-squares routine[11,12] are given in Table I. The equilibrium constants listed are calculated by fitting the data to the SEK model (eq 4 and 6) and to the attenuated $K$ (AK) model (eq 3 and 5), without aggregate size restrictions in either case. The constants previously obtained are also given. A comparison of the minimum values of the root mean square deviation in $C_F$ (RMSD) indicates that the SEK model fits somewhat better than the AK model. Figure 1 shows a plot of $(1 - \phi)$

**TABLE II: Two-Constant Fits of the Equilibrium Data**

| | SEK model | | AK model | |
|---|---|---|---|---|
| | Equilibrium constants | RMSD of fit | Equilibrium constants | RMSD of fit |
| Purine | $K_2 = 2.48 \pm 0.07$<br>$K = 1.90 \pm 0.03$ | 0.0057 | $K_2 = 2.15 \pm 0.04$<br>$K = 7.63 \pm 0.08$ | 0.0028 |
| 6-Methylpurine | $K_2 = 8.00 \pm 0.31$<br>$K = 5.71 \pm 0.06$ | 0.0065 | $K_2 = 5.83 \pm 0.16$<br>$K = 24.9 \pm 0.2$ | 0.0039 |
| Uridine | $K_2 = 0.602 \pm 0.032$<br>$K = 0.635 \pm 0.055$ | 0.0077 | $K_2 = 0.586 \pm 0.035$<br>$K = 2.20 \pm 0.23$ | 0.0077 |
| 5-Bromouridine | $K_2 = 1.24 \pm 0.05$<br>$K = 1.91 \pm 0.06$ | 0.0059 | $K_2 = 1.12 \pm 0.05$<br>$K = 7.37 \pm 0.27$ | 0.0051 |
| Cytidine | $K_2 = 0.726 \pm 0.030$<br>$K = 1.06 \pm 0.05$ | 0.0047 | $K_2 = 0.688 \pm 0.031$<br>$K = 3.86 \pm 0.21$ | 0.0045 |

vs. $C_F\phi^2$, which should be a straight line if the successive equilibrium constants are equal, for the 6-methylpurine solutions. It can be seen that, whereas the SEK model more correctly fits the initial slope of the plot, the AK model correctly anticipates the curvature of the data toward the abscissa.

The behavior of the two models demonstrated by Figure 1 suggests allowing $K_2$, the dimerization equilibrium constant, to vary independently of $K$. This modification makes sense physically, since it allows for a degree of cooperativity in the formation of aggregates, i.e., $K_2 < K$. In this case the equations to be fitted are

$$C_F = \bar{C}_1 + \frac{2K_2\bar{C}_1}{K}[\exp(K\bar{C}_1) - 1]$$

and

$$C_A = \bar{C}_1 + \frac{2K_2\bar{C}_1}{K^2}[\exp(K\bar{C}_1) - 1 - K\bar{C}_1)] \quad (7)$$

for the AK model, and

$$C_F = \bar{C}_1 + K_2\bar{C}_1^2\frac{2 - K\bar{C}_1}{(1 - K\bar{C}_1)^2}$$

and

$$C_A = \bar{C}_1 + \frac{K_2\bar{C}_1^2}{1 - K\bar{C}_1} \quad (8)$$

for the SEK model. The results of these fits are given in Table II and, for 6-methylpurine, displayed in Figure 2. It can be seen that for the weakly associated bases the two models fit equally well, whereas for the more strongly associated solutes (purine and 6-methylpurine) the AK model fits the data decidedly better than the SEK model. In addition, the SEK model results in $K_2 > K$ for these two nucleoside bases, which is not physically reasonable if aggregation is due primarily to dispersive interactions.[2,13,14]

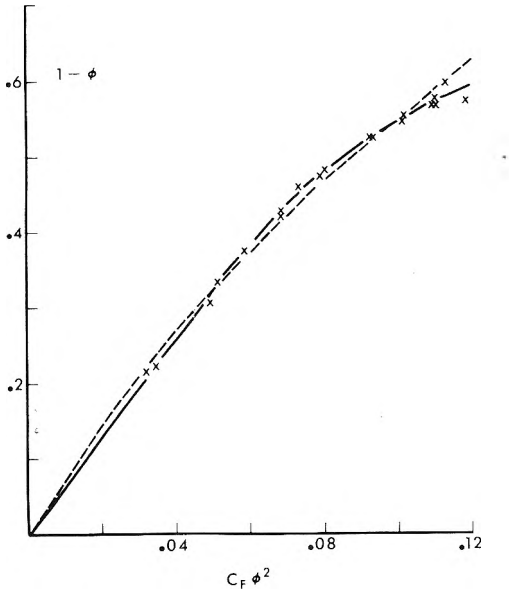


**Figure 2.** Best two-equilibrium constant fits of osmotic coefficient data of 6-methylpurine in water at 25°. The solid curve is calculated according to AK model (eq 7); the dashed curve is calculated according to SEK model (eq 8).

## Kinetics

The ultrasonic absorption spectrum of a multistep reaction mechanism such as that given by eq 2 can be calculated from

$$\frac{\alpha}{f^2} = \sum_{j=1}^{m}\frac{A_j}{1 + (2\pi f\tau_j)^2} + B \quad (9)$$

$\alpha$ is the amplitude absorption coefficient, $f$ is the sound frequency, $\tau_j$ is the $j$th first-order time constant (i.e., relaxation time) and $A_j$ the corresponding amplitude factor, and $B$ is the background absorption. In general, $m$ reaction steps result in $m$ or fewer nonzero relaxation times; however, the individual $\tau_j$'s and $A_j$'s are not a function of any one reaction step only.

The relaxation times of the reaction system are obtained by solving the pertinent rate equations. For the mechanism under consideration (eq 2) the association and dissociation rate constants, $k_i$ and $k_{-i}$, respectively, are defined by

$$K_i = k_i/k_{-i} \quad (10)$$

The rate equations for eq 2 are therefore

$$dC_1/dt = -\sum_{i=2}^{n}\beta(k_iC_{i-1}C_1 - k_{-i}C_i)$$

$$dC_i/dt = k_iC_{i-1}C_1 - (k_{-i} + k_{i+1}C_1)C_i + k_{-(i+1)}C_{i+1}$$

$$dC_n/dt = k_nC_{n-1}C_1 - k_{-n}C_n$$

$$2 \le i \le n - 1 \quad (11)$$

The parameter $\beta$ equals two when $i = 2$ and one otherwise. Introducing the perturbation of the concentrations from their equilibrium values, $C_i = \bar{C}_i + \delta C_i$, a set of linearized rate equations is obtained:

$$d\delta C_1/dt = -\sum \beta^2 k_i \bar{C}_{i-1}\delta C_1 + (\beta k_{-i} - k_{i+1}\bar{C}_1)\delta C_i + k_{-n}\delta C_n$$

$$d\delta C_i/dt = (k_i\bar{C}_{i-1} - k_{i+1}\bar{C}_i)\delta C_1 + k_i\bar{C}_1\delta C_{i-1} - (k_{i+1}\bar{C}_1 + k_{-1})\delta C_i + k_{-(i+1)}\delta C_{i+1}$$

$$d\delta C_n/dt = k_n\bar{C}_{n-1}\delta C_1 + k_n\bar{C}_1\delta C_{n-1} - k_{-n}\delta C_n \qquad 2 \le i \le n-1 \quad (12)$$

Equation 12 is a set of coupled, first-order differential equations whose solution we wish to obtain. This is done by solving the eigenvalue problem for the set. Expressing eq 12 in matrix notation:

$$\delta\dot{\mathbf{c}} = \mathbf{A}\delta\mathbf{c} \qquad (13)$$

$\delta\dot{\mathbf{c}}$ and $\delta\mathbf{c}$ are the column vectors

$$\delta\mathbf{c} = \left\{\frac{d\delta C_i}{dt}\right\}$$

$$\delta\mathbf{c} = \{\delta C_i\}$$

and may be thought of as displacements relative to a reaction coordinate system whose basis vectors consist of the reacting species, $N_i$. The elements of the matrix $\mathbf{A}$ are the coefficients of the $\delta C_i$ of eq 12; these elements have the units of $sec^{-1}$. The desired solution is obtained by performing a coordinate transformation on eq 13 in such a way that all cross terms disappear; i.e., in the transformed coefficient matrix, $\Lambda$, only diagonal elements are nonzero:

$$\Lambda = \mathbf{G}^{-1}\mathbf{A}\mathbf{G} \qquad (14)$$

$\mathbf{G}$ is the transformation matrix whose column vectors, $\mathbf{g}_j$, are the basis vectors of the new coordinate system in terms of the old. The displacement vectors are transformed according to

$$\delta\dot{\xi} = \mathbf{G}^{-1}\,\delta\dot{\mathbf{c}}$$

$$\delta\dot{\xi} = \mathbf{G}^{-1}\,\delta\mathbf{c}$$

so that in the new coordinate system eq 13 is expressed by

$$\delta\dot{\xi} = \Lambda\,\delta\xi \qquad (15)$$

The solutions of these uncoupled, first-order equations are

$$\delta\xi_j = \delta\xi_j{}^0 \exp(\lambda_j t) \qquad (16)$$

The constants $\lambda_j$ are the diagonal elements of $\Lambda$ and have units of $sec^{-1}$; they are the eigenvalues of $\mathbf{A}$ and are usually defined as the negative reciprocal relaxation times of the reaction system:

$$\lambda_j = -1/\tau_j \qquad (17)$$

The new, transformed coordinate system represents the normal coordinates of the reaction mechanism; in this coordinate system the reactions are said to be expressed in their normal modes. The elements of the eigenvectors $\mathbf{g}_j$, designated $g_{ij}$, measure the contribution of $N_i$ to the $j$th normal reaction mode. The $\mathbf{g}_j$ can be calculated from

$$\mathbf{A}\mathbf{g}_j = \lambda_j\mathbf{g}_j \qquad (18)$$

which may be obtained from eq 14.

The amplitude factor corresponding to the $j$th normal mode can be calculated from[15]

$$A_j = \frac{2\pi^2\tau_j[\Delta V_j - (V\theta/C_p)\Delta H_j]^2}{\nu\beta RT\sum_{i=1}^{n}(g_{ij}{}^2/\bar{C}_i)} \qquad (19)$$

$\nu$, $\beta$, $V$, $\theta$, and $C_p$ are the sound velocity, adiabatic compressibility, molar volume, thermal expansion coefficient, and constant pressure heat capacity, respectively, of the solution. $\Delta V_j$ and $\Delta H_j$ are the volume and enthalpy change of the $j$th normal mode and are given by

$$\Delta V_j = \sum_{j=1}^{n} g_{ij}\tilde{V}_i$$

with an analogous expression for $\Delta H_j$. $\tilde{V}_i$ is the partial molar volume of $N_i$. Defining $\Delta V_i$ as the volume change for the formation of $N_i$ from $N_{i-1}$ and $N_1$, and recognizing that $\Sigma_{i=1}^{n} ig_{ij} = 0$ because of mass balance, one can express $\Delta V_j$ in terms of the $\Delta V_i$:

$$\Delta V_j = \sum_{i=2}^{n}\left\{\Delta V_i\sum_{k=1}^{n} g_{kj}\right\} \qquad (20)$$

The expressions developed above are used to simulate the sound absorption spectra of aqueous solutions of 6-methylpurine previously published[7] in order to determine whether the two equilibrium constant AK model is consistent with the kinetic data. The calculation proceeds as follows. It first is necessary to calculate $n$, the size of the coefficient matrix to be used. The criterion used here is that $n$ should be large enough to account for 99% of the aggregates present in solution, i.e.

$$\sum_{i=1}^{n}\bar{C}_i \ge 0.99C_A$$

The value obtained is $n = 4$ for the solutions considered. The coefficient matrix, $\mathbf{A}$, used in the simulation is therefore given by (21). The $\bar{C}_i$'s are calculated from the results

$$\begin{Bmatrix} -\sum_{i=2}^{4}\beta^2 k_i\bar{C}_{i-1} & 2k_{-2} - k_3\bar{C}_1 & k_{-3} - k_4\bar{C}_1 & k_{-4} \\ 2k_2\bar{C}_1 - k_3\bar{C}_2 & -k_3\bar{C}_1 - k_{-2} & k_{-3} & 0 \\ k_3\bar{C}_2 - k_4\bar{C}_3 & k_3\bar{C}_1 & -k_4\bar{C}_1 - k_{-3} & k_{-4} \\ k_4\bar{C}_3 & 0 & k_4\bar{C}_1 & -k_{-4} \end{Bmatrix} \qquad (21)$$

of the previous section, i.e., using $K_2 = 5.83$, $K_3 = 24.9/3 = 8.30$, and $K_4 = 6.23$. The rate constants are obtained by assuming that the interaction energy between adjacent nucleosides in a stack is independent of the size of the stack or of the location of the molecules within the stack. This means that the probability of a monomer dissociating from a stack is independent of the size of the stack so that

$$k_{-2} = k_{-3} = k_{-4} = k_d \qquad (22)$$

The association rate constants are calculated by combining eq 1, 10, and 22:

$$k_i = (K/i)k_d$$

Using eq 15, 16, and 17 the relaxation times of the reaction mechanism may be calculated. The amplitude factors of the normal modes, the $A_j$ of eq 9, may be calculated by (a) assuming that the volume change for adding a monomer to a stack is independent of the size of the stack, i.e.

$$\Delta V_2 = \Delta V_3 = \Delta V_4 = \Delta V$$

and (b) combining eq 9, 18, 19, and 20 with the calculated relaxation times to obtain the best fit of simulated values of $\alpha/f^2$ to the experimental data.

Following the above procedure, a two-dimensional opti-

**TABLE III: Fitted Parameters Resulting from Simulating the Sound Absorption Spectra of 6-Methylpurine (25°) on the Basis of the Two-Constant AK Model**

| $C_F$, $M$ | $f_j$, MHz | $A_j$, sec$^2$/cm | $\lvert\Delta V\rvert$, ml/mol | $k_d$, sec$^{-1}$ | RMSD, sec$^2$/cm |
|---|---|---|---|---|---|
| 0.025 | 50.0 | $0.29 \times 10^{-17}$ | 4.96 ±0.17 | $(1.82 \pm 0.15) \times 10^8$ | $0.25 \times 10^{-17}$ |
| | 36.6 | 1.04 | | | |
| | 21.8 | 2.68 | | | |
| 0.50 | 60.9 | 0.44 | 4.11 ±0.13 | 1.89 ± 0.12 | 0.39 |
| | 43.0 | 1.62 | | | |
| | 24.3 | 4.54 | | | |
| 0.10 | 78.2 | 1.19 | 4.69 ±0.11 | 2.07 ± 0.12 | 1.05 |
| | 54.9 | 3.73 | | | |
| | 30.6 | 9.40 | | | |
| 0.15 | 86.6 | 1.77 | 4.54 ±0.08 | 2.09 ± 0.09 | 0.65 |
| | 60.9 | 4.63 | | | |
| | 33.9 | 10.4 | | | |
| 0.22 | 96.5 | 2.49 | 4.38 ±0.08 | 2.13 ± 0.09 | 0.69 |
| | 67.8 | 5.13 | | | |
| | 37.6 | 10.5 | | | |

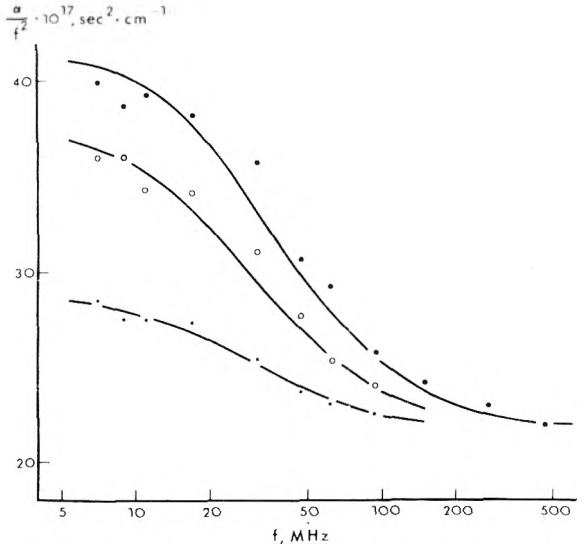


**Figure 3.** Ultrasonic absorption spectra of 6-methylpurine in water at 25°: ★, 0.05 *M*; O, 0.10 *M*; ●, 0.22 *M*. Curves are calculated on the basis of the two-constant AK model (eq 2, 10, 11, and 12) according to the procedure described in the text.

mization method described elsewhere[11] is used to find the values of $k_d$ and $\Delta V$ giving the best fit of calculated spectrum to experimental data for each of the solutions measured. These results, together with the relaxation frequencies (calculated according to $f_j = 1/2\pi\tau_j$) and corresponding amplitude factors, are given in Table III. The standard errors of the fitted parameters and RMSD's of the fits are also given. The simulated relaxation curves and experimental values of $\alpha/f^2$ are plotted in Figure 3. The RMSD's of the fits and Figure 3 show that the two equilibrium constant AK model reproduces the measured sound absorption spectra to within experimental error.

## Discussion

The attenuated constant model introduced here seems to give a more physically reasonable description of the stacking process than the SEK model. The one-equilibrium constant results indicate that while the AK model overestimates the degree of aggregation at low concentrations, the SEK model overpredicts the amounts of higher polymers formed. Both models can, of course, be improved by allowing $K_2$ to vary independently of $K$. This modification allows for cooperativity in the stacking process; i.e. higher polymers are formed relatively easily once dimers are formed from monomers. The two-equilibrium constant AK fits for purine and 6-methylpurine give the expected result, i.e., $K_2 < K$; on the other hand, Table II shows that the two-constant SEK model does not fit the experimental data nearly as well and in addition contradicts the above modification, i.e., the model results in $K_2 > K$. Cytidine, uridine, and 5-bromouridine give equally good fits with both models. Apparently the very low degree of association of these nucleosides obscures any possible cooperativity effect.

The two-constant AK model reproduces the sound absorption spectrum most exactly; the results of the simulation given in Table III clearly show why. A very narrow band of relaxation frequencies having significantly different amplitude factors is obtained (the ratio of the largest to the smallest $f_j$ is about 2.5 in all cases). The reaction modes are thus not resolvable, but appear as a single relaxation time. The results of Table II indicate that the volume change for the addition of a monomer to a stack is $\lvert\Delta V\rvert$ = 4.5 ml ± 10% and that $k_d = 2.0 \times 10^8$ sec$^{-1}$ ± 10%. This value of $k_d$ agrees reasonably well with the value previously obtained by extrapolation.[7] It should be noted that the assumption that the volume change and dissociation rate constant of dimer formation are equal to the general stack formation values (i.e., $\Delta V_2 = \Delta V$ and $k_{-2} = k_d$) is not strictly valid. Since the model used in the kinetic analysis allows for cooperativity in the first step, $k_{-2}$ and $\Delta V_2$ should most properly be allowed to vary independently of $k_d$ and $\Delta V$. Although the introduction of two additional parameters would, of course, improve the already good agreement between the simulated and measured absorption spectrum, we do not feel justified in fitting the absorption data with four adjustable constants.

The results of this work tend to support the growing body of evidence[2,6] which indicates that the stacking process is somewhat different from the "hydrophobic bonding" interaction in which aggregate formation is characterized by positive changes in enthalpy, entropy, and volume.[16] The magnitude of $\Delta V$ reported here is somewhat

less than that given by Porschke and Eggers for the stacking of $N^6,N^9$-dimethyladenine;[6] these authors report $\Delta V = -6.5$ ml/mol. In the absence of information about the effect of pressure on the stacking equilibria of 6-methylpurine, we assume that the sign of $\Delta V$ is also negative for the present system. The smaller magnitude of $\Delta V$ could then be attributed to the fact that 6-methylpurine stacking interactions are weaker than those in $N^6,N^9$-dimethyladenine, resulting in a somewhat larger spacing between the parallel purine rine units. Stacking interactions between the base molecules might have been expected to lead to a positive volume change because of the effect of removal of oriented water molecules from contact with the hydrophobic faces of the purine molecules. However, this effect seems to be outweighed by the relatively strong binding between the $\pi$-electronic systems of the bases. Recent studies of the denaturation of ribonuclease seem to indicate that negative volume changes accompanying hydrophobic exposure of hydrocarbon residues (in proteins) are less than had been predicted from studies of smaller molecular systems.[17]

*Acknowledgments.* Acknowledgment is made to the National Science Foundation (Grant No. GP-43307) for partial support of this work.

### References and Notes

(1) Present address: Department of Biomathematics, P.O. Box 104 Old BSB, University of Alabama in Birmingham, Birmingham, Ala. 35294.
(2) P. O. P. Ts'o in "Fine Structure of Proteins and Nucleic Acids", G. D. Fasman and S. M. Timesheff, Ed., Marcel Dekker, New York, N.Y., 1970, pp 49–190.
(3) P. O. P. Ts'o, I. S. Melvin, and A. C.Olson, *J. Am. Chem. Soc.*, **85**, 1289 (1963).
(4) P. O. P. Ts'o and S. I. Chan, *J. Am. Chem. Soc.*, **86**, 4176 (1964).
(5) T. L. Hill and Y. D. Chen, *Biopolymers*, **12**, 1285 (1973).
(6) D. Porschke and F. Eggers, *Eur. J. Biochem.*, **26**, 490 (1972).
(7) F. Garland and R. C. Patel, *J. Phys. Chem.*, **78**, 848 (1974).
(8) J. Rassing and F. Garland, *Acta Chem. Scand.*, **24**, 2419 (1970).
(9) F. Garland, J. Rassing, and G. Atkinson, *J. Phys. Chem.*, **75**, 3182 (1971).
(10) S. D. Christian, E. L. Enwall, and E. E. Tucker, unpublished work.
(11) S. D. Christian, *J. Chem. Educ.*, **42**, 604 (1965); E. E. Tucker, S. B. Farnham, and S. D. Christian, *J. Phys. Chem.*, **73**, 3820 (1969).
(12) D. W. Marquardt, *J. Soc. Ind. Appl. Math.*, **11**, 431 (1963) (Fortran Share Program No. 1428).
(13) H. Devoe and I. Tinoco, *J. Mol. Biol.*, **4**, 500 (1962).
(14) E. Grunwald and E. Price, *J. Am. Chem. Soc.*, **86**, 4517 (1964).
(15) F. Garland, R. C. Patel, and G. Atkinson, *J. Acoust. Soc. Am.*, **54**, 994 (1973).
(16) W. Kauzmann, *Adv. Protein Chem.*, **14**, 1 (1959).
(17) J. F. Brandts, R. J. Oliveira, and C. Westwort, *Biochemistry*, **9**, 1038 (1970).

# Correlation between Rate Constants for Water Substitution in Inner Coordination Spheres of Metal Ions and Their Electrochemical Activities in Metal Deposition Reactions

**Ashok K. Vijh* and J.-P. Randin**

*Hydro-Quebec Institute of Research, Varennes, Quebec, Canada* *(Received September 16, 1974; Revised Manuscript Received February 13, 1975)*

*Publication costs assisted by Hydro-Quebec Institue of Research*

It has been shown that the homogeneous rate constants for water substitution in the inner coordination spheres of metal ions are directly related to their heterogeneous rate constants for the electrodeposition reactions. Mechanistic significance of these correlations for the electrodeposition reactions is pointed out.

## Introduction

The cathodic deposition of a hydrated metal ion, $(M^{z+})_{nH_2O}$, on the metal electrode $M_E$ may be represented by the forward act of the following reaction:

$$(M^{z+})_{nH_2O} + ze + M_E \underset{k_b}{\overset{k_f}{\rightleftharpoons}} M_E\text{–}M + nH_2O \qquad (1)$$

where $ze$ are the electrons provided by the cathode in the electrolysis reaction and $M_E$–M is a metal atom M deposited on metal lattice $M_E$. The intrinsic activity of the above reaction is represented by the exchange current density, $i_0$, which is a measure of the *rate* at the reversible potential. The exchange current density, $i_0$, is related to the rate constant, $k_s$, of reaction 1 by the relation:

$$i_0 = zFk_s\, a_{M^{z+}}{}^{1-\beta} a_M{}^{\beta} \qquad (2)$$

where $a$ represent the activities of $M^{z+}$ and M in the bulk of the solution, $\beta$ is the transfer coefficient, $z$ is the charge of the metal ion, $F$ is the Faraday constant, and $i_0$ is the rate characteristic of the dynamic equilibrium in reaction 1. At the reversible potential, the rates in the forward and backward directions are equal:

$$i_0 = \vec{i} = \overleftarrow{i} \qquad (3)$$

and both $k_f$ and $k_b$ are equal to the standard rate constant $k_s$, provided that the reactants and the products are in their standard state. In the subsequent discussion, we shall be concerned with the forward reaction only, hence

$$\vec{i} = zFk_f\, a_{M^{z+}}{}^{1-\beta}$$

For our purposes $a$ may be approximated with concentration, $C$; further if one considers reaction 1 for various metal ions at a nearly identical concentration (e.g., in the 0.5–1 $M$ concentration range but mostly near 1 $M$), it follows that the $i_0$ values are proportional to rate constant, $k_f$, values provided that the valences of the depositing ions are

**TABLE I: Appropriate Data for the Deposition of Divalent Metal Ions on Metals**

| Metal ion | Homogeneous rate constant, $k$,[a] $sec^{-1}$ | $-\log i_0$,[b] A $cm^{-2}$ | Medium | Ref |
|---|---|---|---|---|
| $Ni^{2+}$ | $1.5 \times 10^4$ | 8.7 | 1 *M* $NiSO_4$ | 15 |
| $Co^{2+}$ | $3 \times 10^5$ | 6.85 | 0.85 *M* $CoSO_4$ | 16 |
| $Fe^{2+}$ | $1.5 \times 10^6$ | 8 | 1 *M* $FeSO_4$ | 15 |
| $Zn^{2+}$ | $3 \times 10^7$ | 4.7 | 1 *M* $ZnSO_4$ | 15 |
| $Cd^{2+}$ | $2.5 \times 10^8$ | 1.85 | 0.72 *M* $CdSO_4$ | 17 |
| $Cu^{2+}$ | $3 \times 10^8$ | 2.57–4.7 | 1 *M* $CuSO_4$ or 1 *M* $CuSO_4$ + 1 *N* $H_2SO_4$ | 15, 18–19 |
| $Pb^{2+}$ | $3 \times 10^9$ ($Hg^{2+}$)[c] | 1.07 | 0.5 *M* $Pb(NO_3)_2$ | 20 |

[a] The rate constant refers to the substitution of $H_2O$ in the *inner* coordination sphere of the shown ions.[14] [b] $-\log i_0$ (A $cm^{-2}$) are the reported values of the exchange current densities for the reaction $M^{z+} + ze \rightleftharpoons M$ under nearly identical solution conditions and are taken from the references shown in the last column. [c] The datum on the homogeneous rate constant, $k$, for $Pb^{2+}$ is not available in ref 14. However, because of the proximity of Hg and Pb in the periodic table of the elements and the very similar properties of their ions, one may use, in an approximate way, the $k$ values for $Hg^{2+}$ as also representing the $k$ value for $Pb^{2+}$.

**TABLE II: Appropriate Data for the Deposition of Divalent Metal Ions on Mercury**

| Ion | Homogeneous rate constant, $k$,[a] $sec^{-1}$ | Heterogeneous rate constant, $k_f$,[c] cm $sec^{-1}$ |
|---|---|---|
| $Cd^{2+}$ | $2.5 \times 10^8$ | $2.6 \times 10^{-2}$ (0.5 *M* $Na_2SO_4$) |
| $Cu^{2+}$ | $3 \times 10^8$ | $4.5 \times 10^{-2}$ (1 *M* $KNO_3$) |
| $Hg^{2+}$ | $3 \times 10^9$ | 1.3 (1.1 *M* $HClO_4$) |
| $Ni^{2+}$ | $1.5 \times 10^4$ | $3.3 \times 10^{-9}$ (0.1 *M* $HClO_4$) |
| $Pb^{2+}$ | $3 \times 10^9$ ($Hg^{2+}$)[b] | 1.5 (1.0 *M* $HClO_4$) |
| $Zn^{2+}$ | $3 \times 10^7$ | $3.26 \times 10^{-3}$ (1 *M* $NaClO_4$ + $10^{-3}$ *N* $HClO_4$) |

[a] Homogeneous rate constants are taken from ref 14 and electrochemical rate constants are from ref 21. [b] Footnote c of Table I also applies to this table. [c] The values of the electrochemical (i.e., heterogeneous) rate constants, by definition, are for the identical solution concentrations, even though they were calculated from the experimental data obtained in solutions of different concentrations.

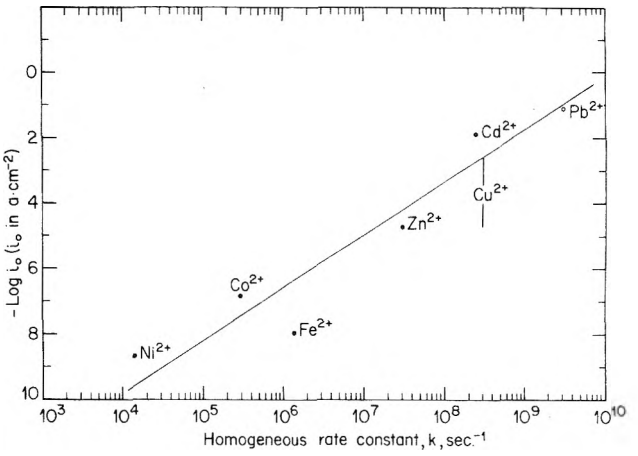


**Figure 1.** A plot of the $-\log i_0$ values for the deposition of divalent metal ions on metals against the homogeneous rate constant for the substitution of $H_2O$ in the inner coordination sphere of the ions shown. For data and their source reference, see Table I.

the same. With the above qualifications (constant value of valence $z$ and roughly constant values of concentrations of the depositing ions), one may assume that $i_0$ values represent the *rate constants* for the series of metal ions to be considered in the next section.

It has been theoretically postulated[1] that deaquation of the hydrated metal ions is the main cause of the overvoltage (and hence the activation energy of the reaction) associated with the cathodic reduction of cations in aqueous media (i.e., the electrodeposition reaction such as in eq 1), at least for small multiply charged cations. This postulate has indeed been used to explain the impossibility of depositing cations such as $Be^{2+}$ and $Al^{3+}$ from aqueous solutions.[1] For the reduction of $Ni^{2+}$,[2-7] $Co^{2+}$,[7-9] $Zn^{2+}$,[10] and $Cu^{2+}$ [11,12] ions, there is experimental evidence that the rate-determining step (rds), or at least the kinetically important step in the electrodeposition reaction is the dehydration.[2-13] Based on this theoretical suggestion[1] and the experimental evidence for a limited number of ions,[2-13] it appears appropriate to explore this point in a more generalized way for all metal ions for which suitable data on the $i_0$ values and the rate constants for dehydration are available. This is carried out in the next section.

### Correlation between Rate Constants of Dehydration and the Rate Constants for Electrodeposition of Ions

The values of characteristic rate constants, $k$, for the water substitution in the inner coordination sphere of metal ions[14] *and* exchange current densities (i.e., a value proportional to the rate constants) for their electrodeposition in aqueous solutions for a *series* of metal ions are available for divalent ions only (Table I). If the theoretical suggestion[1] and the limited experimentally determined mechanistic data[2-7] are valid, one should expect a *direct* correlation between the $i_0$ values and the $k$ values. A plot of data given in Table I shows that this is indeed observed for all the divalent metals for which the relevant data are available (Figure 1).

In order to explore further the general applicability of this correlation (Figure 1), it is of interest to examine the plot of rate constant, $k_f$, for the electrodeposition of divalent ions (aqueous solutions) on a mercury electrode instead of on the metal electrode $M_E$ (where M in $M_E$ and $(M^{z+})_{nH_2O}$ represent the same identical metal, e.g., $(Cu^{2+})_{nH_2O}$ on a Cu electrode). Although only scant data are available (Table II), they are sufficient to demonstrate that increasing values of rate constant, $k_f$, for the deposition of divalent ions on Hg tend to be associated with increasing values of $k$, the characteristic rate constant for water substitution in the inner coordination sphere of the ions (Figure 2).

From Figures 1 and 2, it would appear that, at least for divalent ions, deaquation of the ion is the kinetically important step in the overall electrodeposition reaction. This would then support the previous theoretical viewpoint[1] and

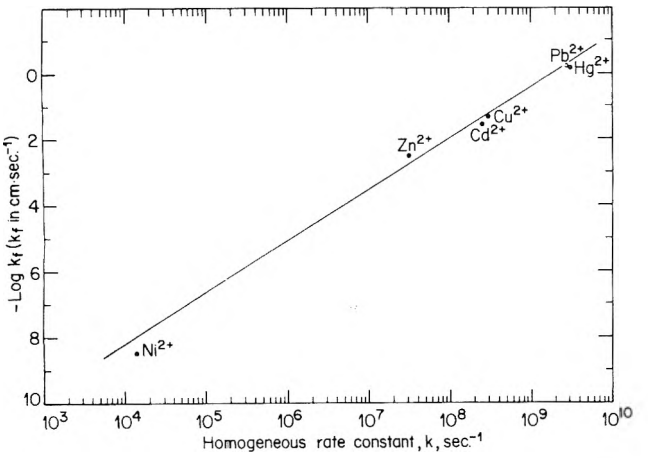


**Figure 2.** A plot of the heterogeneous rate constant, $k_f$, for the deposition of divalent metal ions on mercury against the homogeneous rate constant for the substitution of $H_2O$ in the inner coordination sphere of the ions shown. For data and their source reference, see Table II.

the detailed mechanistic data on the electrodeposition of $Ni^{2+}$,[2-7] $Co^{2+}$,[7-9] $Zn^{2+}$,[10] and $Cu^{2+}$.[11,12] The deaquation model[1] neglects other sources of overvoltage for the electron transfer step. These may be much more important for the less highly charged cations which are the subject of the present note. The deviation of points from the correlation line of Figure 1 draws attention to the fact that other energetically important processes most likely contribute to the activation energy of the electrochemical step. For instance, the conditions of the electrode surface could be of major importance, as indicated by the better correlation of Figure 2 where the metal deposition occurs at a mercury electrode. The present line of argument, although somewhat speculative, does point strongly, however, to one important factor in metal deposition, namely, the deaquation of ions.

It is believed that sufficient appropriate data for investigating the correlations such as in Figures 1 and 2 are not available for monovalent or trivalent ions. Also, it appears that data on rate constants for metal deposition and solvent substitution in *nonaqueous* solutions are too meager to permit exploration of correlations such as in Figures 1 and 2. There is no reason to believe, however, that considerations developed here and previously[1-13] are not valid for nonaqueous systems.

## References and Notes

(1) H. Strehlow and J. Jen, *J. Electroanal. Chem.*, **46**, 181 (1973).
(2) L. Gierst and H. Hurwitz, *Z. Elektrochem.*, **64**, 36 (1960).
(3) J. Dandoy and L. Gierst, *J. Electroanal. Chem.*, **2**, 116 (1961).
(4) H. Shirai, *Nippon Kagaku Zasshi*, **82**, 339 (1961); *Chem. Abstr.*, **55**, 14127*h* (1961).
(5) N. S. Hush and J. W. Scarrott, *J. Electroanal. Chem.*, **7**, 26 (1964).
(6) E. Verdier and R. Pernicelli, *J. Chim. Phys.*, **67**, 965 (1970).
(7) R. Bennes, *J. Electroanal. Chem.*, **44**, 145 (1973).
(8) E. Verdier and F. Rouelle, *J. Chim. Phys.*, **62**, 297 (1965).
(9) E. Eriksrud and T. Hurlen, *J. Electroanal. Chem.*, **36**, 311 (1972).
(10) F. von Strum and M. Ressel, *Microchem. J.*, **5**, 53 (1961).
(11) S. I. Woodburn, T. J. Cardwell, and R. J. Magee, *Recl. Trav. Chim. Pays-Bas*, **88**, 1167 (1969).
(12) F. M. Hawkridge and H. H. Bauer, *Anal. Chem.*, **44**, 364 (1972).
(13) H. H. Bauer, "Electrodics", Wiley, New York, N.Y., 1972, p 14.
(14) M. Eigen, *Pure Appl. Chem.*, **6**, 97 (1963).
(15) R. Parsons, "Handbook of Electrochemical Constants", Butterworths, London, 1959, p. 97.
(16) M. V. Simonova and A. L. Rotinyan, *Elecktrokhimiya*, **2**, 812 (1966).
(17) R. J. Brodd, *J. Res. Natl. Bur. Stand., Sect. A*, **65**, 275 (1961).
(18) T. Hurlen, *Acta. Chem. Scand.*, **15**, 630 (1961).
(19) V. J. Chernenko and K. I. Litovchenko, *Elektrokhimiya*, **7**, 816 (1971).
(20) N. A. Hampson and D. Larkin, *Trans. Faraday Soc.*, **65**, 1660 (1969).
(21) N. Tanaka and R. Tamamushi, *Electrochim. Acta*, **9**, 963 (1964).

# Laser Photolysis Studies on Quenching Processes of Triplet Benzophenone by Amines in Fluid Solution

**Satoshi Arimitsu,***

*Sagami Chemical Research Center, Nishiohnuma, Sagamihara, Kanagawa 229, Japan*

**Hiroshi Masuhara, Noboru Mataga, and Hiroshi Tsubomura**

*Faculty of Engineering Science, Osaka University, Toyonaka, Osaka 560, Japan* *(Received August 29, 1974)*

*Publication costs assisted by the Sagami Chemical Research Center*

The quenching behaviors of triplet benzophenone by some amines in solution have been directly investigated using the nanosecond laser photolysis technique. It has been confirmed in systems of benzophenone and tertiary aromatic amines, such as *N,N*-diethylaniline and *N,N*-dimethyl-*p*-toluidine, that the ionic photodissociation to benzophenone anion and amine cation takes place completely in acetonitrile, while the photoreduction of benzophenone occurs efficiently in benzene. These processes were found to compete with each other depending largely upon solvent polarity. The quenching of the triplet benzophenone by primary and secondary aromatic amines as well as aliphatic amines leads to the formation of a ketyl radical in all solvents used. The marked distinction observed in the quenching processes of triplet benzophenone by various amines has been explained by the difference in ionization potential and the change of molecular structure of the amine in addition to the solvent effect. The solvent effect was discussed on the basis of free-energy calculations regarding the formation of ion pairs and free ions involved in the quenching path. In the case of the benzophenone–tertiary amine system it is concluded that an electron transfer followed by proton transfer results in rapid hydrogen abstraction. The relaxation time for solvent orientation may be a useful guide to the present conclusion. In the case of primary and secondary amines the importance of a hydrogen atom bonded to the N atom of the donor was suggested.

## Introduction

There have been a number of studies on the photochemistry of ketones.[1] Recently, the photophysical and photochemical behavior of triplet ketones in amine solutions has been studied as an attractive subject and the elementary processes are considerably elucidated.[2] Cohen et al. found that the photoreactivity of benzophenone (BP) was enhanced with great efficiency in aliphatic amine solution, and proposed that the enhanced rate for photoreduction was due to the formation of a charge transfer (CT) complex or an ion pair followed by proton transfer.[3] Using the conventional flash photolysis method, Davidson et al. investigated photoreduction and quenching of triplet BP by arylamines in fluid solution and suggested Cohen's postulate.[4] In a related study of the BP–amine system, we have reported spectroscopic evidence for the formation of a CT complex of BP with aromatic amine in rigid solution at 77°K, measuring electronic absorption and emission spectra.[5] In this system, the photoreduction of BP takes place, unusually, at low temperature, which is explained by the lower activation energy of hydrogen abstraction due to CT interaction between BP and aromatic amine.

To clarify the relation between the electron transfer and hydrogen abstraction reaction mechanism for BP–amine systems in fluid and rigid solutions, we have previously reported the time-dependent behavior of the n–$\pi^*$ triplet BP in fluid solution containing *N,N*-diethylaniline by means of laser photolysis.[6] It has been confirmed that the ionic dissociation to BP anion and amine cation competes with the hydrogen abstraction reaction in the BP–*N,N*-diethylaniline system by measuring the yields of product ion and ketyl radicals in various solvents.

In the present paper more detailed studies on the quenching of triplet BP by various amines in some solvents will be reported. The relation between ionic dissociation and hydrogen abstraction processes for BP–amine system will be discussed and the photoreduction mechanism of BP by amine will be clarified.

## Experimental Section

The laser photolysis apparatus used in this research is the same as that described previously.[7] Transient absorption spectra were obtained from 380 to 800 nm with HTV 1P28 and R406 photomultipliers. BP was recrystallized from ethanol and sublimed in vacuo. Acetonitrile was refluxed repeatedly over phosphorus pentoxide, and purified by fractional distillation. Acetone (Nakarai Chemicals, spectrograde), pyridine (Dotaito spectrograde), toluene, and benzene (Merk spectrograde) were used without further purification. Aniline (AN), *N*-ethylaniline (NEA), *N,N*-diethylaniline (DEA), and *N,N*-dimethyl-*p*-toluidine (DMT) were obtained by vacuum distillation and stored under vacuum conditions. *p*-Toluidine (TO) was purified by recrystallization and vacuum sublimation. *p*-Phenylenediamine (PPD) was recrystallized from benzene and sublimed. Pure triethylamine (TEA) was kindly supplied by Mr. Okada. To eliminate the influence of oxygen, all sample solutions were prepared by bubbling with $N_2$ gas, which was saturated with solvent vapor.

## Results

*Quenching of Triplet BP by Amines.* The transient species generated by exciting in the n–$\pi^*$ band of BP with a 347-nm laser pulse was investigated. The transient spec-

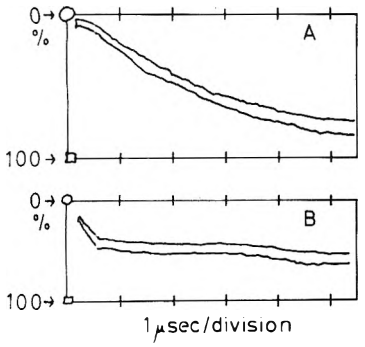


**Figure 1.** Oscillograms showing the decay of the triplet benzophenone observed at 535 nm in benzene: (A) $3.0 \times 10^{-3}$ *M* benzophenone; (B) $3.0 \times 10^{-3}$ *M* benzophenone and $1.8 \times 10^{-3}$ *M* DEA.

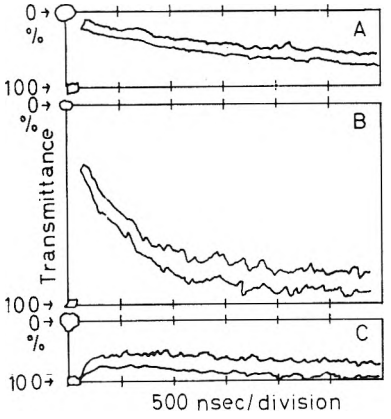


**Figure 2.** Oscillograms showing the decay of the triplet benzophenone as well as the rise of the benzophenone anion in acetonitrile: (A) observed at 515 nm in the case of $2.9 \times 10^{-3}$ *M* benzophenone solution; (B) observed at 535 nm in the case of $2.9 \times 10^{-3}$ *M* benzophenone and $1.34 \times 10^{-4}$ *M* DEA solution; (C) observed at 660 nm in the case of $2.9 \times 10^{-3}$ *M* benzophenone and $1.34 \times 10^{-4}$ *M* DEA solution.

tra obtained just after laser photolysis give rise to the same absorption at around 535 nm in all solvents, the position being consistent with the triplet–triplet absorption of BP.[8] Since the lowest excited singlet state of BP is not detected by our laser photolysis apparatus because of its short lifetime,[9] triplet BP appears as the initial transient. This assignment is supported by measuring the decay kinetics of the transient. The decay times are 2.2 μsec in benzene and 1.6 μsec in acetonitrile solutions, which are fairly consistent with previous data reported by Porter et al.[8] Though the triplet BP disappears mostly within a few microseconds as shown in Figures 1A and 2A, the residue decaying more slowly was found to display similar absorption to that of triplet BP. This transient may be ascribed to a ketyl radical produced by direct hydrogen abstraction of the triplet BP from solvent as found by previous workers.[10]

When a tertiary amine such as DEA, which has abstractable hydrogen, was added to BP–benzene and BP–acetonitrile systems, there appear no spectral changes indicating an attractive interaction between BP and DEA in the ground state. However, the lifetime of triplet BP was found to be remarkably shortened to a few hundred nanoseconds due to the encounter collision with the added amine as shown in Figures 1B and 2B. By a closer comparison between these figures, it should be noted that quenching processes of triplet BP by DEA in benzene and acetonitrile are quite different. In benzene, the degradation of triplet BP

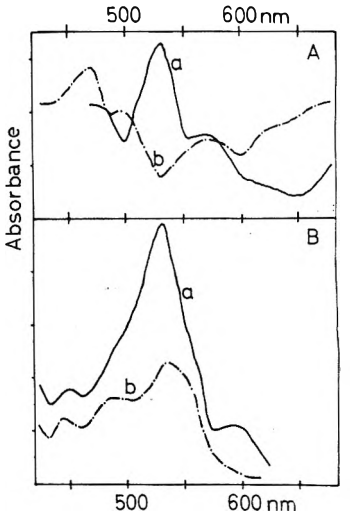


**Figure 3.** Transient absorption spectra of the benzophenone–DEA system: (A) $3.0 \times 10^{-3}$ *M* benzophenone and $1.7 \times 10^{-3}$ *M* DEA in acetonitrile (a) immediately after laser excitation and (b) 200 nsec after laser excitation; (B) $3.0 \times 10^{-3}$ *M* benzophenone and $1.7 \times 10^{-3}$ *M* DEA in benzene (a) immediately after laser excitation and (b) 400 nsec after laser excitation.

leads to a transient absorbing at 535 nm. On the other hand, in acetonitrile solution, such a transient is not observed at all as shown in Figure 2B.

*Transient Absorption Spectra.* As to the quenching of triplet BP by DEA, direct information was obtained by measuring the time-resolved spectra in these solutions. As is clearly seen in Figure 3A and 3B, it was confirmed that the triplet BP appears immediately after laser excitation in both solvents. At a later time, however, we could observe quite different spectra in these solutions. In the case of acetonitrile, the spectrum observed at 200 nsec after laser photolysis consists of two absorption bands around 480 and 660 nm, where the former is attributed to the DEA cation,[11] and the latter to the BP anion,[12] respectively. The formation of the BP anion was directly observed at 660 nm in acetonitrile solution containing DEA. As shown in Figure 2C, it was found that the buildup of BP anion absorption corresponds exactly to the faster decay of triplet BP. On the other hand, in the case of benzene, the absorption of the ketyl radical having a long decay time compared with that of triplet BP was observed at 535 nm as shown in Figure 3B.

The primary quenching reaction of triplet BP in polar and nonpolar media was also investigated in the presence of DMT. It was found that the ionic dissociation led to the formation of DMT cation and BP anion radicals in acetonitrile solution. The former exhibits absorption around 480 nm,[13] and the latter at a longer wavelength region than 600 nm, as shown in Figure 4. On the other hand, the results obtained in benzene were essentially identical with those obtained in the BP–DEA–benzene system.

It has been found that there are many distinctions between the photoreduction of ketones by primary, secondary, and tertiary amines in fluid solutions.[2,14,15] Therefore, we have investigated the quenching processes by some amines such as AN, TO, NEA, PPD, and TEA. The result obtained in the case of the BP–AN system is shown in Figure 5 as a typical one. Figure 5 apparently shows that the degradation of triplet BP produced just after laser pulse is also enhanced by aniline. However, in contrast to the case of tertiary aromatic amines such as DEA and DMT, the

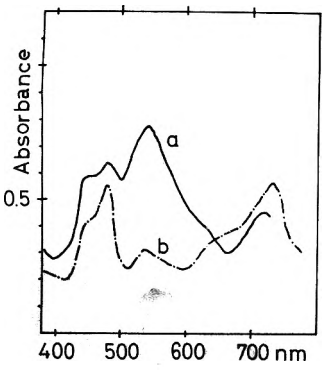


**Figure 4.** Transient absorption spectra of the benzophenone–*N,N*-dimethyl-*p*-toluidine system: 2.75 × $10^{-3}$ *M* benzophenone and 2.22 × $10^{-3}$ *M* *N,N*-dimethyl-*p*-toluidine in acetonitrile (a) immediately after laser excitation and (b) 300 nsec after laser excitation.

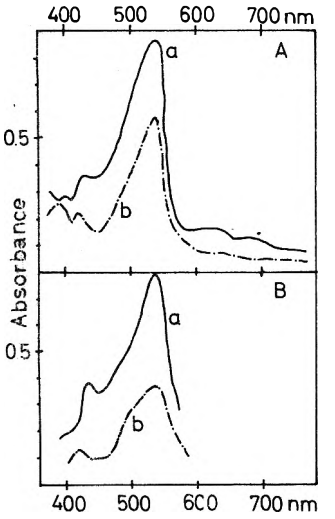


**Figure 5.** Transient absorption spectra of the BP–aniline system: (A) 2.75 × $10^{-3}$ *M* BP and 6.9 × $10^{-3}$ *M* aniline in acetonitrile (a) immediately after laser excitation and (b) 300 nsec after laser excitation; (B) 2.8 × $10^{-3}$ *M* BP and 4.3 × $10^{-3}$ *M* aniline in toluene (a) immediately after laser excitation and (b) 300 nsec after laser excitation.

photoreduction of BP is brought about mainly by the interaction of triplet BP with aniline, leading to a ketyl radical in both polar and nonpolar solvents, though the ionic dissociation occurs appreciably in acetonitrile solution. The situation is similar to the quenching behaviors of BP–PPD, BP–TO, BP–NEA, and BP–TEA systems, though no ion formation was detected in the case of the BP–TEA system.

*Solvent Effect on Triplet BP Quenching by Amines.* More quantitative studies of the solvent effect on quenching of triplet BP with amine were made in various solvents. The quantum yields for ionic dissociation and photoreduction processes in the BP–amine system were determined in acetonitrile, acetone, pyridine, and benzene (toluene). The molar absorption coefficients for triplet BP, ketyl radical, and BP anion obtained by previous workers are 1 × $10^4$ at 535 nm and 5 × $10^3$ at 535 and 660 nm, respectively.[8,12,16] With these values, the concentrations of triplet BP, ketyl radical, and BP anion were calculated in these solvents by measuring the absorbance of these species as well as triplet BP, so that the quantum yields of BP anion and ketyl radicals were determined.[17] These results are shown in Figures 6 and 7. In the case of BP–DEA and BP–DMT systems, the ionic dissociation takes place completely in acetonitrile,

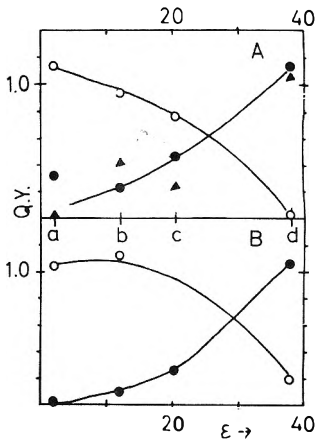


**Figure 6.** The solvent effect on the primary processes of the triplet BP–amine systems. The vertical scale is quantum yield of radicals, calculated by taking into account the extinction coefficients obtained: ketyl radical at 535 nm (○), benzophenone anion at 660 nm (●), and amine cation at 480 nm (▲). The horizontal scale represents the dielectric constant of the solvents (a) benzene or toluene, (b) pyridine, (c) acetone, and (d) acetonitrile: (A) BP–DEA system 400 nsec after excitation; (B) BP–*N,N*-dimethyl-*p*-toluidine 300 nsec after excitation.

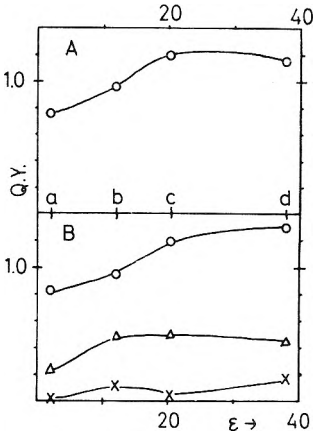


**Figure 7.** The solvent effect on the primary processes of the triplet BP–amine systems. The vertical scale is quantum yield of radicals, calculated by taking into account the extinction coefficients obtained: ketyl radical at 535 nm (○), anilino radical at 410 nm (△), and absorption at 660 nm (×). The horizontal scale represents the dielectric constant of the solvents (a) benzene or toluene, (b) pyridine, (c) acetone, and (d) acetonitrile: (A) BP–TEA system 500 nsec after excitation; (B) BP–aniline system 500 nsec after excitation.

and diminishes with decreasing dielectric constant of solvents while the photoreduction undergoes perfectly in benzene, and reveals inverse dependence on the solvent effect compared with ionic dissociation. Moreover, it was found that the sum of quantum yields for ionic dissociation and photoreduction was approximately equal to unity in BP–DEA and BP–DMT systems. On the other hand, in the case of BP–AN and BP–TEA systems as well as BP–TO and BP–NEA systems, the photoreduction of BP undergoes efficiently in all solvents used as shown in Figure 7. The quantum yield of the ketyl radical decreases slightly with decreasing dielectric constants of solvent molecules. This result implies that another quenching process competing some extent with photoreduction may be involved in nonpolar solvent. In the case of the BP–PPD–acetonitrile system, both BP and PPD are excited with a 347-nm pulse. Although the exciting laser pulse leads to the ionization of

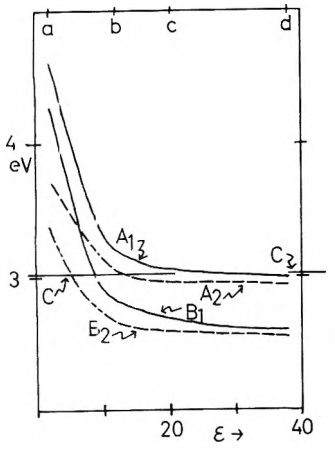


**Figure 8.** Calculated free energies of the ion pairs as well as dissociated ions in various solvents. The horizontal scale represents the dielectric constant of (a) benzene, (b) pyridine, (c) acetone, and (d) acetonitrile: ($A_1$) dissociated $BP^-$ + $TEA^+$ ions; ($A_2$) $BP^-$···$TEA^+$ ion pair; ($B_1$) dissociated $BP^-$ + $DEA^+$ ions; ($B_2$) $BP^-$···$DEA^+$ ion pair; (C) the energy level of triplet BP.

**TABLE I: Ionization and Oxidation Potentials of Amines Used for Calculating Free Energies of Ion States**

| Amine | Ionization potential, eV | Oxidation potential, V |
|---|---|---|
| DEA | | 0.76 |
| (DMA) | 7.14[a] | 0.71[c] |
| DMT | | 0.65[c] |
| PPD | 6.84[b] | |
| NEA | | 1.034[d] |
| TO | 7.50[a] | |
| TEA | 7.50[a] | 1.15,[d] 1.19[c] |
| AN | 7.70[a] | 1.28[d] |

[a] F. I. Vilesov, *Usp. Fiz. Nauk*, **81**, 669 (1963). [b] K. Tsuji, M. Saito, and T. Tani, *Denki Kagaku*, **41**, 688 (1973). [c] N. L. Weinberg and H. R. Weinberg, *Chem. Rev.*, **68**, 449 (1968). [d] The value estimated by using the relation between ionization potential and polarographic half-wave potential. See E. S. Pysh and N. C. Yang, *J. Am. Chem. Soc.*, **85**, 2124 (1963).

PPD, it is possible to analyze ketyl radical formation and ionic photodissociation since the PPD cation has slight absorption at a longer wavelength region than 530 nm.[18] Using the above values of molar absorption coefficients, quantum yields obtained for ketyl radical formation and ionic photodissociation were 0.8 and 0.2, respectively.

## Discussion

The present laser photolysis studies of triplet BP will be discussed from the following viewpoints: solvent effect and mechanism of hydrogen abstraction.

*Solvent Effect.* The difference of quantum yields for ionic photodissociation in several solvents was first demonstrated and explained for the pyrene–*N,N*-dimethylaniline system by Taniguchi et al.[19] They estimated the free energies of solvated ion pair and dissociated ion radical states, and showed that the yield of ionic dissociation increases and the free energies of ion states are lowered as the solvent dielectric constant is increased. We have also calculated the free energies of ion states of BP–amine systems in the same way, and typical examples are given in Figure 8. The values of oxidation potentials of amines used are summarized in Table I. The reduction potential of BP is −1.84 eV.[20] In the case of the BP–TEA–acetonitrile system both initial and dissociated ion radical states have almost the same energy and no BP anion was detected appreciably in the course of quenching reaction. Recent transient photocurrent measurement showed that ionic dissociation occurs in the pyrene–TEA acetonitrile system with a quantum yield of 0.15 although the free energies of excited pyrene and dissociated ionic states are almost equal.[21] The difference between BP–TEA and pyrene–TEA systems may be explained as follows. The competing so-called hydrogen abstraction process is rather fast and dissociation is suppressed in the former system.

The acetonitrile solution of BP containing PPD is an interesting system from the viewpoint of energetic consideration. As shown in Table I the ionization potential of PPD is lower than that of DEA. Then, the ion radical state of this system has a lower energy than that of the BP–DEA system in acetonitrile. Although this means that the quantum yield for ion formation is expected to be about 1.0, the observed value for ion formation is 0.2. Therefore, another quenching path competing with ionic photodissociation in the BP–PPD–acetonitrile system is faster than that of the BP–DEA–acetonitrile system.

Ionic dissociation to BP anion and DEA cation occurs in pyridine, acetone, and acetonitrile, consistent with the energetic consideration shown in Figure 8. Now the following may be concluded from a consideration of the quantum yield for ionic photodissociation (Figures 6–8 and Table I). Ionic dissociation is possible only when the final ionic state is lower in energy than the initial state (triplet BP). However, the quantum yield for ionic dissociation is determined by a delicate balance between dissociation and competing processes. Although in the case of the pyrene–quencher system the energetic consideration may be enough to explain the solvent effect, it is complicated in the present BP system.

*Mechanism of Hydrogen Abstraction of BP.* The rate constant for photoreduction of BP with amines is faster than that of BP with alkanes and alcohols. It has been proposed that the enhanced rate is due to the stepwise mechanism of electron transfer followed by proton transfer. However, no direct observation of this process has been given and the complicated problem of the degree of CT has been discussed.[22,23] The CT quenching of triplet ketones may be summarized into following two groups.[24] The first is of fluorenone, 2-naphthaldehyde, and 2-acetonaphthone, whose lowest triplet states are of $\pi$–$\pi^*$ character. Solvent effect on the quenching rate constant, $k_q$, is efficient and the slope of the linear relation between log $k_q$ and ionization potential is rather large. BP and acetone belong to the second group whose triplet is of n–$\pi^*$ character. No efficient solvent effect on $k_q$ is observed and the slope of plot of log $k_q$ vs. ionization potential is smaller than that observed in the case of complete electron transfer quenching.[25] The CT degree required for the photoreduction of BP are still unclear and the contributions of direct (not stepwise) hydrogen abstraction are not neglected.[22,26] Moreover, it has been pointed out that the direct transfer of a H atom is also accelerated by CT interaction.[5] The problem with this mechanism will be discussed from the viewpoint of solvent effect on ionic photodissociation.

Ionic photodissociation in polar solvents has been directly observed by flash and laser photolysis methods in the

case of aromatic hydrocarbons quenched by aromatic amines as well as nitriles.[19,27] These systems show exciplex emission only in nonpolar solvents and the electronic structures of fluorescent states were deemed to be quite polar, as revealed by $S_n \leftarrow S_1$ absorption spectral measurements and by analysis of solvent effect on exciplex emission.[28-30] On the other hand, the partial CT interaction and less polar structure were confirmed in the case of hexamethylbenzene–biphenyl and naphthalene–naphthonitrile systems.[30] Since these exciplexes show emission even in polar solvents, no ionic photodissociation may be expected. Hence, it is suggested that almost complete CT in the encounter collisional complex is required for ionic dissociation. Detailed analysis of the latter process was obtained for the pyrene–*N,N*-dimethylaniline system in pyridine by measuring the laser-induced photocurrent. The rapid rise of the transient current, which is faster than the decay of exciplex ($\tau \sim 20$ nsec), was observed and its rising curve was identical with the time-integrated function of an exciting pulse.[31] The exciplex formation and ionic photodissociation were concluded to compete with each other in the encounter collisional complex. Moreover, it was shown by time-resolved fluorescence spectra that solvent orientation–relaxation is required for exciplex formation.[32] Hence, photodissociation to solvated ion pairs or ion radicals is considered to consist of electron transfer followed by solvation.

The free-energy difference between excited quenchee and ion radicals, which was calculated for pyrene–*N,N*-dimethylaniline in some solvents, is almost equal to those of BP–DEA and BP–DMT systems. Moreover, the quenching rate constant is a diffusion-limited one both for pyrene and BP systems. Hence, the same mechanism of ionic photodissociation may be expected in the present BP–amine system. Considering the above conclusion, the present result on competing processes of ionic photodissociation and hydrogen abstraction may be reduced to the competition between solvation and proton transfer. Then the reaction mechanism is given as follows:

$$^3BP + A_mH \longrightarrow {}^3(BP^- \cdots A_mH^+)^{\ddagger} \begin{cases} \nearrow BP_s^- + A_mH_s^+ \\ \searrow BPH\cdot + A_m\cdot \end{cases}$$

$A_mH$, BPH·, and $A_m$· represent amine, ketyl radical, and resultant amine radical, respectively. $(BP^- \cdots A_mH^+)^{\ddagger}$ is an encounter collisional complex with high CT and is a nonrelaxed state for solvent orientation. The subscript s represents the solvated state. Hence, it is concluded that the hydrogen abstraction reaction in BP–DEA and BP–DMT systems consists of two steps, electron transfer and proton transfer, and that the relaxation time of solvent orientation is a useful guide to the present consideration.

In the case of TEA, AN, TO, and NEA donors the mechanism of ketyl radical formation is less clear. One possible explanation is due to the same mechanism as in the case of DEA and DMT donors. Because of the relative high values of the ionization potential, which results in a high free energy of the final ionic state, the ionic dissociation occurs slightly as shown in Figure 7. The behavior of the BP–TEA system may be interpreted on this model at present. Another is based on the consideration of the importance of the hydrogen atom bonded to the N atom of the donor. The quantum yield for ionic dissociation of the BP–PPD system in acetonitrile is lower than unity although the latter ionization potential is smaller than that of DEA. This may be due to the faster rate of proton transfer in the above scheme, or to rapid direct hydrogen atom transfer, which competes with electron transfer in the encounter complex. Hence, the second explanation may be given to the results on BP–AN, BP–TO, and BP–NEA systems.

## References and Notes


(1) N. J. Turro, "Molecular Photochemistry", Benjamin, New York, N.Y., 1967; J. G. Calvert and J. N. Pitts, "Photochemistry", Wiley, New York, N.Y., 1967.
(2) S. G. Cohen, A. Parola, and G. H. Parsons, *Chem. Rev.*, **73**, 1411 (1973).
(3) S. G. Cohen and H. M. Chao, *J. Am. Chem. Soc.*, **90**, 165 (1968); S. G. Cohen and J. I. Cohen, *ibid.*, **89**, 164 (1967); *J. Phys. Chem.*, **72**, 3782 (1968).
(4) R. F. Bartholomew, R. S. Davidson, P. F. Lambeth, J. F. Mckellar, and P. H. Tuner, *J. Chem. Soc., Perkin Trans. 2*, 577 (1972).
(5) S. Arimitsu and H. Tsubomura, *Bull. Chem. Soc. Jpn.*, **45**, 1357 (1972).
(6) S. Arimitsu and H. Masuhara, *Chem. Phys. Lett.*, **22**, 543 (1973).
(7) H. Masuhara, M. Shimada, N. Tsujino, and N. Mataga, *Bull. Chem. Soc. Jpn.*, **44**, 3310 (1971).
(8) G. Porter and M. R. Topp, *Proc. R. Soc., Ser. A*, **315**, 163 (1970).
(9) R. M. Hochstrasser, H. Lutz, and G. W. Scott, *Chem. Phys. Lett.*, **24**, 162 (1974).
(10) H. Tubomura, N. Yamamoto, and S. Tanaka, *Chem. Phys. Lett.*, **1**, 309 (1967); T. S. Godfrey, J. W. Halpern, and G. Porter, *ibid.*, **1**, 490 (1967).
(11) T. Shida and W. H. Hamill, *J. Chem. Phys.*, **44**, 2375 (1966).
(12) A. Beckett and G. Porter, *Trans. Faraday Soc.*, **59**, 2038 (1963).
(13) E. Land and G. Porter, *Trans. Faraday Soc.*, **59**, 2027 (1963).
(14) R. S. Davidson and P. F. Lambeth, *Chem. Commun.*, 511 (1968).
(15) P. J. Wagner and A. E. Kemppainen, *J. Am. Chem. Soc.*, **91**, 3085 (1969).
(16) G. Porter and F. Wilkinson, *Trans. Faraday Soc.*, **57**, 1686 (1961).
(17) Although the band position of the BP anion varies slightly with change of solvent, we estimated the concentration of the BP anion by measuring the absorption at 660 nm in all solvents used.
(18) H. Tsubomura, K. Kimura, H. Yamada, and M. Kato, *Tetrahedron Lett.*, 4217 (1965).
(19) Y. Taniguchi, Y. Nishina, and N. Mataga, *Bull. Chem. Soc. Jpn.*, **45**, 764 (1972).
(20) R. O. Loutfy and R. O. Loutfy, *J. Phys. Chem.*, **77**, 336 (1973).
(21) T. Hino, H. Masuhara, and N. Mataga, to be published.
(22) J. B. Guttenplan and S. G. Cohen, *J. Am. Chem. Soc.*, **94**, 4040 (1972).
(23) P. J. Wagner and R. A. Leavitt, *J. Amer. Chem. Soc.*, **95**, 3669 (1973).
(24) S. G. Cohen, G. A. Davis, and W. D. K. Clark, *J. Amer. Chem. Soc.*, **94**, 869 (1972); J. B. Guttenplan and S. G. Cohen, *Tetrahedron Lett.*, 2163 (1972).
(25) D. Rehm and A. Weller, *Ber. Bunsenges. Phys. Chem.*, **73**, 834 (1969).
(26) R. W. Yip, R. O. Loutfy, Y. L. Chow, and L. K. Magdzinski, *Can. J. Chem.*, **50**, 3426 (1972).
(27) T. Okada, H. Oohari, and N. Mataga, *Bull. Chem. Soc. Jpn.*, **43**, 2750 (1970); H. Yamashita, H. Kokubun, and M. Koizumi, *ibid.*, **41**, 2312 (1968); K. Kawai, N. Yamamoto, and H. Tsubomura, *ibid.*, **42**, 369 (1969); H. Leonhardt and A. Weller, *Ber. Bunsenges. Phys. Chem.*, **67**, 791 (1963); H. Knibbe, D. Rehm, and A. Weller, *ibid.*, **72**, 257 (1968); K. H. Grellmann, A. R. Watkins, and A. Weller, *J. Lumin.*, **1, 2**, 678 (1970); K. H. Grellmann, A. R. Watkins, and A. Weller, *J. Phys. Chem.*, **76**, 469, 3132 (1972); D. Dmitriefski and A. N. Terenin, *Dokl. Akad. Nauk SSSR*, **151**, 122 (1963).
(28) R. Potashnik, C. R. Goldschmidt, M. Ottolenghi, and A. Weller, *J. Chem. Phys.*, **55**, 5344 (1971); T. Okada, T. Fujita, M. Kubota, S. Masaki, N. Mataga, R. Ide, Y. Sakata, and S. Misumi, *Chem. Phys. Lett.*, **14**, 563 (1972).
(29) N. Nakashima, N. Mataga, F. Ushio, and C. Yamanaka, *Z. Phy. Chem. (Frankfurt am Main)*, **79**, 150 (1972); N. Nakashima, N. Mataga, and C. Yamanaka, *Int. J. Chem. Kinet.*, **5**, 833 (1973).
(30) H. Beens and A. Weller, *Acta Phys. Polon.*, **34**, 593 (1968); S. Masaki, T. Okada, and N. Mataga, to be published.
(31) Y. Taniguchi and N. Mataga, *Chem. Phys. Lett.*, **13**, 596 (1972).

# Pulse Radiolysis Study of Imidazole and Histidine in Water

P. S. Rao,[1a] M. Simic,[1b] and E. Hayon*[1a]

*Pioneering Research Laboratory, U.S. Army Natick Laboratories, Natick, Massachusetts 01760, and Zoology Department, University of Texas, Austin, Texas 78712* *(Received November 22, 1974)*

*Publication costs assisted by Natick Laboratories*

The reaction rate constants of $e_{aq}^-$ and OH radicals with imidazole (ImH), *N*-methylimidazole (MeIm), histidine, and *N*-methylhistidine were determined. The $k(e_{aq}^- + S)$ values were strongly dependent on the state of protonation of the "pyridine" nitrogen in these molecules, with rates of $\sim 5 \times 10^9\ M^{-1}\ sec^{-1}$ at pH ~6.0 and $(\sim 1\text{–}2) \times 10^7\ M^{-1}\ sec^{-1}$ at pH ~10.0. The $k(OH + S)$ values show only small but significant changes with pH with rates of $\sim 5 \times 10^9\ M^{-1}\ sec^{-1}$ at pH 4–5 and $\sim 9.0 \times 10^9\ M^{-1}\ sec^{-1}$ at pH 9–10. The transient absorption spectra of the $e_{aq}^-$ and OH radical adducts to these molecules were observed. For $e_{aq}^-$ addition to imidazole at pH ~5.0, the $ImH_2$· radical suggested to be formed has maxima at 300 and 360 nm and $\epsilon_{300}$ $5.6 \times 10^3\ M^{-1}\ cm^{-1}$; the MeImH· radical has maxima at 310 and 360 nm with $\epsilon_{360}$ $6.1 \times 10^3\ M^{-1}\ cm^{-1}$. The OH radical adducts to $ImH_2^+$ and ImH have maxima at 295 and 400 nm and at 310 and 390 nm, respectively. A $pK_a$(radical) = 6.1 is observed for the equilibrium $OH\text{·}ImH_2^+ \rightleftharpoons OH\text{·}ImH + H^+$, which is close to $pK_a = 7.1$ for loss of a proton from the "pyridine" nitrogen of imidazole. The results from the OH radical adduct to *N*-methylimidazole support this assignment. Similar results were obtained for histidine and *N*-methylhistidine. The decay kinetics of the free-radical intermediates were determined.

## Introduction

One of the important properties of the imidazole ring is the presence of both a tertiary ("pyridine") and a secondary ("pyrrole") nitrogen.[2] The first nitrogen carries a net negative charge in the molecule and will consequently be a center for electrophilic attack. The second nitrogen carries a net positive charge in the molecule. As a result there is a possibility of mutual interconversion of the nitrogen atoms in the imidazole ring. In slightly acidic solutions when the tertiary nitrogen becomes protonated, the two nitrogens become indistinguishable and transformation changes may result.

The reactions and sites of attack of free radicals on the imidazole nucleus have not been examined in detail. Free radicals add primarily to the ring as demonstrated from ESR investigations.[3,4] Reported below is a pulse radiolysis study of the optical spectra and acid–base properties of the intermediates produced form the reaction of $e_{aq}^-$ and OH radicals in water with imidazole, histidine, and their methyl derivatives.

## Experimental Section

The pulse radiolysis equipment and the experimental procedures used have already been described.[5,6] Single pulses of 2.3-MeV electrons and ~30-nsec duration were employed. The radiolysis of water produces the reaction

$$H_2O \longrightarrow e_{aq}^-\ (2.8),\ OH\ (2.8),\ \text{and}\ H\ (0.6)$$

where the numbers in parentheses are the *G* values (yields per 100 eV) of the radicals. The extinction coefficients reported were based on these *G* values and the KCNS dosimetry.[5]

The chemicals used were the best research grade available. Imidazole and histidine were obtained from Calbiochem; their *N*-methyl derivatives were Aldrich and K & K Laboratories products. The reagents were purchased from Baker and Adamson, Mallinckrodt, and Eastman Chemicals. The solutions were buffered with perchloric acid, potassium hydroxide, and ~1 m*M* phosphates and tetraborate.

**TABLE I: Rate Constants of the Reactions of $e_{aq}^-$ and OH Radicals with Imidazole and Histidine in Water**

| Substrate[a] | pH | $k(e_{aq}^- + S)$, $M^{-1}\ sec^{-1}$ | pH | $k(OH + S)$,[c] $M^{-1}\ sec^{-1}$ |
|---|---|---|---|---|
| Imidazole | 6.3 | $4.3 \times 10^9$ [b] | 3.4 | $5.5 \times 10^9$ |
| (7.1, 14.5) | 10.9 | $2.0 \times 10^7$ | 6.8 | $8.7 \times 10^9$ |
| | | | 10.9 | $1.2 \times 10^{10}$ |
| *N*-Methyl- | 6.0 | $1.9 \times 10^{10}$ | 5.4 | $5.0 \times 10^9$ |
| imidazole (7.0) | 10.2 | $3.3 \times 10^7$ | 9.4 | $8.1 \times 10^9$ |
| Histidine | 5.9 | $3.9 \times 10^9$ [b] | 6–7 | $5.0 \times 10^9$ [d] |
| (6.0, 9.2) | 11.1 | $1.2 \times 10^7$ [b] | | |
| *N*-Methylhistidine | 6.0 | $5.1 \times 10^9$ | | |
| (6.6, 8.6) | 10.9 | $2.2 \times 10^7$ | | |

[a] Numbers in parentheses are the $pK_a$ values. [b] From ref 7. [c] Rates determined by following the formation kinetics of the intermediates at the appropriate wavelength (see text). [d] From ref 10.

## Results and Discussion

*Reaction with $e_{aq}^-$.* Imidazole and histidine have $pK_a$'s of 7.1 and 6.0, respectively, for loss of a proton from the "pyridine" nitrogens. The reactivity of $e_{aq}^-$ with these molecules is strongly dependent on these ionization constants. Table I gives the $k(e_{aq}^- + S)$ values with imidazole, *N*-methylimidazole, histidine, and *N*-methylhistidine determined at two pH values. Values from the literature[7] are also included. These rates were determined in the presence of ~1.0 *M tert*-butyl alcohol (to scavenge the OH radicals[5]) and 1 atm of argon, by monitoring the decay kinetics of $e_{aq}^-$ at 700 nm in the presence of different concentrations of the substrates. The rate of $e_{aq}^-$ with, for example, ImH (ImH = imidazole) is ~500 times slower than the rate with $ImH_2^+$. Methylation of the "pyrrole" hydrogen in imidazole gives very similar results (Table I).

**TABLE II: Absorption Maxima, Extinction Coefficients, Ionization Constants, and Decay Kinetics of the Intermediates Produced from the Reaction of $e_{aq}^-$ and OH Radicals with Imidazole and Histidine**

| Substrate[a] | Reactant | pH | $\lambda_{max}$, nm | $\epsilon_{max}$, $mM^{-1}$ $cm^{-1}$ | $2k$, $M^{-1}$ $sec^{-1}$ | $pK_a$ (radical) | Suggested radical |
|---|---|---|---|---|---|---|---|
| Imidazole (7.1, 14.5) | $e_{aq}^-$ | 5.0 | 300, 360 | 5.6, 2.0 | $2.1 \times 19^9$ | | $ImH_2$· |
| *N*-Methylimidazole (7.0) | $e_{aq}^-$ | 5.0 | 310, 360 | 6.1, 2.5 | $2.3 \times 10^9$ | | MeImH· |
| Histidine (1.8, 6.0, 9.2) | $e_{aq}^-$ | 5.2 | 295, 370 | 4.7, 1.7 | $8.0 \times 10^8$ | | $HisH_2$· |
| *N*-Methylhistidine (6.6, 8.6) | $e_{aq}^-$ | 5.2 | 320, 375 | 4.9, 2.0 | $7.9 \times 10^8$ | | MeHisH· |
| Imidazole (7.1, 14.5) | OH | 4.4 | 295, 400 | 3.3, 1.4 | | 6.1 | OH·$ImH_2^+$ |
| | OH | 8.5 | 310, 390 | 5.5, 1.2 | $5.5 \times 10^9$ | | OH·ImH |
| *N*-Methylimidazole (7.0) | OH | 4.0 | 310, 400 | 4.1, 1.4 | | 6.2 | OH·MeImH$^+$ |
| | OH | 10.0 | 320, 390 | 5.5, 1.2 | $4.8 \times 10^9$ | | OH·MeIm |
| Histidine (1.8, 6.0, 9,2) | OH | 3.5 | 300, 410 | 4.2, 1.4 | | 5.2 | OH·$HisH_2^+$ |
| | OH | 9.2 | 310, 410 | 6.2, 2.3 | $1.2 \times 10^9$ | | OH·HisH |
| *N*-Methylhistidine (6.6, 8.6) | OH | 3.8 | 305, 425 | 4.0, 0.7 | | 5.2 | OH·MeHisH$^+$ |
| | OH | 7.3 | 310, 420 | 5.8, 1.4 | $2.0 \times 10^9$ | | OH·MeHis |

[a] Numbers in parentheses are the $pK_a$ values.

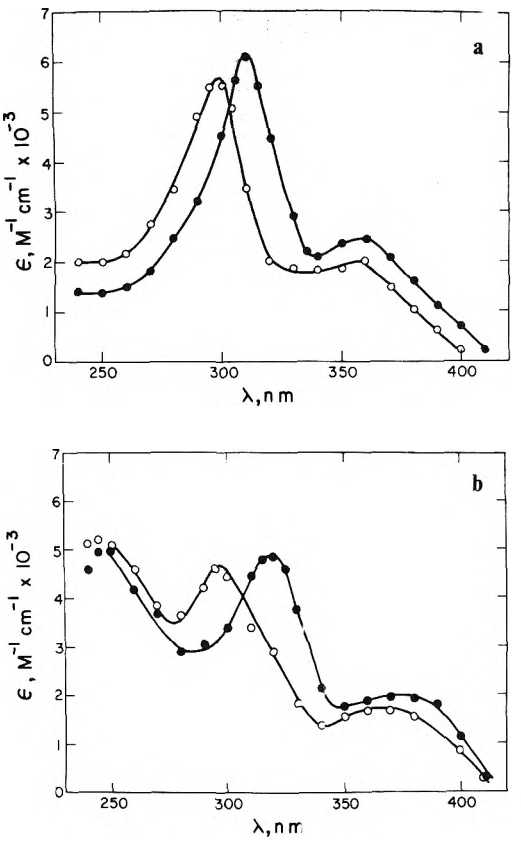


**Figure 1.** Absorption spectra of the intermediates formed from the addition of $e_{aq}^-$ (a) to imidazole (○, pH 5 0, 3 m*M*) and *N*-methylimidazole (●, pH 5.0, 1 m*M*) and (b) to histidine (○, pH 5.2, 2 m*M*) and *N*-methylhistidine (●, pH 5.2, 2 m*M*). A 1.0 *M* concentration of *t*-BuOH was present in these solutions; total dose ~2.7 krads/pulse.

On pulse radiolysis of aqueous solutions of 3 m*M* imidazole at pH 5.0, in the presence of 1.0 *M* *t*-BuOH and 1 atm of argon, a relatively strong transient absorption spectrum is observed with maxima at 300 and 360 nm and extinction coefficients of $5.6 \times 10^3$ and $2.0 \times 10^3$ $M^{-1}$ $cm^{-1}$, respectively; see Figure 1a and Table II. The $e_{aq}^-$ is suggested to add to the "pyridine" nitrogen, via reaction 1, to form radical I.

$$e_{aq}^- + ImH_2^+ \longrightarrow ImH_2\cdot \quad (1)$$


I II

A red shift in the spectrum is observed for radical II formed from the reaction of $e_{aq}^-$ with *N*-methylimidazole at pH 5.0. Radical II has similar extinction coefficients; see Figure 1a and Table II. Due to the low reactivity of $e_{aq}^-$ with the neutral imidazole and *N*-methylimidazole molecules and the high reactivity of the compounds toward OH radical (see below), it was not possible to examine the transient spectra of the electron adducts in alkaline solutions under proper experimental conditions.

The spectra of the intermediates produced from the reaction of $e_{aq}^-$ with histidine and *N*-methylhistidine at pH 5.2 are shown in Figure 1b and Table II. These spectra are quite similar to those observed from imidazole. While the majority of $e_{aq}^-$ are expected to add to the imidazole ring, one cannot exclude the possibility that a small fraction of $e_{aq}^-$ may lead to deamination[8,9] of the side-chain amino acid. The resulting radical would absorb over the same wavelength region as the $e_{aq}^-$ adduct but is expected to have a much lower extinction coefficient.[8]

The electron adducts to the four substrates examined decay by second-order kinetics (Table II). The decay rates of the histidine and *N*-methylhistidine radicals, $2k = 8.0 \times 10^8$ $M^{-1}$ $sec^{-1}$, are a factor of ~3 slower than those of the corresponding imidazole radicals. Under the experimental conditions used, some reaction with the *t*-BuOH radical cannot be excluded.

*Reaction with OH Radicals.* Hydroxyl radicals react with imidazole, histidine, and their *N*-methyl derivatives very rapidly; see Table I. These rates were determined by following the formation kinetics of the intermediates produced from this reaction at the wavelengths where they absorb. From the pseudo-first-order rates, the second-order rate constants were determined. The rate of OH reacting with histidine derived[10] by competition kinetics with KCNS is also given in Table I. A small but significant increase in the $k$(OH + S) rate is observed in alkaline solution, beyond the $pK_a$ of the "pyridine" nitrogen. These re-

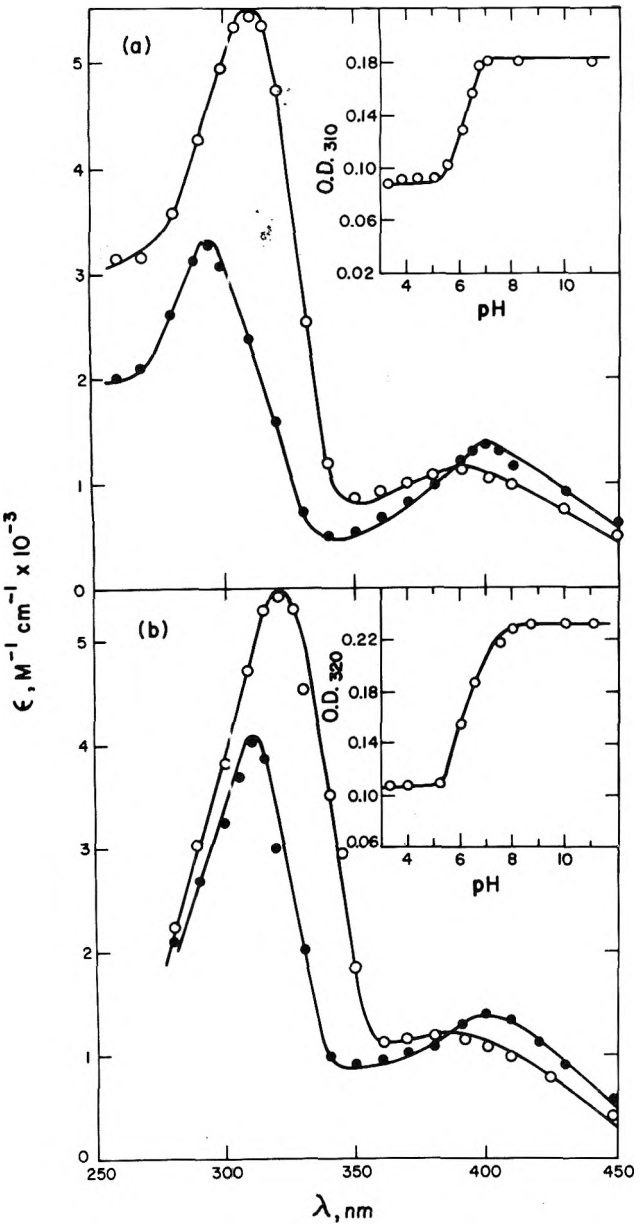


**Figure 2.** Absorption spectra of the intermediates formed from the addition of OH radicals to (a) 2 m*M* imidazole at pH 4.4 (●) and pH 8.5 (O) and (b) 2 m*M* *N*-methylimidazole at pH 4.0 (●) and pH 10.0 (O). Solutions were saturated with $N_2O$; total dose ~2.4 krads/pulse.

sults are consistent with other observations on the dependence of this rate upon the state of protonation of the nitrogen atom in amines[11] and amino acids.[12]

Figure 2a shows the transient absorption spectra produced from the reaction of OH radicals with imidazole at pH 4.4 and 8.5. It is interesting to note that the maxima of the two bands at pH 8.5 are closer to each other than the corresponding bands at pH 4.4. This would seem to suggest that more than one radical adduct is formed. Such a conclusion was also reached from ESR work,[4] and it was suggested that OH radicals add at $C_2$ and $C_5$ positions. Radicals III and IV are the suggested structure at pH > p$K_a$ (radical) = 6.1 (see below). On monitoring the change in absorbance at 310 nm with pH, a titration curve is observed with p$K_a \approx 6.1$ (see Figure 2a). This value is close to the p$K_a$ of imidazole and suggests that in acid solutions radicals V and VI are present. One cannot exclude some protonation at the pyrrole nitrogen.

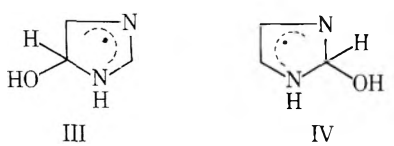

III IV

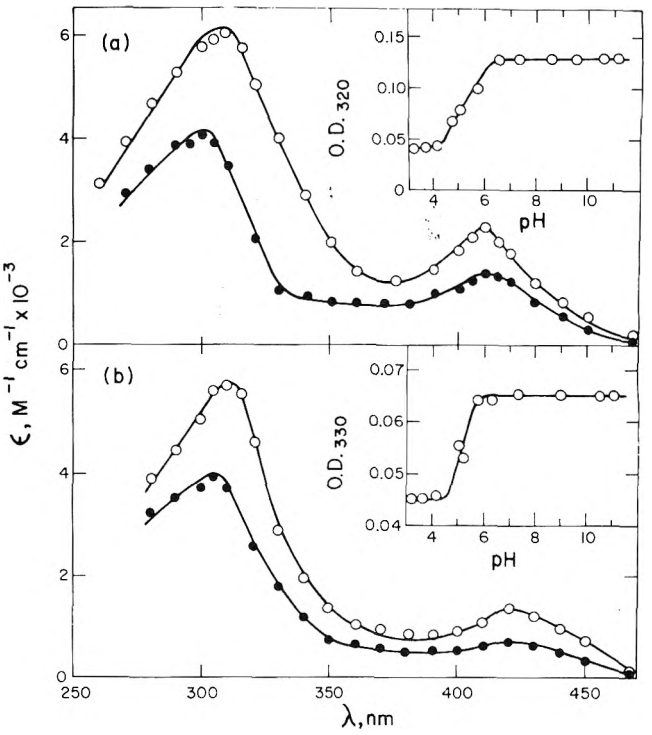


**Figure 3.** Absorption spectra of the intermediates formed from the reaction of OH radicals with (a) 1 m*M* histidine at pH 3.5 (●) and pH 9.2 (O) and (b) 1 m*M* *N*-methylhistidine at pH 3.8 (●) and pH 7.3 (O). Solutions were saturated with $N_2O$; total dose ~2.4 krads/pulse.

V VI

Figure 2b shows the corresponding results with *N*-methylimidazole. A p$K_a$ of 6.2 is observed in this case, indicating that deprotonation of the "pyrrole" -NH- hydrogen is not involved in this acid–base equilibrium reaction.

In alkaline solutions at pH ≥11.0, the spectrum of the OH adduct of imidazole undergoes changes which could not be monitored conveniently. Dehydration of radicals III and IV in alkaline solution has been suggested[4] leading to the deprotonation of the >NH group.

The reaction of OH radicals with histidine and *N*-methylhistidine gave intermediates with absorption spectra similar to those observed from imidazole; see Figure 3. The observed p$K_a$ (see Insert, Figure 3) is also in agreement with the p$K_a$ values of the parent compounds.

These radicals decay by second-order kinetics and the rates are given in Table II.

*Effect of Oxygen.* The reaction of oxygen with the OH radical adduct of imidazole and *N*-methylimidazole was examined in solutions containing 13 m*M* $N_2O$ (½ atm) and 0.7 m*M* $O_2$ (½ atm) in order (a) to convert all the $e_{aq}^-$ to OH radicals, reaction 2, and (b) for all the OH adducts to

$$e_{aq}^- + N_2O \longrightarrow OH + N_2 + OH^- \qquad (2)$$

react fast with $O_2$, reaction 3. At these concentrations of

$$OH\cdot ImH + O_2 \longrightarrow OH\cdot ImHO_2 \quad (3)$$

$N_2O$ and $O_2$, and using 1 m*M* substrates, essentially all the $e_{aq}^-$ react with $N_2O$, $k_2 = 8.6 \times 10^9\ M^{-1}\ sec^{-1}$.[7] Typically, the rate of reaction 3 is $\sim 10^9\ M^{-1}\ sec^{-1}$ so that the formation of the peroxy radical $OH\cdot ImHO_2$ is complete in $\leq 1.5$ μsec. At this time, less than 5% of the OH·ImH radicals have decayed.

The transient spectra observed on pulse radiolysis of 1 m*M* imidazole in the presence of 0.7 m*M* $O_2$ and 13 m*M* $N_2O$ at pH 3.3, 5.3, and 9.3 did not show absorption maxima at ~310 and ~390 nm (cf. Figure 2), absorbances read at ~20 μsec after the pulse. Instead of the OH·ImH radical absorptions, much weaker absorptions were found with maxima at ≤230 nm. Such absorption spectra are characteristic of organic peroxy radicals.[5,13-16] Addition of $O_2$ to the OH adduct of histidine has already been shown using the benzoquinone titration method.[17]

## References and Notes


(1) (a) U.S. Army Natick Laboratories. (b) University of Texas.
(2) B. Pullman and A. Pullman, "Quantum Biochemistry", Interscience, New York, N.Y., 1963; R. J. Suneberg and R. B. Martin, *Chem. Rev.*, **74**, 471 (1974).
(3) P. H. Kasai and D. McLeod, Jr., *J. Am. Chem. Soc.*, **95**, 27 (1973).
(4) A. Samuni and P. Neta, *J. Phys. Chem.*, **77**, 1629 (1973).
(5) M. Simic, P. Neta, and E. Hayon, *J. Phys. Chem.*, **73**, 3794 (1969).
(6) J. P. Keene, E. D. Black, and E. Hayon, *Rev. Sci. Instrum.*, **40**, 1199 (1969).
(7) M. Anbar, M. Bambenek, and A. B. Ross, *Natl. Stand. Ref. Data Ser., Natl. Bur. Stand.*, **No. 43** (1973).
(8) M. Simic and E. Hayon, *Radiat. Res.*, **48**, 244 (1971).
(9) J. P. Mittal and E. Hayon, *J. Phys. Chem.*, **78**, 1790 (1974).
(10) L. M. Dorfman and G. E. Adams, *Natl. Stand. Ref. Data Ser., Natl. Bur. Stand.*, **No. 46** (1973).
(11) M. Simic, P. Neta, and E. Hayon, *Int. J. Radiat. Phys. Chem.*, **3**, 309 (1971).
(12) M. Simic, P. Neta, and E. Hayon, *J. Am. Chem. Soc.*, **92**, 4763 (1970).
(13) M. Simic and E. Hayon, *J. Phys. Chem.*, **75**, 1677 (1971).
(14) E. Hayon and M. Simic, *J. Am. Chem. Soc.*, **95**, 6681 (1973).
(15) R. Stockhausen, A. Henglein, and G. Beck, *Ber. Bunsenges. Phys. Chem.*, **73**, 567 (1969).
(16) E. Hayon and M. Simic, *Acc. Chem. Res.*, **7**, 114 (1974).
(17) M. Simic and E. Hayon, *Biochem. Biophys. Res. Commun.*, **50**, 364 (1973).


# Hydrophobic Interaction in Water–*p*-Dioxane Mixtures


**A. Ben-Naim***

*Laboratory of Molecular Biology, National Institute of Arthritis, Metabolism, and Digestive Diseases, National Institutes of Health, Bethesda, Maryland 20014*

**and M. Yaacobi**

*Department of Inorganic and Analytical Chemistry, The Hebrew University of Jerusalem, Jerusalem, Israel*



*(Received September 16, 1974)*

*Publication costs assisted by the National Institutes of Health*



The solubility, standard free energy, entropy, and enthalpy of solution of methane and ethane were determined in various mixtures of water and 1,4-dioxane. The strength of the hydrophobic interaction as well as its temperature dependence were estimated from the experimental data. It is found that the hydrophobic interaction first increases upon the addition of dioxane to pure water. At higher concentration of dioxane the hydrophobic interaction gradually weakens until it reaches its relatively low value for pure dioxane. The entropy and the enthalpy changes accompanying the process of hydrophobic interaction exhibit a more abrupt behavior as a function of the mole fraction of dioxane. Namely, the anomalously large and positive values of the entropy and the enthalpy changes decrease steeply in the range of $0 \leq x_{dioxane} \leq 0.25$, and then attain almost constant values.


## I. Introduction

As a part of a more general study of the problem of hydrophobic interaction (HI),[1-6] we have recently carried out a systematic investigation of the variation of the strength of the HI and its temperature dependence in mixtures of water and ethanol.[7] This article reports a similar study in the system water–1,4-dioxane.

In its gross features the behavior of the system water–dioxane resembles that of the system water–ethanol. This is true except for a very small region of compositions where the organic component is extremely diluted in water.

In the next section we report the experimental results on the solubilities and the corresponding thermodynamic quantities of solutions of methane and ethane in mixtures of water and dioxane. In section III we process these data to compute an approximate measure of the HI and its temperature dependence. Some remarks and discussions on the results obtained are given in section IV.

The notations used throughout this paper follow closely those employed in previous articles.[7,8] By HI between two particles we refer to the *indirect* part of the work required to bring two particles from fixed positions at infinite sepa-


* To whom all correspondence should be addressed. [After August 1975 address all correspondence to: Department of Physical Chemistry, The Hebrew University, Jerusalem, Israel.]

ration to some close distance $R$. More specifically, if $U(R)$ is the *direct* pair potential operating between two (simple and spherical) particles, we define the HI between this pair at the distance $R$ by

$$\delta G^{HI}(R) = \Delta G(R) - U(R) \tag{1.1}$$

where $\Delta G(R)$ is the change of the Gibbs free energy for the process of bringing the two particles from infinite separation to the distance $R$, the process being carried out within the solvent at constant temperature $T$ and pressure $P$.

The subtraction of the direct part of the work $U(R)$ in the definition of $\delta G^{HI}$ has proved useful in achieving a relation between HI and experimental quantities. We shall omit the details of the derivation of this relation here but we quote the final result (for more details see ref 4 and 5).

The HI between two methane molecules at the distance of $\sigma_1 = 1.533$ Å (which is the C–C distance in ethane) is approximated by

$$\delta G^{HI}(\sigma_1) = \Delta\mu_{Et}^{\,0} - 2\Delta\mu_{Me}^{\,0} \tag{1.2}$$

where on the right-hand side of (1.2) we have the standard free energies of solution of methane and ethane (see the next section for a precise definition).

Relation 1.2 establishes a connection between a molecular quantity on one hand and experimental quantities on the other. This relation may be used, as we have done before, to study the strength of the HI as well as its temperature dependence in various liquids and solutions.

## II. Solubilities and Thermodynamics of Solutions of Methane and Ethane

The measurements of the solubilities of methane and ethane in mixtures of water and dioxane were carried out according to the method developed by Ben-Naim and Baer[9] with some minor modifications as suggested by Wen and Hung.[10] Methane and ethane were purchased from Matheson (with a purity of 99.97 and 99.9%, respectively). Water was doubly distilled after being run through an ion exchanger. Analytical 1,4-dioxane was used for the preparation of the solvent mixtures.

Ostwald absorption coefficients were computed directly from the measurable volume of the gas dissolved in a given volume of the solvent. A more useful definition of the Ostwald absorption coefficient $\gamma_s$ of a solute s is

$$\gamma_s = (\rho_s^{\,l}/\rho_s^{\,g})_{equil} \tag{2.1}$$

where $\rho_s^{\,l}$ and $\rho_s^{\,g}$ are the molar concentrations of the solute s in the liquid and in the gas at equilibrium.

The standard free energy of solution required for the forthcoming computations is formally defined by

$$\Delta\mu_s^{\,0} = \lim_{\rho_s^{\,g} \to 0} [-RT \ln (\rho_s^{\,l}/\rho_s^{\,g})_{equil}] \tag{2.2}$$

where the limit may be taken when either $\rho_s^{\,l}$ or $\rho_s^{\,g}$ tends to zero.

If the solubility of the gas is sufficiently low, as is the case for methane and ethane in water, one may compute $\Delta\mu_s^{\,0}$ directly from one value of $\gamma_s$ without recourse to the limiting procedure required in (2.2). In pure dioxane, however, the solubilities are appreciably larger than in water in which case the quantity, defined by

$$\Delta\mu_s^{\,0} = -RT \ln (\rho_s^{\,l}/\rho_s^{\,g})_{equil} \tag{2.3}$$

may not, in general, be identified with the conventional standard free energy change as defined in (2.2). Nevertheless there is a possibility of reinterpreting $\Delta\mu_s^{\,0}$ as a "non-conventional" standard free energy of solution (for more details the reader is referred to ref 5). For all our purposes in studying the strength of the HI and its temperature dependence, it will be sufficient to adopt the following interpretation: $\Delta\mu_s^{\,0}$ is the free energy change for transferring the solute s (presumed to be simple and spherical) from a *fixed* position in the gas to a *fixed* position in the liquid. The process being carried out at a constant temperature $T$ and pressure $P$.

With the above interpretation we may immediately write the change in entropy and in enthalpy associated with the same process, i.e.

$$\Delta S_s^{\,0} = -\partial\Delta\mu_s^{\,0}/\partial T \tag{2.4}$$

$$\Delta H_s^{\,0} = \Delta\mu_s^{\,0} + T\Delta S_s^{\,0} \tag{2.5}$$

It must be noted that the quantities $\Delta S_s^{\,0}$ and $\Delta H_s^{\,0}$ defined above differ from the conventional standard entropy and enthalpy of solution of a solute s.[5]

The experimental values of $\gamma_s$ were processed as follows. About eight values of $\gamma_s$ were measured for each solvent in the range of temperatures between 5 and 25°. Then the temperature dependence of $\Delta\mu_s^{\,0}$, computed from (2.3), was fitted to a second-degree polynomial of the form

$$\Delta\mu_s^{\,0} = a + bT + cT^2 \tag{2.6}$$

($T$ is the absolute temperature.)

Tables I and II report the coefficients $a$, $b$, and $c$ in (2.6) as well as the standard deviation for each series of measurements (Tables III–VII are available as supplementary material, see paragraph at end of text).

The smoothed values of $\Delta\mu_s^{\,0}$ obtained from (2.6) may be inverted to obtain the Ostwald absorption coefficient, these are reported in Tables III and IV.

The dependence of $\Delta\mu_s^{\,0}$ on the mole fraction of dioxane, depicted in Figures 1 and 2, is very similar to that found in the water–ethanol system.[7] A possible exception is the behavior at very dilute solution of dioxane in water. This aspect will be further discussed in section IV.

The standard entropies and enthalpies of solution of methane and ethane were computed from (2.4) and (2.5) and are reported in Tables V and VI. Figures 3–6 exhibit the composition dependence of $\Delta S_s^{\,0}$ and $\Delta H_s^{\,0}$. We note that the general appearance of these curves is very similar to the ones obtained in the water–ethanol system.[7] We estimate that the values of $\Delta S_s^{\,0}$ are accurate to within ±1.5 eu. For the values of $\Delta H_s^{\,0}$ the corresponding range would be $\pm 1.5\,T$ cal/mol.

The essential behavior is that both the entropy and the enthalpy of solution steeply decrease in the water-rich region (i.e., in the range of compositions $0 \leq x \leq 0.2$), followed by a very weak composition dependence in the remaining region.

As in the previous paper[7] we concluded that the anomalously large and negative entropy and enthalpy of solution of gases is confined to solutions in which the water is the dominant component. This anomaly quickly disappears as the mole fraction of the nonaqueous component increases beyond, e.g., $x \geq 0.2$.

## III. Hydrophobic Interaction

In the context of this paper the term HI refers to the quantity

$$\delta G^{HI}(\sigma_1) = \Delta\mu_{Et}^{\,0} - 2\Delta\mu_{Me}^{\,0} \tag{3.1}$$

**TABLE I: Polynomial Coefficients in (2.6) and the Standard Deviation for Each Set of Measurements of Methane in Mixtures of Water–Dioxane**

| $X_{dioxane}$ | $c$ | $b$ | $a$ | Std dev |
|---|---|---|---|---|
| 0.00 | −0.09371 | 71.360 | −10,944.7 | 0.807 |
| 0.015 | −0.17992 | 119.80 | −17,760.1 | 1.067 |
| 0.03 | −0.03996 | 37.010 | −5,531.6 | 3.372 |
| 0.06 | −0.06330 | 47.420 | −6,618.2 | 2.295 |
| 0.09 | −0.26015 | 159.50 | −22,607.1 | 3.974 |
| 0.12 | −0.09338 | 60.790 | −8,080.5 | 2.054 |
| 0.15 | −0.12050 | 75.164 | −10,045.7 | 2.906 |
| 0.20 | −0.09391 | 58.510 | −7,584.7 | 3.012 |
| 0.40 | 0.00075 | 2.3096 | 313.4 | 2.01 |
| 0.70 | 0.04805 | −26.118 | 4,296.2 | 2.446 |
| 1.00 | 0.00988 | −4.781 | 1,099.8 | 3.997 |

**TABLE II: Polynomial Coefficients in (2.6) and the Standard Deviation for Each Set of Measurements of Ethane in Mixtures of Water–Dioxane**

| $X_{dioxane}$ | $c$ | $b$ | $a$ | Std dev |
|---|---|---|---|---|
| 0.00 | −0.11611 | 89.432 | −14,509.6 | 2.039 |
| 0.015 | −0.20115 | 136.17 | −20,962.7 | 1.753 |
| 0.03 | −0.11940 | 86.676 | −13,529.1 | 3.150 |
| 0.06 | −0.13816 | 94.065 | −14,189.3 | 4.453 |
| 0.09 | −0.04252 | −14.214 | 1,884.3 | 5.833 |
| 0.12 | −0.11005 | 72.342 | −10,532.7 | 2.019 |
| 0.15 | −0.01961 | 17.708 | −2,437.0 | 5.424 |
| 0.20 | −0.06735 | 44.768 | −6,505.4 | 1.790 |
| 0.40 | −0.08963 | 56.511 | −8,689.7 | 5.736 |
| 0.70 | −0.06322 | 40.696 | −6,717.0 | 2.677 |
| 1.00 | −0.20190 | −115.36 | 15,942.3 | 3.056 |

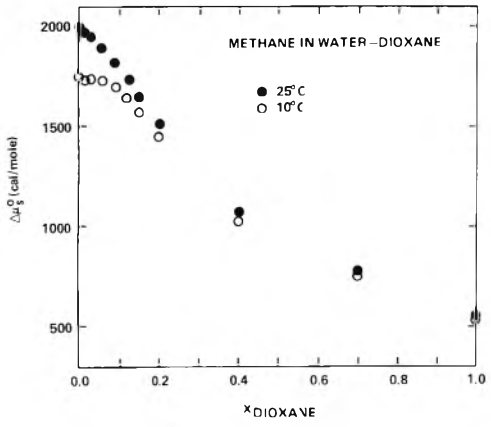


**Figure 1.** Standard free energy of solution of methane as a function of the mole fraction of dioxane at two temperatures.

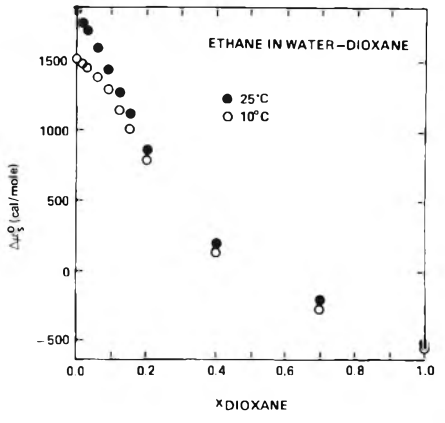


**Figure 2.** Standard free energy of solution of ethane as a function of the mole fraction of dioxane at two temperatures.

where $\Delta\mu_{Et}^0$ and $\Delta\mu_{Me}^0$ are the standard free energy of solution of ethane and methane, respectively. The quantity $\delta G^{HI}$ serves as a measure of the indirect work required to bring two methane molecules from infinite separation to a very close distance (for more details see ref 4 and 5). In this respect $\delta G^{HI}$ reflects a property of the *solvent* rather than of the solutes involved.

With the above understanding in mind we use $\delta G^{HI}$ as a convenient probe to follow the change of the property of the solvent, as a medium for HI, in the whole range of compositions of mixtures of water and dioxane.

Figure 7 depicts the variation of the strength of HI as a function of the mole fraction of dioxane. Clearly the most conspicuous feature of the curve is the strengthening of the HI as we add dioxane to pure water, in the region $0 \leq x \lesssim 0.15$, followed by a steady weakening of the HI in the remaining region of $0.15 \lesssim x \leq 1.0$. This behavior is similar, in its gross features, to the one we have observed previously in the system water–ethanol.[7] The only important difference is the behavior at very dilute solutions. Namely, addition of very small quantities of ethanol ($x \lesssim 0.05$) to water *weakens* the HI, whereas in the same region of composition dioxane strengthen the HI.

The entropy and the enthalpy change associated with

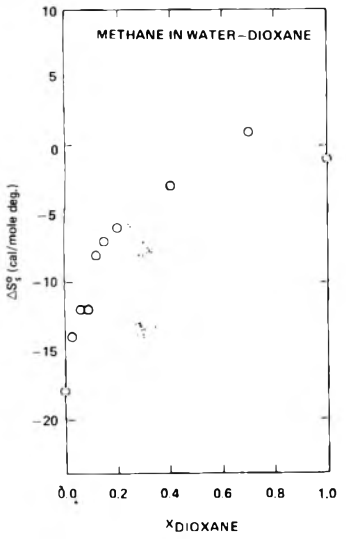


**Figure 3.** Standard entropy of solution of methane as a function of the mole fraction of dioxane at 10°.

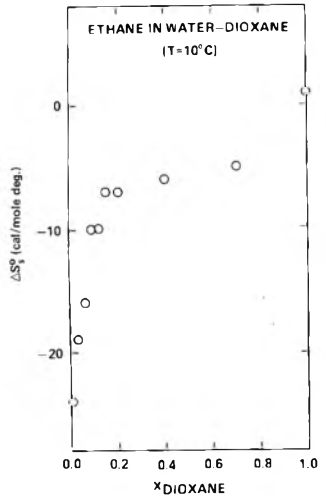


**Figure 4.** Standard entropy of solution of ethane as a function of the mole fraction of dioxane at 10°.

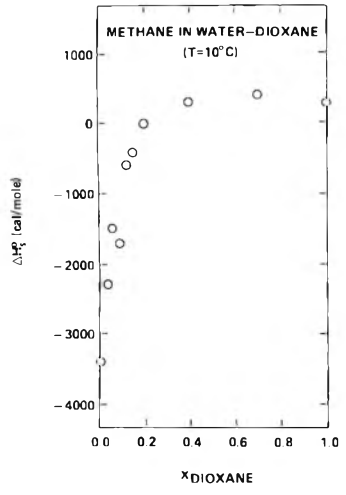


**Figure 5.** Standard enthalpy of solution of methane as a function of the mole fraction of dioxane at 10°.

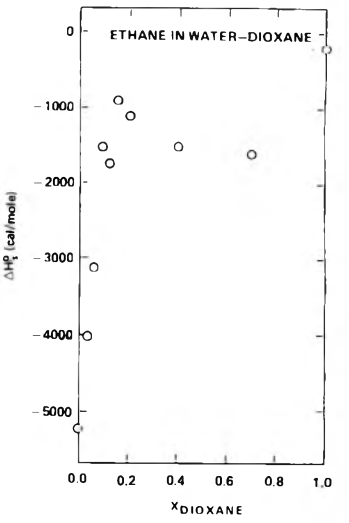


**Figure 6.** Standard enthalpy of solution of ethane as a function of the mole fraction of dioxane at 10°.

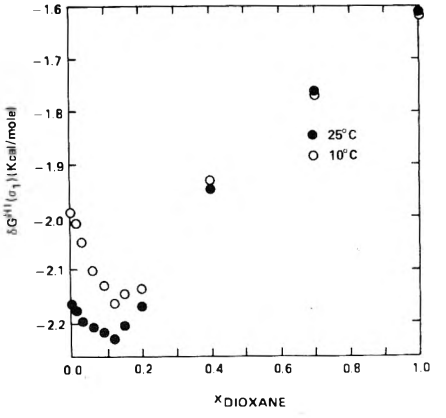


**Figure 7.** Variation of the hydrophobic interaction with the mole fraction of dioxane at two temperatures.

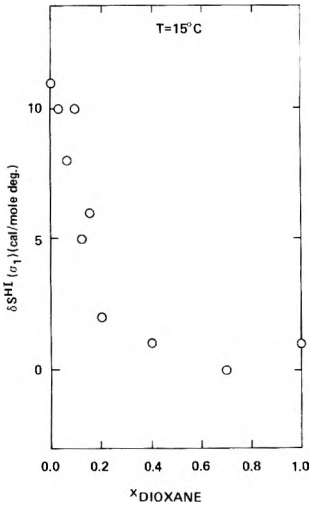


**Figure 8.** Variation of the entropy change associated with the process of hydrophobic interaction as a function of the mole fraction of dioxane at 15°.

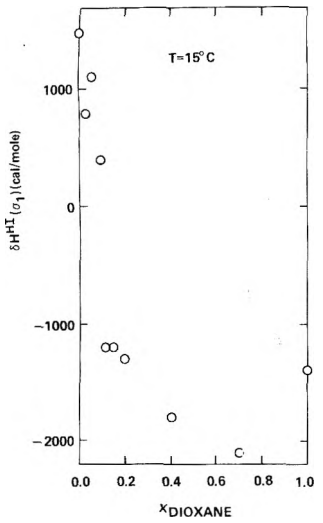


**Figure 9.** Variation of the enthalpy change associated with the process of hydrophobic interaction as a function of the mole fraction of dioxane at 15°.

the process of bringing the two methane molecules from infinite separation to a close distance is computed from the relations[5]

$$\delta S^{HI} = \Delta S_{Et}{}^{0} - 2\Delta S_{Me}{}^{0} \quad (3.2)$$

$$\delta H^{HI} = \Delta H_{Et}{}^{0} - 2\Delta H_{Me}{}^{0} \quad (3.3)$$

The dependence of $\delta S^{HI}$ and $\delta H^{HI}$ on the mole fraction of dioxane is depicted in Figures 8 and 9. Table VII includes the values of $\delta G^{HI}$, $\delta S^{HI}$, and $\delta H^{HI}$ in the system water–dioxane at two temperatures. We note again that the anomalously large values of $\delta S^{HI}$ and $\delta H^{HI}$ in water quickly disappear as we add an organic component to the solvent. In the region of $0.2 \lesssim x_{dioxane} \leq 1.0$ the values of $\delta S^{HI}$ and $\delta H^{HI}$ are almost constant. This behavior is very similar to the one observed for $\Delta S_s{}^0$ and $\Delta H_s{}^0$.

## IV. Discussion

Perhaps the most important difference between the behavior of water–ethanol as compared with water–dioxane is in the very small region of compositions where the organic component is very dilute in water.

In our previous paper[7] we have discussed a possible correlation between changes in the structure of water and changes in the strength of HI. On the basis of some experimental findings we concluded that for any reasonable definition of the "structure of water" one should expect that a small *increase* in the structure is accompanied by a small *decrease* in the strength of the HI. If this statement is correct we arrive at the conclusion that addition of dioxane to water has a destabilizing effect on the structure of water in the range of compositions $0.0 < x < 0.15$. Ethanol, on the other hand, shows a stabilization effect on the structure in the very small region of compositions $0.0 < x < 0.03$. Some theoretical arguments as to the reasons for such a stabilization effect have been discussed earlier.[5,11]

In principle it is possible that differences in the behavior of dioxane and ethanol could be detected also in the composition dependence of the entropy and the enthalpy of the HI (as well as the corresponding quantities for the process of solution). Unfortunately data are not sufficiently accurate for that purpose and the general behavior of the entropy and the enthalpy curves looks very similar in both systems.

*Acknowledgment.* This work has been supported in part by the Israel Commission for Basic Research, for which the authors are very grateful.

*Supplementary Material Available.* Tables III–VII will appear following these pages in the microfilm edition of this volume of the journal. Photocopies of the supplementary material from this paper only or microfiche (105 × 148 mm, 24× reduction, negatives) containing all of the supplementary material for the papers in this issue may be obtained from the Journals Department, American Chemical Society, 1155 16th St., N.W., Washington, D.C. 20036. Remit check or money order for $4.00 for photocopy or $2.50 for microfiche, referring to code number JPC-75-1263.

## References and Notes

(1) W. Kauzmann, *Adv. Protein Chem.*, **14**, 1 (1959).
(2) G. Némethy and H. A. Scheraga, *J. Chem. Phys.*, **36**, 3382, 3401 (1962); *J. Phys. Chem.*, **66**, 1773 (1962).
(3) G. Némethy, *Angew. Chem.*, **6**, 195 (1967).
(4) A. Ben-Naim, *J. Chem. Phys.*, **54**, 1387, 3696 (1971); **57**, 5257 (1972).
(5) A. Ben-Naim, "Water and Aqueous Solutions, Introduction to a Molecular Theory", Plenum Press New York, N.Y., 1974.
(6) C. Tanford, *Adv. Protein Chem.*, **23**, 121 (1968); **24**, 1 (1970).
(7) M. Yaacobi and A. Ben-Naim, *J. Solution Chem.*, **2**, 425 (1973).
(8) A. Ben-Naim, J. Wilf, and M. Yaacobi, *J. Phys. Chem.*, **77**, 95 (1973).
(9) A. Ben-Naim and S. Baer, *Trans. Faraday Soc.*, **59**, 2735 (1963).
(10) Wen-Yang Wen and J. H. Hung, *J. Phys. Chem.*, **74**, 170 (1970).
(11) A. Ben-Naim, *J. Statistical Phys.*, **7**, 3 (1973).

# Structure-Breaking and Structure-Promoting Processes in Aqueous Solutions

**A. Ben-Naim***

*Laboratory of Molecular Biology, National Institute of Arthritis, Metabolism, and Digestive Diseases, National Institutes of Health, Bethesda, Maryland 20014* *(Received November 13, 1974; Revised Manuscript Received March 7, 1975)*

*Publication costs assisted by the National Institutes of Health*

A new measure is devised to estimate the structural changes in the solvent induced by processes occurring in aqueous solutions. This measure relates the isotope effect in the standard free energy of the process involved, in light and heavy water, with the change in the average number of hydrogen bonds that occurs in the solvent. Some numerical examples for the process of dissolution are presented, from which one can classify solutes as either structure promoters or structure breakers. A possible generalization of this method for more complicated processes is also indicated.

## 1. Introduction

The classification of solutes, dissolved in water, as "structure breakers" and "structure promoters" has been the subject of a great number of research works.[1-4] These concepts have evolved from the two fundamental works of Bernal and Fowler,[5] and Frank and Evans,[6] on the properties of aqueous solutions.

These authors were, perhaps, the first to recognize and to stress the importance of the role of the "structure of water" in the understanding of the unusual properties of aqueous solutions.

Yet in spite of the large number of articles written on this subject, the very basic questions of how to define the "structure of water" and which experiment should be done to measure the "structural changes" in water were left unanswered.

To be sure, there has been a great deal of discussion on this topic, nevertheless in most cases it appears that this subject has evaded a quantitative treatment. To cite one example out of many, suppose one measures the viscosity of pure water. Then the same measurement is carried out in aqueous solutions of various solutes. Now if a solution is found to have a larger viscosity than that of pure water, the traditional interpretation of such an observation is that the added solute has increased the "structure of the solvent".

Clearly because of the ambiguity in the very meaning of the "structure of water" as conceived by different authors, and because of a lack of a clear-cut relationship between the measurable quantity on one hand, and the changes of the structure of water on the other, there has been a widespread disagreement among authors who have used different experimental techniques.

The central purpose of this article is, in a way, to fill the gap in this field. In the first place we shall present a quantitative measure of the "structure of water" which we believe is in close conformity with current views on this concept as expressed by many authors. Furthermore we devise an approximate relationship between a simple experimental quantity on one hand and a change in the structure of water induced by the pertinent process. To the best of the authors knowledge this is the first relation that makes such a connection. Although it involves certain approximations, the application of this relationship leads to results that are in qualitative agreement with conclusions reached earlier using other methods.

As a subsidiary result, this work provides new and independent support to the theoretical argument presented earlier,[7,8] that simple solutes such as argon, methane, and the like do indeed stabilize the structure of water, in the sense which is described in sections 3 and 4. This topic has been continuously discussed and debated in the literature ever since it was originally conjectured by Frank and Evans.[6]

The next two sections contain the assumptions leading to, and the derivation of a relation between the isotope effect in the standard free energy of solution and structural changes in water. Section 4 provides a few numerical results and section 5 indicates possible generalizations of this relationship to include more complex processes taking place in aqueous media.

## 2. Definitions and Assumptions

In this section we consider the simplest process that occurs in aqueous solution; i.e., the dissolution of a spherical nonpolar solute, such as argon, methane, and the like, in a system of $N$ water molecules at a given temperature $T$ and pressure $P$.

The standard free energy of solution of a solute, S, is related to the Ostwald absorption coefficient, $\gamma_S$, by [8]

$$\Delta\mu_S^0 = -kT \ln \gamma_S \tag{2.1}$$

where $k$ is the Boltzmann constant. The statistical mechanical expression for $\gamma_S$ is

$$\gamma_S = \frac{\int dV \int d\mathbf{X}^N \exp[-\beta U_N(\mathbf{X}^N) - \beta B_S(\mathbf{X}^N) - \beta PV]}{\int dV \int d\mathbf{X}^N \exp[-\beta U_N(\mathbf{X}^N) - \beta PV]} = \langle \exp(-\beta B_S) \rangle_0 \tag{2.2}$$

Here $\beta = (kT)^{-1}$, $U_N(\mathbf{X}^N)$ represents the total potential energy of interaction among the solvent molecules being at a fixed configuration $\mathbf{X}^N = \mathbf{X}_1, \mathbf{X}_2, \cdots, \mathbf{X}_N$ ($\mathbf{X}_i$ comprises the six coordinates required to describe the position and the orientation of a single water molecule, the latter is treated here as a rigid particle).

The quantity $B_S(\mathbf{X}^N)$ represents the total interaction energy between a solute particle, at some fixed position, e.g., $\mathbf{R}_S$, and the solvent molecules at the configuration $\mathbf{X}^N$. The integrations in (2.2) is over all possible volumes $V$ and con-

* After August 1975 correspondence should be addressed to the author at the Department of Physical Chemistry, the Hebrew University, Jerusalem, Israel.

figurations $\mathbf{X}^N$. The symbol $\langle\rangle_0$ designates an average, in the *TPN* ensemble, over all the configurations of the solvent molecules.

In addition to the very usage of the classical expression (2.2) for the Ostwald absorption coefficient we also employ the following assumptions.

*a*. The water molecules are viewed as rigid particles interacting via a pair potential $U(\mathbf{X}_i, \mathbf{X}_j)$. For the total potential energy of interaction we assume the full pairwise additivity,[9] namely

$$U_N(\mathbf{X}^N) = \sum_{i<j} U(\mathbf{X}_i, \mathbf{X}_j) \tag{2.3}$$

$$B_S(\mathbf{X}^N) = \sum_{i=1}^{N} U(\mathbf{X}_i, \mathbf{R}_S) \tag{2.4}$$

where $U(\mathbf{X}_i, \mathbf{R}_S)$ represents the solute–solvent pair potential. The precise location of $\mathbf{R}_S$ is of no importance, this is the reason for suppressing the dependence of $B_S$ on $\mathbf{R}_S$ in eq 2.4.

*b*. A model for the solvent–solvent pair potential is presumed to have the following form:[8,10]

$$U(\mathbf{X}_i, \mathbf{X}_j) = U(R_{ij}) + U_{el}(\mathbf{X}_i, \mathbf{X}_j) + \epsilon_{HB} G(\mathbf{X}_i, \mathbf{X}_j) \tag{2.5}$$

The first term is a spherical symmetrical contribution to the total interaction potential. This part may be conveniently chosen to have the Lennard-Jones form, and its main importance is to account for the strong repulsive forces which are operative at very short distances, e.g., $R_{ij} \lesssim 2.5$ Å. The electrostatic part $U_{el}$ may include interaction between a few electric multipoles. The most important contribution to this part of the potential is clearly the dipole–dipole interaction, which accounts for the long-range interaction between two molecules. The third term on the right-hand side of (2.5) is perhaps the most characteristic part of the pair potential for water. We shall refer to this part as the hydrogen bond (HB) potential. It consists of an energy parameter $\epsilon_{HB}$ which may be referred to as the HB energy and a geometrical factor $G(\mathbf{X}_i, \mathbf{X}_j)$ which is essentially a stipulation on the relative configuration of the two water molecules. The function $G(\mathbf{X}_i, \mathbf{X}_j)$ attains a maximum value of unity whenever the two molecules are hydrogen bonded to each other, and its value declines sharply to zero when the configuration $\mathbf{X}_i, \mathbf{X}_j$ deviates considerably from the one required for the formation of a HB. We have recently suggested an explicit analytical form for this function,[8,10] however, for the purpose of the present article the above qualitative description of the major properties of this function will be sufficient.

The essential reason underlying the split of the pair potential as in (2.5) is the recognition of the fact that a HB is formed only when the two molecules attain a very precise configuration, at which case, a strong binding potential energy $\epsilon_{HB}$ is operative. We stress again, however, that (2.5) is only a *model* for such a pair potential.

Substituting (2.5) into (2.3) and lumping the first two terms on the right-hand side of (2.5) into one, we get

$$U_N(\mathbf{X}^N) = U_N'(\mathbf{X}^N) + \epsilon_{HB} G(\mathbf{X}^N) \tag{2.6}$$

with

$$G(\mathbf{X}^N) = \sum_{i<j} G(\mathbf{X}_i, \mathbf{X}_j) \tag{2.7}$$

In section 3 we shall assign to the average of the function $G(\mathbf{X}^N)$ the meaning of a measure of the structure of water.

*c*. The third, and perhaps the most important assumption, is that the solvent isotope effect on $\Delta\mu_S^0$ for a simple solute S in $H_2O$ and in $D_2O$ may be ascribed to the difference in the parameter $\epsilon_{HB}$ only. In other words, in order to account for the difference in $\Delta\mu_S^0$ for S in light and heavy water it is sufficient to consider two liquids having exactly the same molecular properties except for the difference in the HB energy. The value of $\epsilon_{HB}$ for $H_2O$ and for $D_2O$ will be denoted by $\epsilon_H$ and $\epsilon_D$, respectively

The attitude taken here with respect to these two liquids is not new,[4,11] i.e., one views $D_2O$ as essentially the same as $H_2O$, slightly perturbed by a change in the HB energy $\epsilon_{HB}$. Of course one can trace back the difference in the HB energy to the differences in the masses of hydrogen and deuterium. In fact this kind of treatment is necessary if we are going to study the properties of liquid $H_2O$ and $D_2O$ as was actually done by Swain and Bader.[12] However, for the purpose of calculating $\gamma_S$ or $\Delta\mu_S^0$ we observe that the internal partition function of the water molecule does not appear explicitly in (2.1). This fact permits us to evade any consideration of the internal properties of a single water molecule.

Furthermore, it is well known that the bond length and bond angle in $H_2O$ are almost the same as in $D_2O$. Also both molecules are isoelectronic to neon. Hence we can assume that the spherical symmetrical part $U(R_{ij})$ is the same for the two liquids. Similarly the dipole moment of $H_2O$ and $D_2O$ have almost identical magnitude,[11] hence we shall also take $U_{el}$ to be the same for the two liquids.

There are several arguments indicating that the HB energy is greater in $D_2O$ as compared to $H_2O$.[11] Hence we take

$$\epsilon_D < \epsilon_H \tag{2.8}$$

Note however that the geometrical requirements for the formation of a HB, as prescribed by the function $G(\mathbf{X}_i, \mathbf{X}_j)$ are also presumed to be the same for the two liquids.[11,13] The statement that $D_2O$ is "more structured" than $H_2O$ is frequently found in the literature.[4,11] In Appendix A we show that this statement is equivalent to the assumption made in (2.8). The equivalence is proved by the use of the definition of the "structure" of water as presented in the next section.

Though clearly the difference $\epsilon_D - \epsilon_H$ originates from quantum mechanical considerations,[12] once we have adopted this result in our model pair potential (2.5), all our further considerations will be purely classical. In principle we are treating in this paper a system of particles subjected to the laws of classical statistical mechanics and which are characterized by the assumptions made above. The essence of the approximation to be introduced in the next section is that the isotope effect in $\Delta\mu_S^0$ may be accounted for by two model systems, which differ only in the parameter $\epsilon_{HB}$.

*d*. The last assumption concerns the solute–solvent interaction $U(\mathbf{X}_i, \mathbf{R}_S)$. Following arguments similar to the ones advanced in the previous paragraph we assume that the difference in the HB energy affects only the solvent–solvent interaction, and not the solute–solvent interaction.

## 3. An Approximate Relation between the Isotope Effect in $\Delta\mu_S^0$ and Structural Changes in the Solvent

Consider the statistical mechanical expression (2.2) for $\gamma_S$, once for $H_2O$ (designated by H) and once for $D_2O$ (designated by D). Assuming that the difference $\epsilon_D - \epsilon_H$ is small compared with the value of the HB energy (see sec-

tion 4), we expand $\gamma_S(D)$ in power series, using $\epsilon_{HB}$ as a parameter that takes the values $\epsilon_H$ and $\epsilon_D$, i.e.

$$\gamma_S(D) = \gamma_S(H) + (\epsilon_D - \epsilon_H)\frac{\partial \gamma_S}{\partial \epsilon_{HB}}\Big|_H + \cdots \quad (3.1)$$

The first derivative of $\gamma_S$ with respect to $\epsilon_{HB}$ is obtained directly from (2.2), the result being

$$\partial\gamma_S/\partial\epsilon_{HB} = -\beta[\langle G(-\exp(-\beta B_S))\rangle_0 - \langle G\rangle_0\langle\exp(-\beta B_S)\rangle_0] \quad (3.2)$$

Here, as in (2.2) the symbol $\langle\ \rangle_0$ represent an average in the $TPN$ ensemble over all the configurations of the solvent molecules, using the distribution function

$$P(\mathbf{X}^N, V) = \frac{\exp[-\beta U_N(\mathbf{X}^N) - \beta PV]}{\int dV \int d\mathbf{X}^N \exp[-\beta U_N(\mathbf{X}^N) - \beta PV]} \quad (3.3)$$

Relation 3.2 may be transformed to a somewhat simpler form by using the conditional distribution function of finding a configuration $\mathbf{X}^N$ and volume $V$, given a solute particle at some fixed position $\mathbf{R}_S$, namely

$$P(\mathbf{X}_N, V/\mathbf{R}_S) = \frac{\exp[-\beta U_N(\mathbf{X}^N) - \beta B_S(\mathbf{X}^N) - \beta PV]}{\int dV \int d\mathbf{X}^N \exp[-\beta U_N(\mathbf{X}^N) - \beta B_S(\mathbf{X}^N) - \beta PV]} \quad (3.4)$$

The joint average on the right-hand side of (3.2) may be rewritten as

$$\begin{aligned}\langle G \exp(-\beta B_S)\rangle_0 &= \int dV \int d\mathbf{X}^N P(\mathbf{X}^N, V) G(\mathbf{X}^N) \exp[-\beta B_S(\mathbf{X}^N)] \\ &= \langle\exp(-\beta B_S)\rangle_0 \int dV \int d\mathbf{X}^N P(\mathbf{X}^N, V/\mathbf{R}_S) G(\mathbf{X}^N) \\ &= \langle\exp(-\beta B_S)\rangle_0 \langle G\rangle_S \end{aligned} \quad (3.5)$$

where the symbol $\langle\ \rangle_S$ represents the conditional average, using the distribution function given in (3.4).

With the help of (3.5) we may rearrange (3.2) to get the final identity

$$-kT\left(\frac{\partial \ln \gamma_S}{\partial \epsilon_{HB}}\right)_{T,P,N} = \left(\frac{\partial \Delta\mu_S{}^0}{\partial \epsilon_{HS}}\right)_{T,P,N} = \langle G\rangle_S - \langle G\rangle_0 = \lim_{N_S \to 0}\left(\frac{\partial \langle G\rangle_S}{\partial N_S}\right)_{T,P,N} \quad (3.6)$$

The last equality on the right-hand side of (3.6) follows from the extensive character of the function $\langle G\rangle_S$, i.e., in the macroscopic limit, the derivative with respect to $N_S$ may be approximated by the change due to the addition of one solute particle S.

Substituting (3.6) into (3.1) we get the first-order expansion of $\gamma_S(D)$ as

$$\gamma_S(D) = \gamma_S(H)[1 - \beta(\epsilon_D - \epsilon_H)(\langle G\rangle_S - \langle G\rangle_0) + \cdots] \quad (3.7)$$

Thus the isotope effect in $\gamma_S$ is determined by the quantity $\langle G\rangle_S - \langle G\rangle_0$ which we now show has the meaning of a structural change in the solvent, induced by the addition of S.

Consider the function $G(\mathbf{X}_i,\mathbf{X}_j)$ which has been introduced as a part of the pair potential in (2.5). As we have stated before, there is no need, for the present purpose, to provide an explicit form for this function, though this may be done in various ways.[8] It is sufficient to acknowledge the property that $G(\mathbf{X}_i,\mathbf{X}_j)$ attains the maximum value of unity whenever the pair of molecules are in a "good" configuration to form a HB (e.g., the O–O distance is about 2.76 Å and the O–H···O angle is 180°), and the value drops steeply to zero for any other configuration.

With this property in mind we define the function

$$\psi_i(\mathbf{X}^N) = \sum_{\substack{j=1 \\ j\neq i}}^{N} G(\mathbf{X}_i, \mathbf{X}_j) \quad (3.8)$$

which is a measure of the number of HB's in which molecule $i$ participates when the whole system is at a specific configuration $\mathbf{X}^N$. This is true since the sum on the right-hand side of (3.8) essentially "counts" the number of HB's formed by the $i$th molecule. Hence $\psi_i(\mathbf{X}^N)$ may serve as a measure of the local structure around the $i$th molecule at the specific configuration $\mathbf{X}^N$. The range of values attainable by $\psi$ is $0 \leq \psi \leq 4$. Note that if the function $G(\mathbf{X}_i,\mathbf{X}_j)$ has been defined in a discrete way, i.e., it is unity whenever $i$ and $j$ are hydrogen bonded and zero otherwise, the function $\psi$ will attain only the five values 0, 1, 2, 3, 4.

The average structure around a specific molecule in the system, e.g., $i = 1$, may be defined as the average value of $\psi_1(\mathbf{X}^N)$, namely

$$\begin{aligned}\bar{\psi}(0) &= \int dV \int d\mathbf{X}^N P(\mathbf{X}^N, V)\psi_i(\mathbf{X}^N) \\ &= \frac{1}{N}\int dV \int d\mathbf{X}^N P(\mathbf{X}^N, V) \sum_{i=1}^{N} \psi_i(\mathbf{X}^N) \\ &= \frac{1}{N}\int dV \int d\mathbf{X}^N P(\mathbf{X}^N, V) \sum_{i=1}^{N}\sum_{\substack{j=1 \\ j\neq 1}}^{N} G(\mathbf{X}_i, \mathbf{X}_j) \\ &= \frac{2}{N}\langle G\rangle_0 \end{aligned} \quad (3.9)$$

Thus either the average number of HB's $\langle G\rangle_0$ in the system, or the average number of HB's formed by a specific particle of the system may be used as a measure of the degree of the structure of water.

Similarly one may define the conditional average

$$\begin{aligned}\bar{\psi}(S) &= \int dV \int d\mathbf{X}^N P(\mathbf{X}^N, V/\mathbf{R}_S)\Psi_1(\mathbf{X}^N) \\ &= \frac{2}{N}\langle G\rangle_S \end{aligned} \quad (3.10)$$

Hence the quantity $\Delta\langle G\rangle_S = \langle G\rangle_S - \langle G\rangle_0$ may be assigned the meaning of the structural change in the solvent induced by the dissolution of the solute S. We believe that $\Delta\langle G\rangle_S$ reflects in its content, the concept of structural changes in the solvent as referred to by many authors.

Having assigned meaning to $\Delta\langle G\rangle_S$ we may view relation 3.6 as an *exact* relation for a system of model particles obeying the assumptions of section 2. Alternatively, adopting the first-order expansion in (3.7) to account for the isotope effect in $\gamma_S$ (or in $\Delta\mu_S{}^0$), we get the following approximate relation:

$$\Delta\mu_S{}^0(D) - \Delta\mu_S{}^0(H) = (\epsilon_D - \epsilon_H)\Delta\langle G\rangle_S \quad (3.11)$$

where on the left-hand side we have an experimental quantity, whereas on the right-hand side we have molecular quantities. Once we agree upon the numerical value for $\epsilon_D - \epsilon_H$, we may extract information on $\Delta\langle G\rangle_S$ by the application of this relation. Some numerical values for $\Delta\langle G\rangle_S$ are presented in the next section.

Finally we note that in deriving relation 3.11 we did not make use of the full pairwise additivity (2.3). Instead, it is sufficient to assume the split of the total potential energy as in (2.6). The more refined split in (2.7) was employed, however, in the interpretation of the quantity $\langle G\rangle$ as a measure of the structure of water.

## 4. Some Numerical Examples

In this section we make use of relation 3.11 to estimate the magnitude and direction of the structural changes in water induced by the dissolution of different solutes. We note that in the past the isotope effect in the thermodynamic properties of aqueous solution was frequently interpreted in terms of structural changes in the solvent.[14-18] We believe that relation 3.11 provide a more direct and explicit means for that goal.

Experimental values for $\Delta\mu_S^0(H)$ and $\Delta\mu_S^0(D)$ were collected from the literature.[19] As for $\epsilon_D - \epsilon_H$, it is well known that there exist no universally agreed method of estimating the HB energy.[13] We believe, however, that the estimates made by Némethy and Scheraga[11,20] are quite reasonable for our purposes. They used the values of $\epsilon_H = -3.57$ kcal/mol of bonds, and $\epsilon_D = -3.80$ kcal/mol of bonds, for their model of liquid water. (These estimates were based on the experimental values for the energies of sublimation and vaporization of light and heavy ice.[4,11,21]) Using these values we get

$$\epsilon_D - \epsilon_H = -0.23 \text{ kcal/mol of bonds} \qquad (4.1)$$

which we shall adopt in all the forthcoming calculation. Note that $\epsilon_D - \epsilon_H$ is indeed small compared with the value of the HB energy. This fact supports the use of only first-order terms in the expansion in (3.1). Clearly the exact values of $\epsilon_H$ and $\epsilon_D$ depends strongly on the method one chooses to measure the strength of the HB. However in relation 3.11 the difference $\epsilon_D - \epsilon_H$ appears as a proportionality factor, therefore different choices of $\epsilon_D - \epsilon_H$ would have no effect on the relative magnitude of $\Delta\langle G\rangle_S$ for different solutes.

Table I reports some values for the isotope effect in $\Delta\mu_S^0$ for argon in $H_2O$ and in $D_2O$ along with the computed values of $\Delta\langle G\rangle_S$ at different temperatures. In accordance with many previous conclusions, based on either experimental or theoretical arguments, the dissolution of argon in water increases, or stabilizes, the structure of water, in the sense that the average number of HB's becomes larger in the presence of the solute. This effect diminishes with the increase of temperature. The plot of $\Delta\langle G\rangle_S$ vs. temperature shows a clearcut positive curvature, Figure 1.

Table II includes values of $\Delta\langle G\rangle_S$ for methane, ethane, propane, and butane. The temperature dependence is similar to the one observed for argon in Table I.

From these data it appears that the extent of the stabilization effect becomes smaller the larger the hydrocarbon molecule. This finding suggests that geometrical restrictions on the shape of the molecule are important in achieving a large stabilization effect, a topic which clearly deserves further study.

In Table III we report similar results for ionic solutions. Note however that we are using only the final relation (3.11) which was derived for *nonionic* solutes. The fact that a salt dissociates into ions in water may alter the whole argument leading to (3.11), therefore these figures should be regarded as tentative ones only. We have used part of Table 6-9 from Arnett and McKelvey[4] as a source for our computations. Perhaps the most remarkable difference between the values of $\Delta\langle G\rangle_S$ in this table and in the previous two tables is the appearance of negative values for most of the salts, i.e., most ionic solutions have a destabilizing effect on the structure of water. Exceptional cases are the fluoride salts such as LiF and NaF, and the tetraalkylammonium salts such as $(n\text{-Bu})_4NCl$.

**TABLE I: Values of $\Delta\mu_S^0(D) - \Delta\mu_S^0(H)$, in cal/mol, and $\Delta\langle G\rangle_S$ for Argon at Different Temperatures[a]**

| $t$, °C | 5 | 10 | 15 | 20 | 25 |
|---|---|---|---|---|---|
| $\Delta\mu_S^\circ(D) - \Delta\mu_S^\circ(H)$ | −63.9 | −58.5 | −53.9 | −49.8 | −46.2 |
| $\Delta\langle G\rangle_S$ | 0.278 | 0.254 | 0.234 | 0.216 | 0.201 |

[a] Based on data from Ben-Naim.[22]

**TABLE II: Values of $\Delta\langle G\rangle_S$ for Some Hydrocarbons at Different Temperatures[a]**

| $t$, °C | 5 | 10 | 15 | 20 | 25 |
|---|---|---|---|---|---|
| Methane | 0.21 | 0.19 | 0.17 | 0.15 | 0.13 |
| Ethane | 0.19 | 0.14 | 0.12 | 0.12 | 0.14 |
| Propane | (0.14) (4°) | | | | (0.11) |
| Butane | 0.17 (0.17) (4°) | 0.13 | 0.08 | 0.03 | −0.03 (0.14) |

[a] Based on data from Ben-Naim et al.[23] and Kresheck et al.[24] Values in brackets were computed from Kresheck et al.,[24] who reported some values at 4 and 25°.

**TABLE III: Values of $\Delta\langle G\rangle_S$ for Some Ionic Solutions[a]**

| | $F^-$ | $Cl^-$ | $Br^-$ | $I^-$ | $BPh_4^-$ |
|---|---|---|---|---|---|
| $Li^+$ | +0.42 | −0.10 | −0.31 | −0.53 | −0.71 |
| $Na^+$ | +0.01 | −0.51 | −0.72 | −0.95 | −1.13 |
| $K^+$ | −0.04 | −0.56 | −0.78 | −1.00 | −1.18 |
| $Rb^+$ | −0.03 | −0.55 | −0.76 | −0.98 | −1.16 |
| $Cs^+$ | +0.21 | −0.31 | −0.52 | −0.74 | −0.92 |
| $NH_4^+$ | −0.19 | −0.71 | −0.93 | −1.15 | −1.33 |
| $(Me)_4N^+$ | −0.06 | −0.58 | −0.79 | −1.02 | −1.19 |
| $(n\text{-Bu})_4N^+$ | +0.97 | +0.45 | +0.23 | −0.01 | −0.16 |

[a] All entries are for one temperature, 25°. Data taken from Tables 6-9 of ref 4.

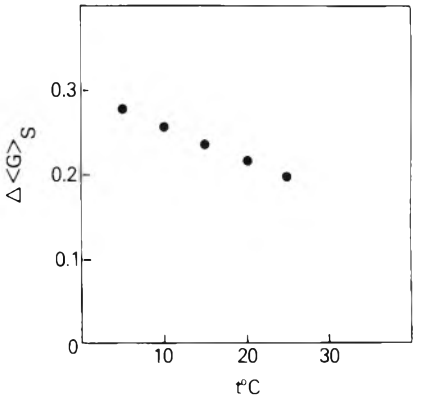


**Figure 1.** Values of $\Delta\langle G\rangle_S$ for argon in water as a function of temperature.

In the case of small ions such as $Li^+$ or $F^-$, the strong electrical field in the immediate surroundings of the ion produce a large perturbation effect on the internal properties of the water molecules in that region. If this effect is large then the factorization of the internal partition func-

tion for single water molecules may not be justified and hence relation 2.2 will not be valid. For this reason one should interpret with some care the figures of Table III for small ions. In the case of tetralkylammonium salts, we probably have a competitive effect of stabilization and destabilization by the two ions involved. This conclusion is similar to the ones reached by others using different experimental techniques.[1,2]

From Table III it is difficult to draw a clear-cut relation between the ionic size and the extent of the effect that ion has on the structure of water. It appears that the larger the *anion* the larger the destabilization effect. No such a simple relation appears to exist for *cations*.

## 5. Further Generalizations for Other Processes

In previous sections we treated the process of dissolution of simple molecules in water. This process is sufficient to establish a classification of solutes as "structure breakers" or "structure promoters" in aqueous solutions. However by a simple generalization of the result of section 3 one can deal with more complex processes, such as conformational changes or association of subunits to form a multisubunit biopolymer, etc. In fact information gathered for such processes is more important and interesting than the mere knowledge of which solutes stabilizes or destabilizes the structure of water. The ability to predict the effect of various processes on the structure of water will eventually prove helpful in the understanding of the role of liquid water as a medium in which most biochemical processes take place.

Consider as a simple example the isomerization reaction

$$A \rightleftharpoons B \tag{5.1}$$

The standard free energy for this reaction is

$$\Delta\mu^0 = \mu_B{}^0 - \mu_A{}^0 \tag{5.2}$$

and the isotope effect in $\Delta\mu^0$ may be approximated by

$$\Delta\mu^0(D) - \Delta\mu^0(H) = [\mu_B{}^0(D) - \mu_B{}^0(H)] - [\mu_A{}^0(D) - \mu_A{}^0(H)] \approx (\epsilon_D - \epsilon_H)[\langle G\rangle_B - \langle G\rangle_A] \tag{5.3}$$

The quantity in the squared brackets on the right-hand side of (5.3) may be interpreted as the structural change in the solvent induced by reaction 5.1.

Care must be exercised in interpreting $\langle G\rangle_B - \langle G\rangle_A$ when A and B are complex molecules. In the first place, one has to interpret the quantity $\langle G\rangle_B$ as an average over all the conformations of the molecules that are included in the definition of the isomer B. Similar comment applies to $\langle G\rangle_A$. More important, if the reaction in (5.1) involve formation or breaking of hydrogen bonds within the molecules A and B, or between these molecules and the solvent, relation 5.3 no longer applies since it has been based on the assumption (see section 2) that the solute–solvent interaction does not change when we replace $H_2O$ by $D_2O$. In such a case we have to modify (5.3) to account for the fact that the execution of reaction A → B involve different HB energies in the two solvents. A simple example of such a case would be the dissociation of carboxylic acids, for which the isotope effect in the dissociation constants have been tabulated.[25]

We now turn to one specific example for which we can cite some numerical values. The process to be considered is the so-called "hydrophobic interaction" (HI) process.[26–28] The change in the Gibbs free energy for the process of bringing two simple solutes from infinite separation to some close distance $R$ may be written as

$$\Delta G(R) = U(R) + \delta G^{HI}(R) \tag{5.4}$$

where $U(R)$ is the direct pair potential between the two solutes and $\delta G^{HI}(R)$ is referred to as the strength of the HI at the distance $R$.[8]

For a specific distance $R = \sigma_1 = 1.53$ Å we have recently suggested the following approximate relation:[8,28]

$$\delta G^{HI}(\sigma_1) = \Delta\mu_{Et}{}^0 - 2\Delta\mu_{Me}{}^0 \tag{5.5}$$

where $\Delta\mu_{Et}{}^0$ and $\Delta\mu_{Me}{}^0$ are the standard free energies of solution of ethane and methane, respectively.

The corresponding isotope effect in the strength of the HI at $R = \sigma_1$ is

$$\delta G^{HI}(\sigma_1, D) - \delta G^{HI}(\sigma_1, H) = \Delta\mu_{Et}{}^0(D) - \Delta\mu_{Et}{}^0(H) - 2[\Delta\mu_{Me}{}^0(D) - \Delta\mu_{Me}{}^0(H)] \approx [\langle G\rangle_{Et} - 2\langle G\rangle_{Me} + \langle G\rangle_0] \times (\epsilon_D - \epsilon_H) \tag{5.6}$$

(Note the different meaning of the letter $G$ on the two sides of eq (5.6).)

The expression in the squared brackets on the right-hand side of (5.6) can be readily interpreted as the structural change in the solvent involved in the HI process, in fact this term may be shown to equal the quantity $\langle G\rangle_{Et} - \langle G\rangle_{2Me}$ which has a more obvious meaning, see also Appendix B.

**TABLE IV: Structural Changes Induced by the Process of Hydrophobic Interaction[a]**

| $t$, °C | 5 | 10 | 15 | 20 | 25 |
|---|---|---|---|---|---|
| $\langle G\rangle_{Et} - \langle G\rangle_{2Me}$ | −0.23 | −0.23 | −0.22 | −0.18 | −0.12 |

[a] These figures refer to the process of bringing two methane molecules from a fixed position at infinite separation to a distance $R = \sigma_1 = 1.533$ Å. Based on data from ref 23.

Table IV lists some values for the structural changes in the solvent for the HI process. As is expected all the figures are negative, a result which is consistent with previous conclusions that the net effect of the HI process is a breakdown of the structure of water.[8,27]

## 6. Conclusion

In view of the fact that concepts such as "structure-making" and "structure-breaking" solutes are so ubiquitous in the literature on aqueous solutions, it is desirable to have a simple and well-defined measure of these quantities. We believe that the approximate relation 3.11 achieves that goal.

Of course the numerical values given in Tables I–IV may not have absolute significance, since they depend on the assumptions listed in section 2 as well as on the numerical value chosen for $\epsilon_D - \epsilon_H$. However we believe that the relative magnitude of these quantities is meaningful, so that different solutes may be compared as to the extent of their effect on the structure of water.

The knowledge of the effect of solute on the structure of water is clearly crucial in the understanding the properties of aqueous solutions. It is difficult to claim any practical advantages to such a knowledge, except, perhaps, in con-

nection with the Pauling theory of anesthesia, where it has been suggested that gaseous molecules such as xenon form "microcrystals of ice" around them. If this occurs in the brain, the theory argues, it may affect the passage of electrical impulses in the nerve system.[29]

A more important aspect of this work is its potential application to more complex processes. This possibility has been indicated in section 5. However, because of lack of the relevant data on the isotope effect for such processes this aspect has not been developed to the point where numerical quantities could have been computed. We believe that effort in generalizing the relation discussed in sections 3 and 4, as well as in measuring the pertinent isotope effect, would be quite rewarding in understanding the role of water as a medium where most biochemical processes take place.[30]

*Acknowledgment.* The author is very grateful to Drs. R. Tenne and W. Kauzmann for reading the manuscript and offering helpful comments.

## Appendix A

It is often claimed in the literature[4,14] that $D_2O$ is more "structured" than $H_2O$. We show here that the "structure" as measured by $\langle G\rangle_0$ is a monotonic increasing function of $-\epsilon_{HB}$. Hence the above statement is equivalent to the assumption (2.8).

To show that we consider the derivative of $\langle G\rangle_0$ with respect to $\epsilon_{HB}$, i.e.

$$\langle G\rangle_0 = \frac{\int dV \int d\mathbf{X}^N \exp[-\beta U_N(\mathbf{X}^N) - \beta PV] G(\mathbf{X}^N)}{\int dV \int d\mathbf{X}^N \exp[-\beta U_N(\mathbf{X}^N) - \beta PV]} \quad (A.1)$$

$$\left(\frac{\partial\langle G\rangle_0}{\partial(-\epsilon_{HB})}\right)_{T,P,N} = \beta[\langle G^2\rangle_0 - \langle G\rangle_0^2] \geq 0 \quad (A.2)$$

Hence increasing the strength of the HB energy for a model system obeying the assumptions of section 2 will result in an increase of the structure of the system. This result is almost self-evident on intuitive grounds.

At this junction it is interesting to show that $\langle G\rangle_0$ is not necessarily a monotonic decreasing function of the temperature. This assumption underlies the usage of the concept of "structural temperature" for aqueous solutions.[5,8]

The temperature derivative of $\langle G\rangle_0$ is

$$\left(\frac{\partial\langle G\rangle_0}{\partial T}\right)_{P,N} = \frac{1}{kT^2}[\langle G U_N\rangle_0 - \langle G\rangle_0\langle U_N\rangle_0 + P(\langle G V\rangle_0 - \langle G\rangle_0\langle V\rangle_0)] \quad (A.3)$$

It may be shown that the cross fluctuation $\langle GV\rangle_0 - \langle G\rangle_0\langle V\rangle_0$ is related to the difference in the molar volumes of $H_2O$ and $D_2O$. Since the latter is small at room temperature, we expect that this will have negligible contribution to the right-hand side of (A.3).

Putting $U_N = U_{N'} + \epsilon_{HB}G$ as in (2.6) we get

$$\langle G U_N\rangle_0 - \langle G\rangle_0\langle U_N\rangle_0 = \epsilon_{HB}(\langle G^2\rangle_0 - \langle G\rangle_0^2) + (\langle G U_N'\rangle_0 - \langle G\rangle_0\langle U_N'\rangle_0) \quad (A.4)$$

In order to secure a negative temperature dependence to $\langle G\rangle_0$ we must assume that the term

$$P(\langle GV\rangle_0 - \langle G\rangle_0\langle V\rangle_0) + \langle G U_N'\rangle_0 - \langle G\rangle_0\langle U_N'\rangle_0 \quad (A.5)$$

is either negative or positive but small compared with $\epsilon_{HB}(\langle G^2\rangle_0 - \langle G\rangle_0^2)$. We believe that the second possibility is the correct one. Nevertheless, it is clear from the above relations that it is much safer to correlate changes of structure with changes in HB energies rather than with changes in temperature.

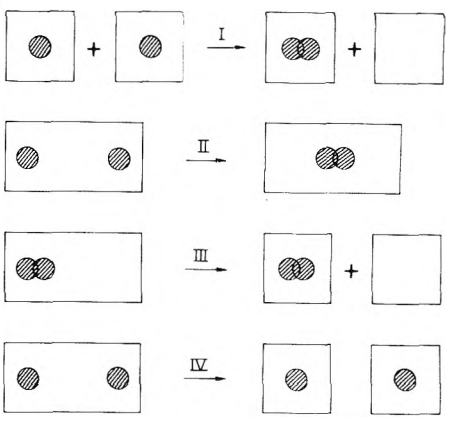


**Figure 2.** Schematic processes referred to in Appendix B.

## Appendix B

In section 5 we have interpreted the quantity in the squared brackets on the right-hand side of (5.6) as the change in the structure of water for the hydrophobic interaction process. This statement needs further clarification. To simplify our notation we denote by $\phi(S;N)$ the value of $\langle G\rangle_S$ in a system of $N$ water molecules. The quantity on the right-hand side of (5.6) strictly refers to the change of the structure due to process I in Figure 2, i.e.

$$\Delta\phi(I) = \phi(Et;N) - 2\phi(Me;N) + \phi(0;N) \quad (B.1)$$

where $\phi(0;N)$ is the structure of $N$ water molecules without any solutes. However, we are interested in the change of structure for process II which may be written as

$$\Delta\phi(II) = \phi(Et;N) - \phi(2Me;N) \quad (B.2)$$

where by 2Me we denote two methane molecules at infinite separation (for more details see ref 8). We want to show that in macroscopic systems $\Delta\phi(I)$ and $\Delta\phi(II)$ are equal to each other. To do that we note that in macroscopic systems the quantity $\Delta\phi(II)$ does not depend on $N$. This is true since all the changes of the structure must occur in the local environments of the solute. In particular, if we take $2N$ instead of $N$ we get the same quantity, i.e. (note that $T$ and $P$ are constants)

$$\Delta\phi(II) = \phi(Et;2N) - \phi(2Me;2N) \quad (B.3)$$

Since the solutes are at fixed positions, and the systems are macroscopically large, the two processes depicted as III and IV in Figure 2 involve the same, if any, structural change, due to the introduction of a partition in the system, i.e.

$$-\Delta\phi(III) = \phi(Et;2N) - \phi(Et;N) - \phi(0;N) \quad (B.4)$$

$$-\Delta\phi(IV) = \phi(2Me;2N) - 2\phi(Me;N) \quad (B.5)$$

$$\Delta\phi(III) = \Delta\phi(IV) \quad (B.6)$$

Using (B.4) to (B.6) in (B.3) we get the equality

$$\Delta\phi(II) = \Delta\phi(I) \quad (B.7)$$

which is the required relation.

NOTE ADDED IN PROOF.

Recently Jolicoeur and Lacroix (*Can. J. Chem.*, **51**, 3051 (1973)) have published an interesting paper on the free energies of transfer from $H_2O$ to $D_2O$ for a series of ketones. Processing their data according to relation 3.11 leads to the following conclusion. Most unsaturated ketones show a positive stabilization of the structure of water, whereas most of the unsaturated and polycyclic isomers have an opposite effect. There are also some interesting effects due to the degree of branching in the hydrocarbon chains that certainly deserve further detailed study both experimentally and theoretically. I am indebted to Dr. Jolicoeur for drawing my attention to this paper.

## References and Notes


(1) R. A. Horne, Ed., "Water and Aqueous Solutions, Structure, Thermodynamics and Transport Processes", Wiley-Interscience, New York, N.Y., 1972.
(2) F. Franks, Ed., "Water, A Comprehensive Treatise", Vol. II and III, Plenum Press, New York, N.Y., 1973.
(3) J. E. Desnoyers and C. Jolicoeur in "Modern Aspects of Electrochemistry", Vol. 5, J. O'M Bockris and B. E. Conway, Ed., Plenum Press, New York, N.Y., 1969
(4) E. M. Arnett and D. R. McKelvey in "Solute-Solvent Interaction", J. F. Coetzee and C. D. Ritchie, Ed., Marcel Dekker, New York, N.Y., 1969.
(5) J. D. Bernal and R. H. Fowler, *J. Chem. Phys.*, **1**, 515 (1933).
(6) H. S. Frank and M. W. Evans, *J. Chem. Phys.*, **13**, 507 (1945).
(7) A. Ben-Naim, *J. Statistical Phys.*, **7**, 3 (1973).
(8) A. Ben-Naim, "Water and Aqueous Solutions, an Introduction to a Molecular Theory", Plenum Press, New York, N.Y., 1974.
(9) The assumption of full pairwise additivity as written in (2.3) is a very severe one for a complex fluid such as water. In fact the derivation in section 3 requires somewhat a weaker assumption, namely, that the total potential energy $U_N$ may be written as $U_N = U_N' + \epsilon_{HB}G$ where the meaning of these symbols are defined in (2.6). However the treatment in section 2 becomes simpler by using the more explicit forms (2.3) and (2.5).
(10) A. Ben-Naim in "Water, A Comprehensive Treatise", Vol. I, F. Franks, Ed., Plenum Press, New York, N.Y., 1972.
(11) G. Némethy and H. A. Scheraga, *J. Chem. Phys.*, **41**, 680 (1964).
(12) C. G. Swain and R. F. W. Bader, *Tetrahedron*, **10**, 182 (1960).
(13) D. Eisenberg and W. Kauzmann, "The Structure and Properties of Water", Oxford University Press, Oxford, 1969.
(14) H. L. Friedman and C. V. Krishman in "Water, A Comprehensive Treatise", Vol. III, F. Franks, Ed., Plenum Press, New York, N.Y., 1973.
(15) B. E. Conway and L. H. Laliberté, *Trans. Faraday Soc.*, **66**, 3032 (1970).
(16) W. Y. Wen and K. Nara, *J. Phys. Chem.*, **72**, 1137 (1968).
(17) B. E. Conway and L. H. Laliberté, *J. Phys. Chem.*, **72**, 4317 (1968).
(18) J. Greyson, *J. Phys. Chem.*, **71**, 2210 (1967).
(19) Note that we have defined $\Delta\mu_S^0$ in (2.1) in terms of the Ostwald absorption coefficient, which is a ratio of molar concentrations. The advantages of using this particular definition have been discussed elsewhere.[8] In the literature, $\Delta\mu_S^0$ is often reported in terms of a ratio in mole fractions. However, since the molar volumes of $H_2O$ and $D_2O$ are almost identical, around room temperature, the isotope effect in $\Delta\mu_S^0$ will be almost insensitive to whether we have chosen molar or mole-fraction concentration scales.
(20) G. Némethy and H. A. Scheraga, *J. Chem. Phys.*, **36**, 3382, 3401 (1962).
(21) I. Kirshenbaum, "Physical Properties and Analysis of Heavy Water", National Nuclear Energy Series, McGraw-Hill, New York, N.Y., 1951.
(22) A. Ben-Naim, *J. Chem. Phys.*, **42**, 1512 (1965).
(23) A. Ben-Naim, J. Wilf, and M. Yaacobi, *J. Phys. Chem.*, **77**, 95 (1973).
(24) G. C. Kresheck, H. Schneider, and H. A. Scheraga, *J. Phys. Chem.*, **69**, 3132 (1965).
(25) P. M. Laughton and R. E. Robertson in "Solute-Solvent Interaction", J. F. Coetzee and C. D. Ritchie, Ed., Marcel Dekker, New York, N.Y., 1969.
(26) W. Kauzmann, *Adv. Protein Chem.*, **14**, 1 (1959).
(27) G. Némethy and H. A. Scheraga, *J. Phys. Chem.*, **66**, 1773 (1962).
(28) A. Ben-Naim, *J. Chem. Phys.*, **54**, 1387, 3696 (1971).
(29) See, for example, J. F. Catchpool in "Structural Chemistry and Molecular Biology, A. Rich and N. Davidson, Ed., W. H. Freeman, San Francisco, Calif., 1968.
(30) A. L. Lehninger, "Biochemistry", Worth Publishers, New York, N.Y., 1970.


# Interfacial Free Energies between Polymers and Aqueous Electrolyte Solutions


**R. Williams**

*PCA Laboratories, Princeton, New Jersey 08540*


*(Received December 18, 1974)*

*Publication costs assisted by RCA Laboratories*



Contact angle measurements were made for aqueous solutions of $CaCl_2$ and $K_2CO_3$ on Teflon and polyethylene. The variation of interfacial free energy with salt concentration is the same as that of the surface tension of the solution. This can be understood by considering the effect of the electrostatic image force on the distribution of ions near the interface.


The surface tension of water is increased by dissolving an ionic salt in it. If we exclude a few materials that are wetting agents this is a general effect. At a given concentration all salts of the same charge type behave about the same. With the possible exception of certain very dilute solutions the surface tension increases monotonically with increasing salt concentration. For concentrated solutions the surface tension can be 50% greater than that of pure water. A recent review of earlier experimental and theoretical work on the problem was given by Randles.[1]

The physical basis for the increase in surface tension is the electrostatic image force. A charge, $q$, in a dielectric medium, 1, is repelled from an interface with a medium, 2, having a smaller dielectric constant. Consider the case for media with dielectric constants, $\epsilon_1$ and $\epsilon_2$ with $\epsilon_1 > \epsilon_2$. If the interface lies in the $x$–$y$ plane at $z = 0$, the image potential, $U(z)$, is

$$U(z) = (q^2/4\epsilon_1 z)\frac{\epsilon_1 - \epsilon_2}{\epsilon_1 + \epsilon_2} = (q^2/4\epsilon_1 z)\alpha \qquad (1)$$

where $\alpha = (\epsilon_1 - \epsilon_2)/(\epsilon_1 + \epsilon_2)$. For the surface tension problem, medium 2 is air and $\epsilon_2$ is 1. For water, $\epsilon_1$ is 79, giving $\alpha = 0.98$. As an ion in the water approaches the interface its energy is increased by the amount, $U(z)$. This becomes

equal to $kT$ when $z$ = 2 Å. The higher energy leads to depletion of ions in a thin layer very near the surface. Those ions that remain near the surface have higher energy. As a result, the surface free energy or surface tension is increased. Using this model, Onsager and Samaras[2] calculated the magnitude of the increase in surface tension and obtained a result in reasonable agreement with experiment.

It would appear that there should be a parallel effect on the interfacial free energy between an aqueous electrolyte solution and any insulator having a small dielectric constant. For example, the dielectric constant of Teflon is 2.1 and that of polyethylene is 2.25. An ion in water, near an interface with either of these materials, experiences an image potential given by eq 1 with $\alpha$ = 0.94. The same considerations used in the analysis of the surface tension problem can now be applied to the interfacial free energy. We expect the interfacial free energy to increase when ionic solutes are dissolved in water. The following experiments and analysis will show that this is, indeed, the case.

### Contact Angle Equations

In the simplest case, the contact angle, $\theta$, is determined by three interfacial free energies. $\gamma_{LA}$ is the surface tension of the liquid. $\gamma_{SA}$ and $\gamma_{SL}$ are the unit free energies of the solid–air interface and the solid–liquid interface, respectively. The relation among these quantities is[3]

$$\gamma_{LA} \cos \theta = \gamma_{SA} - \gamma_{SL} \quad (2)$$

We now consider what happens when we use a given solid and measure the contact angle for aqueous solutions containing various concentrations, $c$, of a given salt. The above quantities now become functions of the concentration: $\theta(c)$, $\gamma_{LA}(c)$, and $\gamma_{SL}(c)$. The exception to this, of course, is $\gamma_{SA}$. The corresponding values for pure water will be denoted by $\theta(0)$, $\gamma_{LA}(0)$, and $\gamma_{SL}(0)$. We further define increments of surface tension, $\Delta\gamma_{LA}(c)$, and interfacial free energy, $\Delta\gamma_{SL}(c)$, by the equations:

$$\gamma_{LA}(c) = \gamma_{LA}(0) + \Delta\gamma_{LA}(c) \quad (3)$$

$$\gamma_{SL}(c) = \gamma_{SL}(0) + \Delta\gamma_{SL}(c) \quad (4)$$

Since the image-force contribution to the energy of an ion near the interface is very similar for water–air and water–polymer interfaces we *assume* that

$$\Delta\gamma_{LA}(c) = \Delta\gamma_{SL}(c) \quad (5)$$

The experiments reported here test this assumption. For solutions of $CaCl_2$ and $K_2CO_3$ in water, the surface tensions are known as a function of concentration over a wide range.[4] We have measured the contact angle of such solutions against Teflon and polyethylene as a function of concentration. We combine eq 2–5 to get

$$\gamma_{LA}(c) \cos \theta(c) = [\gamma_{SA} - \gamma_{SL}(0)] - \Delta\gamma_{SL}(c) = [\gamma_{SA} - \gamma_{SL}(0)] - \Delta\gamma_{LA}(c) \quad (6)$$

The measured contact angles, $\theta(c)$, were then used with the known surface tensions, $\gamma_{LA}(c)$, to obtain a plot of $-\gamma_{LA}(c) \cos \theta(c)$ vs. $\Delta\gamma_{LA}(c)$. According to eq 6, this should give a straight line with a slope of unity. If this relation is obeyed it means that the effect of dissolved ions on the interfacial energy is the same as their effect on the surface tension. It would then be reasonable to conclude that both are dominated by the same image-force considerations.

**TABLE I**[a]

| $K_2CO_3$ | | $CaCl_2$ | |
|---|---|---|---|
| $c$ | $\gamma_{LA}(c)$, erg/cm$^2$ | $c$ | $\gamma_{LA}(c)$, erg/cm$^2$ |
| 2.0 | 79.1 | 1.0 | 75.2 |
| 3.0 | 82.9 | 2.0 | 78.9 |
| 4.0 | 87.2 | 4.0 | 86.9 |
| 6.0 | 97.0 | 5.0 | 90.4 |
| 7.0 | 102.6 | 7.0 | 97.1 |
| 8.3 | 110.8 | | |

[a] All concentrations are in mol/kg of $H_2O$. Data for $K_2CO_3$ are for 20° and those for $CaCl_2$ are for 25°. Contact angle measurements were made at the corresponding temperatures for the two solutions. For pure water the surface tension is 72.8 at 20° and 72.0 at 25°. The unit of erg/cm$^2$ is equivalent to the more usual unit of dynes/cm.

### Experimental Section

Solutions were made up from deionized water and reagent grade $CaCl_2$ and $K_2CO_3$. The concentrations used, along with the corresponding values[4] reported for the surface tension, are given in Table I. The Teflon and polyethylene were in the form of rectangles, several centimeters on a side, cut from sheets 1 mm thick. The surfaces were smooth but not polished. The Teflon was cleaned in hot Caro's acid and thoroughly rinsed in deionized water. The polyethylene was cleaned in Tide detergent as recommended by Dann.[5] Contact angles were measured by applying a drop of solution to the horizontal surface and photographing the drop from the side through a low-power microscope.[6] Angles were measured on the resulting photographs. A method, described by Ellison and Zisman,[7] to apply the drop in order to get a uniform advancing contact angle, was followed here.

### Results

The contact angle is larger for the solutions than for pure water and increases with increasing concentration. For example, the contact angle of pure water on Teflon was 103°. For $CaCl_2$ solutons $\theta(c)$ was larger, increasing monotonically with concentration to a value of 120° when the $CaCl_2$ concentration reached 7.0 mol/kg of $H_2O$. (The value of $\theta(0)$ found here for polyethylene was 93°, equal to that found by Zisman[3] and 2° less than that found by Dann.[5] Our value of $\theta(0)$ for pure water on Teflon was 5° less than Zisman's value and 9° less than Dann's value, probably due to surface roughness in our sample. The primary interest in this work was to establish the trend with salt concentration rather than to obtain absolute values.) Results were generally similar for both solutes on both substrates, but with a significant difference to be discussed below.

A summary of the experimental results is shown in Figure 1. The data are plotted in the form suggested by eq 6: $-\gamma_{LA}(c) \cos \theta(c)$ vs. $\gamma_{LA}(c) - \gamma_{LA}(0)$. The solid lines are drawn in with a slope of 1. This conforms reasonably well to the trend of the data points in all cases. For Teflon the points for both $CaCl_2$ and $K_2CO_3$ fall nearly on the same line. The interfacial free energy in this case is not dominated by specific chemical interactions. Conformity to the line of unit slope shows that the dissolved salt affects the interfacial free energy quantitatively the same as it affects the surface tension. This strongly suggests that the image-force interaction is dominant in both cases.

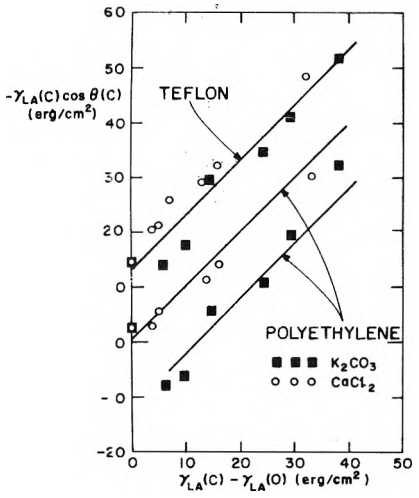


**Figure 1.** $-\gamma_{LA}(c)\cos\theta$ vs. $\gamma_{LA}(c) - \gamma_{LA}(0)$ for aqueous solutions on Teflon and polyethylene. The data for $CaCl_2$ solutions all refer to 25°. The data for $K_2CC_3$ all refer to 20°.[2] The surface tension data reported in the literature was available only for these temperatures and the contact angle measurements were made at the corresponding temperatures. Note that, on a given substrate, there is only one value for the contact angle at zero concentration, since this refers to pure water.

With polyethylene, solutions of $CaCl_2$ and $K_2CO_3$ behave somewhat differently. In both cases the points fall on lines of unit slope but the lines are displaced from each other in the vertical direction. The line for $K_2CO_3$ lies below that for $CaCl_2$ and does not extrapolate to the proper point at zero concentration. Apparently there is some specific chemical interaction between the surface and $K_2CO_3$. It may be due to reaction of hydroxyl ions, produced by hydrolysis of the carbonate, with acid groups retained by the polyethylene after washing. This is superimposed on the general image-force effect to give a line, of unit slope, but displaced.

It is concluded that, for the cases investigated, dissolved ions affect the interfacial free energy in the same way that they affect the surface tension. With the exception of the displacement due to the chemically specific effect, the results can be well explained by the image-force effect. The results also show that the work of adhesion, $\gamma_{LA}(c)[1 + \cos\theta(c)]$, is independent of salt concentration for this system. This result, together with a simplified model for the effect of ions on interfacial free energies, will be presented in a future article.

### References and Notes

(1) J. E. B. Randles in "Advances in Electrochemistry and Electrochemical Engineering", P. Delahay, Ed., Vol. 3, Interscience, New York, N.Y., pp 1–30.
(2) L. Onsager and N. T. Samaras, *J. Chem. Phys.*, **2**, 528 (1934).
(3) W. A. Zisman, *Adv. Chem. Ser.*, **No. 43**, 1–52 (1964).
(4) "Lange's Handbook of Chemistry", 11th ed, McGraw-Hill, New York, N.Y., 1973, pp 10-267-8.
(5) J. R. Dann, *J. Colloid Interface Sci.*, **32**, 302 (1970).
(6) R. Williams and A. M. Goodman, *Appl. Phys. Lett.*, **25**, 531 1974.
(7) A. H. Ellison and W. A. Zisman, *J. Phys. Chem.*, **85**, 503 (1954).

# An Infrared Study of Isolated Hydroxyl Groups on Silica Surfaces

**P. R. Ryason* and B. G. Russell**

*Chevron Research Company, Richmond, California 94802* *(Received February 4, 1974; Revised Manuscript Received March 20, 1975)*

*Publication costs assisted by Chevron Research Company*

A reinvestigation of isolated hydroxyl groups on silica surfaces shows the 3750-$cm^{-1}$ SiOH band to be structureless and asymmetric, for wafers prepared at pressures ≤200,000 lb/in.$^2$. Band peak positions vary linearly with temperature with a temperature coefficient of 0.0176 $cm^{-1}$/deg. The log of the band half-widths varies linearly with $1/T$ above ~100°. Hydroxyl group rotational activation energies are about 0.9 kcal/mol. Identical surface environments have been found for hydroxyl groups on two different silicas (Cab-o-Sil and Aerosil) by the precise spectroscopic measurements reported here.

### Introduction

Isolated hydroxyl groups are readily produced on silica surfaces by heating high area silicas under vacuum to temperatures above 500°. Infrared spectra of silica wafers so treated show a sharp band at about 3750 $cm^{-1}$.[1] There is disagreement in the literature as to whether this is a single band or consists of several bands. Hair and Hertl claimed to resolve the 3750-$cm^{-1}$ SiOH band and reported reaction orders of chlorosilanes with the various components of this band.[2] Hockey, however, pointed out that the spectral features reported by Hair and Hertl for the SiOH band were due to water vapor in the optical path of the infrared spectrometer.[3] He found that conversion of the OH groups to OD groups eliminated the structure observed in the absorption spectrum of the surface hydroxyl species. Clearly, the inference must be drawn that residual traces of water vapor in the instrument were responsible for the structure observed in the OH region. More recently, Van Cauwelaert and coworkers claim to have resolved the OH absorption

* Address correspondence to this author at the Jet Propulsion Laboratory, Pasadena, Calif. 91103.

**TABLE I: Description of Wafers Used in This Work**

| Wafer no. | 1 | 2 | 3 | 4 | 5 |
|---|---|---|---|---|---|
| Manufacturer | Cabot | Cabot | Degussa | Degussa | Degussa |
| Designation | Cab-o-Sil M5 | Cab-o-Sil M5 | Aerosil 200 | Aerosil 200 | Aerosil 200 |
| Lot no. | None | IC 262 | 520 | 520 | 520 |
| BET area, $m^2/g$ | 251 | 256 | 269 | 269 | 269 |
| Wt of wafer/area of wafer, $mg/cm^2$ | 4.2 | 2.2 | 3.8 | 4.4 | 9.3 |
| Pressure used to prepare wafer, $lb/in.^2$ | <1000 | <1000 | <1000 | <1000 | 200,000 |

band of isolated hydroxyl groups on silica surfaces.[4] Curiously, the structure of the OH band became more pronounced as the temperature was increased. Furthermore, on deuteration, the structure on the high-frequency side of the band maximum disappeared. Subsequently, Morrow and Cody[5] reported they were unable to reproduce Van Cauwelaert's results. Van Cauwelaert and coworkers[6] responded to this, suggesting that the pressure used in compressing the silica powder into self-supporting wafers was an important variable. Only those wafers compressed at pressures >300,000 lb/in.$^2$ showed a high-frequency shoulder of the surface hydroxyl absorption band. The work reported in this paper was nearly completed when the latter two accounts[5,6] appeared. Evidence bearing on these issues is presented in this work. In addition, precise information is provided on the dependence of the frequency of the band maximum and of the half band width on temperature, over a 1000° temperature range.

## Experimental Section

Three different samples of fumed silicas were used, an Aerosil 200 grade and two batches of Cab-o-Sil M5 grade. For the work on band structure and the temperature dependence of band properties, wafers were prepared by compressing a few milligrams of the powder in a Perkin-Elmer KBr die. Finger pressure (for 4 sec) was sufficient to yield a very fragile, though self-supporting wafer. To obtain some information on the effect of pressure,[6] a wafer was compressed at 200,000 lb/in.$^2$, the limit imposed by the strength of the available dies. This wafer was kept at pressure 43 sec, and brought to atmospheric pressure in 8 sec. Samples of the silicas used were submitted for area measurements. Materials used in the present work and relevant data are given in Table I.

Spectra of these wafers were obtained in a Perkin-Elmer Model 180 infrared specrophotometer. The cell and vacuum system used have been described.[7] Unlike previous workers who heated wafers to 800° outside the cell then transferred it, we were able to heat wafers to 800° directly in the cell, simultaneously pumping to pressures of $2.5 \times 10^{-7}$ Torr. To remove hydrocarbons possibly adsorbed during wafer making and handling, all wafers were heated in 160 Torr of oxygen at 300° for 1 hr, the oxygen was pumped out, the cell again brought to 160 Torr with $O_2$, heated for 1 hr at 500°, the oxygen pumped out, and then heated 0.5 hr at 800° while pumping. Qualitative spectra were obtained of the wafers prior to any heating, then after each stage of heating. For these spectra, the spectral slit width was 2 $cm^{-1}$ and the scanning speed was 166 $cm^{-1}$/min; the range 4000–180 $cm^{-1}$ was scanned. Particular attention was paid to the region of intense absorption at 1100 $cm^{-1}$. Since the wafer diameter (13 mm) was only slightly larger than the infrared beam at that point in the optical path, the transmission was checked on 20-fold scale expansion to determine that, to within the limits of detection, the wafer had 0% transmission at 1100 $cm^{-1}$. This procedure also assured that there were no pinholes or cracks in the wafer. Both cell compartments, the source region, and the monochromator of the Model 180 are very efficiently flushed by dried air. No compensating cell was required or used in the reference beam. Either beam of the Model 180 can be used as sample or reference beam; we used the instrument in the $I_0/I$ mode. That is, the sample cell was in the beam designated $I_0$ by the manufacturer. All spectra were recorded in absorbance. Spectral slit widths of 1 $cm^{-1}$ and scanning speeds of 0.5 $cm^{-1}$/min were used in the scans of the OH region. Wafer spectra at different temperatures were obtained in a random order. To attain the lowest temperatures, a few Torr of noble gas were introduced into the cell. In the first stages, He was used. However, the fused silica manometer capsule had a sealed off reference side; concern for He diffusing through the spiral into the reference side led to the substitution of neon. In both cases, the noble gas was passed over Ti sponge at 800° to remove impurities before being introduced into the vacuum system.

Water vapor and $CO_2$ were used to calibrate the frequency scale of the spectrometer. Since mechanical problems with the grating table were being corrected over the period of time these spectra were obtained, calibration spectra were run immediately after the wafer spectra. The frequency accuracy is believed to be $\pm 0.2$ $cm^{-1}$. Two methods of determining band areas were used. For wafers 1 and 3, the spectra were planimetered, using a tangent background. For wafers 2 and 4, the ordinate and abscissa data were transmitted to an IBM 1800 as spectrum was being scanned. Band areas were then determined by numerical integration (Simpson's rule) again using a tangent background.

## Results

*Wafers Pressed at Low Pressures.* Examples of the spectra obtained are shown in Figure 1 and 2. Plots of $\nu_{max}$ vs. $T$ for wafers 1–4 are shown in Figure 3. Following Hisatsune,[8] plots of log $\Delta\nu_{1/2}$ vs. $1/T$ were also made, as shown in Figure 4. Since the bands were asymmetric, $\Delta\nu_{1/2}$ was estimated as follows. A perpendicular was dropped from the band maximum to the tangent background of the band. At the half-height point, the distance to the high-frequency side of band was measured. This distance was doubled to obtain $\Delta\nu_{1/2}$, the band width at half-height. Ten points were picked on the high-frequency side of the SiOH bands for

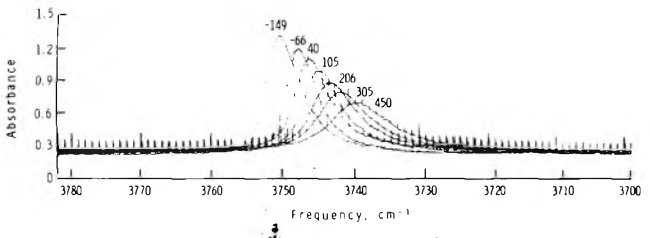


**Figure 1.** Cab-o-Sil M 5 wafer, 2.18 mg/cm$^2$, temperature as indicated, °C.

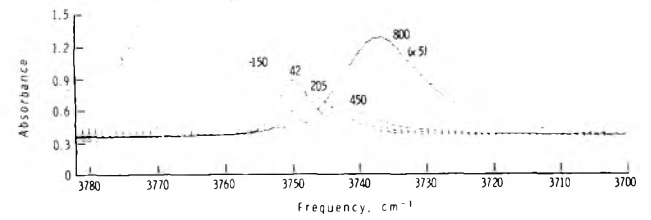


**Figure 2.** Aerosil 200 wafer, 4.3 mg/cm$^2$, temperature as indicated, °C; 800° spectrum run on expanded scale (×5).

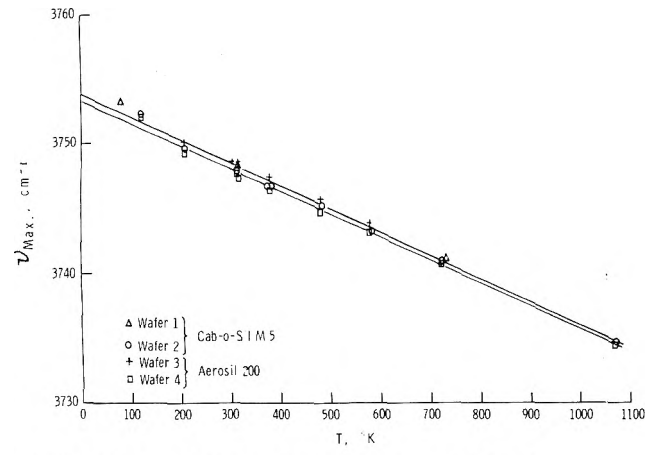


**Figure 3.** Cab-o-Sil M 5 and Aerosil 200 $\nu_{max}$. (OH) vs. $T$.

the following: wafer 2 (450, 305, and 206°) and wafer 4 (800, 450, and 105°). These were then fitted to a Lorentz curve. For both wafers, the 800° bands were fitted by a Lorentz curve to within 0.5%; at 100°, the deviations were ~2% for wafer 2 and ~1% for wafer 4. The slope of the log $\Delta\nu_{1/2}$ vs. $1/T$ plot is proportional to the activation energy of rotation of the OH group if the band is Lorentzian.[8]

Least-squares fitting of the $\nu_{max}$ vs. $T$ plots yielded the following results: Cab-o-Sil wafers 1 and 2 (77–1072°K)

$$\nu_{max} = 3753.8 \pm 0.2 - (1.79 \pm 0.04) \times 10^{-2}T$$

Aerosil wafers 3 and 4 (123–1073°K)

$$\nu_{max} = 3753.3 \pm 0.2 - (1.74 \pm 0.05) \times 10^{-2}T$$

The indicated uncertainties are one standard deviation. Below ~100° the band width appears to be determined by factors other than rotation. These data were excluded in the least-squares fitting of the ln $\Delta\nu_{1/2}$ vs. $1/T$ data, which yielded the following results: Cab-o-Sil wafers 1 and 2

$$\ln \Delta\nu_{1/2} = -\frac{(4.26 \pm 0.21) \times 10^2}{T} + (2.75 \pm 0.04)$$

$$\Delta E_{ROT} = 0.85 \pm 0.04 \text{ kcal/mol}$$

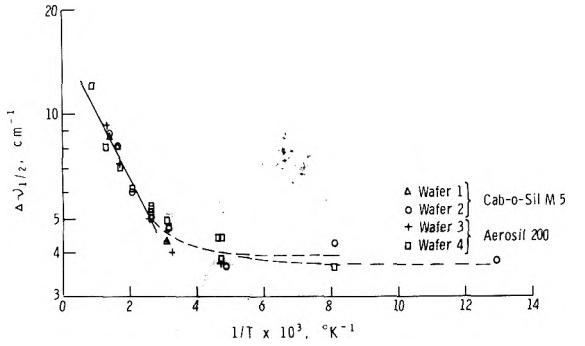


**Figure 4.** Cab-o-Sil M 5 and Aerosil 200. $\Delta\nu_{1/2}$ vs. $1/T$.

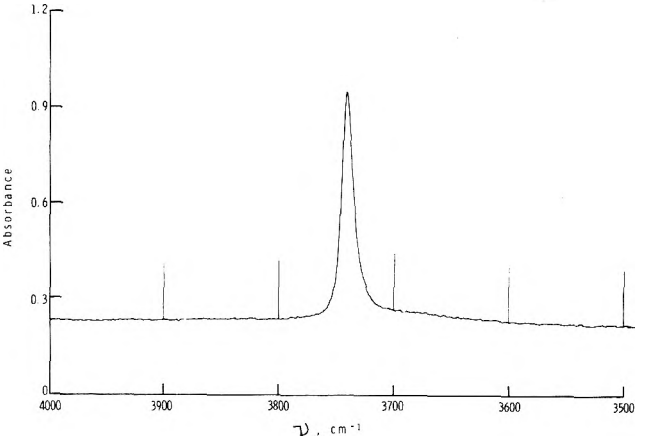


**Figure 5.** Spectrum of Aerosil 200 wafer pressed at 200,000 psi (450°).

Aerosil wafers 3 and 4

$$\ln \Delta\nu_{1/2} = -\frac{(4.42 \pm 0.35) \times 10^2}{T} + (2.79 \pm 0.08)$$

$$\Delta E_{ROT} = 0.88 \pm 0.07 \text{ kcal/mol}$$

The indicated uncertainties are one standard deviation.

Plots of band areas vs. temperature indicated that the band area decreased with temperature. For wafers 1–3, the data were badly scattered; for wafer 4, the SiOH band area appeared to decrease exponentially with temperature. Band areas for wafers 1–3 were in the range of 2–7 cm$^{-1}$; those for wafer 4 were in the range 8–13 cm$^{-1}$. It is not known if the larger areas in the second case are responsible for the apparently higher precision of that case.

*Wafers Pressed at High Pressure.* A spectrum of this wafer is shown in Figure 5. Spectra on the expanded scale of Figures 1 and 2 were also obtained. These also do not show a shoulder on the high-frequency side of the band. Frequencies of the band maxima of the SiOH band of this wafer at various temperatures were measured and found to be identical (to within one standard deviation) with the SiOH frequencies of the wafers pressed at lower pressure. The biggest difference between the high pressure and low pressure wafers was the broad hydrogen bonded SiOH absorption band at ~3520 cm$^{-1}$ observed in the spectra of the wafers prior to heating. At the band maximum, this band was about 12 times more intense in the high pressure wafer than the low pressure wafer. Of course, this band was also more intense at each stage of heating the high pressure

wafer. After heating to 800°, then decreasing the wafer temperature to room temperature, however, the hydrogen bonded SiOH band appeared to have been eliminated in the spectrum of the high pressure wafer.

## Discussion

None of our infrared spectra of isolated surface hydroxyl groups on silica surfaces show evidence of a shoulder on the high-frequency side. In this respect, the present results agree with those of Hockey[3] and of Morrow and Cody[5] for low pressure wafers and disagree with the results of Van Cauwelaert et al.[6] for high pressure wafers. Other reported spectra[9,10] of silicas heated to high temperatures also fail to show structure on the high-frequency side of the surface SiOH band. However, the pressures used by Van Cauwelaert et al. in making wafers were not exactly reproduced because of the limited strength of the die. Thus, the question of structure in the surface OH absorption band of silicas pressed at pressures greater than 200,000 lb/in.$^2$ remains open.

As judged by the frequencies of the band maxima at various temperatures, the surface hydroxyl groups of the high pressure wafer are in very similar surroundings to those of the low pressure wafers. Results of adsorption measurements and reactions with reagents demonstrate the heterogeneity of the surface hydroxyl groups on silicas heated to 800°.[2,4] Spectroscopic results reported here show that the local environments of the SiOH groups are not perfectly uniform. The band width of the SiOH band below 100° is wider than one would expect for a perfectly uniform surface SiOH environment and is temperature independent. What this work does show is that the 3750-cm$^{-1}$ band of surface hydroxyl groups on silicas heated to 800° probably cannot be spectroscopically resolved, even though the spectroscopic evidence also indicates surface heterogeneity.

All workers' results show the SiOH band for isolated surface SiOH groups to be asymmetric. Van Cauwelaert et al.[6] interpreted this asymmetry in terms of a second band on the low-frequency side, using a curve resolver to fit the observed shape. Morrow and Cody[5] interpreted this "tail" as evidence for random intramolecular perturbations. However, the asymmetry and the slight temperature dependence of this asymmetry make it probable that it is due to a sum of hot bands, the thermally excited levels being low-frequency lattice vibrations. In that case, the low-frequency band carries no direct structural information regarding the isolated surface hydroxyl groups. Klier[11] has analyzed band shapes of the $\nu_3 + \nu_2$ bands of liquid water, ice, and absorbed water at various temperatures. He concluded from the rotational correlation functions that the asymmetry was due to an attractive perturbation of the rotary motion. For his systems, hydrogen bonding is the most probable attractive perturbation. Another source of asymmetry is hot bands, especially likely in systems with low-frequency vibrations, such as hydrogen bonded systems or solids.

Linear dependence of the frequency of the band maximum with temperature has previously been noted by Ward.[12] Morrow and Cody[5] found an approximate value for the temperature coefficient of about 0.02 cm$^{-1}$/deg. The more precise values here reported strongly suggest that the isolated surface hydroxyl groups of these silicas are in identical environments. Not only the temperature coefficients of the band maxima are equal, but the frequencies of the band maxima extrapolated to absolute zero and the activation energies for rotation are also equal. Spectroscopic measures of surface properties, therefore, establish the identical nature of these two surfaces.

Hisatsune[8] found the activation energies for rotation of nitrate ions in KCl, KBr, and KI matrices were 1.44, 1.41, and 0.99 kcal/mol, respectively. These values are comparable with the activation energy for rotation of surface hydroxyl groups found in this work. From Figure 4, it is clear that the band width is nearly constant below room temperature. This may be due to nonuniformity of the fixed local environments of the surface OH groups. A similar effect has been noted for cyanate ion in alkali halide matrices.[13]

Band area data for wafer 4 were analyzed on the assumption that the decrease in band area was due to ionization:

$$\underline{OH} \rightleftharpoons \underset{\sim}{H^+} + \underline{O^-}$$

where $\underline{OH}$ and $\underline{O^-}$ indicate fixed surface species and $\underset{\sim}{H^+}$ indicates a mobile surface species. If one assumes that $(\underline{O^-}) \gg (\underset{\sim}{H^+})$, the equilibrium constant for the above reaction yields the equation:

$$\ln\left[\frac{(\underline{OH})_0}{(\underline{OH})} - 1\right] = -\frac{\Delta H}{RT} + \frac{\Delta S}{R} - \ln(\underline{O^-})$$

Plotting $\log\{[(\underline{OH})_0/(\underline{OH})] - 1\}$ vs. $1/T$ yields a very good straight line, the slope of which corresponds to an enthalpy of ionization of about 1 kcal/mol. This is surprisingly low and may not correspond to the postulated process. In the absence of a more extensive body of precise data, interpretation of a decrease in band area as due to ionization and the formation of free surface protons is speculative.

## Conclusions

The infrared absorption bands of isolated surface hydroxyl groups on high area silicas pressed at pressures ≤200,000 lb/in.$^2$ are asymmetric and structureless. Hot bands probably are the source of the asymmetry. Frequencies of band maxima depend linearly on temperature. Above ~100°, the high-frequency sides of the bands are lorentzian. From the band half-width vs. $1/T$ plot, an activation energy of ~0.9 kcal/mol is found for $\underline{OH}$ group rotation. Band areas decrease with increasing temperature. This may imply ionization of the $\underline{OH}$ group; the data are too imprecise to draw this conclusion without reservation. Detailed spectroscopic information on the surface hydroxyl groups show the two silicas, Cab-o-Sil and Aerosil, to have identical surfaces.

*Acknowledgment.* We are grateful for the advice and encouragement of Dr. H.F. Harnsberger. The constructive and helpful suggestions of the reviewers are also appreciated.

## References and Notes

(1) J. B. Peri, *J. Phys. Chem.*, **70**, 2937 (1966).
(2) M. L. Hair and W. Hertl, *J. Phys. Chem.*, **73**, 2372 (1969).
(3) J. A. Hockey, *J. Phys. Chem.*, **74**, 2570 (1970).
(4) F. H. Van Cauwelaert, P. A. Jacobs, and J. B. Uytterhoeven, *J. Phys. Chem.*, **76**, 1434 (1972).
(5) B. A. Morrow and I. A. Cody, *J. Phys. Chem.*, **77**, 1465 (1973).
(6) F. H. Van Cauwelaert, P. A. Jacobs, and J. B. Uytterhoeven, *J. Phys. Chem.*, **77**, 1470 (1973).
(7) P. R. Ryason, *Rev. Sci. Instrum.*, **44**, 772 (1973).
(8) M. Tsuboi and I. C. Hisatsune, *J. Chem. Phys.*, **57**, 2087 (1972).
(9) M. L. Hair and W. Hertl, *J. Phys. Chem.*, **77**, 1965 (1973).
(10) M. J. D. Low and N. Ramasubramanian, *J. Phys. Chem.*, **70**, 2740 (1966).
(11) K. Klier, *J. Chem. Phys.*, **58**, 737 (1973).
(12) J. Ward, *J. Catal.*, **16**, 386 (1970).
(13) V. Schettino and I. C. Hisatsune, *J. Chem. Phys.*, **52**, 9 (1970).

# Isotherms and Energetics of Carbon Dioxide Adsorption on γ-Alumina at 100–300°

**Michael P. Rosynek**

*Department of Chemistry, Texas A&M University, College Station, Texas 77843* *(Received December 16, 1974)*

*Publication costs assisted by the Petroleum Research Fund*

Adsorption isotherms and isosteric heats of adsorption were measured for the interaction of carbon dioxide with γ-alumina at five temperatures in the range 100–300°. A decrease in heat of adsorption with increasing surface coverage was observed at all temperatures, and the isotherms conformed well at low coverages to the Freundlich equation, indicating an energetically heterogeneous alumina surface. Entropy calculations indicate that at >150° the surface species are extremely mobile, even at low coverages. Consideration of previous infrared and catalytic site poisoning studies of $CO_2$ on alumina suggests that at >150°, the adsorbed layer consists almost entirely of relatively free carbonate-type structures, formed by interaction of $CO_2$ molecules with surface oxide ions. At <150°, particularly at low coverages, the surface species appear much less mobile. Bicarbonate-type entities are probably formed only at high coverages (>6%) and at low temperatures (<150°) after the most energetic sites have interacted with $CO_2$ to produce carbonate species.

## Introduction

The interaction of carbon dioxide with the surface of catalytic (γ) alumina has been the subject of several investigations during the past 10 years. These studies have been of two general types: (1) kinetic investigations of catalytic site poisoning by $CO_2$, and (2) infrared studies of surface species that are formed by $CO_2$ adsorption. In the former category, it has been demonstrated, for example, that $CO_2$ selectively poisons surface sites on alumina that catalyze deuterium exchange reactions of hydrogen,[1] methane,[2] benzene,[3,4] *n*-butenes,[5] and various cyclic olefins.[6] In addition, quantitative poisoning by $CO_2$ has established an upper limit of 2–3 × $10^{12}$/cm$^2$ (less than 0.2% of the total available surface) for the concentration of these deuterium exchange sites.[2,4] On the other hand, the rates of alumina-catalyzed isomerization (double-bond migration and cis–trans rotation) of *n*-butenes are largely unaffected by $CO_2$ adsorption,[5] and this observation led to the postulate that olefin isomerization sites and deuterium exchange sites on alumina are unrelated and operate independently of each other.

The natures of surface species that result from $CO_2$ adsorption on alumina have been elucidated chiefly by the infrared studies of Peri,[7] Parkyns,[8,9] Amberg,[10] and others.[11–13] The results of Parkyns,[8] for example, indicate that on alumina pretreated at 500° chemisorption of $CO_2$ at 25° occurs primarily by interaction with surface hydroxyl groups to form monomeric bicarbonate ($HCO_3$) species. Moreover, this process apparently involves transfer of a complete OH group to the carbon atom, rather than a proton transfer from the OH group to an oxygen atom of $CO_2$. Although one of Parkyns' band assignments has recently been questioned,[13] the formation of $HCO_3$-type species is undoubtedly a process of major importance in the $CO_2$/$Al_2O_3$ system at low temperatures. In addition, various workers[9,12] have observed evidence for a much slower and less extensive formation of uni- and bidentate carbonate ($CO_3$) moieties on alumina, which presumably occurs by interaction of $CO_2$ with surface oxide ions.

Despite this variety of studies, fundamental information about the extent and thermodynamics of $CO_2$ adsorption on alumina over a significant range of surface coverage appears to be lacking. Gregg and Ramsay[12] measured adsorption isotherms for $CO_2$ on κ-$Al_2O_3$ in the temperature range 150–400°, but limited their study to equilibrium pressures of less than 20 Torr. The present investigation was undertaken to provide data on heats and entropies of $CO_2$ adsorption on alumina for significant ranges of temperature and surface coverage. The intent is to correlate the results with those of previous infrared and site poisoning studies, in an effort to obtain a fuller understanding of the principal modes of interaction in the $CO_2$/$Al_2O_3$ system.

## Experimental Section

*Materials.* Commercial γ-alumina was obtained from the American Cyanamid Co., as described previously,[4,5] and 0.4-g samples were used in the form of irregular 30–40 mesh particles. Nitrogen adsorption at −196° gave a BET surface area of 172 m$^2$/g, and a pore volume of 0.35 cc/g. Sample pretreatment prior to each experiment involved heating under vacuum at 10°/min to 550°, treatment with 100 Torr of oxygen for 2 hr, followed by overnight evacuation at the same temperature.

Oxygen (99.9%) and helium (99.995%) were obtained from Airco and were purified before use by passage through a trap at −196°. Carbon dioxide was Matheson's Coleman Instrument grade (99.99%) and was purified by distillation from −78 to −196°, followed by three freeze–pumping cycles at the latter temperature.

*Apparatus.* All adsorption measurements were performed using a Cahn Model RG recording electrobalance which was connected to a conventional diffusion-pumped high-vacuum gas handling system. Pressures were measured with a McLeod gauge (0–5 Torr) and mercury manometer (>5 Torr). A vacuum of <$10^{-5}$ Torr could be routinely achieved in the balance chamber. Sample temperatures were regulated to ±0.2° with a digital proportional band controller.

*Data Treatment.* Fractional surface coverages (θ) were calculated from adsorbate weights by assuming a value of 16.4 Å$^2$ for the area occupied by a $CO_2$ molecule in a filled monolayer, as given by[14]

$$A = 0.96(b/N)^{2/3} \quad (1)$$

where $N$ is Avogadro's number, and $b$ is the van der Waals volume constant (42.67 cc/mol for $CO_2$). Isosteric heats of adsorption ($\Delta H_a$) were evaluated from families of isotherms at selected surface coverages by application of the Clausius–Clapeyron equation.[15] Thus, assuming ideal gas behavior and adsorption reversibility

$$\Delta H_a(\theta) = R\left(\frac{\ln (P_1/P_2)}{\frac{1}{T_1} - \frac{1}{T_2}}\right) \quad (2)$$

where $P_1$ and $P_2$ are the equilibrium pressures required to effect a surface coverage of $\theta$ at temperatures $T_1$ and $T_2$, respectively. The differential molar entropy, $\bar{S}_a$, of the adsorbed species at temperature $T$ and equilibrium pressure $P$ is then given by[16]

$$\bar{S}_a(\theta) = S_g^0 - R \ln (P/P^0) + \frac{\Delta H_a(\theta)}{T} \quad (3)$$

where $S_g^0$ is the total entropy of the gas-phase material at standard pressure, $P^0$. Values of $S_g^0$ for $CO_2$ at various temperatures were taken from the compilation of Barin and Knacke.[17]

Experimentally determined entropies were compared to theoretical values calculated from statistical thermodynamic considerations, and based upon two extreme models of the adsorption process. In the first model, complete mobility of the surface species is assumed, the molecules retaining all rotational and vibrational degrees of freedom and two translational degrees; the third translational degree is converted to a vibration perpendicular to the adsorbent surface. The adsorbate layer thus resembles a two-dimensional gas, and if the partition functions of the adsorbed molecules are assumed to be separable, the differential molar entropy of the surface species will be given by

$$\bar{S}_a = {}_2\bar{S}_{a,tr} + \bar{S}_r + \bar{S}_v \quad (4)$$

where ${}_2\bar{S}_{a,tr}$ is the two-dimensional translational contribution to the total entropy, and $\bar{S}_r$ and $\bar{S}_v$ are the rotational and vibrational contributions, respectively. Values of ${}_2\bar{S}_{a,tr}$ were calculated from[16]

$${}_2\bar{S}_{a,tr} = R \ln (MTA/\theta) + 63.8 \text{ eu} \quad (5)$$

where $M$ is the molecular weight of the adsorbate, and $A$, the molecular area, is defined by eq 1. $\bar{S}_r$ and $\bar{S}_v$, which are essentially independent of surface coverage, were determined from the standard statistical thermodynamic equations,[18] viz.

$$\bar{S}_r = R \ln \left\{\frac{1}{\pi\sigma}\left[8\pi^3 ekT\left(\prod_{i=1}^{n} I_i\right)^{1/n}/h^2\right]^{n/2}\right\} \quad (6)$$

and

$$\bar{S}_v = R\sum_{i=1}^{n}\left[\frac{h\nu_i/kT}{\exp(h\nu_i/kT) - 1} - \ln\left[1 - \exp(h\nu_i/kT)\right]\right] \quad (7)$$

For $CO_2$, $\sigma$ (the symmetry factor) = 2; $I_1 = I_2 = 7.32 \times 10^{-39}$ g cm$^2$; $\nu_1$, $\nu_2$, $\nu_3$, and $\nu_4$ = (6.97, 3.92, 1.98, and 1.98) × $10^{13}$ sec$^{-1}$, respectively.[18]

In the other model of the adsorption process, the surface species are assumed to be completely immobile. In this case, all translational and rotational degrees of freedom are lost (i.e., converted to vibrational degrees), and the only significant entropy contribution remaining is the so-called configurational or localization entropy:[15]

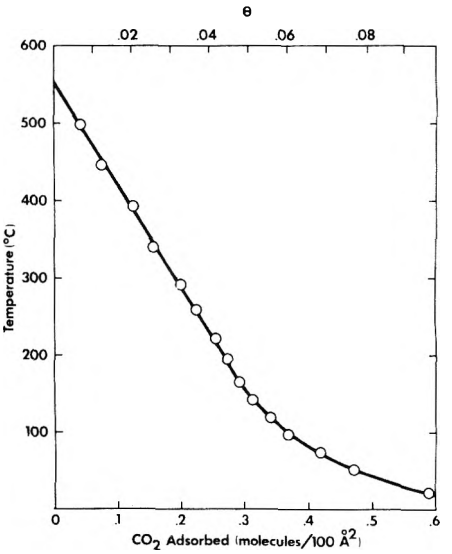


**Figure 1.** Vacuum isobar for $CO_2$ on γ-alumina; 24-hr evacuation at each temperature.

$$\bar{S}_{a,c} = -R \ln\left(\frac{\theta}{1 - \theta}\right) \quad (8)$$

which represents the entropy of $X$ molecules distributed over $X_0$ sites.

## Results

In order to determine initially the extent of "strong" chemisorption of $CO_2$ on alumina as a function of temperature, a vacuum isobar was measured by exposing an alumina sample to an equilibrium $CO_2$ pressure of 700 Torr for 24 hr at 22°. The sample was then evacuated for 24 hr at 22°, and for the same length of time at successively higher temperatures, and the weight of adsorbed $CO_2$ remaining at each temperature was recorded. Mass spectral analysis confirmed that the desorbate in all cases consisted only of $CO_2$ (<0.1% of other material could have been detected). The resulting isobar is shown in Figure 1. The break in the curve at approximately 150° indicates the presence of at least two forms of adsorbed $CO_2$, with the more weakly adsorbed type (desorbing in the range 25–150°) accounting for about 40% of the total. Larson and Hall[2] observed the same behavior for the $CO_2/Al_2O_3$ system, although the corresponding slope change occurred at a somewhat higher temperature.

Adsorption isotherms were measured at five sample temperatures in the range 100–300°. At each temperature, $CO_2$ doses were admitted through a trap at −78°, and the sample was allowed to equilibrate for 1 hr at each pressure before a weight reading was taken. (Virtually identical results were obtained when duplicate isotherms were run at 102° in which 1-hr equilibration times were used in one case and 6-hr times in the other.) A 20 Torr partial pressure of dry helium was present during each experiment to obviate corrections for apparent weight losses due to thermomolecular flow at low $CO_2$ pressures. The resulting isotherms (Figure 2) were temperature reversible and were of the type I (Langmuir) variety, but did not obey the Langmuir equation. Much better results were obtained when the data were fitted to the Freundlich equation, viz.

$$\theta = kP^{1/n} \quad (9)$$

TABLE I: Values of $n$ and $Q_0$ from Slopes of Freundlich Plots for $CO_2$ Isotherms on Alumina

| Temp, °C | $n$ | $Q_0$, kcal/mol |
|---|---|---|
| 102 | 5.7 | 4.2 |
| 148 | 4.5 | 3.8 |
| 199 | 4.1 | 3.8 |
| 251 | 3.5 | 3.7 |
| 299 | 3.3 | 3.8 |

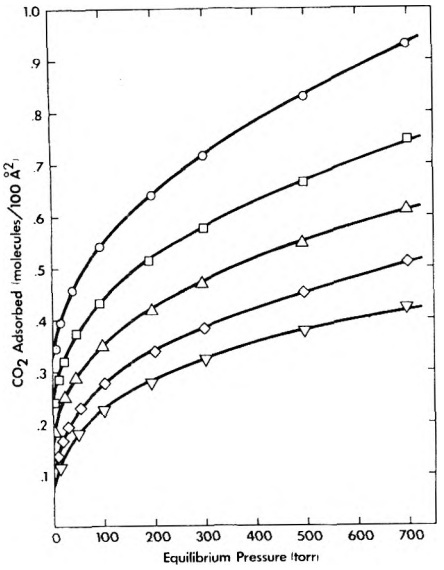


**Figure 2.** Adsorption isotherms for $CO_2$ on $\gamma$-alumina; 1-hr equilibration at each pressure: O, 102°; □, 148°; △, 199°; ◇, 251°; ▽, 299°.

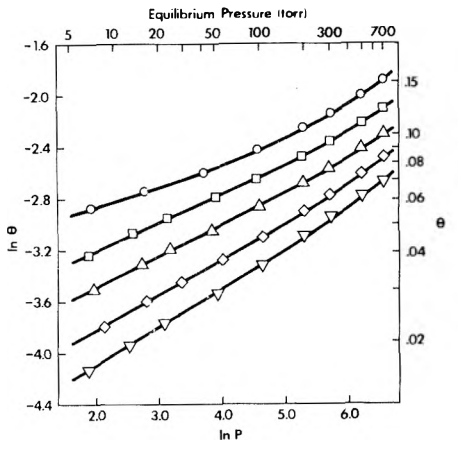


**Figure 3.** Freundlich plots for $CO_2$ isotherms on $\gamma$-alumina; O, 102°; □, 148°; △, 199°; ◇, 251°; ▽, 299°.

where $k$ and $n$ ($= Q_0/PT$) are constants. Plots of ln $\theta$ vs. ln $P$ are shown for each temperature in Figure 3, and are quite linear in the low surface coverage region ($\theta < \sim 0.06$) in which the Freundlich equation is expected to apply.[19] Even at 102°, where uniformly higher coverages are involved, the curvature is not severe. Values of $n$ and $Q_0$, calculated from slopes of the linear portions of the curves in Figure 3, are summarized in Table I, and $n$ is seen to decrease with increasing temperature, as expected.[20]

Isosteric heats of adsorption at selected coverages were calculated by applying eq 2 to the four pairs of adjacent isotherms in Figure 3. Values of $\Delta H_a$ at individual temperatures were obtained by interpolation, and these are presented in Figure 4. Uniform decreases of $-\Delta H_a$ with increasing coverage were observed at all temperatures. A "limiting" value of $\sim -4$ kcal/mol is approached at high coverages for the three lowest temperatures (102, 148, and 199°) but no apparent levelling off is evident at the two highest temperatures (251 and 299°).

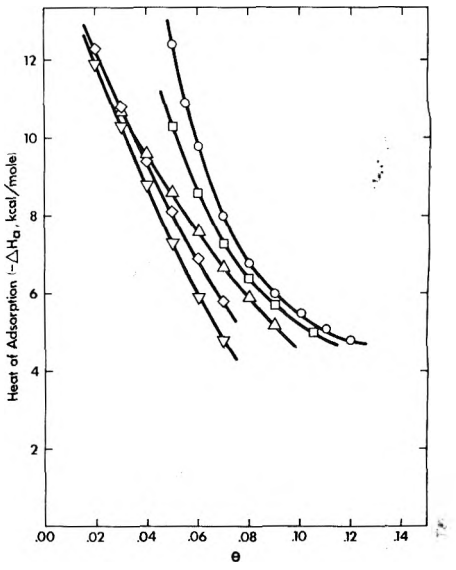


**Figure 4.** Variation of heat of adsorption with surface coverage for $CO_2$ on $\gamma$-alumina. Adsorption at 102° (O), 148° (□), 199° (△), 251° (◇), and 299° (▽).

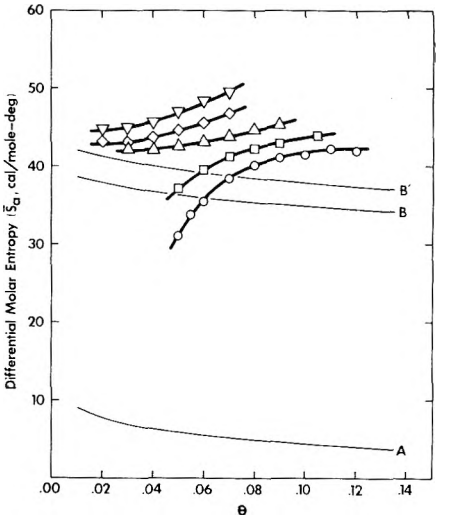


**Figure 5.** Experimental differential molar entropy of $CO_2$ adsorbed on $\gamma$-alumina as a function of surface coverage at 102° (O), 148° (□), 199° (△), 251° (◇), and 299° (▽): curve A, predicted entropy for immobile adsorption model (eq 8); curves B and B′, predicted entropies for mobile adsorption model (eq 4) at 102 and 299°, respectively.

Differential molar entropies of the adsorbed species were computed from eq 3 for each point in Figure 4, and these are shown in Figure 5. Here, curve A represents entropies predicted by the model of immobile surface species (eq 8), and curves B and B′ represent values calculated from the mobile adsorption model (eq 4) at 102 and 299°, respectively; predicted mobile entropies for the other three temperatures lie between B and B′. It is apparent from Figure 5 that, except for the lowest coverages at 102 and 148°, the

experimentally determined entropies considerably exceed the predicted values, even for the model of completely mobile surface species.

## Discussion

*Surface Heterogeneity.* Conformity of the $CO_2$ isotherms at low coverages to the Freundlich equation (Figure 3) indicates an energetically heterogeneous alumina surface on which the number of sites of a given adsorption potential decreases exponentially with increasing $-\Delta H_a$. This finding is supported by the decrease in heat of adsorption with increasing surface coverage observed at all five temperatures (Figure 4). Such behavior might also be caused by increasing adsorbate–adsorbate lateral interactions with increasing surface population, but this possibility is almost certainly negligible at the low surface coverages encountered. At $\theta = 0.15$, for example, the average $CO_2$ density on the surface is less than one molecule per 100 Å$^2$. In addition, an exponential decrease in heat of adsorption cannot be explained on the basis of lateral repulsions between adsorbed molecules.[20]

Another possible contribution to the observed $\Delta H_a$–$\theta$ behavior is a dependence of the mode of adsorbate–surface bonding on coverage. Increasing competition for adsorption sites may, for example, force a transition from predominantly bidentate-type surface species at low coverages to exclusively unidentate-type structures at higher coverages. But again, the uniformly low surface coverages involved in the present study make this possibility seem unlikely also.

Evidence for heterogeneity of the alumina surface in its interaction with $CO_2$ has been observed previously. Temperature-programmed desorption of adsorbed $CO_2$ from a saturated surface, for example, occurs slowly and uniformly over a wide temperature range (50–500°), indicating an array of sites with a broad spectrum of adsorption heats. This behavior is in sharp contrast to the relatively narrow temperature ranges (e.g., 50–150°) typically observed for hydrocarbon desorption from alumina,[4,21] at comparable rates of temperature increase. The linear portion of the vacuum isobar for $CO_2$ at $>\sim$150°, shown in Figure 1, is also consistent with this observation.

The source of such surface heterogeneity on alumina is difficult to assess precisely. It may arise from site differences caused by purely physical surface features such as point defects, corner and edge locations on microcrystallites, exposure of different crystal planes, etc. Another possible cause may be small variations in structure and/or surrounding environment of a single kind of site. It is likely that all of these factors play important roles on alumina surfaces.

*Nature of Adsorbed Species.* As demonstrated in Figure 5, at low to intermediate coverages ($\theta < 0.06$) at 102 and 148°, the surface species are evidently less than completely mobile. $CO_2$ adsorption under these conditions results in the loss of more than one translational degree of freedom, and perhaps rotational degrees as well. At 102°, for example, a partially mobile surface species (one which has lost all three translational degrees of freedom but retains complete rotational and vibrational freedom) would have a differential molar entropy (eq 6 and 7) of ~15 eu. At higher coverages ($\theta > 0.07$) and/or higher temperatures (>148°), on the other hand, entropies of the surface species considerably exceed the predicted values, even for the model of complete mobility of the adsorbed species. Such excess entropy or "super mobility" is usually attributed to a very low-frequency vibration of the surface–adsorbate bond,[22] since the internal vibrations of molecules make only small contributions to the total entropy, and are normally altered only slightly upon adsorption.[16]

**TABLE II: Pertinent Frequencies in the Infrared Spectra of Two Classes of Co(III) Carbanato Complexes[a]**

| Complex | Carbonate bonding | Absorption frequency, cm$^{-1}$: $\nu_1$ $\nu$(C–O$_b$) + $\nu$(C–O$_a$) | $\nu_5$ $\nu$(C–O$_a$) |
|---|---|---|---|
| $[Co(NH_3)_5CO_3]Br$ | Unidentate | 1373 | 1453 |
| $[Co(NH_3)_5CO_3]I$ | Unidentate | 1366 | 1449 |
| | | $\nu$(C–O$_b$) | $\nu$(C–O$_a$) + $\delta$(O$_a$–C–O$_b$) |
| $[Co(NH_3)_4CO_3]Cl$ | Bidentate | 1593 | 1265 |
| $[Co(NH_3)_4CO_3]ClO_4$ | Bidentate | 1602 | 1284 |

[a] Reference 24.

Speculation about the nature of this bond and that of the corresponding surface species may be guided by the results of previous infrared and site poisoning studies of the $CO_2$/$Al_2O_3$ system. On alumina pretreated at 500–550°, adsorption of $CO_2$ at 25° gives rise to major infrared bands at 3605, 1640, 1480, and 1233 cm$^{-1}$.[7-12] By comparison to the spectrum of crystalline $KHCO_3$, Parkyns, in an excellent study,[8] assigned these four bands to the O–H, asymmetric C–O, and symmetric C–O stretching, and C–O–H bending modes, respectively, of monomeric bicarbonate species (I), formed by interaction of $CO_2$ molecules with surface hydroxyl groups:

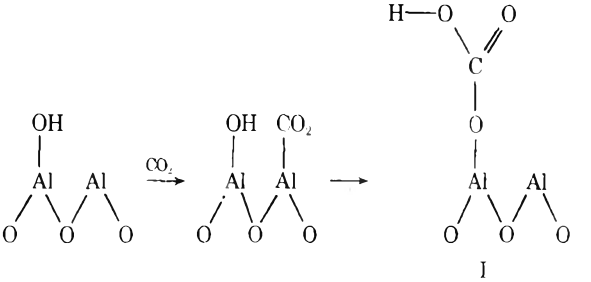


I

The key to this assignment was the appearance of the 3605-cm$^{-1}$ band, together with a concomitant decrease in intensity of the band due to the highest frequency OH groups of the alumina.

Contrary to the prediction of this model, however, the behavior of the band at 1480 cm$^{-1}$ does not parallel that of the other three bands.[13] Heating under vacuum from 25 to 150°, for example, almost completely removes the bands at 3605, 1640, and 1233 cm$^{-1}$, while only slightly reducing the 1480-cm$^{-1}$ band intensity. Similarly, when $CO_2$ is slowly added to a bare alumina surface at 100°, the 1480-cm$^{-1}$ band selectively appears first, and only after it has almost reached its limiting intensity do the other three bands begin to appear. Similar addition of $CO_2$ at 25° causes all four bands to increase simultaneously. In addition, the intensity of the 1480-cm$^{-1}$ band is directly proportional to

the poisoning effect of $CO_2$ on alumina-catalyzed benzene–deuterium exchange reactions; no such correlation exists for the other three bands. Hence, since surface hydroxyl groups are known to play a negligible role in low-temperature (<100°) deuterium exchange reactions on alumina,[13] it is likely that assignment of the bands at 3605, 1640, and 1233 $cm^{-1}$ to a bicarbonate entity is correct, but that some other surface species (the only persistent one above ≈150°) is responsible for the band at 1480 $cm^{-1}$.

One possibility for the identity of this species is a uni- or bidentate carbonate structure, generated by interaction of a $CO_2$ molecule with a surface oxide ion in one or both of two ways:

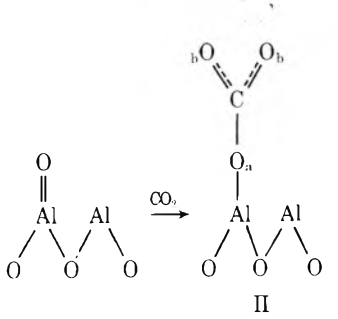

II

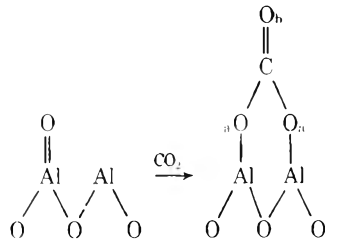

III

Assessment of the relative importances of the two structures II and III may be made by considering bands that occur in the infrared spectra of two classes of cobalt(III) carbonato complexes,[24] as summarized in Table II. (Six additional infrared-active vibrations exist for each of these complexes but are not tabulated since they occur at frequencies below the transmission limit of alumina, viz., ≈1100 $cm^{-1}$.) Clearly, the 1480-$cm^{-1}$ band observed in the $CO_2/Al_2O_3$ system corresponds closely to the $\nu_5$ vibration of the unidentate carbonato complexes, but it is not, however, accompanied by a second band in the 1300–1400-$cm^{-1}$ region that would characterize the surface species as a true unidentate carbonate structure (Table II). A more likely possibility for the adsorbed species is a relatively free carbonate ion that experiences only transitory localization at any given surface oxide ion. Infrared spectra of inorganic metallic carbonates, for example, invariably exhibit a single intense absorption band in the 1435–1475-$cm^{-1}$ region as their only spectral feature at frequencies above 1000 $cm^{-1}$.[23]

The "supermobility" observed for the adsorbed species (Figure 5) may therefore be explained by a very low frequency vibration of the C–$O_a$ bond in structure II. Calculation from eq 7 illustrates, for example, that an excess differential molar entropy of 10 eu can be generated by a vibrational frequency of $1.4 \times 10^{11}$ $sec^{-1}$ at 100° and $2.2 \times 10^{11}$ $sec^{-1}$ at 300°. Such frequencies are not unreasonable for weak surface–adsorbate bonds.[16] This weak vibration reflects the tendency toward desorption as molecular $CO_2$, and at a given coverage this desorption tendency would, of course, increase with increasing temperature, as demonstrated in Figure 5. At low coverages, only the most energetic sites, which most firmly bind the adsorbate, are occupied; hence, the frequency of the surface–adsorbate bond vibration is higher, and the entropy decreases, approaching that predicted by the model of completely mobile adsorbate, and, at 102 and 148°, even falling below it. Bicarbonate entities probably begin to form on the surface only at high coverages ($\theta > \approx 0.06$) and at low temperatures (<150°) after the most energetic sites have interacted with $CO_2$ to form carbonate species. In this connection, the slope change observed in the vacuum isobar of Figure 1 may indicate desorption of predominantly $HCO_3$-type species in the temperature range 25–150°, and desorption of primarily $CO_3$ moieties at higher temperatures.

## Conclusions

The surface of γ-alumina, activated at 550°, is energetically heterogeneous in its interaction with carbon dioxide, as demonstrated by a decrease in heat of adsorption with increasing coverage and by conformity of $CO_2$ adsorption isotherms to the Freundlich equation at low coverages. Entropy calculations indicate that at temperatures higher than 150° the surface species are extremely mobile, even at low coverages. Consideration of previous infrared and catalytic site poisoning studies of $CO_2$ on alumina suggests that at >150° the adsorbed layer consists almost entirely of relatively free carbonate structures, formed by interaction of $CO_2$ molecules with surface oxide ions. At <150°, particularly at low coverages, the differential molar entropy of the surface species is much lower. Bicarbonate entities probably exist on the surface only at higher coverages ($\theta > \approx 0.06$), and not at all at >150°.

*Acknowledgment.* Acknowledgment is made to the Donors of the Petroleum Research Fund, administered by the American Chemical Society, for support of this research.

## References and Notes

(1) F. H. van Caulwelaert and W. K. Hall, *Trans. Faraday Soc.*, **66**, 454 (1970).
(2) J. G. Larson and W. K. Hall, *J. Phys. Chem.*, **69**, 3080 (1965).
(3) P. C. Saunders and J. W. Hightower, *J. Phys. Chem.*, **74**, 4323 (1970).
(4) M. P. Rosynek and J. W. Hightower, *Proc. Int. Congr. Catal., 5th*, 851 (1973).
(5) M. P. Rosynek, W. D. Smith, and J. W. Hightower, *J. Catal.*, **23**, 204 (1971).
(6) J. W. Hightower and W. K. Hall, *Trans. Faraday Soc.*, **66**, 477 (1970).
(7) J. B. Peri, *J. Phys. Chem.*, **70**, 3168 (1966).
(8) N. D. Parkyns, *J. Chem. Soc. A*, 410 (1969).
(9) N. D. Parkyns, *J. Phys. Chem.*, **75**, 526 (1971).
(10) L. H. Little and C. H. Amberg, *Can. J. Chem.*, **40**, 1997 (1962).
(11) Ya. M. Grigor'ev, D. V. Pozdnyakov, and V. N. Filimonov, *Russ. J. Phys. Chem.*, **46**, 186 (1972).
(12) S. J. Gregg and J. D. F. Ramsay, *J. Phys. Chem.*, **73**, 1243 (1969).
(13) J. W. Hightower, *Prepr., Div. Petr. Chem., Am. Chem. Soc.*, **18**, 262 (1973).
(14) S. Ross and J. P. Olivier, "On Physical Adsorption", Wiley-Interscience, New York, N.Y., 1964.
(15) J. J. F. Scholten and S. Kruyer in "Physical and Chemical Aspects of Adsorbents and Catalysts", B. G. Linsen, Ed., Academic Press, London, 1970.
(16) A. Clark, "The Theory of Adsorption and Catalysis", Academic Press, New York, N.Y., 1970.
(17) I. Barin and O. Knacke, "Thermochemical Properties of Inorganic Substances", Springer-Verlag, Berlin, 1973.
(18) T. L. Hill, "An Introduction to Statistical Thermodynamics", Addison-Wesley, Reading, Mass., 1960.
(19) J. M. Thomas and W. J. Thomas, "Introduction to the Principles of Heterogeneous Catalysis", Academic Press, London, 1967.
(20) G. C. Bond, "Catalysis by Metals", Academic Press, London, 1962.
(21) R. J. Cvetanovic and Y. Amenomiya, *Adv. Catal.*, **17**, 103 (1967).
(22) C. Kemball, *Adv. Catal.*, **2**, 233 (1950).
(23) K. Nakamoto, "Infrared Spectra of Inorganic and Coordination Compounds", 2nd ed, Wiley-Interscience, New York, N.Y., 1970.
(24) J. Fujita, A. E. Martell, and K. Nakamoto, *J. Chem. Phys.*, **36**, 339 (1962).

# Studies on the Orientation of Acrylonitrile Adsorbed on Interlamellar Surfaces of Montmorillonites

**Shoji Yamanaka,*[1] Fumikazu Kanamaru, and Mitsue Koizumi**

*The Institute of Scientific and Industrial Research, Osaka University, Suita, Osaka 565, Japan*
*(Received June 17, 1974; Revised Manuscript Received September 3, 1974)*

Montmorillonite–acrylonitrile complexes have the following three different values of basal spacings depending on the kind of the interlayer cation and on the amount of adsorbed water: 17.8, 16.3, and approximately 13 Å. The arrangement of the molecules adsorbed in the interlayer space of these complexes is determined from the results of studies on infrared pleochroism and deuterium exchange and of basal spacing measurements. The stability of the complex is directly related to the polarizing power of the interlayer cation. However, the orientation of adsorbed molecules is affected by other important factors such as amount of adsorbed water and hydrogen-bond formation.

## Introduction

Montmorillonite is a layered aluminosilicate containing exchangeable cations between the layers. Various polar organic molecules are introduced into the interlayer spaces to form organo–clay complexes. In a previous paper,[2] we studied the reaction of acrylonitrile (hereafter called AN) with montmorillonites and found that the stability of the complex was directly related to the polarizing power of the interlayer cation. From preliminary work conducted by the authors, it was found that the basal spacings of montmorillonite–acrylonitrile complexes varied according to the kind of the interlayer cation and the condition of sample preparation. In the present research, the orientation of AN adsorbed in the interlayer space is determined on the basis of the results of infrared pleochroic study and basal spacing measurement.

## Experimental Section

*Materials.* Montmorillonite used in this study was identical with that used in a previous study.[2] The clay from Kambara in Niigata, Japan, was supplied by Nihon Chikagaku-sha Ltd. The <2-$\mu$ particle size fraction was converted to the $Li^+$, $Na^+$, $K^+$, $Ca^{2+}$, $Mg^{2+}$, $Ba^{2+}$, $Co^{2+}$, $Ni^{2+}$, and $NH_4^+$ forms, and the thin films of the converted forms were prepared using the methods described previously.[2] Since a film sample was highly oriented with planes of the silicate sheet lying parallel to the film surface, it was possible to investigate pleochroic effects by observing the difference in absorption intensity of the film inclined to the path of a spectrophotometer beam at various angles.[3]

AN was purified by distillation at atmospheric pressure after refluxing with $P_2O_5$ for 5 hr. It was redistilled in a vacuum line through a $P_2O_5$ tube.

$\alpha$-Deuterioacrylonitrile (AN-$\alpha d$) was prepared from AN by H–D exchange in $D_2O$ with CaO as a catalyst.[4] The deuterium content at the $\alpha$ position was estimated to be more than 90% by measuring the intensities of infrared absorption bands at 1413 and 1396 $cm^{-1}$ which were assigned to the $CH_2$ deformation vibration of AN and AN-$\alpha d$, respectively.

*Infrared Spectrum.* Infrared spectra of the oriented films were measured in an evacuable glass cell with NaCl windows, using a Hitachi Perkin-Elmer EPI-2G spectrometer. The cell was designed in such a way that the film could be heated up to 100° and inclined to an infrared beam, as it was maintained under vacuum, in order to investigate a pleochroic effect under a reduced pressure. After the film mounted in the cell was dried by evacuation at room temperature, its infrared spectrum was recorded to see the degree of dehydration. More highly dehydrated samples were prepared by evacuation at 80°. Then the film was allowed to react with vapor AN which was introduced into the cell through a vacuum line. Prior to running the spectra, the excess vapor in the cell was evacuated; the spectral measurement was carried out in the presence of a very small amount of the vapor (ca. 1 Torr), because AN adsorbed on some of the samples was easily removed by a continuous evacuation.[2] The pleochroism was measured on three incidence angles, 90, 60, and 30°. In an effort to confirm the assignment of the C–H stretching bands of AN, the same spectroscopic measurement as described above was conducted using AN-$\alpha d$ instead of AN.

*Basal Spacing.* Basal spacings were measured on the oriented films placed in a capillary, using a powder X-ray camera. Flakes (5 × 0.2 mm) cut out of an oriented film were dried in a Pyrex glass capillary under vacuum at room temperature or at 80°. After introducing AN vapor into the capillaries, they were sealed off. In some cases, the capillaries were evacuated for 6 hr before sealing. The plane of the film was placed parallel to nickel filtered Cu K$\alpha$ radiation to get intense (00$l$) reflections.[5]

## Results and Interpretation

*Infrared Spectrum.* The spectrum of one of montmorillonite–acrylonitrile complexes in the range 4000–1200 $cm^{-1}$ is shown in Figure 1 together with that of vapor AN. Bands due to adsorbed AN appearing in the region below 1200 $cm^{-1}$ were omitted since they suffered interference by vibrations due to the silicate structure. The positions of absorption peaks of the adsorbed AN are summarized in Table I, together with those of vapor AN. The assignments were taken from the paper by Halverson et al.[6]. Besides the absorption peaks listed in Table I, additional bands due to exchangeable $NH_4^+$ were observed at 3270, 3070, 2860, and 1425 $cm^{-1}$ in the spectrum of the $NH_4^+$–mont–AN complex (mont = montmorillonite). These frequencies were identical with those of dehydrated $NH_4^+$–mont. In compar-

**TABLE I: Positions of the Infrared Absorption Peaks for Adsorbed AN and for Vapor AN**

| Vapor AN freq, $cm^{-1}$ | Branch | Adsorbed AN freq, $cm^{-1}$ | Assignment[a] |
|---|---|---|---|
| 3136 | R | | |
| 3127 | Q | 3130 | $\nu_1$, C—H str |
| 3118 | P | | |
| | | 3070 | $\nu_2$, C—H str |
| 3056 | R | | |
| 3047 | Q | 3030 | $\nu_3$, C—H str |
| 3036 | P | | |
| 2290 | R | | |
| | | 2280–2295[b] | $\nu_6 + \nu_{11}$ |
| 2267 | P | | |
| 2246 | R | | |
| 2237 | Q | 2235–2271[b] | $\nu_4$, C≡N str |
| 2228 | P | | |
| 1915 | R | | |
| 1906 | Q | | $\nu_9 + \nu_{10}$ |
| 1898 | P | | |
| 1657 | ? | [c] | $\nu_6 + \nu_{15}$ |
| 1641 | ? | [c] | |
| 1622 | R | | |
| 1615 | Q | 1602 | $\nu_5$, C=C str |
| 1604 | P | | |
| 1421 | R | | |
| 1415 | Q | 1413 | $\nu_6$, $CH_2$ in-plane def |
| 1405 | P | | |

[a] Assignment for vapor AN was taken from ref 6. [b] Frequencies varied in the range indicated according to the kinds of interlayer cations involved. [c] The band expected in this region was obscured by the deformation vibration of adsorbed water.

ison with vapor AN, the observed bands for adsorbed AN are very simple; they do not have PQR structure. This fact is ascribable to loss of the rotational freedom of AN because the molecules adsorbed in the interlayer space are restricted in their movement.[7] The band at 1602 $cm^{-1}$ was tentatively assigned to the C=C stretching vibration, though it was obscured by the absorption due to the deformation vibration of adsorbed water. The bands appearing in the CN stretching region were shifted to higher frequencies corresponding to the polarizing power of the interlayer cation involved as described previously.[2] The 3070-$cm^{-1}$ band observed for mont–AN complexes has no counterpart in the spectrum of vapor AN; however, it appears in the spectrum of liquid AN at 3072 $cm^{-1}$ and is assigned to a fundamental vibration, $\nu_2$.[6] In order to assign this band to one of the three C–H stretching vibrations of AN, infrared spectra of the complexes containing AN-$\alpha d$ were measured. In these spectra, the 3070-$cm^{-1}$ band disappeared but the other two C–H stretching bands at 3130 and 3030 $cm^{-1}$ were essentially unchanged by deuteration. Therefore, it is apparent that the 3070-$cm^{-1}$ band can be assigned to the C–H stretching vibration concerned with the $\alpha$-positioned hydrogen.

The intensity of this band increased as the incidence angle increased as shown in Figure 2. The value of the pleochroism measurement is affected by several factors such as the "imperfection" of the orientation, so that the information may be of qualitative nature. But it will be reasonable to interpret Figure 2 as indicating that the direction of the

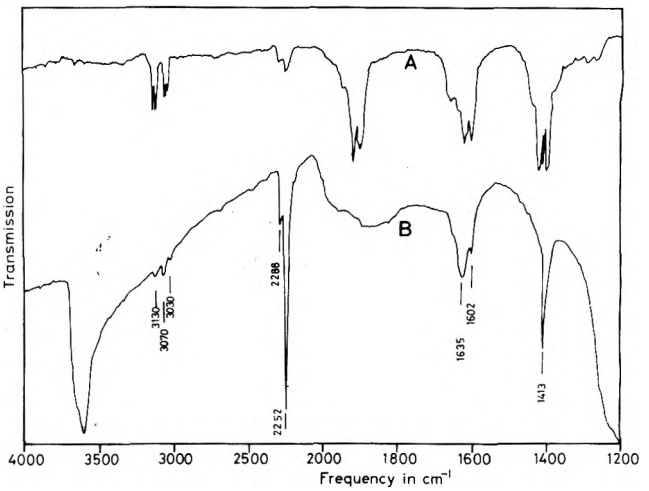


**Figure 1.** Infrared spectra of (A) vapor AN (60 Torr) and (B) the Ca–mont–AN complex.

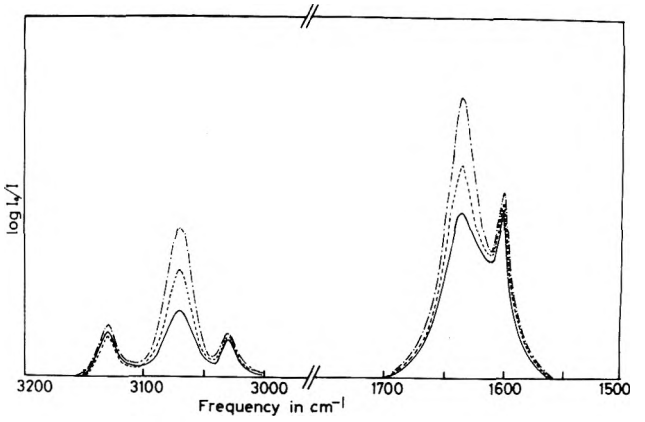


**Figure 2.** Pleochroism of the Ca–mont–AN complex with a basal spacing of 17.8 Å in the regions of 3200–3000 and 1700–1500 $cm^{-1}$, for three angles of incidence: ——, 0°; - - - -, 30°; — · — · —, 60°.

C–H band ($\alpha$ position) must be at a high angle to the silicate layer.

In the case of AN–mont complexes with large polarizing power cations, the existence of retained water was recognized as an infrared absorption near 1630 $cm^{-1}$ ($H_2O$ deformation), and an appreciable pleochroic effect was observed for this band for which the transition moment was along the molecular principal axis of $C_{2v}$ symmetry. Moreover, this band was shifted toward higher frequency in comparison with that of the evacuated sample when AN was introduced into the cell; the magnitude of the shift varied corresponding to the kind of cation, from 1617 to 1640 $cm^{-1}$ for Mg and from 1625 to 1635 $cm^{-1}$ for Ca, Co, and Ni. These observations on the deformation vibration are quite similar to the finding by Serratosa[8] on water contained in montmorillonite–benzonitrile complexes. Therefore, the model proposed in his study can be applied to picturing the molecular arrangement in mont–AN complexes; adsorbed water is placed with its molecular principal axis at a high angle to the silicate sheets, forming hydrogen bonds with the oxygen layers of the silicate structure.

When the complexes with small polarizing power cations such as $Na^+$, $K^+$, $NH_4^+$, $Li^+$, and $Ba^{2+}$ were subjected to evacuation for 6 hr, the intensities of the absorption bands due to AN decreased. In the case of larger polarizing power

**TABLE II: X-Ray Diffraction Data**

| Montmorillonite | Polarizing power of cation[a] | Pre-treatment[b] | Basal spacing data of mont–AN complex: Spacing with AN vapor, Å | No. of obsd orders | Spacing after evacuation for 6 hr, Å | No. of obsd orders |
|---|---|---|---|---|---|---|
| K–mont | 0.75 | A | 13.0 | 5 | 9.9 | 5 |
| Na–mont | 1.05 | A | 13.0 | 5 | 9.6 | 5 |
| Ba–mont | 1.48 | A | 13.0 | 5 | 13.0 | 5 |
| Li–mont | 1.67 | A | 13.2 | 3 | 13.0 | 4 |
| | | B | 13.0 | 5 | 13.0 | 4 |
| Ca–mont | 2.02 | A | 17.8 | 5 | 13.0 | 4 |
| | | B | 13.0 | 4 | | |
| Co–mont | 2.78 | A | 17.9 | 6 | 13.2 | 4 |
| | | B | 13.2 | 4 | | |
| Ni–mont | 2.90 | A | 17.8 | 6 | 13.3 | 4 |
| | | B | 13.3 | 4 | | |
| Mg–mont | 3.08 | A | 17.8 | 5 | 13.2 | 4 |
| | | B | 13.3 | 4 | | |
| $NH_4$–mont | 0.68 | A | 16.3 | 5 | 10.1 | 5 |

[a] See ref 2. [b] A = dehydration under vacuum at room temperature; B = dehydration under vacuum at 80°.

cations such as Mg, Ca, Co, and Ni, on the other hand, the intensities of the bands due to AN did not essentialy change on the same treatment, but instead those due to retained water decreased. Even when the Mg–, Ca–, Co–, and Ni–mont–AN complexes were heated up to 80° under vacuum, AN could not be removed.

*Basal Spacing.* Basal spacings of the samples prepared under various conditions are listed in Table II. Values of these spacings of the complexes can be classified into three main groups: 17.8, 16.7, and approximately 13 Å. Magnesium, calcium, cobalt, and nickel montmorillonites formed two types of complexes depending on the degree of hydration of the minerals. The basal spacings of the complexes obtained using highly dehydrated samples were approximately 13 Å, whereas the montmorillonites which contained an appreciable amount of water even after degassing formed the complexes with the basal spacing of 17.8 Å. The latter type was converted into the former type by evacuation. The decrease of the basal spacing from 17.8 to 13 Å is attributed to the removal of retained water instead of AN adsorbed, because the infrared study mentioned above indicated that the intensities of the bands due to AN did not essentially change but those due to adsorbed water decreased. For sodium, potassium, and ammonium montmorillonites, the decrease in the value by evacuation was due to complete desorption of AN.

A (001) spacing of 16.3 Å was observed only for ammonium montmorillonite. Since ammonium montmorillonite was subject to complete dehydration by evacuation even at room temperature, absorption bands due to retained water could not be observed in the infrared spectrum of $NH_4$–mont–AN complex. Therefore, the characteristic spacing value for this complex was not ascribable to water as in the 17.8-Å form. The pleochroism of the 3070-$cm^{-1}$ band of the $NH_4$–mont–AN complex was also measured; however, we could not observe obvious changes because of the interference of a broad absorption at 3080 $cm^{-1}$ arising from the $NH_4$ cation.[9]

## Discussion

On the basis of the value of the basal spacing, mont–AN complexes can be classified into three groups: (1) complexes with Na, K, Li, and Ba cations; (2) complexes with Ca, Mg, Co, and Ni cations; (3) the complex with the $NH_4$ cation. The possible orientation of AN contained in these complexes is estimated as follows.

*Group 1.* All of the basal spacings of the complexes belonging to this group are 13.0 Å as shown in Table II. The value indicates that the sorbed AN molecules are oriented with their molecular planes parallel to the silicate sheets. If we make a reasonable assumption that the effective thicknesses of the $\pi$-electron cloud of AN and of the silicate layer are 3.4 and 9.6 Å, respectively, the calculated spacing, 13.0 Å, is in good agreement with the observed one.

Sodium and potassium montmorillonites could be easily dehydrated even by evacuation at room temperature and changed into the montmorillonites with the basal spacings of 9.6 and 9.9 Å, respectively. These values mean that the complete dehydration caused adjacent silicate sheets to come together. It is interesting to note that AN molecules take the trouble to penetrate into the interlayer space, enlarging the basal spacing up to 13.0 Å. Such a strong affinity of AN for montmorillonite cannot be attributed to only the ion–dipole interaction of Na and K cations with AN, because the polarizing power of these cations seems to be too small to overcome the difficulties of internal adsorption. For a better understanding of the intercalation reaction mechanism, some additional factors must be taken into account.

*Group 2.* Montmorillonites classified into group 2 are distinguished by the large polarizing power of their interlayer cations from the other groups. These complexes have two types of basal spacings corresponding to the amount of adsorbed water retained. The complexes with the basal spacing of 13 Å are the dehydration form of those with a 17.8-Å spacing. Summarizing the results of the pleochroic study, together with the observations of a previous paper,[2] we can present a possible arrangement of the molecules adsorbed in the complexes with 17.8-Å spacing as shown in Figure 3, where four AN molecules surround a cation through CN groups with the C–H ($\alpha$ position) bond axis at a high angle to the silicate sheet and two water molecules are placed above and below the cation. The water molecules are hydrogen bonding with the oxygen of the silicate surface. The fact that the basal spacings of the dehydrated

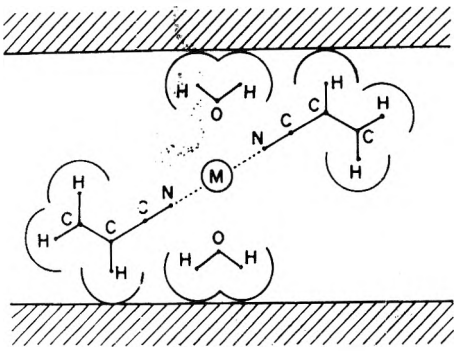

Figure 3. An idealized arrangement of interlayer materials in mont–AN complexes with a basal spacing of 17.8 Å. M indicates one of Mg, Ca, Co, and Ni cations. (The other two AN molecules are not shown.)

complexes vary from 13.0 to 13.3 Å according to the samples cannot be explained yet, but the orientation of the adsorbed AN seems to be essentially similar to that of group 1. The change in color of cobalt montmorillonite is of particular interest. Cobalt montmorillonite equilibrated in air was "pink" and converted into a "light purple" color by evacuation. The Co–mont–AN complex with a basal plane spacing of 17.8 Å was also "pink", but it changed into a "deep sky blue" form with a basal spacing of 13.2 Å, losing only water by evacuation at 80°. The change in color of the Co–mont–AN complex can be reasonably interpreted in terms of the change of the coordination number from 6 for the 17.8-Å form with four AN and two water molecules into 4 for the 13.0-Å form with two water molecules lost.

*Group 3.* Ammonium montmorillonite has properties similar to those of potassium montmorillonite as far as it is concerned with adsorption isotherms for AN, the shift of CN frequency, and ease of dehydration. However, the basal plane spacing of the $NH_4$–mont–AN complex (16.3 Å) was clearly distinguished from that of the K–mont–AN complex (13.0 Å). One remarkable difference between $NH_4$ and K cations is that $NH_4$ can furnish its hydrogen atoms to hydrogen bonds. The characteristic value of the basal spacing for the $NH_4$–mont–AN complex can be explained by taking hydrogen bonds into account, as shown in Figure 4. An idealized model proposed in Figure 4 seems to have a favorable arrangement, because many hydrogen bonds such as NH- - -O and NH- - -N can stabilize the complex. As mentioned above, we could not ascertain the formation of the NH- - -N hydrogen bond from the results of the infrared study. However, it is not strange that the frequencies of the bands due to exchangeable $NH_4^+$ of dehydrated montmorillonite are not shifted on exposure to AN, because $NH_4^+$ forms hydrogen bonds with oxygen layers of the silicate sheets before the NH- - -N bonds are produced with adsorbed AN.

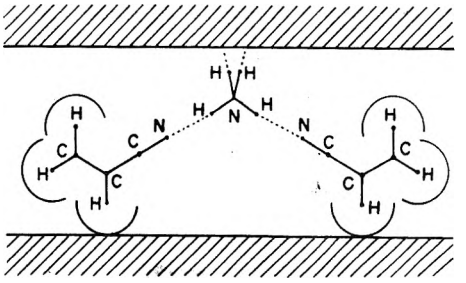

Figure 4. Proposed orientation of AN molecules and the $NH_4$ cation in the $NH_4$–mont-AN complex.

The fact that AN adsorbed on ammonium montmorillonite was removed as easily as the molecules adsorbed on potassium montmorillonite indicates that hydrogen-bond formation contributes only a little to the stabilization of the complex. It is noteworthy that such a weak interaction is sufficient to affect the orientation of adsorbed molecules.

These considerations lead to an important conclusion: the stability of the complexes is mainly due to the polarizing power of the interlayer cations involved, and the orientations of adsorbed molecules are much more influenced by other important factors such as the amount of the adsorbed water and hydrogen-bond formation.

*Acknowledgment.* The expense of this study was partly defrayed by a Grant-in-Aid for Special Research Projects from the Ministry of Education.

## References and Notes

(1) To whom correspondence should be addressed at the Department of Applied Chemistry, University of Osaka Prefecture, Sakai, Osaka 591, Japan.
(2) S. Yamanaka, F. Kanamaru, and M. Koizumi, *J. Phys. Chem.*, **78**, 42 (1974).
(3) J. M. Serratosa, *Clays Clay Miner.*, **14**, 385 (1967).
(4) L. C. Leitch, *Can. J. Chem.*, **35**, 345 (1957).
(5) W. F. Bradley, *J. Am. Chem. Soc.*, **67**, 975 (1945).
(6) F. Halverson, R. F. Stamm, and J. J. Whalen, *J. Chem. Phys.*, **16**, 808 (1948).
(7) L. H. Little, "Infrared Spectra of Adsorbed Species", Academic Press, London and New York, 1966, Chapter 11.
(8) J. M. Serratosa, *Am. Mineral.*, **53**, 1244 (1968).
(9) M. M. Mortland, J. J. Fripiat, J. Chaussidon, and J. Uytterhoeven, *J. Phys. Chem.*, **67**, 248 (1963).

# Lithium-7 Nuclear Magnetic Resonance Study of Lithium Cryptates in Various Solvents

**Yves M. Cahen, James L. Dye, and Alexander I. Popov***

*Department of Chemistry, Michigan State University, East Lansing, Michigan 48824* *(Received November 6, 1974)*

*Publication costs assisted by Michigan State University*

Lithium-7 NMR studies were performed on lithium ion complexes with cryptands C222, C221 and C211 in water and in several nonaqueous solvents. In the case of the first two cryptands the exchange between the free and complexed lithium ion was fast by the NMR time scale and only one population-average resonance was observed. Cryptand 211 forms much more stable lithium complexes and two $^7Li$ resonances (corresponding to the free and the bound $Li^+$) were observed for solutions containing excess of the $Li^+$ ion. The limiting chemical shifts of the complex were found to be independent of the solvent indicating that the lithium ion is completely shielded by the cryptand. Formation constants of lithium–C222 complexes were determined in water and pyridine solutions. The values obtained were, log $K_{H_2O} = 0.99 \pm 0.15$ and log $K_{Py} = 2.94 \pm 0.10$.

## Introduction

In recent years a number of new macrocyclic ligands have been synthesized which form stable complexes with alkali metal ions. Crown ethers, developed by Pedersen,[1] were the first such complexing agents to appear. Shortly thereafter Lehn[2] introduced a new class of complexing agents of hexaoxadiamine macrobicyclic type called "cryptands"[3] which complex alkali metal cations to an even greater extent than the crown ethers. Cryptands form an inclusion type complex where the metal ion is trapped inside the cavity of the ligand. Lehn and coworkers have studied extensively alkali metal cryptates in solutions[4] primarily by potentiometric technique and by proton NMR. For example they were able to study potassium and barium cryptates in deuteriochloroform by proton NMR.[5]

We wish to report the effects of the formation of lithium cryptates on the $^7Li$ NMR spectra and the determination of the formation constant of lithium–C222 complexes in water and pyridine by this technique. A preliminary communication of some of our results was published earlier.[6]

## Experimental Section

The 211 and 221 cryptands (I) were obtained from E. M.

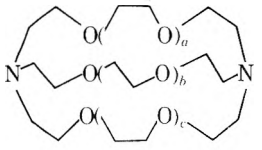

I

2,2,2, $a = b = c = 1$

2,2,1, $a = 0$, $b = c = 1$ 2,1,1, $a = b = 0$, $c = 1$

Laboratories Inc. and were used as received. Lithium-7 NMR measurements indicate that their purity is greater than 98%. Cryptand 222 (I) was prepared by a modification[7] of the method of Dietrich et al.[2] These compounds will be identified in the following text by C211, C221, and C222, respectively. Nitromethane, dimethyl sulfoxide, tetrahydrofuran, pyridine, propylene carbonate, dimethylformamide, formamide, and chloroform were purified and dried by previously described techniques.[8] Lithium perchlorate (Fisher) was dried at 190° for several days (water content 0.2% as determined by Karl Fischer titration). Lithium iodide (K & K Laboratories) was purified by recrystallization from acetone and dried under vacuum over $P_2O_5$ by elevating the temperature progressively from 28 to 82° (water content, 0.1%). Solutions of cryptands and lithium salt were prepared at various ligand/$Li^+$ mole ratios in all of the above solvents except chloroform where solutions with excess lithium salt could not be prepared due to the lack of solubility. In this case, at least an equimolar amount of a cryptand was necessary to solubilize the lithium salt.

Nuclear magnetic resonance experiments were carried out on a Varian DA-60 spectrometer in a V-4333 probe at 23.3 MHz and 1.4092 T. Spinning 5 mm sample tubes were used. A 1-mm o.d. melting point capillary inserted coaxially in the sample tube and filled with an appropriate solution (usually a 4 $M$ aqueous $LiClO_4$ solution) was used as an external standard. The observed chemical shifts were corrected for the bulk diamagnetic susceptibility of the solvents. The measurements were made at probe temperature of 30 ± 1°.

## Results and Discussion

The $^7Li$ chemical shifts were determined as a function of cryptand/$Li^+$ mole ratios with the results shown in Table I. Typical spectra obtained with C211 are shown in Figure 1.

The stability of a cryptate complex is largely determined by the size of the crypt cavity and by the solvating ability of the solvent. If the rate of exchange of the lithium ion between the two sites, free ion in the bulk solution and the complex, is greater than $\sqrt{2}/\pi\Delta\nu$, where $\Delta\nu$ is the difference between the characteristic resonance (in Hz) in each site, only one population-average resonance is observed. This is the case with C222 which has a much larger cavity (2.8 Å) than the bare lithium ion (1.56 Å). In nitromethane, dimethyl sulfoxide, pyridine, and water only one $^7Li$ resonance is observed.

In dimethyl sulfoxide and water, the solvent molecules have a strong solvating ability and compete quite successfully with the ligand. Consequently, only a weak lithium cryptate complex is formed and a large excess of ligand is necessary to produce a variation of the observed $^7Li$ chemi-

**TABLE I: $^7$Li NMR Study of 222-, 221-, 211-Lithium Complexes in Various Solvents at 30 ± 1°**

| Solvent | Salt | [Li$^+$], $M$ | [Crypt-and]/[Li$^+$] | $^7$Li chemical shift, ppm[a] |
|---|---|---|---|---|
| Crypt 222 | | | | |
| $CH_3NO_2$ | $LiClO_4$ | 0.025 | 0.0 | 0.35 |
| | | | 0.5 | 0.75 |
| | | | 1.0 | 1.02 |
| | | | 2.0 | 1.03 |
| DMSO | $LiClO_4$ | 0.025 | 0.0 | 0.97 |
| | | | 0.5 | 0.97 |
| | | | 1.0 | 0.96 |
| | | | 2.0 | 0.96 |
| Pyridine | $LiClO_4$ | 0.025 | 0.0 | −1.52 |
| | | | 0.7 | 0.30 |
| | | | 1.0 | 1.04 |
| | | | 2.5 | 1.61 |
| | | | ∞[b] | 1.73 |
| $H_2O$ | LiI | 0.010 | 0.0 | 0.00 |
| | | | 1.0 | $0.00_5$ |
| | | | 10.0 | $0.09_5$ |
| | | | 20.0 | 0.11 |
| | | | ∞[b] | 0.18 |
| Crypt 221 | | | | |
| $CH_3NO_2$ | $LiClO_4$ | 0.05 | 0.0 | 0.38 |
| | | | 0.5 | 0.81 |
| | | | 1.0 | 1.04 |
| | | | 2.0 | 1.03 |
| DMSO | $LiClO_4$ | 0.05 | 0.0 | 0.94 |
| | | | 0.5 | 0.96 |
| | | | 1.0 | 0.97 |
| | | | 2.0 | 0.98 |
| Pyridine | $LiClO_4$ | 0.05 | 0.0 | −2.16 |
| | | | 0.5 | −2.21, 1.87 |
| Crypt 211 | | | | |
| $CH_3NO_2$ | $LiClO_4$ | 0.15 | 0.0 | 0.61 |
| | | | 1.0 | *0.41*[c] |
| | LiI | 0.14 | 0.0 | 0.49 |
| | | | 1.0 | *0.42* |
| | $LiI_3$ | 0.14 | 0.0 | 0.11 |
| | | | 0.4 | 0.01 and *0.37* |
| | | | 0.9 | *0.37* |
| | LiCl | 0.13 | 1.0 | *0.41* |
| DMSO | $LiClO_4$ | 0.20 | 0.0 | 0.97 |
| | | | 0.8 | 0.95 and *0.39* |
| | | | 1.0 | *0.39* |
| | LiI | 0.14 | 0.0 | 0.95 |
| | | | 1.0 | *0.39* |
| | LiCl | 0.11 | 0.0 | 0.88 |
| | | | 1.0 | *0.39* |
| | $LiBPh_4$ | 0.10 | 0.0 | 0.97 |
| | | | 1.0 | *0.42* |
| THF | $LiI_3$ | 0.10 | 0.0 | 0.48 |
| | | | 0.5 | 0.44 and *0.36* |
| | | | 1.0 | *0.36* |
| PC | $LiClO_4$ | 0.25 | 0.0 | 0.45 |
| | | | 0.5 | 0.52 and *0.38* |
| | | | 1.0 | *0.38* |
| $CHCl_3$ | $LiI_3$ | 0.15 | 1.0 | *0.38* |
| $H_2O$ | LiI | 0.25 | 0.0 | 0.00 |
| | | | 0.5 | 0.00 and *0.38* |
| DMF | $LiClO_4$ | 0.25 | 0.0 | −0.50 |
| | | | 0.5 | −0.40 and *0.42* |
| Formamide | $LiClO_4$ | 0.25 | 0.0 | −0.39 |
| | | | 0.5 | −0.43 and *0.38* |

[a] Vs. aqueous $LiClO_4$ at infinite dilution (corrected for magnetic susceptibility). [b] Calculated. [c] Chemical shifts of C-211 cryptates.

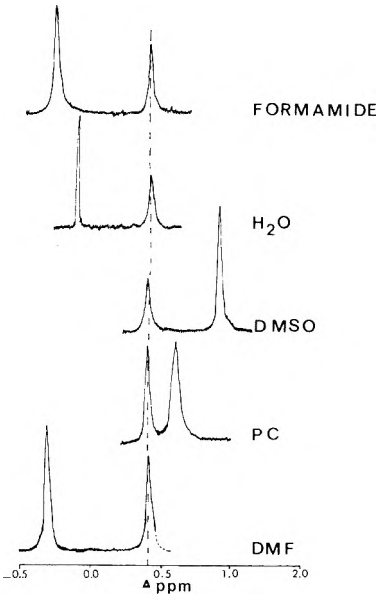


**Figure 1.** Lithium-7 NMR spectra of lithium-C211 cryptate in various solvents: [C211] = 0.25 *M*, [Li$^+$] = 0.50 *M*. Chemical shift of Li-C211 is at 0.41 ppm vs. aqueous $LiClO_4$ solution at infinite dilution.

cal shift (see Table I) from the position characteristic of the solvated Li$^+$ ion in the given solvent. In nitromethane and pyridine, which are poor solvating solvents, the respective complexes are readily formed as evidenced by the chemical shift of the $^7$Li resonance upon addition of the ligand.

With C221 the exchange is slower because of the smaller cavity size of this ligand (2.2 Å). In dimethyl sulfoxide C221 forms a weak complex with Li$^+$ ion while in nitromethane the complex is more stable and the limiting chemical shift for Li$^+$–C221 complex is reached at 1:1 ligand/Li$^+$ mole ratio. In both cases only one population-averaged resonance line is observed because the exchange is fast on the NMR time scale. In pyridine at room temperature the exchange is slow enough and the difference between the chemical shift of both sites is large enough (97 Hz) so that two $^7$Li resonances are obtained, one for the complexed lithium at at 1.87 ppm and one for the free lithium at −2.02 ppm vs aqueous $LiClO_4$ solution at infinite dilution (Figure 2).

Cryptand 211 has a cavity radius nearly equal to that of the unsolvated lithium ion. It is expected, therefore, that very stable lithium complexes will be formed and that the exchange will be slow. The Li$^+$–C211 system was investigated in nitromethane, dimethyl sulfoxide, tetrahydrofuran, propylene carbonate, chloroform, dimethylformamide, formamide, and water solutions. The data shown in Table I indicated that in all solvents the addition of the ligand in less than stoichiometric amounts results in two resonances

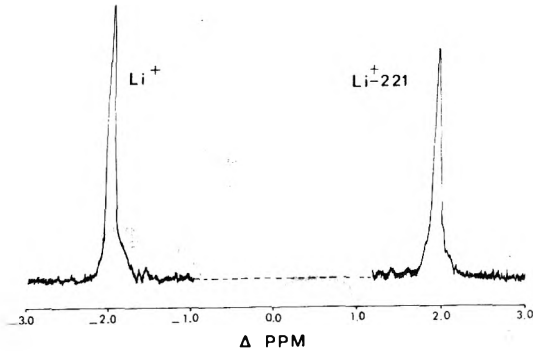


**Figure 2.** Lithium ion and lithium–C221 resonances in pyridine solutions: [C221] = 0.25 *M*, [$Li^+$] = 0.50 *M* vs. aqueous $LiClO_4$ solution at infinite dilution.

corresponding to the free and the complexed lithium ion. Similar results were found in a $^{23}Na$ NMR study of sodium–C222 complexes in ethylenediamine[8] and in other solvents.[9]

Not surprisingly, the chemical shift of the lithium ion complexed by C211 is essentially independent of the solvent and of the counterion used (Figure 1). In all cases it is found at 0.40 ± 0.03 ppm. In the complex, the lithium ion is completely encased by the ligand and, since the $^7Li$ chemical shifts are dependent almost exclusively on the nearest neighbors of the lithium ion, they are insensitive to either the solvent molecules surrounding the cryptate or to counterion in cases where a low dielectric constant of the solvent (such as THF or chloroform) would lead to ion pair formation.

On the other hand, the limiting chemical shifts of $Li^+$–C222 and especially $Li^+$–C221 complexes are definitely solvent dependent indicating that the looser structure of the complex permits the solvent molecules to approach sufficiently close to the metal ion so as to affect its resonance frequency.

Lithium NMR has been shown to be a useful technique for the determination of the formation constants of weak and medium strength complexes.[10,11] This technique was described in detail in an earlier publication which dealt with the determination of the formation constants of $Li^+$–glutarimides and $Li^+$–tetrazole complexes in nitromethane. This approach was used in this work to determine the formation constants of $Li^+$–C222 complexes in water and in pyridine. The technique involves the measurement of $^7Li$ chemical shifts as a function of ligand/$Li^+$ mole ratio followed by a computer fit of the data with the equation

$$\delta_{obsd} = [(KC_t^M - KC_t^L - 1) \pm (K^2C_t^{L^2} + K^2C_t^{M^2} - 2K^2C_t^LC_t^M + 2KC_t^L + 2KC_t^M + 1)^{1/2}]\left[\frac{\delta_f - \delta_c}{2KC_t^M}\right] + \delta_c$$

which has two adjustable parameters, the formation constant $K$ and the limiting chemical shift of the complex $\delta_c$. The other factors are the total concentration of the ligand, $C_t^L$, total concentration of the $Li^+$ ion, $C_t^M$, chemical shift of the uncomplexed $Li^+$, $\delta_f$, and the observed chemical shift, $\delta_{obsd}$.

The values obtained were log $K$ = 0.99 ± 0.15 and log $K$ = 2.94 ± 0.10, respectively. The previously reported value in methanol[12] is log $K$ = 2.65 which reflects its intermediate solvating ability for the lithium ion between that of water and of pyridine. Previous estimates of the log $K$ values in water were ~0[2] and <2.[13,14]

It should be noted that the above values are the *concentration* constants. However, since the complexation reaction

$$Li^+ + C222 \rightleftarrows Li^+\text{–}C222$$

does not involve separation of charges, these values should represent reasonable approximations of the thermodynamic constants.

*Acknowledgment.* The authors gratefully acknowledge the support of this work by the National Science Foundation Grant No. GP-36427 and the U.S. Atomic Energy Commission Contract No. AT(11-1)-958.

## References and Notes

(1) C. J. Pedersen, *J. Am. Chem. Soc.*, **89**, 7017 (1967).
(2) B. Dietrich, J. M. Lehn, anc J. P. Sauvage, *Tetrahedron Lett.*, 2885, 2889 (1969).
(3) Following the suggestion of Lehn (personal communication) we designate the ligands as *cryptands* and the corresponding complexes as *cryptates*.
(4) B. Dietrich, J. M. Lehn, and J. P. Sauvage, *J. Chem. Soc., Chem. Commun.*, 15 (1973), and references cited therein.
(5) B. Dietrich, J. M. Lehn, and J. P. Sauvage, *Tetrahedron Lett.*, **29**, 1647 (1973).
(6) J. L. Dye, M. T. Lok, F. J. Tehan, J. Ceraso, and K. Voorhees, *J. Org. Chem.*, **38**, 1773 (1973).
(7) Y. M. Cahen, P. R. Handy, E. T. Roach, and A. I. Popov, *J. Phys. Chem.*, in press.
(8) J. M. Ceraso and J. L. Dye, *J. Am. Chem. Soc.*, **95**, 4432 (1973).
(9) Unpublished work, this laboratory.
(10) R. L. Bodner, M. S. Greenberg, and A. I. Popov, *Spectrosc. Lett.*, **5**, 489 (1972).
(11) Y. M. Cahen, R. F. Beisel, and A. I. Popov, *J. Inorg. Nucl. Chem.*, in press.
(12) J. M. Lehn, *Structure Bonding*, **16**, 1 (1973).
(13) J. M. Lehn and J. P. Sauvage, *Chem. Commun.*, 440 (1971).
(14) J. M. Lehn and J. P. Sauvage, paper presented at conference de thermodynamique chimique, Societe chimique de France, Bordeaux France, Oct 20, 1972.

# Lithium-7 Nuclear Magnetic Resonance Study of Lithium Ion–Lithium Cryptate Exchange Rates in Various Solvents

**Yves M. Cahen, James L. Dye, and Alexander I. Popov***

*Department of Chemistry, Michigan State University, East Lansing, Michigan 48824* *(Received January 20, 1975)*

*Publication costs assisted by Michigan State University*

The kinetics of complexation reactions of the lithium ion with cryptand C211 in pyridine, water, dimethyl sulfoxide, dimethylformamide, and formamide and with cryptand C221 in pyridine were investigated by temperature-dependent $^7$Li NMR. The energies of activation for the release of $Li^+$ from $Li^+$–C211 complexes *increase* with the increasing donicity of the solvent as expressed by the Gutmann donor number. The transition state of the complexation reaction must involve substantial ionic solvation. Using the formation constants of the $Li^+$–C211 cryptate in water the rate constant for the forward reaction was found to be $k_f = 0.98 \times 10^3$ sec$^{-1}$.

## Introduction

During recent years a number of synthetic macrocyclic polyethers and polyamines have been synthesized which are capable of forming strong complexes with the alkali and alkaline earth ions. Among the most effective of these compounds are the polyoxadiamine macrobicyclic ligands ("cryptands",[1] I) synthesized and studied extensively by Lehn and coworkers.[2]

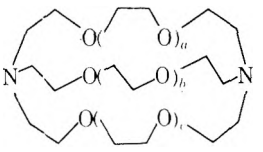

I

C222, a = b = c = 1

C221, $a = b = 1$, $c = 0$ C211, $a = 1$, $b = c = 0$

The stability of the cryptate complexes depends to a large extent on the size relationship between the three-dimensional cavity of the cryptand and the diameter of the complexed ion. Thus cryptand C211, with a cavity diameter of 1.6 Å, forms a very stable complex with the lithium ion ($d$ = 1.56 Å). On the other hand, cryptands C221 and C222 with cavity diameters of 2.2 and 2.8 Å, respectively, form only weak complexes with $Li^+$ but strong complexes with the sodium ($d$ = 2.24 Å) and potassium ($d$ = 2.88 Å) ions.

In the case of the weaker complexes, the solvating ability of the solvent plays an important role in the complexation reaction. We have shown recently[3,4] that the $Li^+$–C221 and $Li^+$–C222 complexation reactions occur readily in a poorly solvating solvent, such as nitromethane, but cannot be detected in the strongly solvating solvent, dimethyl sulfoxide. The drastic effect of the solvent on the complexation reaction is also illustrated by the formation constants for the $Li^+$–C222 complex which were found to be 9.8 in water and 960 in pyridine. Thus, the strong solvating ability of water drastically depresses the value of the $Li^+$–C222 formation constant.

The kinetics of complexation reactions of the $Na^+$–C222 complex in ethylenediamine solutions were investigated by Ceraso and Dye[5] by using $^{23}$Na NMR techniques. Similar studies on this system in a variety of solvents have recently been completed in our laboratory.[6] Complexation reaction rates were also studied by Lehn and coworkers in aqueous and methanol solutions by NMR methods.[7,8]

The lithium ion forms stable complexes with the cryptand C211, and the exchange between the free and the bound lithium ions is slow on the NMR time scale. Thus solutions containing lithium in excess can be examined by measuring the $^7$Li resonances. The exchange kinetics can be deduced from changes in line shapes as a function of temperature. We wish to report a study of the $Li^+$–cryptate exchange kinetics in water and in several nonaqueous solvents.

## Experimental Section

Cryptands 211 and 221 were obtained from E. M. Laboratories Inc., Elmsford, N.Y., and were used as received. From $^7$Li NMR measurements it was estimated that their purity was ≥98%. Pyridine, dimethyl sulfoxide, dimethylformamide, formamide, lithium perchlorate, and lithium iodide were purified and dried by previously described techniques.[9] Lithium perchlorate was used in nonaqueous solvents. Since this compound is only sparingly soluble in water it was replaced by lithium iodide for studies in aqueous solutions.

Nuclear magnetic resonance measurements were carried out on a Varian DA-60 spectrometer by using the side band technique, with a V 4333 probe at 23.3 MHz and 1.4092 T. Spinning 5-mm sample tubes were used with a 1-mm o.d. melting point capillary inserted coaxially in the spinning tube and filled with an external reference solution (usually 4 $M$ $LiClO_4$ in water). Temperatures were measured with a calibrated thermocouple. Pressurized NMR tubes (30 to 50 psi of $N_2$) were used when it was necessary to record a spectrum above the boiling point of the sample solution.

## Results and Discussion

The complexation process between a ligand L and a cation $M^+$ in a solvent S can be represented by the following general equation

$$L + M^+_{solv} \underset{k_b}{\overset{k_f}{\rightleftharpoons}} LM^+ + solvent \qquad (1)$$

which assumes a first-order process for the backward reaction, e.g., in our case, the dissociation reaction or the release of the lithium ion from the cryptate cavity. Such a mechanism was found to be predominant for the complexation of sodium ions by several 18-crown-6 complexing agents.[10] The general case of exchange between two sites A and B with different relaxation times is described by the following modified Bloch equations[6,11]

$$G = u + iv \tag{2}$$

$$v = -\gamma H_1 M_0 \left[ \frac{SU + TV}{S^2 + T^2} \right] \tag{3}$$

$$u = -\gamma H_1 M_0 \left[ \frac{UT - SV}{S^2 + T^2} \right] \tag{4}$$

where $G$ is the complex moment of magnetization, $v$ and $u$ are the pure absorption and pure dispersion line shapes, respectively, and

$$S = \frac{p_A}{T_{2A}} + \frac{p_B}{T_{2B}} + \frac{\tau}{T_{2A}T_{2B}} - \tau(\omega_A - \omega)(\omega_B - \omega) \tag{5}$$

$$U = 1 + \tau(p_B/T_{2A} + p_A/T_{2B}) \tag{6}$$

$$T = (p_A\omega_A + p_B\omega_B - \omega) + \tau\left[ \frac{(\omega_A - \omega)}{T_{2B}} + \frac{(\omega_B - \omega)}{T_{2A}} \right] \tag{7}$$

$$V = \tau(p_B\omega_A + p_A\omega_B - \omega) \tag{8}$$

where $p_A$ and $p_B$ are the relative population at sites A and B, respectively, and $\tau$ is the lifetime of interaction defined by

$$\tau = \tau_A\tau_B/(\tau_A + \tau_B) \tag{9}$$

$\omega_A$ and $\omega_B$ are the resonance frequencies at the two sites at a given temperature in the absence of exchange and $T_{2A}$ and $T_{2B}$ are the respective relaxation times at each site at a given temperature in the absence of exchange. If at a given temperature the lifetime $\tau$ is greater than $\sqrt{2}/(\pi\Delta\omega)$, where $\Delta\omega = |\omega_A - \omega_B|$, two separate resonances are observed for the two respective sites; if $\tau$ is less than $\sqrt{2}/(\pi\Delta\omega)$, only one population-averaged resonance is observed.

Since it was experimentally difficult and inconvenient in the case of coalescing lines to obtain a pure absorption mode signal, a phase correction was made and the observed line shape was fitted by the following equation:

$$v' = u \sin\theta + v\cos\theta + c \tag{10}$$

where $\theta$ is the phase correction parameter and $c$ the base line adjustment parameter. An example of the spectra obtained at various temperatures for aqueous solutions is shown in Figure 1. Spectra were analyzed on a CDC 6500 computer by using the Fortran IV KINFIT program[12] based on a generalized weighted nonlinear least-squares analysis. Each spectrum was fitted with four parameters; the lifetime $\tau$, the phase correction $\theta$, the base line adjustment $c$, and a normalization factor. A typical computer output (Figure 2) shows the fit of a spectrum ($LiClO_4$, C211) in formamide at 143.3°.

Respective populations $p_A$ and $p_B$ were obtained from the stoichiometry (lithium to ligand) used, assuming a large complex formation constant, and were checked by the integration of each resonance line below the coalescence temperature. The areas were found to be temperature independent within experimental error.

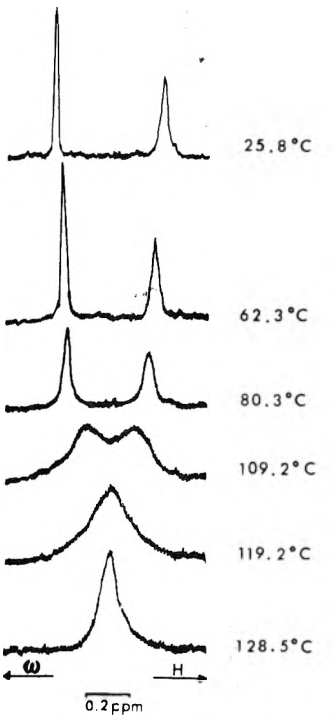


**Figure 1.** Spectra at various temperatures for an aqueous solution containing 0.50 *M* LiI, 0.25 *M* C211.

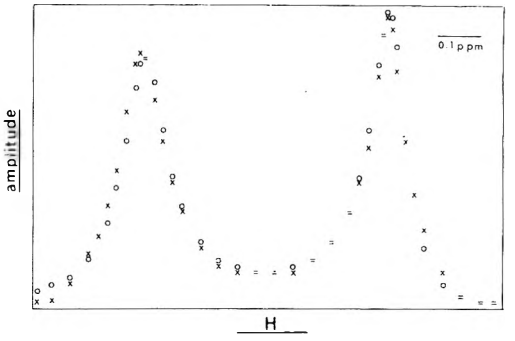


**Figure 2.** Computer fit of spectra obtained with 0.50 *M* $LiClO_4$, 0.25 *M* C211 in formamide at 143.3°. × represents an experimental point, O, a calculated point, =, an experimental and calculated point are the same within the resolution of the plot.

For the $Li^+$–C211 systems, no exchange is observable at room temperature. Measurable exchange, detected by the onset of broadening of both resonance lines, begins at higher temperatures, $t_E$, which were found to be about 75, 80, 105, 145, and 85° in dimethyl sulfoxide, water, formamide, pyridine, and dimethylformamide, respectively. It was noted that $\omega_A$ and $\omega_B$ varied linearly with temperature relative to the lock frequency. The difference between the chemical shift (ppm) of the solvated ion A and that of the complexed ion B is a linear function of temperature as expressed by

$$\delta_A - \delta_B \equiv \Delta(\delta) = \Delta(\delta_0) - S(t - 25) \tag{11}$$

in which $\Delta(\delta_0)$ is $\delta_A - \delta_B$ at 25°. The values of $\Delta(\delta_0)$ and $S$ are given in Table I. At temperatures higher than $t_E$, $\omega_A$ and $\omega_B$ were obtained by extrapolation. The validity of this extrapolation was verified by separate experiments on solutions which contained only A or B. The $T_{2A}$ and $T_{2B}$ values given in Table I were determined by measurement of the full width at half-height of each resonance line and were

**TABLE I: Description of $\Delta(\delta)$ as a Function of Temperature[a]**

| Solvent | Salt | Cryptand | $\Delta(\delta_0)$, ppm | $S$, ppm/°C | $T_{2A}$, sec | $T_{2B}$, sec |
|---|---|---|---|---|---|---|
| Pyridine | $LiClO_4$ | 211 | 3.425 | −0.00696 | 0.796 | 0.637 |
| Water | LiI | 211 | 0.520 | −0.00222 | 0.796 | 0.354 |
| Dimethyl sulfoxide | $LiClO_4$ | 211 | −0.525 | 0.00181 | 0.909 | 0.374 |
| Dimethylformamide | $LiClO_4$ | 211 | 0.999 | −0.00364 | 1.061 | 0.455 |
| Formamide | $LiClO_4$ | 211 | 1.010 | −0.00370 | 0.909 | 0.374 |
| Pyridine | $LiClO_4$ | 221 | −3.986 | −0.00746 | 0.707 | 0.637 |

[a] $\Delta(\delta) = \Delta(\delta_0) + S(t - 25)$; $\Delta(\delta) = \delta_A - \delta_B$ at a given temperature $t$ (°C); $\Delta(\delta_0) = \delta_A - \delta_B$ at 25° (A = solvated ion, B = complexed ion).

**TABLE II: Exchange Rates and Thermodynamic Parameters of Lithium Cryptate Exchange in Various Solvents**

| Solvent | DN[a] | $\epsilon$[b] | $E_a$, kcal mol$^{-1}$ | $k_b \times 10^3$, sec$^{-1}$ (298°K) | $\Delta H_0^{\ddagger}$, kcal mol$^{-1}$ | $\Delta S_0^{\ddagger}$, cal °K$^{-1}$ mol$^{-1}$ | $\Delta G_0^{\ddagger}$, kcal mol$^{-1}$ (298°K) |
|---|---|---|---|---|---|---|---|
| Cryptand 211 | | | | | | | |
| Pyridine | 33.1 | 12.3 | 19.6 (3.5)[c] | 0.12 (0.24) | 19.0 (3.4) | −12.5 (9.2) | 22.7 (1.1) |
| Water | 33.0 | 78.6 | 21.3 (1.2) | 4.9 (2.0) | 20.7 (1.1) | +0.4 (3.0) | 20.6 ($0.2_5$) |
| Dimethyl sulfoxide | 29.8 | 45.0 | 16.1 (0.6) | 23.2 (5.4) | 15.5 (0.6) | −13.8 (1.4) | 19.7 ($0.1_4$) |
| Dimethylformamide | 26.6 | 36.1 | 16.0 (0.6) | 13.0 (3.3) | 15.4 (0.6) | −15.5 (1.4) | 20.0 ($0.1_5$) |
| Formamide | 24.0 | 111.0 | 14.1 (0.7) | 7.4 (2.9) | 13.5 (0.7) | −22.8 (1.8) | 20.8 ($0.2_3$) |
| Cryptand 221 | | | | | | | |
| Pyridine | 33.1 | 12.3 | 13.5 (0.4) | 1230 (196) | 12.9 (0.4) | −14.9 (0.9) | 17.9 (0.1) |

[a] Gutmann donor number.[14] [b] Dielectric constant. [c] Standard deviation.

found to be temperature independent. It should be noted that the cryptate resonance line is 2 to 3 times broader than the resonance line for the solvated ion. Therefore, the width of the cryptate resonance line cannot be entirely caused by field inhomogenities.

In the case of the $Li^+$–C221 system in pyridine, $\omega_A$, $\omega_B$, $T_{2A}$, and $T_{2B}$ were measured by separate experiments since some exchange occurs at room temperature.

Activation energy plots, log $k_b$ vs. $1/T$ are shown in Figure 3. Activation energies ($E_a$), rate constants ($k_b$), and values of $\Delta H_0^{\ddagger}$, $\Delta S_0^{\ddagger}$, and $\Delta G_0^{\ddagger}$ for the release of $Li^+$ from the cryptate are given in Table II. A complete error analysis[13] including cross correlation terms which account for the coupling of parameters (particularly evident between $\Delta H_0^{\ddagger}$ and $\Delta S_0^{\ddagger}$) was performed in all cases. Not surprisingly, $\Delta G_0^{\ddagger}$, which is directly determined from $k_b$, has the smallest standard deviation.

The accuracy of the determination of the activation energy depends upon the range of temperatures over which exchange can be measured. For example, with the $Li^+$–C211 system in pyridine, the difference between the chemical shift of the solvated and the complexed lithium ion is 2.7 ppm, which is considerably larger than the shifts found in other solvents (0.5–1 ppm). Thus, for this system the exchange is observable over only a limited temperature range and coalescence could not be observed. Therefore, the activation energy could only be determined from the line broadening below the coalescence temperature, which accounts for the relatively large standard deviation. On the other hand for the $Li^+$–C221 system in the same solvent, the exchange is observable over a large temperature range, 62.6–159.4°, and the activation energy can be determined with a higher accuracy.

The energies of activation for the release of $Li^+$ from the $Li^+$–C211 complexes in pyridine, water, dimethyl sulfoxide, dimethylformamide, and formamide seem to be determined by the donicity of the solvent as expressed by the Gutmann donor number,[14] rather than the dielectric constant. The activation energies vary from 14.1 kcal mol$^{-1}$ in formamide (DN = 24) to 21.3 kcal mol$^{-1}$ in water (DN = 33.0). By contrast, Shchori et al.[10] found that the (smaller) activation energies for release of $Na^+$ from dibenzo-18-crown-6 were independent of the solvent used. However, two of the three solvents used, methanol and dimethylformamide, have the same donicity while that of the third solvent, dimethoxyethane, is not known.

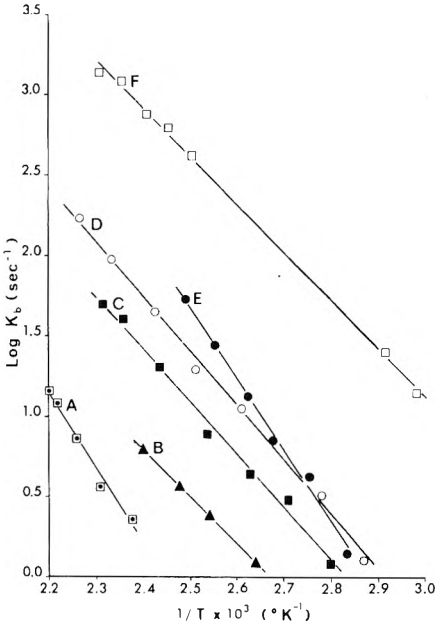


**Figure 3.** Log $k_b$ vs. $1/T$ plot for 0.50 *M* $LiClO_4$, 0.25 *M* C211 in (A) pyridine, (B) formamide, (C) dimethylformamide, (D) dimethyl sulfoxide, (E) 0.50 *M* LiI, 0.25 *M* C211 in water, and (F) 0.50 *M* $LiClO_4$, 0.25 *M* C221 in pyridine.

We expect that the *net* energy required to transfer $Li^+$ from the cryptate to the solvent should decrease with increasing donicity of the solvent since this scale is a good

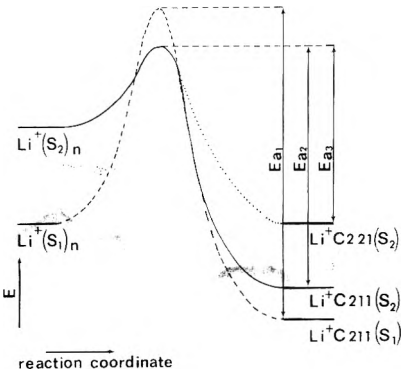


**Figure 4.** Schematic representation of the complexation of lithium ion by cryptands 211 and 221. $S_1$ represents a good donor solvent, $S_2$ a poor one.

measure of the primary solvation energy. The solvation energy of the cryptate and the secondary solvation energy of the lithium ion both depend primarily upon the dielectric constant of the solvent and change in the same direction from solvent to solvent.

Since the activation energy *increases* with increasing donicity, opposite to the overall energy change, the transition state must involve substantial ionic solvation. The energy profile is illustrated schematically in Figure 4. The solid line represents the complexation path of $Li^+$–C211 in a poor donor solvent ($S_2$) and the dashed line in a good donor solvent ($S_1$) with reverse activation energies of $E_{a_1}$ and $E_{a_2}$, respectively ($E_{a_1} > E_{a_2}$). In the same solvent, for example $S_2$, the energy level of the 221 cryptate will be higher than for the 211 cryptate because of the better fit of the lithium ion in the C211 cavity. On the other hand, if the transition state is similar to the solvated lithium ion, its energy should not depend strongly upon the cryptand used. The energy of activation for $Li^+$–C221 ($E_{a_3}$) is lower than for $Li^+$–C211 ($E_{a_2}$) in pyridine, 13.5 and 19.6 kcal $mol^{-1}$, respectively.

Although $E_a$ and hence $\Delta H_0^{\ddagger}$ are very sensitive to the solvent used, the values of $\Delta G_0^{\ddagger}$ (298°K) are nearly independent of solvent. Changes in $\Delta H_0^{\ddagger}$ are compensated for by corresponding changes in $\Delta S_0^{\ddagger}$, a not uncommon occurrence.[15]

Using the formation constant of $Li^+$–C211 cryptate in water determined by Lehn and coworkers[2] ($\log K = 5.3$) we can calculate the rate constant for the forward reaction, $k_f = Kk_b = 0.98 \times 10^3$ $sec^{-1}$ for $Li^+$–C211 in water.

*Acknowledgment.* The authors gratefully acknowledge the support of this work by the National Science Foundation Grant No. GP-36427 and the U.S. Atomic Energy Commission Contract No. AT(11-1)-958.

## References and Notes

(1) Following the suggestion of Lehn (private communication) we shall refer to the ligands as *cryptands* and to the complexes as *cryptates*.
(2) J. M. Lehn, *Structure Bonding*, **16**, 1 (1973), and references cited therein.
(3) Y. M. Cahen, J. L. Dye, and A. I. Popov, *Inorg. Nucl. Chem. Lett.*, **10**, 899 (1974).
(4) Y. M. Cahen, J. L. Dye and A. I. Popov, preceding article in this issue.
(5) J. M. Ceraso and J. L. Dye, *J. Am. Chem. Soc.*, **95**, 4432 (1973).
(6) Unpublished work, this laboratory.
(7) J. M. Lehn, J. P. Sauvage, and B. Dietrich, *J. Am. Chem. Soc.*, **92**, 2916 (1970).
(8) J. P. Kintzinger and J. M. Lehn, *J. Am. Chem. Soc.*, **96**, 3313 (1974).
(9) Y. M. Cahen, P. R. Handy, E. T. Roach, and A. I. Popov, *J. Phys. Chem.*, **79**, 80 (1975).
(10) E. Shchori, J. J. Grodzinski, and M. Shporer, *J. Am. Chem. Soc.*, **95**, 3842 (1973).
(11) J. A. Pople, W. G. Schneider, and H. J. Bernstein, "High Resolution Nuclear Magnetic Resonance", McGraw-Hill, New York, N.Y., 1959, pp 218–224. An error in their equation (10–14) in which $p_A$ and $p_B$ are interchanged was propagated in ref 5. In the latter case $p_A$ and $p_B$ were equal so the error did not affect the final results.
(12) J. L. Dye and V. A. Nicely, *J. Chem. Educ.*, **48**, 443 (1971).
(13) W. E. Wentworth, *J. Chem. Educ.*, **42**, 96 (1965).
(14) (a) V. Gutmann and E. Wycheva, *Inorg. Nucl. Chem. Lett.*, **2**, 257 (1966); (b) V. Gutmann, "Coordination Chemistry in Nonaqueous Solvents", Springer Verlag, Vienna, 1968.
(15) K. J. Laider, "Chemical Kinetics", McGraw-Hill, New York, N.Y., 1965, pp 251–253.

# Dissociation of Hydroxyl Protons of β-Hydroxyalkyl Radicals as Studied by Electron Spin Resonance[1]

**Yutaka Kirino**

*Radiation Research Laboratories and Department of Chemistry, Mellon Institute of Science, Carnegie-Mellon University, Pittsburgh, Pennsylvania 15213* *(Received September 9, 1974)*

*Publication costs assisted by the U.S. Energy Research and Development Administration and Carnegie-Mellon University*

The ESR spectra of seven β-hydroxyalkyl radicals produced by OH addition to olefinic compounds have been examined in strong base by the in situ radiolysis method. Above pH 13 significant changes in ESR parameters, especially large changes in β-proton coupling constants, are observed and can be interpreted in terms of the dissociation of the hydroxyl protons. The p$K$ values of the radicals have been determined to be 14.6 for $^-O_2CĊHCH_2OH$, 14.9 for $^-O_2CĊ(CH_3)CH_2OH$, 13.3 for $NCĊHCH_2OH$, 14.7 for $ĊH_2CH_2OH$, 14.6 for $CH_3ĊHCH_2OH$, 15.1 for $CH_3OĊHCH_2OH$, and 15.2 for $^-O_2CĊHCH(CO_2^-)OH$. The p$K$ values for the β-hydroxyalkyl radicals derived from ethanol and propanol are, respectively, 1.2 and 1.5 units lower than for the parent alcohols. Limitations to the meaning of certain of the above values resulting from the applicability of the available acidity functions at very high base concentrations are discussed in detail. A correlation is obtained between p$K$ values and Hammett $\sigma_p$ values for substituents on the trivalent carbon atom. In all radicals a decrease in the α-proton coupling constants and an accompanying slight increase in $g$ factors are observed upon dissociation, indicating an increase in the amount of spin density on the oxygen atom in the dissociated form.

## Introduction

There are, as of yet, no reports on the dissociation of hydroxyl protons in β-hydroxyalkyl radicals while the dissociation equilibria of α-hydroxyalkyl radicals have been examined in detail both by optical pulse radiolysis[2] and by ESR methods.[3] The p$K$ values of the latter radicals are within the conventional pH scale (typically 10–12)[2,3] and are lower by about 4–5 units than those of the corresponding alcohols (typically 15–16). It was generally considered that a β-hydroxyalkyl radical should be as weak an acid as the corresponding alcohol so that the measurement of their p$K$ values would be difficult. Our recent finding[4] that the p$K$ values for β-sulfhydrylalkyl radicals are about 2 units lower than those for the corresponding thiols suggests by analogy that β-hydroxyalkyl radicals may be somewhat stronger acids than the corresponding alcohols. Values of p$K$ for the latter type of radical are thus anticipated to be around 14. This paper presents a detailed ESR study on the acid dissociation equilibria of β-hydroxyalkyl radicals produced by OH addition to olefinic compounds.

## Experimental Section

*Materials.* Acrylic acid, methacrylic acid, acrylonitrile, fumaric acid, and maleic acid were from Aldrich. Ethylene and propylene were from Phillips and methyl vinyl ether was from Matheson. Potassium hydroxide or sodium hydroxide was taken from newly opened bottles of "Baker Analyzed" reagent. Nitrous oxide was from Linde. Water was distilled and freed from organic impurities by passing the vapor with oxygen through a silica tube at ~600°. Other chemicals were of the highest grade commercially available.

*Radical Production and ESR Observation.* All measurements were made at about 20°. Most of the experiments were carried out by the in situ radiolysis–ESR method.[5] A strongly basic (KOH or NaOH) solution of an appropriate olefinic compound (5–10 m$M$) was saturated with $N_2O$ which served both to remove oxygen and to convert $e_{aq}^-$ formed in the radiolysis to OH. In the case of the gaseous olefinic compounds, mixtures with nitrous oxide were bubbled through basic solutions. A β-hydroxyalkyl radical in the equilibrium with its dissociated form was produced by the processes 1–3. With the increase of base concentration

$$OH + OH^- \rightleftharpoons O^- + H_2O \quad (pK = 11.85)^6 \qquad (1)$$

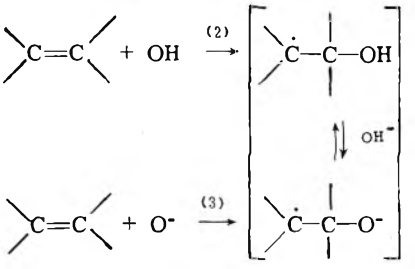


it became more difficult to get a spectrum of sufficient intensity for these observations. A large portion of this decrease in spectral intensity was probably the result of conversion of OH to $O^-$, which adds only slowly to double bonds.[7] Decrease of cavity Q also caused a decrease of intensity and impurities introduced by the large amount of base might scavenge OH or a radical of interest. Another production method was tried unsuccessfully for $ĊH_2CH_2OH$, i.e., reductive dechlorination of 2-chloroethanol by reaction with $e_{aq}^-$[8] and hydrogen abstraction from ethanol by OH.[9] In the former method 2-chloroethanol hydrolyzed rapidly in strongly basic solution; in the latter only the α-hydroxyethyl radical was observed. The in situ photolysis[10] of persulfate solutions[11] could be used in a limited region of basicity for the production of $^-O_2C$-$ĊHCH_2OH$, $NCĊHCH_2OH$, and $^-O_2CĊHCH(CO_2^-)OH$. Sodium or potassium persulfate (5–30 m$M$) solutions containing olefinic compounds (2–5 m$M$) were photoirradiated with a mercury–xenon lamp. The sulfate radical anion

($SO_4^{\cdot-}$) initially produced by photolysis is converted to OH rapidly in strongly basic solutions[12] (pH >12) and the latter radical follows the reaction sequence 1–3. However, insolubility of persulfates in very concentrated KOH solutions limited the applicability of the method.

*Acidity Scale.* Throughout the experiment potassium hydroxide was mainly used as a base and sodium hydroxide was used only in limited cases. For potassium hydroxide solutions of pH <13, pH measurement was carried out with an Orion Research Model 801 digital pH meter equipped with a Sargent-Welch S-30070-10 glass electrode. For more concentrated KOH or NaOH solutions, the concentration of the base was determined by titration with 0.1 or 0.4 *N* hydrochloric acid prepared from an "Acculute" standard solution of Anachemia Chemicals. There are few basicity scales available above the pH scale for concentrated aqueous potassium or sodium hydroxide solutions. Using the ionization of indoles, Yagil[13] has determined an $H_-$ acidity function for aqueous KOH or NaOH which parallels well at relatively low hydroxide concentrations (below 11 *M* in NaOH and below 8 *M* in KOH) the scale of Schwarzenbach and Sulzberger,[14] who used a series of indigo derivatives as indicators. The $H_{2-}$ function for aqueous KOH has been measured by Yagil[13] using indole carboxylates while the $H_{2-}$ function for aqueous NaOH has been determined by Hallé et al.,[15] using sulfonate and carboxylate derivatives of aniline and diphenylamine. In the present work Yagil's $H_-$ scale was chosen for neutral radicals ($NC\dot{C}HCH_2OH$, $\dot{C}H_2CH_2OH$, $\dot{C}H_3CHCH_2OH$, and $CH_3O\dot{C}HCH_2OH$) in KOH or NaOH solutions and Yagil's $H_{2-}$ scale for radicals with a single negative charge ($^-O_2C\dot{C}HCH_2OH$ and $^-O_2C\dot{C}(CH_3)CH_2OH$) and for the radical $^-O_2C\dot{C}HCH(CO_2^-)OH$ in KOH solutions.

## Results

Around pH 11 ESR spectra of good quality were observed for the following seven radicals produced by OH addition: $^-O_2C\dot{C}HCH_2OH$ (I) from acrylate, $^-O_2C\dot{C}(CH_3)CH_2OH$ (II) from methacrylate, $NC\dot{C}HCH_2OH$ (III) from acrylonitrile, $\dot{C}H_2CH_2OH$ (IV) from ethylene, $CH_3\dot{C}HCH_2OH$ (V) from propylene, $CH_3O\dot{C}HCH_2OH$ (VI) from methyl vinyl ether, and $^-O_2C\dot{C}HCH(CO_2^-)OH$ (VII) from fumarate or maleate. These spectra are very similar, respectively, to those previously observed in more acidic solutions.[16] ESR parameters for these radicals found in the present study are shown in the second column of Table I. From methacrylonitrile, only weak lines were detected partly because of the large number of splittings and further study in concentrated base solutions was not possible. No spectra were observed from vinyl fluoride, vinyl chloride, vinylidene chloride, and methyl vinyl ketone.

With the increase in base concentration above $10^{-3}$ *M* changes in ESR parameters of the radicals I–VII were found. Especially large changes (1.4–5.4 G) in the β coupling constants (increase for the radicals I–VI and decrease for VII) were observed. In all radicals the α-proton coupling constants decreased with increasing basicity but most changes were small. Radical VI, however, showed a decrease in $a_\alpha$ as large as that for $a_\beta$. These large dependences of the coupling constants ($a_\beta$ for all the radicals and also $a_\alpha$ for VI) on basicity were analyzed in terms of the dissociation equilibrium of the hydroxyl protons (eq 4). If the in-

$$\underset{\text{A}}{\text{>}\dot{C}CH_2OH} + OH^- \overset{K}{\rightleftharpoons} \underset{\text{B}}{\text{>}\dot{C}CH_2O^-} + H_2O \qquad (4)$$

**TABLE I: ESR Parameters[a] for the Acid and Base Forms of the β-Hydroxyalkyl Radicals and Their Dissociation Constants**

| Radical in acid form | Acid form[b] (A) | | | | | Base form (B) | | | | | [KOH] at half-neutralization, *M* | p*K* of corresponding alcohol |
|---|---|---|---|---|---|---|---|---|---|---|---|---|
| | Hf coupling const | | | | | Hf coupling const | | | | p*K* of radical | | |
| | β-H | α-H | $CH_3$ | N | *g* factor | β-H | α-H | $CH_3$ | N | *g* factor | | |
| I, $^-O_2C\dot{C}HCH_2OH$ | 27.53 | 20.46 | | | 2.00308 | 31.75 | 19.80 | | | 2.00313 | 14.6 ± 0.1 | 1.24 | Unknown |
| | | | | | | (+4.22 | −0.66 | | | +0.00005)[c] | | | |
| II, $^-O_2C\dot{C}(CH_3)CH_2OH$ | 20.15 | | 22.92 | | 2.00306 | 21.52 | | 22.43 | | 2.00306 | 14.9 ± 0.1 | 1.98 | Unknown |
| | | | | | | (+1.40 | | −0.49 | | ~0)[c] | | | |
| III, $NC\dot{C}HCH_2OH$ | 28.20 | 20.07 | | 3.54 | | 30.85 | 19.40 | | 3.48 | 2.00285 | 13.3 ± 0.2 | 0.46 | Unknown |
| | | | | | | (+2.65 | −0.67 | | −0.06 | +0.00003)[c] | | | |
| IV, $\dot{C}H_2CH_2OH$ | 27.25 | 21.92 | | | 2.00236 | 30.24[d] | 21.56[e] | | | 2.00242[e] | 14.7 ± 0.2 | *f* | 15.9[g] |
| | | | | | | (+2.49 | −0.36 | | | +0.00006)[c] | | | |
| V, $CH_3\dot{C}HCH_2OH$ | 19.77 | 21.58 | 25.40 | | 2.00244 | 21.71[d] | 21.21[e] | 25.22[e] | | 2.00245[e] | 14.6 ± 0.2 | *f* | 16.1[g] |
| | | | | | | (+1.94 | −0.37 | −0.18 | | ~0)[c] | | | |
| VI, $CH_3O\dot{C}HCH_2OH$ | 8.89 | 17.14 | 1.81 | | 2.00293 | 10.66[d] | 15.25[d] | 1.66[e] | | 2.00291[e] | 15.1 ± 0.2 | *f* | 14.8[h] |
| | | | | | | (+1.71 | −1.79 | −0.25 | | ~0)[c] | | | |
| VII, $^-O_2C\dot{C}HCH(CO_2^-)OH$ | 15.58 | 20.29 | | | 2.00317 | 10.20 | 19.76 | | | 2.00321 | 15.2 ± 0.2 | 2.78 | Unknown |
| | | | | | | (−5.38 | −0.53 | | | +0.00004)[c] | | | |

[a] The hyperfine coupling constants are given in gauss and are accurate to ±0.02 G. The *g* factors are accurate to ±0.00003. Second-order corrections have been made: R. W. Fessenden, *J. Chem. Phys.*, **37**, 747 (1962). [b] Cf. ref 16. [c] Changes in parameters with dissociation, i.e., $a_B - a_A$ or $g_B - g_A$. [d] Determined by extrapolation using eq 7 in text. [e] Value observed in the most basic medium which allowed spectral detection. [f] Half-neutralization point could not be determined because of lack of the observation of the fully dissociated radical. The p*K* values shown correspond to KOH concentrations of 2.50, 2.25, and 3.67 *M* for radicals IV, V, and VI, respectively. [g] From ref 19. [h] From ref 20.

terchange between the acid form (A) and the base form (B) is rapid, the observed coupling constant, $a$, represents the weighted average of the concentrations of the two forms. If one knows the limiting values corresponding to the acid and base forms ($a_A$ and $a_B$, respectively), then the measured parameter gives a direct measure of the contribution of each, i.e.

$$a = a_A f_A + a_B f_B \quad (5)$$

where $f_A$ and $f_B$ refer to the fraction of A and B ($f_B = 1 - f_A$). For a given solution the dissociation constant can be calculated by eq 6 or 6′, where $H_x$ is an acidity function of

$$pK = pH + \log (f_A/f_B) = pH + \log [(a - a_B)/(a_A - a)] \quad (6)$$

$$pK = H_x + \log (f_A/f_B) = H_x + \log [(a - a_B)(a_A - a)] \quad (6')$$

the medium. A p$K$ value calculated from eq 6′ has the thermodynamic meaning only when an appropriate acidity function is employed, which means that the activity coefficient behavior of the compound in question must be the same as that of the indicators used to establish the $H_x$ scale.[17] An experimental criterion for appropriateness of a chosen acidity function is the plot of log $[(a - a_B)/(a_A - a)]$ against $-H_x$[17] which should be a straight line of slope 1. Actually, however, there is little choice for acidity scales applicable for the present work because only a few acidity functions are known for concentrated hydroxide solutions[13-15] as already mentioned above. Yagil's $H_-$ or $H_{2-}$ scale[13] was used for the radicals I–VI according to the charge of the radical. For the radical VII, the $H_{2-}$ scale was also employed since what should be called the $H_{3-}$ function is not known.

Figure 1a shows the $\beta$-proton coupling constant for $^-O_2C\dot{C}HCH_2OH$ in aqueous KOH as a function of the $H_{2-}$ acidity function. The usual calculation method[18] by eq 6′, using the six experimental points within 1 unit of the equilibrium constant, gave the p$K$ value of 14.56 with a scatter of 0.10. The concentration of KOH at $H_{2-}$ = p$K$ was 1.24 $M$. Also shown in Figure 1a is the solid curve calculated using eq 5 and 6′ and the parameters $a_A$ = 27.53 G, $a_B$ = 31.75 G, and p$K$ = 14.56 [$a = (a_A + a_B \times 10^{pH-pK})/(1 + 10^{pH-pK})$]. As anticipated from the good agreement found between the experimental points and the calculated sigmoid curve, the plot of log $[(a - a_B)/(a_A - a)]$ vs. $-H_{2-}$ gave a good straight line with a slope of 0.97. The same procedure for the radical $^-O_2C\dot{C}(CH_3)CH_2OH$ gave the p$K$ value of 14.94 ± 0.05 which corresponded to 1.98 $M$ KOH at an acidity equal to the p$K$. The slope of the linear plot of log $[(a - a_B)/(a_A - a)]$ vs. $-H_{2-}$ in this case was 1.03. These results described above show that the $H_{2-}$ function used is appropriate to the conjugate acid–base pairs of these radicals and that the p$K$ values obtained are meaningful. It is worth noting that the $H_{2-}$ function for aqueous NaOH determined by Hallé et al.[15] is not on the same scale as the Yagil $H_{2-}$ function for aqueous KOH, for, when the $\beta$-proton coupling constants for $^-O_2C\dot{C}HCH_2OH$ were measured in NaOH solutions and plotted against Hallé's $H_{2-}$ scale, the points were located far from the sigmoid curve as shown by the two triangles (corresponding to 1.97 and 5.04 $M$ NaOH) in Figure 1a.

Dependence of the $\beta$-proton coupling constant for $NC\dot{C}HCH_2OH$ on pH and the $H_-$ function is shown in Figure 1b. The calculation by eq 6′ using seven points within 1

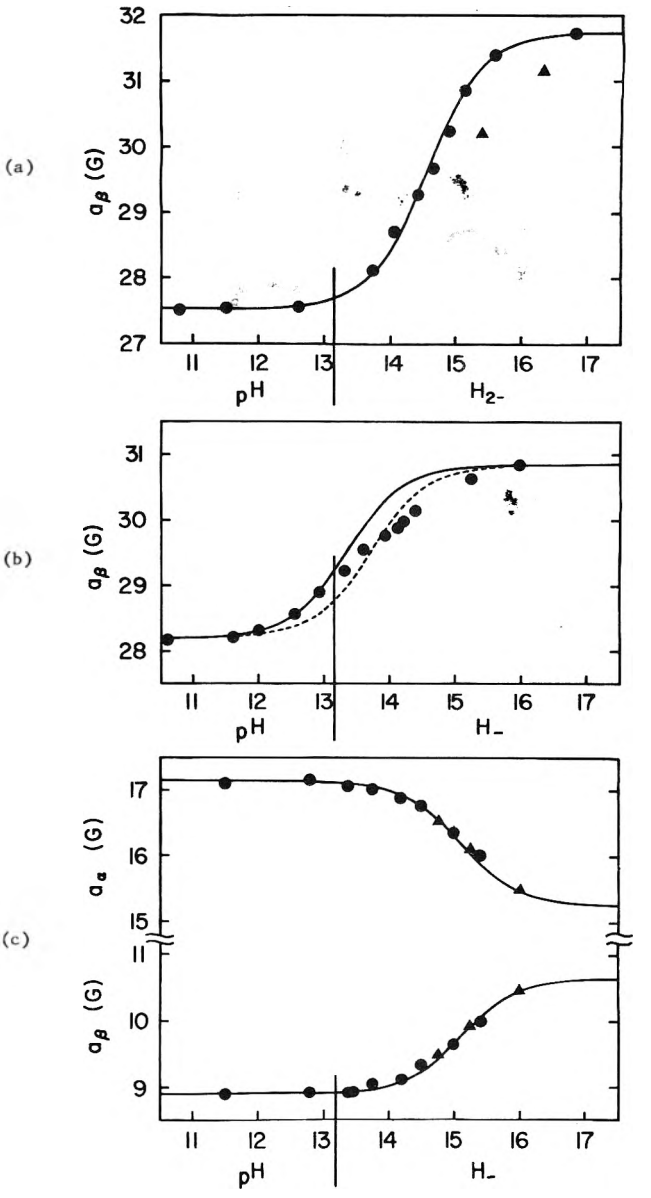


**Figure 1.** The $\beta$-proton coupling constants as a function of basicity for the radicals (a) $^-O_2C\dot{C}HCH_2OH$, (b) $NC\dot{C}HCH_2OH$, and (c) $CH_3O\dot{C}HCH_2OH$ ($a_\alpha$ also shown). Circles and triangles indicate measurement in aqueous KOH and NaOH, respectively. The solid curves are calculated from the data in Table I under the assumption that the spectrum represents the weighted average of the concentrations of the acid and base forms of the radicals. The dashed curve in (b) is based on p$K$ = 13.7.

unit of the half-neutralization point and the limiting values of $a_A$ = 28.20 G and $a_B$ = 30.85 G gave a nominal p$K$ value of 13.7 ± 0.3. However, the deviation of the experimental points from the curve calculated by use of this p$K$ value (shown by the dashed line in the figure) is large. The slope of the plot of log $[(a - a_B)/(a_A - a)]$ vs. $-H_-$ was only 0.85. These facts indicate either that the $H_-$ function used is inappropriate or that there were unknown factors specific for this radical causing large errors. The former is favored since the latter seems unlikely. Therefore, we have concluded that the use of only the experimental points in the pH range and the two limiting values must give a more accurate p$K$ value. Using three points between pH 12 and 13, eq 6 gave the p$K$ value of 13.3. This p$K$ value has been used to calculate the solid curve in Figure 1b.

In Figure 1c changes in $\alpha$ and $\beta$ coupling constants for $CH_3\dot{O}CHCH_2OH$ are plotted against the $H_-$ scale. Circles and triangles indicate measurements in KOH and NaOH solutions, respectively. The two bases did not show any significant difference. For this radical, $\dot{C}H_2CH_2OH$, and for $CH_3\dot{C}HCH_2OH$, ESR spectra for the completely dissociated forms could not be obtained because of the difficulty of detection in the very highly basic solutions. The coupling constants for the dissociated forms ($a_B$) were determined by eq 7, using four experimental points in the higher region

$$a = a_B + (1/K)(a_A - a) \text{ antilog } (-H_-) \quad (7)$$

of basicity. A linear plot of $a$ against $(a_A - a)$ antilog $(-H_-)$, using the method of least squares, gave the value for $a_B$ as an intercept. The value of $a_B$ thus obtained was in turn used to calculate p$K$ from eq 6′. The p$K$ values determined were 14.7 ± 0.1 for $\dot{C}H_2CH_2OH$, 14.6 ± 0.1 for $CH_3\dot{C}HCH_2OH$, and 15.1 ± 0.2 for $CH_3O\dot{C}HCH_2OH$. It should be noted that the use of eq 7 for estimation of $a_B$ assumes the appropriateness of the acidity function used[17] and that good fit of the experimental points to the calculated curve obtained in these findings cannot verify the appropriateness of the acidity function.

The p$K$ value of $^-O_2C\dot{C}HCH(CO_2^-)OH$ was determined to be 15.2 ± 0.2 from the decrease in the $\beta$ coupling constant with the basicity which was represented by Yagil's $H_{2-}$ function. The slope of the plot of log $[(a - a_B)/(a_A - a)]$ *vs.* $-H_{2-}$ was 0.90. All the results are summarized in Table I.

As mentioned above the low intensities of the β-hydroxyalkyl radicals in concentrated base solution result from the tendency of $O^-$ to abstract hydrogen rather than add to double bonds. In fact, the predominant radicals from propylene and methacrylate above about 3 $M$ in hydroxide were allylic radicals, $CH_2\cdots CH\cdots CH_2$ [$a_H$ = 14.85 (2 H), 13.96 (2 H), and 4.17 G, $g$ = 2.00258] and $CH_2\cdots C(CO_2^-)\cdots CH_2$ [$a_H$ = 14.78 (2 H) and 13.95 G (2 H), $g$ = 2.00231], respectively. From methacrylate yet another radical $(CH_3)_2\dot{C}CO_2^-$ [$a_H$ = 21.69 G (6 H), $g$ = 2.00317] was detected with high intensity. This radical can be produced by hydrogen addition to methacrylate and/or partial addition of $e_{aq}^-$, which escaped the scavenging by $N_2O$, followed by protonation. ESR spectral parameters for these radicals were independent of the basicity of the medium.

## Discussion

The ESR method can follow the acid–base equilibrium of a radical as long as the ESR lines of the radical can be identified and their positions measured.[3] This method, therefore, does not depend directly on the concentration of the radical under study and is independent of the coexistence of other radicals. The other common methods used, such as optical pulse radiolysis, usually depend directly on the radical concentration and, therefore, are subject to the complications resulting from changes in radical yields, side reactions, impurities, and related problems which complicate the chemistry, particularly in highly alkaline solutions. Moreover the weighted average contribution of the acid and base forms of the radical is manifested in the ESR parameters, which can be determined very accurately, so that the accuracy of p$K$ values determined is limited largely by that of a basicity scale.

ESR parameters have been measured over the entire range of acid–base equilibria for the radicals $^-O_2C\dot{C}HCH_2OH$ (I), $^-O_2C\dot{C}(CH_3)CH_2OH$ (II), and $NC\dot{C}HCH_2OH$ (III) and their p$K$ values determined. The p$K$ values of 15.2 for the radical $^-O_2C\dot{C}HCH(CO_2^-)OH$ (VII) based on the Yagil $H_{2-}$ function seems reasonable, for radical VII is expected to be a weaker acid than the radical I because the former has an electron-releasing (+$I$ effect) substituent on the carbon atom adjacent to the OH group. However, the observed p$K$ value must be the upper limit since the slope of the plot of log $[(a - a_B)/(a_A - a)]$ against $-H_{2-}$ is less than unity. The KOH concentration, 2.78 $M$, at half-neutralization can be used to provide a better estimate of the p$K$ value when an appropriate acidity scale is established. It is somewhat difficult to evaluate the reliability of the p$K$ values 14.7, 14.6, and 15.1 observed for the radicals $\dot{C}H_2CH_2OH$ (IV), $CH_3\dot{C}HCH_2OH$ (V), and $CH_3O\dot{C}HCH_2OH$ (VI), respectively, since it is necessary to assume the appropriateness of the $H_-$ function used to estimate the coupling constants for the fully dissociated forms of these radicals. It is also possible that the $H_-$ scale used is inappropriate as in the case of radical III. If this is the case, the plot shown in Figure 1c may be similar to that obtained by omitting a few experimental points in highly basic region in Figure 1b. If one omitted two points in the most highly basic region in Figure 1b, one would estimate from the rest of the points $a_B$ = 30.30 G and p$K$ = 13.3 which is fortuitously the same as the true p$K$ value for III. In either case, therefore, it is likely that the p$K$ values obtained for the radicals IV–VI are close to the true values and in no case should be in error by more than 0.2 unit.

Even though one should avoid putting too much meaning on the absolute values of p$K$ obtained for IV–VI, relative values do have meaning, and so undoubtedly $CH_3O\dot{C}HCH_2OH$ (VI) is a weaker acid than $\dot{C}H_2CH_2OH$ (IV). On the other hand, when comparison is made between the corresponding alcohols, $CH_3OCH_2CH_2OH$ is definitely a stronger acid than $CH_3CH_2OH$[19,20] as seen from the values cited in the last column of Table I. The acidity of an alcohol is known to depend on the inductive effect ($I$ effect) of substituents and has a linear energy relationship with Taft $\sigma^*$ values.[20,21] The result for radicals IV and VI indicates that, while the $-I$ effect (electron withdrawing) of the methoxy group enhances the acidity of alcohol, a $+M$ effect (electron releasing) of the substituent dominates to weaken the acidity of the radical through the conjugation between the substituent and $\alpha$ carbon. Indeed, a plot of the p$K$ values of the radicals I–VI against Hammett $\sigma_p$ values gave a good straight line as shown in Figure 2 while a plot against Taft $\sigma^*$ values failed. The finding that the points for the radicals IV–VI are on a line together with the points for I–III seems to support again the p$K$ values determined for IV–VI.

The p$K$ values for radicals IV and V are respectively 1.2 and 1.5 units lower than those for the parent ethanol[19] and propanol.[19] Moreover, the p$K$ for $^-O_2C\dot{C}H_2CH_2OH$ can be estimated to be 16.0 from the relationship[20,21] between p$K$ values of alcohols and Taft $\sigma^*$ values so that the p$K$ for radical I is 1.4 units lower than for the corresponding alcohol. Therefore, it is concluded that the loss of a hydrogen atom from the position $\beta$ to the hydroxyl group in the alcohols enhances the acidity of hydroxyl proton by 1–1.5 units, except where the $I$ and $M$ effects of a substituent are in opposite directions.

Some characteristic changes in ESR parameters with dissociation should be pointed out. In all the radicals the $\alpha$-proton coupling constant decreased, indicating the decrease of spin density on the $\alpha$-carbon atom upon dissocia-

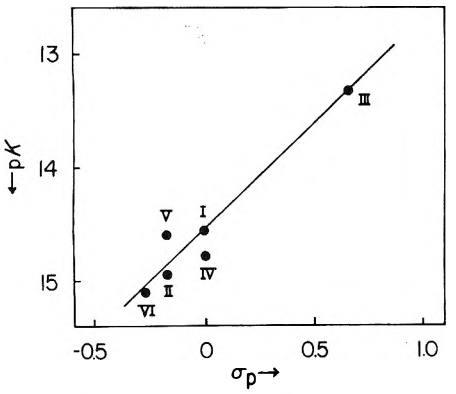


**Figure 2.** p$K$ values plotted against Hammett $\sigma_p$ values for the $\alpha$ substituent X in $XCHCH_2OH$: I, X = $CO_2^-$; III, X = CN; IV, X = H; V, X = $CH_3$; VI, X = $CH_3O$; II, $^-O_2CC(CH_3)CH_2OH$ (sum of $\sigma_p$ values for $CO_2^-$ and $CH_3$ was taken). Values for $\sigma_p$ are from ref 21.

tion. In four of the seven examples a slight but significant increase in the $g$ factors occurs and suggests the greater amount of spin density on oxygen atoms in the dissociated forms. The radical $^-O_2CCHCH(CO_2^-)OH$ showed a large decrease in the $\beta$-proton coupling constant upon dissociation in contrast to the increase shown by all the other radicals. Clearly this results from the effect of the substituent $CO_2^-$ attached to the carbon atom which bears the OH group. Qualitative explanation in this particular case is a change in the conformational preference from VIII to IX

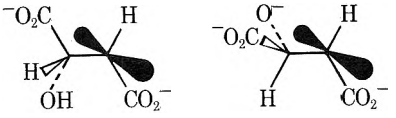


VIII IX

due to the repulsion between the negative charges on the $\alpha$ and $\beta$ sites.

*Acknowledgments.* The author gratefully acknowledges Professor R. H. Schuler, Professor R. W. Fessenden, and Dr. P. Neta for stimulating and helpful discussions.

## References and Notes

(1) Supported in part by the U.S. Atomic Energy Commission.
(2) K.-D. Asmus, A. Henglein, A. Wigger, and G. Beck, *Ber. Bunsenges. Phys. Chem.*, **70**, 756 (1966); M. Simic, P. Neta, and E. Hayon, *J. Phys. Chem.*, **73**, 4214 (1969).
(3) G. P. Laroff and R. W. Fessenden, *J. Phys. Chem.*, **77**, 1283 (1973).
(4) Y. Kirino and R. W. Fessenden, *J. Phys. Chem.*, **79**, 834 (1975).
(5) K. Eiben and R. W. Fessenden, *J. Phys. Chem.*, **75**, 1186 (1971).
(6) J. Rabani and M. S. Matheson, *J. Phys. Chem.*, **70**, 761 (1966); J. L. Weeks and J. Rabani, *ibid.*, **70**, 2100 (1966).
(7) P. Neta, M. Z. Hoffman, and M. Simic, *J. Phys. Chem.*, **76**, 847 (1972); P. Neta and R. H. Schuler, *ibid.*, **79**, 1 (1975).
(8) M. Anbar and E. J. Hart, *J. Phys. Chem.*, **69**, 271 (1965).
(9) T. Shiga, *J. Phys. Chem.*, **69**, 3805 (1965).
(10) D. Behar and R. W. Fessenden, *J. Phys. Chem.*, **75**, 2752 (1971).
(11) O. P. Chawla and R. W. Fessenden, *J. Phys. Chem.*, **79**, 76 (1975).
(12) L. Dogliotti and E. Hayon, *J. Phys. Chem.*, **71**, 2511 (1967); L. Dogliotti and E. Hayon, *ibid.*, **71**, 3807 (1967); E. Hayon and J. J. McGarvey, *ibid.*, **71**, 1472 (1967); O. P. Chawla, Ph.D. Dissertation, Carnegie-Mellon University, Aug 1973.
(13) G. Yagil, *J. Phys. Chem.*, **71**, 1034 (1967).
(14) G. Schwarzenbach and R. Sulzberger, *Helv. Chim. Acta*, **27**, 348 (1944).
(15) J.-C. Hallé, F. Terrier, and R. Schaal, *C. R. Hebd. Seances Acad. Sci., Ser. C*, **267**, 29 (1968).
(16) (a) H. Fischer, *Z. Naturforsch., Teil A*, **19**, 866 (1964), for $HO_2C$-$CHCH_2OH$, $HO_2CC(CH_3)CH_2OH$, $NCCHCH_2OH$, and $HO_2CCHCH$-$(CO_2H)OH$; (b) R. O. C. Norman, P. M. Storey, and P. R. West, *J. Chem. Soc. B*, 1087 (1970), for $^-O_2CCHCH_2OH$; (c) J. Dewing, G. P. Longster, J. Myatt, and P. F. Todd, *Chem. Commun.*, 391 (1965), for $CH_2CH_2OH$; (d) W. E. Griffiths, G. F. Longster, J. Myatt, and P. F. Todd, *J. Chem. Soc. B*, 530 (1967), for $CH_3CHCH_2OH$; (e) D. J. Edge, B. C. Gilbert, R. O. C. Norman, and P. R. West, *J. Chem. Soc. B*, 189 (1971), for $CH_3O$-$CHCH_2OH$; (f) P. Neta, *J. Phys. Chem.*, **75**, 2570 (1971), for $^-O_2C$-$CHCH(CO_2^-)OH$.
(17) R. F. Cookson, *Chem. Rev.*, **74**, 5 (1974).
(18) A. Albert and E. P. Serjeant, "The Dermination of Ionization Constants", Chapman and Hall, London, 1971.
(19) J. Murto, *Acta Chem.Scand.*, **18**, 1043 (1964).
(20) P. Balinger and F. A. Long, *J. Am. Chem. Soc.*, **82**, 795 (1960).
(21) G. B. Barlin and D. D. Perrin, *Q. Rev., Chem. Soc.*, **20**, 87 (1966).

# Sequence Peptide Polymers. IV. Poly(leucylleucyllysine) Conformational Study in Aqueous Solution

**E. Corsi and M. D'Alagni***

*Istituto di Chimica delle Macromolecole, Nucleo di Roma, c/o Laboratorio di Chimica Fisica, Istituto Chimico, Università, 00185 Rome, Italy* *(Received December 3, 1973; Revised Manuscript Received August 5, 1974)*

The synthesis and some conformational aspects of a sequential polypeptide, poly(leucylleucyllysine), are reported. The conformational properties have been studied by ir, uv, CD, ORD, and potentiometric titrations in 0.1 *M* KCl. The spectral data show a similarity between the conformations of the poly(leucylleucyllysine) in the charged and uncharged states, characterized by the presence of $\alpha$-helical segments. The unionized state is stabilized by more hydrophobic interactions. The values of $\Delta G°$, $\Delta H°$, and $\Delta S°$ for the residue (Leu-Leu-Lys), for the transition from the charged to the uncharged state, excluding the electrostatic work, have been obtained from potentiometric titrations, applying the Zimm and Rice method at different temperatures. The following values have been determined at 25°: $\Delta G° = -690$ cal mol$^{-1}$; $\Delta H° = 2784$ cal mol$^{-1}$. The value of $\Delta S°$ is 11.7 cal deg$^{-1}$ mol$^{-1}$. The results are compared with those of the poly(leucylleucylaspartic acid) and with others reported in the literature for random copolymers of lysine and leucine.

## Introduction

In previous papers, the conformational features of the sequential polypeptides poly(leucylleucylaspartic acid $\beta$-benzyl ester) (PLLAB)[1] and poly(leucylleucylaspartic acid) (PLLAA)[2] were studied by spectroscopic and potentiometric methods in order to analyze the role of the hydrophobic interactions in stabilizing the conformations of these macromolecules.

Interesting information was obtained from investigating aqueous solutions of PLLAA at different degrees of neutralization of the $\beta$-carboxyl group of the aspartyl residues.

The experimental results established the presence of $\alpha$-helical segments, stabilized by strong hydrophobic interactions in PLLAA, when the $\beta$-carboxyl group of the aspartate group is in the uncharged state. The values of the characteristic thermodynamic functions were derived from potentiometric titration data at various temperatures. The values of $\Delta G° = -1575$ cal mol$^{-1}$ and $\Delta H° = 6173$ cal mol$^{-1}$ have been obtained at 25° with $\Delta S°$ being 26.0 cal deg$^{-1}$ mol$^{-1}$ (per monomeric unit of Leu-Leu-Asp).

We have extended this investigation to the sequential polypeptide poly(leucylleucyllysine) (PLLL), containing a cationic residue in the repetitive unit.

The substitution of the aspartic residue with the lysine one gives rise to a more favorable solubility of the macromolecule in water. This property allows us to study better the physicochemical behavior of PLLL. In addition, the presence of the lysine may cause some change in the conformational features of the polymer.

The work described in this paper utilizes the Zimm–Rice[3a,b] approach to obtain the variation of free energy, $\Delta G°$, related to the charge-induced conformational transition: $\alpha$ helix $\rightarrow$ coil and coil $\rightarrow$ $\beta$ helix.[3c]

The standard entropy, $\Delta S°$, and enthalpy, $\Delta H°$, change per monomeric unit (Leu-Leu-Lys), characterizing the transition process, are obtained too. The ionization and temperature effects on the CD spectra have been considered. The presence of the $\alpha$-helix conformation in PLLL in the charged and uncharged state is estimated by means of spectroscopic data.

## Experimental Section

*Synthesis of Poly(leucylleucyllysine) Hydrochloride (PLLL·HCl).* PLLL·HCl has been obtained by the decarbobenzyloxylation of the corresponding poly(leucylleucyl-$\epsilon$-benzyloxycarbonyllysine) (PLL-$\epsilon$-ZL), synthesized as described in another paper.[4]

The decarbobenzyloxylation was accomplished as follows. A 0.210-g sample of poly(leucylleucyl-$\epsilon$-benzyloxycarbonyllysine) was suspended in 90 ml of anhydrous, freshly distilled dioxane and 90 ml of chloroform and stirred magnetically, overnight at room temperature. This resulted in swelling of the polymer. Hydrogen chloride gas was bubbled for 30 min through the solution, which became clear. Successively, hydrogen bromide gas was added for 2 hr, and the polymer precipitated as a white powder. Then nitrogen was bubbled for 2 hr.

The polymer, recovered by filtration, was washed with anhydrous ether and dissolved in dilute hydrochloric acid and dialyzed against 0.01 *N* hydrochloric acid.

Dialysis was performed with a 4465.A2 dialyzing tube (A. Thomas Co., Philadelphia, Pa.), which does not retain materials with a molecular weight lower than 12,000.

The dialyzed solution was filtered to remove any undissolved material, lyophilized, and dried under vacuum over phosphorus pentoxide at 140°. Spectrophotometric tests allowed us to establish the completion of the reaction. The yield was 95%. Anal. Calcd for $C_{18}H_{34}N_4O_3$·HCl: C, 55.30; H, 9.02; N, = 14.33. Found: C, = 55.27; H, 9.08; N, 14.38.

*Molecular Weight Distribution.* The molecular weight of PLLL·HCl was determined by the gel filtration method on a Sephadex G-100, using a thermostated column 100 × 1.6 cm, equilibrated with a 0.05 *M* tris(hydroxymethyl)aminomethane hydrochloride buffer, pH 7.5, containing 0.1 *M* KCl.

The column was calibrated with protein markers such as cytochrome c, chymotrypsinogen, ovalbumin, and bovine serum albumin, and the void volume was obtained with blue dextran of mol wt $\sim 2 \times 10^6$.

The experiments were performed with a flow rate through the column of 9.5 ml/hr at 4°. The optical density

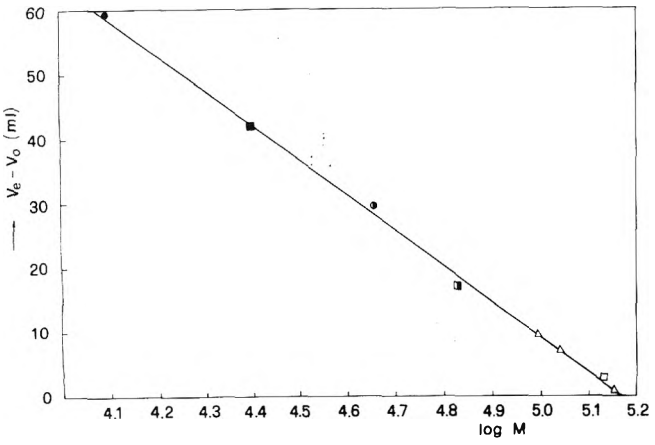


**Figure 1.** Plot of retention volumes ($V_e - V_0$) against log (molecular weight): ●, cytochrome c; ■, chymotrypsinogen A; ◑, ovalbumin; ◨, bovine serum albumin; □, bovine serum albumin dimer (optical density of the eluted fractions at 280 nm); △, PLLL (optical density at 230 nm).

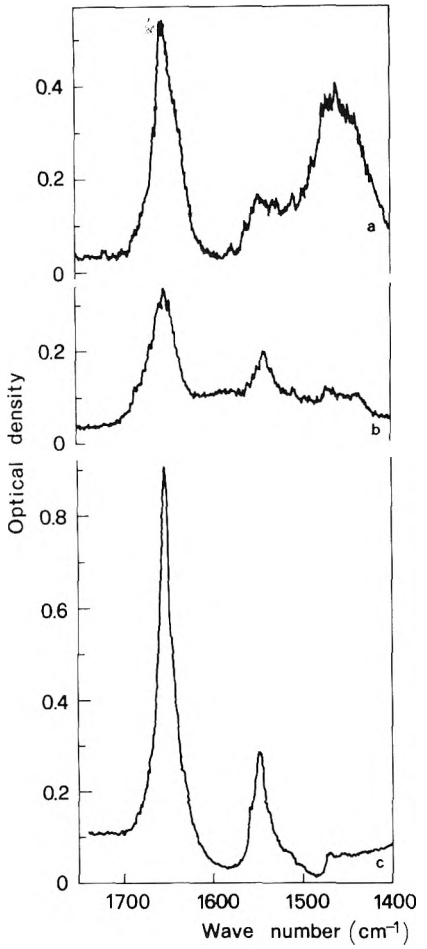


**Figure 2.** Infrared spectra of PLLL: a, in $D_2O$ solution at pH 1.95 (pD ≃2.35), $c$ = 1.35%, registration at 18 hr from polymer dissolution; b, film obtained from a solution in $D_2O$ at pH 10.8 (pD ≃11.20); c, in $CD_3OD$–$D_2O$ (90:10, v/v), pH 5.60 (pD ≃6.00). Registration at 30 ft from polymer dissolution.

of the eluted fractions was estimated at 280 nm with the exception of PLLL (230 nm).

The results of the calibration, given in Figure 1, allowed us to get an approximate idea concerning the molecular weight distribution of PLLL. There are three main fractions with molecular weights, respectively, around 140,000, 110,000, and 94,000.

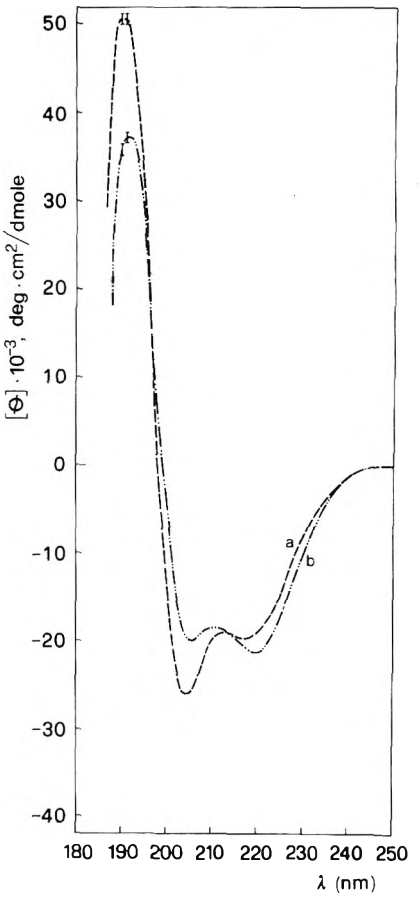


**Figure 3.** CD spectra of PLLL in $H_2O$: a, at pH 1.47; b, at pH 11.28. $c = 1.842 \times 10^{-4}$ $M$.

These estimates may be inaccurate, since the separation capacity[5] of the Sephadex G-100 was limited and since globular proteins were used in the column calibration. However, the molecular weights are sufficiently high to allow us to study the physicochemical behavior of PLLL at the macromolecular level.

*Determination of Concentration.* The concentrations of all polymer solutions were determined by amino acid analyses on a Beckman Model 120 C analyzer after complete hydrolysis in 6 $N$ HCl for 48 hr at 106–110° in sealed tubes under vacuum.

*Infrared Spectra.* Infrared absorption spectra were taken on a Beckman IR9 spectrophotomer in $D_2O$ and in $CD_3OD$–$D_2O$ (90:10, v/v) solutions, using 0.1-mm $BaF_2$ cells, or in films cast from $D_2O$ solutions.

We have not been able to obtain an oriented sample. In Figure 2 are shown some characteristic ir spectra of PLLL: curve a refers to a solution in $D_2O$ at pH 1.95 (pD ≃2.35; $c$ = 1.35%); curve b refers to a film of PLLL in a $D_2O$ solution at pH 10.80 (pD ≃11.20), since the polymer precipitates at the latter pH value; curve c refers to a solution in $CD_3OD$–$D_2O$ (90:10, v/v) at pH 5.60 (pD ≃6.00).

*Far-Ultraviolet Absorption Spectra.* The ultraviolet (uv) absorption measurements were performed on a Beckman DK 2A spectrophotometer using matched stoppered (Hellma) quartz cells of 2-mm path length.

Prepurified nitrogen was flushed through the instrument before and during the registration to minimize oxygen ab-

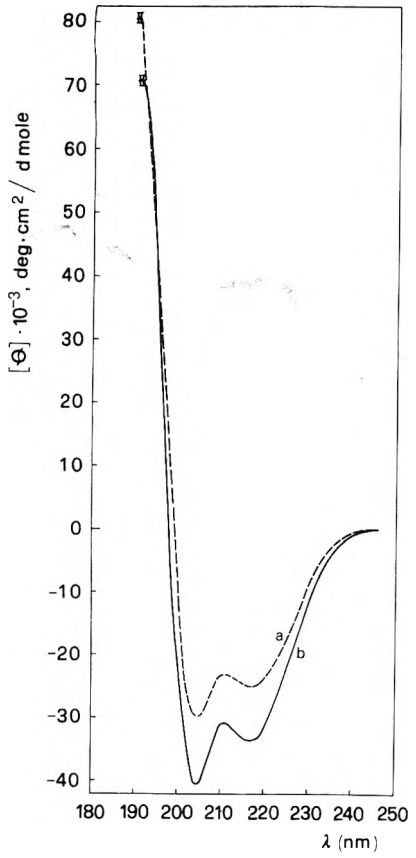


**Figure 4.** CD spectra of PLLL in $CH_3OH$–$H_2O$ (90:10, v/v): a, at pH 11.69; b, at pH 5.62. $c = 1.374 \times 10^{-4}$ *M*.

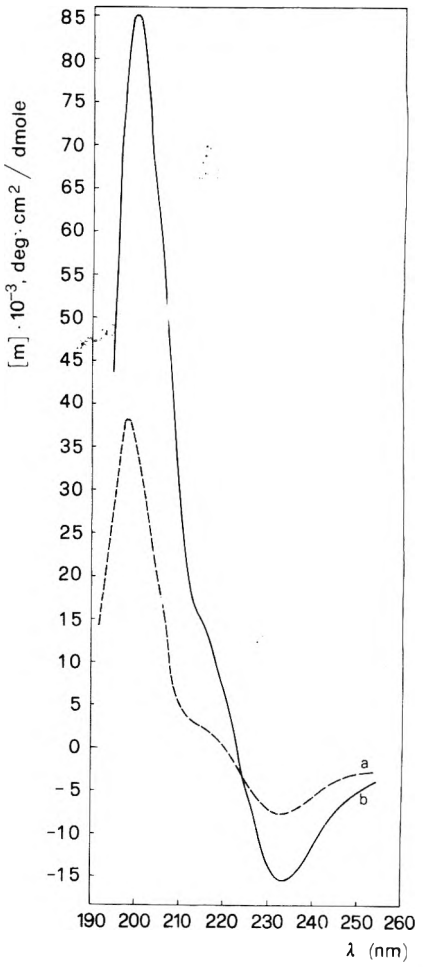


**Figure 5.** ORD curves of PLLL: a, in $H_2O$ solution at pH 5.30; b, in $CH_3OH$–$H_2O$ (90:10, v/v) at pH 5.62.

sorption below 200 nm. Identical absorption spectra with the same extinction coefficients per repetitive unit have been obtained for aqueous solutions at pH 1.47 and 10.38, with $\epsilon$ 4900 at 189 nm.

Uv spectral measurements have been performed to control the effects of concentration in the range $10^{-3}$–$10^{-5}$ *M* at pH 6.89 and 9.20. No deviation from the Lambert–Beer law was detected.

*Circular Dichroism and Optical Rotatory Dispersion.* Ultraviolet circular dichroism (CD) and optical rotatory dispersion (ORD) spectra were recorded on Cary 61 and 60 spectropolarimeters, respectively. Measurements on polymer solutions at different pH values in water and in methanol–water (90:10, v/v) were performed with the polymer concentration being 0.01–0.02% w/v.

The $[\theta]$ and $[m]$ values have been computed by assuming the mean residue molecular weight to be one-third that of the repetitive unit (Leu-Leu-Lys).

Some typical CD spectra of PLLL are reported in Figures 3 and 4. In Figure 3, curves a and b are given for PLLL in aqueous solution at pH 1.47 and 11.28, respectively. In Figure 4 are shown the CD spectra of PLLL dissolved in the methanol–water mixture (90:10, v/v) at two different pH values: curve a for the solution at pH 11.69 and curve b, for the solution at pH 5.62.

CD spectra as a function of the temperature in the range 20–72° were obtained for aqueous solutions at two different pH values. We have not been able to obtain CD spectra at temperatures higher than 30° for PLLL solutions above pH 9.50 since the polymer precipitates beyond that pH level.

The dependence of $[m]$ on $\lambda$ for aqueous and methanol–water solutions of PLLL is shown in Figure 5.

*Titrations.* The potentiometric titration curves were obtained, as described previously,[2] by using a Radiometer titrator, pH meter 26, with a Radiometer 2222 B glass electrode and a K 4112 calomel electrode in a thermostated titration cell.

The pH meter was initially standardized using buffers (Fisher Scientific Co.) at pH 4.00, 7.00, and 10.00.

The water, used to make the solutions, was doubly distilled and was $CO_2$ free. Some hydrochloric acid was added to the PLLL·HCl solution. Each titration was accomplished with 5 ml of solution at a PLLL·HCl concentration of 0.07% in 0.1 *M* KCl. The polymer solutions were titrated with $CO_2$-free 0.1 *M* KOH by use of a micrometer syringe.

The cell was constantly flushed with prepurified nitrogen to prevent absorption of carbon dioxide.

The results of the potentiometric titrations are shown in Figures 6 and 7.

## Results and Discussion

The PLLL·HCl, obtained from the decarbobenzyloxylation of the corresponding PLL-$\epsilon$-ZL, has a rather wide distribution of satisfactorily high molecular weights. This leads to consider very favorably the employed method of synthesis. At the same time, the lack of low molecular weight fractions confers a greater reliability to the results of the conformational study.

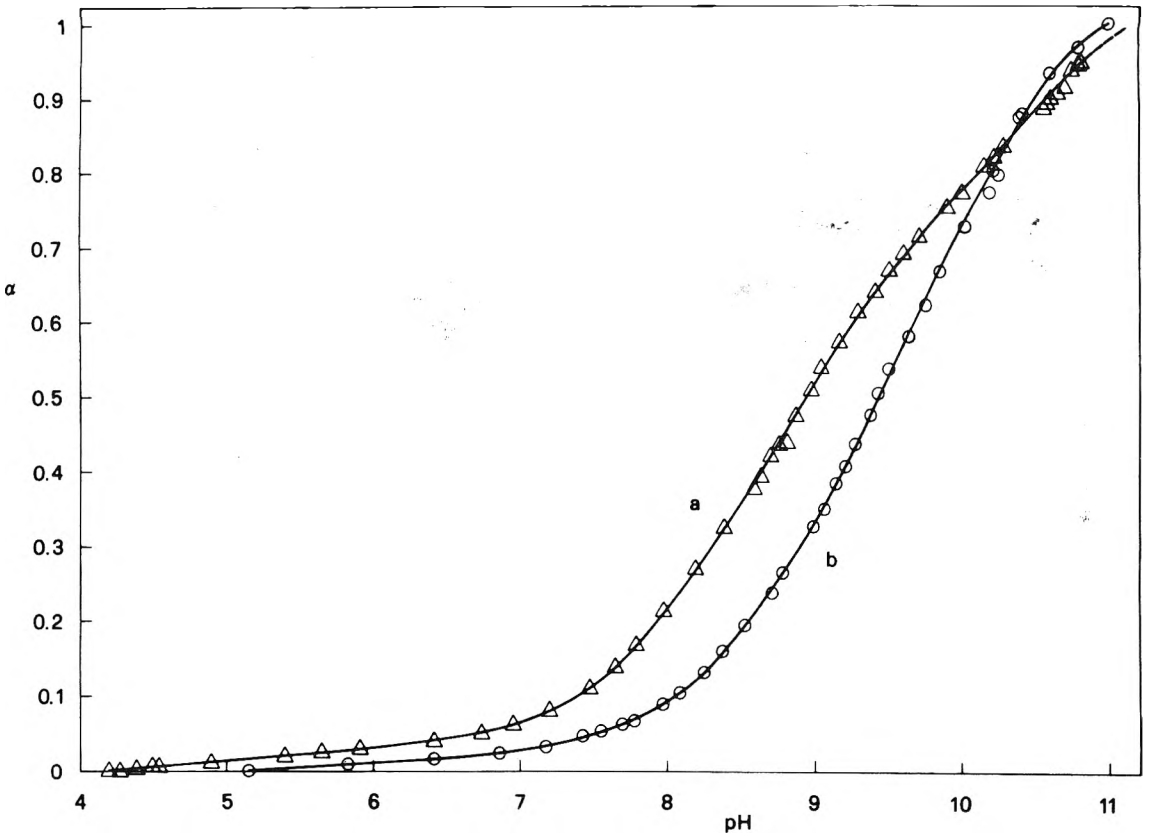


**Figure 6.** Plot of $\alpha$ vs. pH, for PLLL in 0.10 *M* KCl at two different temperatures: a, 58.1°; b, 30.2°.

Curves of the ir spectra of PLLL recorded at pH 1.95 and 10.80, respectively, exhibit the amide I absorption band at 1653 $cm^{-1}$ (see Figure 2a and b).

The band position,[6-8] together with the lack of shift[9] toward lower frequencies when the peptide groups are deuterated, indicates the presence of the $\alpha$-helical conformation for the PLLL in the charged and uncharged form. This interpretation is supported by the uv absorption spectra because identical spectra are given by solutions at pH 1.47 and 10.38. The difference in the amide II frequencies at 1552 and 1460 $cm^{-1}$ in curve a and at 1545 $cm^{-1}$ in curve b arises from the deuteration effect which has caused the shift of this absorption band and from the contribution[10] of the strong absorption band of the HOD at 1455 $cm^{-1}$.

Thus, the spectral data demonstrate a common feature among the conformations of PLLL in going from the charged to the nearly uncharged state.

Furthermore, the value of $\epsilon_{189}$ 4900 allows us to ascribe[11] to the polypeptide a prevalence of the $\alpha$-helical conformation.

The CD results in Figures 3 and 4, in agreement with the previous interpretations, display for PLLL an ordered conformation, characterized by the presence of segments in a right-handed $\alpha$-helical structure.[12] The degree of order is strictly dependent on the nature of the solvent and, within certain limits, on the charged state of PLLL. In fact, in passing from an aqueous solution to one in methanol–water, the absolute magnitude of $[\theta]$ remarkably increases, as shown, respectively, by curve b in Figure 3 and curve a in Figure 4. This feature is emphasized for PLLL in a charged state (curve b, Figure 4). Further evidence is given by the ORD results.

In Figure 5 are reported the ORD profiles of PLLL in aqueous solution at pH 5.30 (curve a) and in the previously mentioned methanol–water solution (90:10, v/v) at pH 5.62 (curve b). The profiles exhibit a trough at 233 nm as well as a shoulder and a peak near 215 and 199 nm, respectively, which are characteristic[13] of the right-handed $\alpha$-helical conformation. The comparison of the two patterns leads us to assign a quite higher $\alpha$-helical content for the methanol–water solution. Moreover, the considerable content of $\alpha$ helix for this PLLL solution at pH 5.60 (pD $\simeq$6.00) is further supported by its ir spectrum in curve c of Figure 2.

Potentiometric titrations of a polyelectrolyte, which can undergo a conformational transition, have been performed[3,14,15] to determine the free energy change associated with the transition. In addition, such a system can be studied as a function of the temperature, since the strength of the inter- and intramolecular interactions, respectively, between macromolecules and within the macromolecule, as well as the interaction of the macromolecule with the solvent molecules, are dependent on the thermic conditions.[15] Therefore, we have analyzed the titration data of PLLL at 30.2, 44.0, 50.2, and 58.1°, following the method of Zimm and Rice.[3a,b]

The experimental data at 58.1° (curves a) and 30.2° (curves b) are shown in Figures 6 and 7, where plots of $\alpha$ vs. pH and pH $-$ log $[\alpha/(1-\alpha)]$ vs. $\alpha$ are reported. $\alpha$ represents the degree of dissociation in the equilibrium process $-NH_3^+ \rightleftarrows -NH_2 + H^+$. The gradient of $\alpha$ (see Figure 6) is steepest at the lowest temperature in the upper part of the curves, probably because the thermal motion of the ionic species opposes the neutralization process of the lysine residues.

Another cause, which might explain this behavior may be a more compact state, stabilized by hydrophobic interactions, occurring at higher temperature.[16,17] The intramolecular interactions, arising from a more compact conforma-

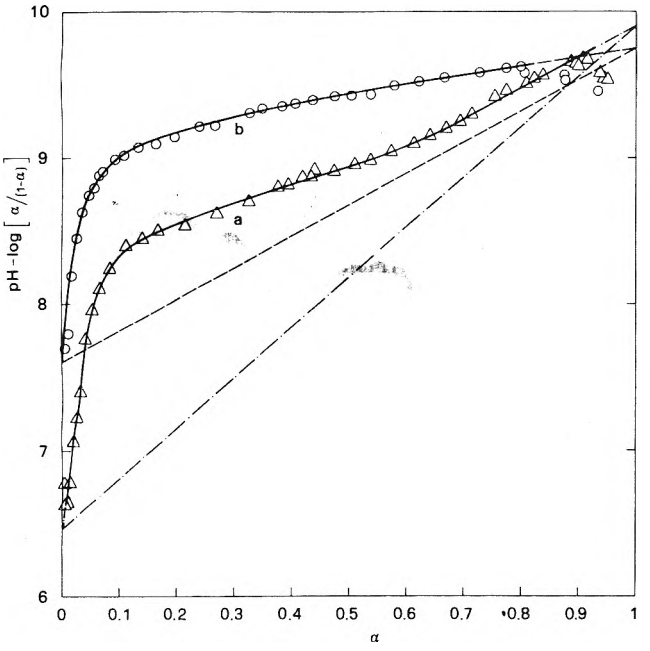


**Figure 7.** Plot of $pK_a$ as a function of $\alpha$ for PLLL at two different temperatures: a, 58.1°; b, 30.2°.

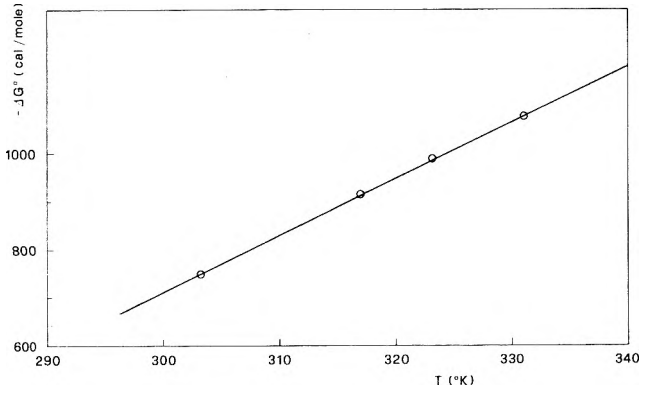


**Figure 8.** Free energy change for the conformational transition of PLLL as a function of the temperature. Values are expressed in calories per mole of repeating unit.

tion of the polypeptide, and the intermolecular ones, which could lead to intermolecular aggregates, may both contribute to the formation of the more compact state.

The absolute magnitude of $\Delta G°$, determined as reported in a previous paper,[2] becomes larger in the temperature range 30.2–58.1° (see Figure 8), denoting a gradual gain in stability when the temperature increases. However, the $\alpha$-helix content seems to change very little with temperature, as can be inferred from inspection of Figure 9, where [θ] at 205 and 208 nm is plotted against temperature for PLLL at pH 1.47 and 9.44.

It could be astonishing that the $\alpha$-helix content is greater at a lower pH, corresponding to a charged state, as may be deduced from the [θ] values of Figures 3 and 4, since the repulsive electrostatic interactions favor the breaking of the $\alpha$ helix. However, it may be supposed that the charged $-NH_3$ groups, which can be, approximately, at least 10–11 Å from each other, in the $\alpha$-helix conformation, are strongly bonded to the solvent molecules, mainly, by means of ion–dipole and hydrogen-bonding forces and give rise to weak Coulomb forces between them. Such a situation leads

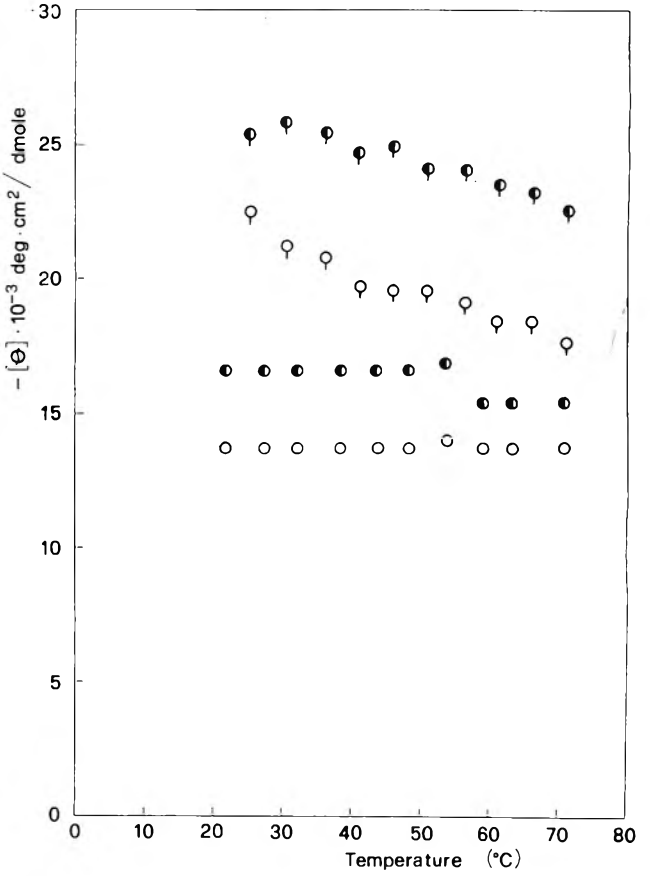


**Figure 9.** Effect of the temperature on the CD spectrum of PLLL in $H_2O$; [θ] vs. temperature: ♀, λ 208 nm, and ◐, λ 205 nm, at pH 1.47; ○, λ 208 nm, and ●, λ 205 nm, at pH 9.44.

to the stabilization of the helical segments which are joined by loops and probably interact only in narrow zones. The interactions arise when two helical segments overlap each other. Wider binding regions are forbidden by the repulsion between charged lysine residues.

The uncharged state may be characterized by more hydrophobic contacts occurring between segments arranged with their helical axes parallel or approximately parallel. The very apolar groups of the side chains allow a remarkable gain of free energy by means of the folding back of the macromolecule. This could explain the rather constant value of [θ] at pH 9.44 as a function of the temperature (see Figure 9). In fact, the increasing of the temperature determines the weakening of the hydrogen bonds and of interactions such as coulombic, ion–dipole, dipole–dipole, etc.,[17-19] destabilizing the $\alpha$ helix. On the other hand, the hydrophobic interactions are enhanced by increasing the temperature to 60°, as reported for random copolypeptides of glutamic acid and leucine.[20] These two competitive effects are balanced in the nearly uncharged state (pH 9.44), while repulsive interactions are present, in addition, among $-NH_3^+$ groups in the charged state (pH 1.47), giving rise to a small decrease of the $\alpha$-helix content (see Figure 9).

Some thermodynamic functions can be evaluated from the potentiometric data by using the plot of $\Delta G°$ vs. $T$ (see Figure 8). The values of $\Delta S°$ and $\Delta H°$, 11.7 cal $deg^{-1}$ $mol^{-1}$ and 2784 cal $mol^{-1}$, respectively, are easily obtained from the straight line of Figure 8. At 25°, $\Delta G°$ is −690 cal $mol^{-1}$ and refers to the conformational transition from the charged to the uncharged state, excluding the electrostatic work.

It is interesting to compare, at the same temperature, the above-mentioned data with those of PLLAA[2] which are as follows: $\Delta S^\circ = 26.0$ cal deg$^{-1}$ mol$^{-1}$, $\Delta H^\circ = 6173$ cal mol$^{-1}$, and $\Delta G^\circ = -1575$ cal mol$^{-1}$. The larger values of both $\Delta S^\circ$ and $\Delta H^\circ$ for PLLAA seem to indicate that this polypeptide is more stabilized by hydrophobic interactions than is PLLL. This may be plausible since the lysine residue is more bulky than the aspartic one and therefore is more in opposition to the folding back of the macromolecule.

The conformational transition of PLLAA appears to involve a greater change in the $\alpha$-helix content and this may explain its more than doubled $\Delta G^\circ$ value as compared to that of PLLL.

It is worthwhile to note that, at 25°, both polylysine, in water in the uncharged state, and polyleucine, although in nonaqueous solvents, are considered to be in the $\alpha$-helix conformation.

Random copolymers ($Lys^xLeu^y$) have been studied in 0.05 *M* KF solution by Snell and Fasman,[21] using potentiometric and circular dichroism methods. The increase of the Leu:Lys ratio determines a smaller $[\theta]_{222}$ absolute value. A difference in $[\theta]_{222}$ of about 4500° cm$^2$ dmol$^{-1}$ occurs between polylysine ($[\theta]_{222} = -36{,}000°$ cm$^2$ dmol$^{-1}$) and poly ($Lys^{59}leu^{41}$) ($[\theta]_{222} = -31{,}500°$ cm$^2$ dmol$^{-1}$). The composition of the PLLL corresponds to poly($Lys^{33}Leu^{67}$) and has $[\theta]_{222} = -21{,}000°$ cm$^2$ dmol$^{-1}$ (see curve b of Figure 3), showing a higher decrease of the $[\theta]_{222}$ absolute magnitude than would be expected in the random copolymers series. However, it must be stressed that PLLL has a lower $\alpha$-helix content than the random copolymers. The above-mentioned data demonstrate that the primary structure of the copolypeptides is strongly influencing their conformations.

In fact, one can predict the $\alpha$-helix conformation to be energetically stable for both polylysine (in the uncharged state) and polyleucine, but PLLL does not retain, completely, this conformation, as explained previously. On the contrary, the copolypeptides ($Lys^xLeu^y$) are hindered in folding back, since a random sequence of the leucyl residues limits the formation of several hydrophobic interactions among them.

The behavior of PLLL in the methanol–water mixture deserves some remarks. Figures 4 and 5, previously cited, show a considerable increase in the formation of the $\alpha$-helix conformation in PLLL in the methanol–water solution as compared with the conformation assumed in water solution. The ability of the methanol–water mixture to stabilize the $\alpha$-helix conformation may be explained by taking into account the hydrophobic interactions between the methyl group of methanol and the side chains of PLLL, which are competitive with the intramolecular ones. Furthermore, the methanol molecules are able to form a network of hydrogen bonds among themselves as well as with the polypeptide.

*Acknowledgments.* We gratefully wish to thank Professor E. Giglio for the helpful discussion and criticism of this work. We also thank Mr. R. Santucci for skilled technical assistance in the circular dichroism measurements.

## References and Notes

(1) M. D'Alagni, P. Bemporad, and A. Garofolo, *Polymer*, **13**, 419 (1972).
(2) M. C. Morelli and M. D'Alagni, *Polymer*, **13**, 515 (1972).
(3) (a) B. H. Zimm and S. A. Rice, *J. Mol. Phys.*, **3**, 391 (1960); (b) S. A. Rice and M. Nagasawa in "Polyelectrolyte Solutions", Academic Press, New York, N.Y., 1961, Section 7.7, (c) D. Pederson, D. Gabriel, and J. Hermans, Jr., *Biopolymers*, **10**, 2133 (1971).
(4) L. Bravin and M. D'Alagni, in preparation.
(5) P. Andrews, *Biochem. J.*, **91**, 222 (1964).
(6) E. J. Ambrose and A. Elliott, *Proc. R. Soc. London, Ser. A* **205**, 47 (1951).
(7) A. Elliott, W. E. Hanby, and B. R. Malcolm, *Discuss. Faraday Soc.*, **25**, 167 (1958).
(8) T. Miyazawa, and E. R. Blout, *J. Am. Chem. Soc.*, **83**, 712 (1961).
(9) S. N. Timasheff et al. in "Conformation of Biopolymers", Vol. I, G. M. Ramachandran, Ed., Academic Press, London, 1967, p 173.
(10) A. Hvidt and S. O. Nielsen, *Adv. Protein Chem.*, **21**, 288 (1966).
(11) K. Rosenheck and P. Doty, *Proc. Natl. Acad. Sci. U.S.A.*, **47**, 1775 (1961).
(12) S. N. Timasheff et al. in "Conformation of Biopolymers", Vol. I, G. M. Ramachandran, Ed., Academic Press, London, 1967, p 173.
(13) J. T. Yang in "Poly-$\alpha$-amino Acids", G. D. Fasman, Ed., Marcel Dekker, New York, N.Y., 1967, p 239.
(14) M. Nagasawa and A. Holtzer, *J. Am. Chem. Soc.*, **86**, 538 (1964).
(15) O. B. J. Ptitsyn, *J. Polym. Sci., Polym. Symp.*, **No. 30**, 615 (1970).
(16) H. A. Scheraga in "The Proteins", Vol. I, H. Neurath, Ed., Academic Press., New York, N.Y., 1963, p 477.
(17) W. F. Harrington and J. A. Schellman, *C. R. Trav. Lab. Carlsberg, Ser. Chim.*, **30**, 21 (1956).
(18) J. G. Foss and J. A. Schellman, *J. Phys. Chem.*, **63**, 2007 (1959).
(19) J. A. Schellman, *C. R. Trav. Lab. Carlsberg, Ser. Chim.*, **29**, 230 (1955).
(20) G. D. Fasman, C. Lindblow, and E. Bodenheimer, *Biochemistry*, **3**, 155 (1964).
(21) C. R. Snell and G. D. Fasman, *Biopolymers*, **11**, 1723 (1972).

# Membrane Potentials and Electrolyte Permeation Velocities in Charged Membranes

**Masayasu Tasaka,* Norio Aoki,**

*Department of Industrial Chemistry, Faculty of Engineering, Shinshu University, Wakasato, Nagano, Japan, 380*

**Yozo Kondo, and Mitsuru Nagasawa**

*Department of Synthetic Chemistry, Faculty of Engineering, Nagoya University, Chikusa-Ku, Nagoya, Japan, 464*

*(Received January 24, 1974; Revised Manuscript Received February 26, 1975)*

Permeation velocities of various electrolytes through a homogeneous (negatively) charged membrane, under no externally applied electric field and zero pressure difference, as well as the electrostatic potential appearing across the membrane, are observed at various concentrations of electrolytes of the 1–1 type. Equations for those phenomena are presented and compared with the experimental data. In particular, the effects of water transport on the permeation velocity of electrolyte and membrane potential are quantitatively discussed.

## Introduction

When two solutions of different concentrations of an electrolyte are placed on both sides of a membrane, we can observe various membrane phenomena. In particular, if there are no temperature and pressure differences across the membrane and also if no electric field is applied, the permeation velocities of water and ions through the membrane as well as the electrostatic potential difference appearing on both sides of the membrane (membrane potential) may be our subjects for research. These membrane phenomena have been extensively studied by many investigators since 1920. From those studies, it is now well established that there is a strong interaction between fluxes of water and ions through a charged membrane.[1–6] So-called anomalous osmosis is caused by the interaction between both fluxes.[4–6] The permeation velocities of ions and the membrane potential must also be affected by the flow of water.

Data on permeation velocities of electrolytes through a charged membrane and also on membrane potential were obtained together with data on water permeation as reported in a previous paper.[6] The purpose of this paper is to analyze these data on permeation of electrolytes and membrane potential based on the same model as in the previous paper. In the previous paper, we discussed the anomalous permeation behavior of water, for which the thermodynamic properties of the electrolyte solution inside the membrane need not be discussed, whereas in this work they must be carefully taken into account.

Our present analysis is not very different from the theories so far published by various authors, which are summarized in recent text books.[7,8] Most important fundamental problems have already been given in separate papers.[9–32] However, it is our impression that there appears to be some confusion among the theories and it seems meaningful to combine a number of approximations into an approach and illustrate these with the experimental data. In particular, the effect of water transport on the permeation velocity and membrane potential should be more carefully discussed.

In this paper, we define the fluxes relative to the membrane as in the previous paper.[6] However, the reciprocal relationship of Onsager between phenomenological coefficients is not assumed.

## Theory

The system considered is a cell in which a charged membrane separates two aqueous solutions of different concentrations ($c'$ and $c''$ in mol/cm$^3$) of an electrolyte. The solutions on both sides of the membrane are maintained at the same pressure and temperature. The fluxes of water and ions relative to the cell may be expressed by the linear equations

$$-J_0 = L_{00}\,\mathrm{grad}\,\tilde{\mu}_0 + L_{0+}\,\mathrm{grad}\,\tilde{\mu}_+ + L_{0-}\,\mathrm{grad}\,\tilde{\mu}_- \quad (1a)$$

$$-J_+ = L_{+0}\,\mathrm{grad}\,\tilde{\mu}_0 + L_{++}\,\mathrm{grad}\,\tilde{\mu}_+ + L_{+-}\,\mathrm{grad}\,\tilde{\mu}_- \quad (1b)$$

$$-J_- = L_{-0}\,\mathrm{grad}\,\tilde{\mu}_0 + L_{-+}\,\mathrm{grad}\,\tilde{\mu}_+ + L_{--}\,\mathrm{grad}\,\tilde{\mu}_- \quad (1c)$$

Here, subscripts +, −, and 0 refer to cation, anion, and water molecules, respectively, $J$'s the mass fluxes (mol/cm$^2$ min), $L$'s the phenomenological coefficients, and $\tilde{\mu}$'s the chemical potentials including contribution due to external forces.

$$\tilde{\mu}_i = \mu_i + z_i F\psi + v_i P \quad (2)$$

In eq 2, $z_i$ and $v_i$ are the valence and partial molar volume of component i, respectively, $\psi$ is the electrostatic potential, $P$ is the pressure, and $F$ is the Faraday constant. Substituting eq 1a into eq 1b and 1c, we have

$$-J_+ = -\frac{L_{+0}}{L_{00}}J_0 + \left(L_{++} - \frac{L_{+0}L_{0+}}{L_{00}}\right)\mathrm{grad}\,\tilde{\mu}_+ + \left(L_{+-} - \frac{L_{+0}L_{0-}}{L_{00}}\right)\mathrm{grad}\,\tilde{\mu}_- \quad (3a)$$

$$-J_- = -\frac{L_{-0}}{L_{00}}J_0 + \left(L_{-+} - \frac{L_{-0}L_{0+}}{L_{00}}\right)\mathrm{grad}\,\tilde{\mu}_+ + \left(L_{--} - \frac{L_{-0}L_{0-}}{L_{00}}\right)\mathrm{grad}\,\tilde{\mu}_- \quad (3b)$$

Therefore, the water flow causes a term in the flux equation for each ion. In dilute electrolyte solutions, however, it may be assumed that the cross terms in eq 3a and 3b, i.e., the third term in eq 3a and the second term in eq 3b, are negligible compared with the other terms.[33] The assumption was employed by Spiegler, Kedem, and Katchalsky for transport of ions through charged membranes.[3,4] We also adopt the assumption in this paper. If the forces grad $\tilde{\mu}_+$ and grad $\tilde{\mu}_-$ in eq 1a are replaced by $J_+$ and $J_-$, we have the equation for water transport with which we discussed the anomalous osmosis through charged membranes.[6]

It is now necessary to express the phenomenological coefficients in eq 3a and 3b in terms of usual parameters in electrochemistry such as concentration, mobility, etc. In electrolyte solutions, the flux of an ion is usually proportional to the concentration of the ion $c_i$, its mobility $l_i$, and the force acting on the ion $F_i$, such as in

$$-J_i = c_i l_i F_i \tag{4}$$

Therefore, it is clear that the second term in eq 3a and the third term in eq 3b are proportional to $\bar{c}_i l_i$. $\bar{c}_i$ is the concentration of the ith ion contained in the solution inside the membranes.

The first terms in eq 3a and 3b show the direct effect of water flow on the ion fluxes and, therefore, should be proportional to the concentration of the ion contained in the solution, $\bar{c}_i$ (mol/cm$^3$), and the flow rate of the solution, $J_v$ (cm$^3$/cm$^2$ min), *if the ions are distributed uniformly in the membrane.* Moreover, the concentration of the electrolyte in the solution is so low that $J_v$ may be approximated as $J_0/\bar{c}_0$ where $J_0$ and $\bar{c}_0$ are defined by (mol/cm$^2$ min) and (mol/cm$^3$), respectively. Thus, we have

$$-(L_{10}/L_{00})J_0 \approx -(\bar{c}_i/\bar{c}_0)J_0$$

However, the distribution of ions in the membrane is not uniform. Most counterions are accumulated around fixed charges on membrane matrix due to their strong electrostatic forces. In other words, the solution inside membranes having a high charge density is not ideal, thermodynamically and hydrodynamically. The most convenient method to take into account the nonideality of the solution may be to decrease the effective concentration of counterion, i.e., the charge density of the matrix.[34,35] That is, since the coion (anion in anionic membranes) is not accumulated around the fixed charges, the effective concentration of coion is approximately equal to $\bar{c}_-$, whereas the effective concentration of counterion may be expressed by $(\bar{c}_- + \phi X)$ where $X$ is the concentration of fixed charge and $\phi$ is a parameter expressing the nonideality of the solution. If the solution is ideal, $\phi$ should be unity. The parameter $\phi$ decreases from unity to zero with increasing charge density of membrane matrix.

Thus, eq 3a and 3b may be approximated as

$$-J_+ = -\frac{(\bar{c}_- + \phi X)}{\bar{c}_0}J_0 + (\bar{c}_- + \phi X)l_+ \operatorname{grad} \bar{\mu}_+ \tag{5a}$$

$$-J_- = -\frac{\bar{c}_-}{\bar{c}_0}J_0 + \bar{c}_- l_- \operatorname{grad} \bar{\mu}_- \tag{5b}$$

These are the Nernst–Planck equations containing the contribution of water flow. The $l$'s are the mobilities of ions in the membrane phase and may be expressed by $l^0 f$ where $l^0$ is the mobility in aqueous solution at a concentration of the electrolyte and $f$ is a tortuosity factor.[32]

*Permeability Coefficient of Electrolyte.* It is assumed that the rate-determining step for the permeations of ions and water is the mass transfer in the membrane phase and that the electrolyte solutions inside and outside the membrane are in thermodynamic equilibrium on both sides of the membrane. Therefore, the effect of a stagnant layer on the permeation velocities[8,16] is neglected in this work. This assumption is valid for thick membranes. From the condition of no current at the steady state, i.e., since $J_+ = J_- = J_s$ for 1–1 electrolytes we have

$$-F \operatorname{grad} \psi = -\left(\frac{J_0}{\bar{c}_0}\right)\frac{\phi X}{(\bar{c}_- + \phi X)l_+ + \bar{c}_- l_-} + \frac{(\bar{c}_- + \phi X)l_+}{(\bar{c}_- + \phi X)l_+ + \bar{c}_- l_-} \operatorname{grad} \mu_+ - \frac{\bar{c}_- l_-}{(\bar{c}_- + \phi X)l_+ + \bar{c}_- l_-} \operatorname{grad} \mu_- \tag{6}$$

Substituting eq 6 into eq 5, we have

$$-J_s = -\left(\frac{J_0}{\bar{c}_0}\right)\frac{\bar{c}_-(\bar{c}_- + \phi X)(l_+ + l_-)}{(\bar{c}_- + \phi X)l_+ + \bar{c}_- l_-} + \frac{\bar{c}_-(\bar{c}_- + \phi X)l_+ l_-}{(\bar{c}_- + \phi X)l_+ + \bar{c}_- l_-} \operatorname{grad} (\mu_+ + \mu_-) \tag{7}$$

If the membrane phase may be approximated as a homogeneous polyelectrolyte solution, the concentration of the simple electrolyte in the membrane phase may be calculated from the theory of Donnan,[36,37] as was assumed by Teorell, Meyer, and Sievers.[9-11] In this case, too, the solution in the membrane phase is not thermodynamically ideal and a parameter must be introduced to supplement the nonideality. That is

$$(\gamma_\pm c)^2 = \bar{\gamma}_\pm \bar{c}_-(\bar{\gamma}_\pm \bar{c}_- + \bar{\gamma}_p X) \tag{8}$$

where $\gamma_\pm$ is the mean activity coefficient of the electrolyte in solution, $\bar{\gamma}_\pm$ is that in the membrane, and $\bar{\gamma}_p$ is the activity coefficient of counterion in the charged membrane. Equation 8 was proposed from various studies on the thermodynamic properties of linear polyelectrolyte solutions.[34,35] The assumptions and concepts concerning eq 8 are recently discussed in ref 38. If the mean activity coefficient of the electrolyte absorbed in the membrane $\bar{\gamma}_\pm$ is assumed to be the same as in aqueous solutions of the electrolyte at the concentration of $\bar{c}_-$, $\bar{\gamma}_p$ is usually found to be approximately equal to the value in the polyelectrolyte solution equilibrated with pure water. Thus, $\bar{\gamma}_p$ is approximately a constant independent of $c$ or $\bar{c}_-$. If we denote $\bar{\gamma}_p/\bar{\gamma}_\pm = \phi$, therefore, eq 8 may be expressed by

$$(\gamma_\pm c)^2 = \bar{\gamma}_\pm^2 \bar{c}_-(\bar{c}_- + \phi X) \tag{9}$$

The concentrations of ions inside the membrane at both interfaces of the membrane, $\bar{c}''$ and $\bar{c}'$, can be calculated as a function of electrolyte concentration from eq 8 or 9 if we know $\bar{\gamma}_p$ or $\phi$. On the contrary, $\bar{\gamma}_p$ or $\phi$ may be determined by measuring $\bar{c}_-$ as a function of $c$. The physical meaning of $\phi$ in eq 5a is equivalent to that in eq 9, since $l^0$'s are defined as the values in aqueous solutions at the same concentration of the electrolyte. Although $\phi$ in eq 5a is defined hydrodynamically whereas $\phi$ in eq 9 is defined thermodynamically, we do not distinguish between them in this paper, as will be discussed in the Discussion. Thus, in this paper, $\phi X$ is a parameter to give the effective concentration of the membrane charge.

The value of $\bar{\gamma}_\pm$ varies with concentration of electrolyte. The variation is taken into account in the comparison between theory and experiments, though the variation is neglected in the following formulation to simplify our discussion. If we neglect the variation of $\bar{\gamma}_\pm$ and $l^0$'s with concentration of electrolyte, eq 5 is rewritten as

$$-J_s = -\left(\frac{J_0}{\bar{c}_0}\right)\frac{\bar{c}_-(\bar{c}_- + \phi X)(l_+ + l_-)}{(\bar{c}_- + \phi X)l_+ + \bar{c}_- l_-} + \frac{(2\bar{c}_- + \phi X)l_+ l_- RT}{(\bar{c}_- + \phi X)l_+ + \bar{c}_- l_-} \operatorname{grad} \bar{c}_- \tag{10}$$

Performing the integration of eq 10 from one side of the membrane (′) to the other (″), we have

$$-J_s = \left(\frac{RT}{\delta}\right)\frac{2l_+l_-A_1(A_1 - \phi X)\left(A_1 - \frac{\phi X}{2}\right)}{(l_+ + l_-)(A_1 - A_2)\left(A_1 - \frac{\phi X l_+}{l_+ + l_-}\right)} \times \ln\frac{\bar{c}_-'' + A_1}{\bar{c}_-' + A_1} + \left(\frac{RT}{\delta}\right) \times \frac{2l_+l_-A_2(A_2 - \phi X)\left(A_2 - \frac{\phi X}{2}\right)}{(l_+ + l_-)(A_2 - A_1)\left(A_2 - \frac{\phi X l_+}{l_+ + l_-}\right)} \ln\frac{\bar{c}_-'' + A_2}{\bar{c}_-' + A_2} \quad (11)$$

where we have used the abbreviation

$$A_i = \frac{1}{2(l_+ + l_-)}\left[\phi X l_+ + \frac{2RT\bar{c}_0 l_+ l_- k}{J_0} + (-1)^i\left\{\left(\phi X l_+ - \frac{2RT\bar{c}_0 l_+ l_- k}{J_0}\right)^2 + 4(\phi X)^2 l_+ l_-\right\}^{1/2}\right] \quad (12)$$

The parameter $\delta$ is the thickness of membrane and $k$ is a constant which can be determined by integrating the equation

$$\frac{d\bar{c}_-}{dX} = \left(\bar{c}_- + \frac{\phi X}{2}\right)^{-1}\left[\bar{c}_-^2\frac{J_0(l_+ + l_-)}{2RT\bar{c}_0 l_+ l_-} + \bar{c}_-\left(\frac{\phi X J_0}{2RT\bar{c}_0 l_-} + k\right) - \frac{(\phi X)^2 J_0}{2RT\bar{c}_0(l_+ + l_-)} + \frac{\phi X l_+ k}{l_+ + l_-}\right] \quad (13)$$

Equation 13 gives the steady distribution of the electrolyte inside the membrane. Performing the integration of eq 13, we have

$$k \approx \frac{1}{\delta}(\bar{c}_-'' - \bar{c}_-') - \frac{\phi X(l_+ - l_-)}{2\delta(l_+ + l_-)} \times \ln\left(\frac{\bar{c}_-'' + \frac{\phi X l_+}{l_+ + l_-}}{\bar{c}_-' + \frac{\phi X l_+}{l_+ + l_-}}\right) - \frac{J_0(l_+ + l_-)}{2\bar{c}_0 l_+ l_- RT}\left[(\bar{c}_-'' - \bar{c}_-') - \frac{\phi X(l_+ - l_-)}{2(l_+ + l_-)}\ln\left(\frac{\bar{c}_-'' + \frac{\phi X l_+}{l_+ + l_-}}{\bar{c}_-' + \frac{\phi X l_+}{l_+ + l_-}}\right)\right]^{-1} \times \left[\frac{1}{2}(\bar{c}_-''^2 - \bar{c}_-'^2) - \frac{\phi X(l_+ - l_-)}{2(l_+ + l_-)}(\bar{c}_-'' - \bar{c}_-') - \frac{l_+ l_-(l_+ - l_-)(\phi X)^3}{2(l_+ + l_-)^3}\left(\frac{1}{\bar{c}_-'' + \frac{\phi X l_+}{l_+ + l_-}} - \frac{1}{\bar{c}_-' + \frac{\phi X l_+}{l_+ + l_-}}\right) + \frac{l_+(l_+ - 3l_-)(\phi X)^2}{2(l_+ + l_-)^2}\ln\left(\frac{\bar{c}_-'' + \frac{\phi X l_+}{l_+ + l_-}}{\bar{c}_-' + \frac{\phi X l_+}{l_+ + l_-}}\right)\right] \quad (14)$$

If $J_0$ is small and $\phi X l_+ \ll 2RT\bar{c}_0 l_+ l_- k/J_0$, as is fulfilled at usual experimental conditions, we have

$$-J_s = \left(\frac{RT}{\delta}\right) \times \frac{2l_+l_-\left\{1 - \frac{(l_+ + l_-)\phi X J_0}{2RT\bar{c}_0 l_+ l_- k}\right\}\left\{1 - \frac{(l_+ + l_-)\phi X J_0}{4RT\bar{c}_0 l_+ l_- k}\right\}}{(l_+ + l_-)\left(1 - \frac{\phi X J_0}{2RT\bar{c}_0 l_- k}\right)^2} \times (\bar{c}_-'' - \bar{c}_-') - \left(\frac{RT}{\delta}\right)\frac{l_+l_-(l_+ - l_-)\phi X}{(l_+ + l_-)^2\left(1 - \frac{\phi X J_0}{2RT\bar{c}_0 l_- k}\right)} \times \ln\left(\frac{\bar{c}_-'' + \frac{\phi X l_+}{l_+ + l_-}}{\bar{c}_-' + \frac{\phi X l_+}{l_+ + l_-}}\right) \quad (15)$$

If $J_0$ is zero, moreover, this is further simplified to

$$-J_s = \left(\frac{RT}{\delta}\right)\left(\frac{2l_+l_-}{l_+ + l_-}\right)(\bar{c}_-'' - \bar{c}_-') - \left(\frac{RT}{\delta}\right)\frac{l_+l_-(l_+ - l_-)\phi x}{(l_+ + l_-)^2}\ln\left(\frac{\bar{c}_-'' + \frac{\phi X l_+}{l_+ + l_-}}{\bar{c}_-' + \frac{\phi X l_+}{l_+ + l_-}}\right) \quad (16)$$

In general, if the electrolyte solutions are dilute enough, we have the limiting form from eq 11

$$-J_s = \left(\frac{RT}{\delta}\right)l_-(\bar{c}_-'' - \bar{c}_-') \quad (17)$$

If we define the permeability coefficient of electrolyte by

$$P_s = |J_s|/(c'' - c') \quad (18)$$

$P_s$ can be calculated by inserting eq 15 or 11 into eq 18. At the limit of high concentration, it becomes

$$P_s = \left(\frac{RT}{\delta}\right)\frac{2l_+l_-}{l_+ + l_-} - \left(\frac{RT}{\delta}\right)\frac{l_+l_-(l_+ - l_-)\phi X \ln r}{(l_+ + l_-)^2(r - 1)c'} \quad (19)$$

where $r$ is $c''/c'$. In dilute solutions where $\phi \approx \bar{y}_p$ can be assumed, eq 17 and 18 give

$$P_s = \left(\frac{RT}{\delta}\right)fl_-^0\left(\frac{r + 1}{\phi X}\right)c' \quad (20)$$

Equation 20 shows that the permeability coefficient does not depend on the mobility of counterion but depends only on the mobility of coion.

*Membrane Potential.* The membrane potential appearing on both sides of the membrane ($\Delta\psi = \psi'' - \psi'$) is the sum of the diffusion potential inside the membrane and the electrostatic potential differences between the membrane and electrolyte solution phases on both sides of the membrane. The diffusion potential $\Delta\psi_d$ can be obtained by integrating eq 6 from one side of the membrane to the other, while the equilibrium potential difference between membrane and solution phases $\Delta\psi_e$ can be calculated from the theory of Donnan.[36,37] That is

$$\Delta\psi = \Delta\psi_d + \Delta\psi_e \quad (21a)$$

where

$$-\Delta\psi_d = -\int_{'}^{''}\left(\frac{J_0}{Fc_0}\right)\frac{\phi X}{(\bar{c}_- + \phi X)l_+ + \bar{c}_- l_-}dx + \frac{RT}{F}\int_{'}^{''}\frac{(\bar{c}_- + \phi X)l_+}{(\bar{c}_- + \phi X)l_+ + \bar{c}_- l_-}d\ln\bar{a}_+ - \frac{RT}{F}\int_{'}^{''}\frac{\bar{c}_- l_-}{(\bar{c}_- + \phi X)l_+ + \bar{c}_- l_-}d\ln\bar{a}_- \quad (21b)$$

and

$$-\Delta\psi_e = -\frac{RT}{F}\ln\left(\frac{\bar{a}_-'a_-''}{a_-'\bar{a}_-''}\right) \quad (21c)$$

If $J_0$ is zero, eq 21 corresponds the form reported by Schlögl and Helfferich.[13] Performing the integration of eq 21, we have

$$-\Delta\psi = \frac{RT}{2F}\ln\frac{\bar{c}_-''(\bar{c}_-' + \phi X)}{\bar{c}_-'(\bar{c}_-'' + \phi X)} + \left(\frac{RT}{F}\right)\times$$
$$\frac{2\phi X l_+ l_-\left(A_1 - \frac{\phi X}{2}\right)}{(l_+ + l_-)^2(A_1 - A_2)\left(A_1 - \frac{\phi X l_+}{l_+ - l_-}\right)}\ln\frac{\bar{c}_-'' + A_1}{\bar{c}_-' + A_1} +$$
$$\left(\frac{RT}{F}\right)\frac{2\phi X l_+ l_-\left(A_2 - \frac{\phi X}{2}\right)}{(l_+ + l_-)^2(A_2 - A_1)\left(A_2 - \frac{\phi X l_+}{l_+ + l_-}\right)}\ln\frac{\bar{c}_-'' + A_2}{\bar{c}_-' + A_2} \quad (22)$$

If $J_0$ is small and $\phi X J_0 \ll 2RT\bar{c}_0 l_- k$, eq 22 becomes

$$-\Delta\psi = \frac{RT}{2F}\ln\frac{\bar{c}_-''(\bar{c}_-' + \phi X)}{\bar{c}_-'(\bar{c}_-'' + \phi X)} +$$
$$\frac{RT}{F}\left(\frac{l_+ - l_-}{l_+ + l_-}\right)\left[\frac{1 - \frac{\phi X J_0}{RT\bar{c}_0(l_+ - l_-)k}}{1 - \frac{\phi X J_0}{2RT\bar{c}_0 l_- k}}\right]\times$$
$$\ln\left[\frac{\bar{c}_-'' + \frac{\phi X l_+}{l_+ + l_-} - \frac{(\phi X)^2 J_0}{2RT\bar{c}_0(l_+ + l_-)k}}{\bar{c}_-' + \frac{\phi X l_+}{l_+ + l_-} - \frac{(\phi X)^2 J_0}{2RT\bar{c}_0(l_+ + l_-)k}}\right] +$$
$$\frac{RT\phi X}{2Fl_+ l_-}\left(\frac{J_0}{RT\bar{c}_0 k}\right)^2\frac{\left[1 - \frac{\phi X J_0(l_+ + l_-)}{4RT\bar{c}_0 l_+ l_- k}\right]}{\left(1 - \frac{\phi X J_0}{2RT\bar{c}_0 l_- k}\right)^2}(\bar{c}_-'' - \bar{c}_-') \quad (23)$$

If $J_0$ is zero, moreover, it turns out to be

$$-\Delta\psi = \frac{RT}{2F}\ln\frac{\bar{c}_-''(\bar{c}_-' + \phi X)}{\bar{c}_-'(\bar{c}_-'' + \phi X)} +$$
$$\frac{RT}{F}\left(\frac{l_+ - l_-}{l_+ + l_-}\right)\ln\left(\frac{\bar{c}_-'' + \frac{\phi X l_+}{l_+ + l_-}}{\bar{c}_-' + \frac{\phi X l_+}{l_+ + l_-}}\right) \quad (24)$$

This corresponds to the equation of Teorell, Meyer, and Sievers.[9-11]

At the limit of low concentrations, eq 22 becomes

$$-\Delta\psi = \frac{RT}{F}\ln\frac{c''}{c'} \quad (25)$$

At high concentrations, it becomes

$$-\Delta\psi = \frac{RT}{F}\left(\frac{\phi X}{2}\right)\left(\frac{r-1}{r}\right)\frac{1}{c'} +$$
$$\frac{RT}{F}\left(\frac{l_+ - l_-}{l_+ + l_-}\right)\left[\frac{1 - \frac{\phi X J_0}{RT\bar{c}_0(l_+ - l_-)k}}{1 - \frac{\phi X J_0}{2RT\bar{c}_0 l_- k}}\right]\ln r +$$
$$\frac{RT\phi X}{2Fl_+ l_-}\left(\frac{J_0}{RT\bar{c}_0 k}\right)^2\frac{\left[1 - \frac{\phi X J_0(l_+ + l_-)}{4RT\bar{c}_0 l_+ l_- k}\right]}{\left(1 - \frac{\phi X J_0}{2RT\bar{c}_0 l_- k}\right)^2}(r-1)c' \quad (26)$$

It is to be noted that, if we neglect the stagnant layer on the membrane surface and the effect of water flow on $P_s$ and $\Delta\psi$, eq 11 and 22 are the same as the corresponding equations reported by Toyoshima, Kobatake, and Fujita.[16]

*Equations for KCl Solution System.* In KCl solutions, all equations may be simplified since $l_{Cl^-}{}^0 = l_{K^+}{}^0$. That is, eq 11, 12, 14,and 22 are

$$-J_s = \left(\frac{RT}{\delta}\right)\frac{l_- A_1(A_1 - \phi X)}{A_1 - A_2}\ln\frac{\bar{c}_-'' + A_1}{\bar{c}_-' + A_1} +$$
$$\left(\frac{RT}{\delta}\right)\frac{l_- A_2(A_2 - \phi X)}{A_2 - A_1}\ln\frac{\bar{c}_-'' + A_2}{\bar{c}_-' + A_2} \quad (27)$$

and

$$-\Delta\psi = \frac{RT}{2F}\ln\frac{\bar{c}_-''(\bar{c}_-' + \phi X)}{\bar{c}_-'(\bar{c}_-'' + \phi X)} +$$
$$\frac{RT}{2F}\left(\frac{\phi X}{A_1 - A_2}\right)\ln\frac{(\bar{c}_-'' + A_1)(\bar{c}_-' + A_2)}{(\bar{c}_-' + A_1)(\bar{c}_-'' + A_2)} \quad (28)$$

where

$$A_i = \frac{1}{4}\left[\phi X + \frac{2RT\bar{c}_0 l_- k}{J_0} + (-1)^i\left\{\left(\phi X - \frac{2RT\bar{c}_0 l_- k}{J_0}\right)^2 + 4(\phi X)^2\right\}^{1/2}\right] \quad (29)$$

and

$$k = \frac{1}{\delta}(\bar{c}_-'' - \bar{c}_-') - \frac{(\bar{c}_-'' + \bar{c}_-')J_0}{2RT\bar{c}_0 l_-} +$$
$$\frac{(\phi X)^2 J_0}{4RT\bar{c}_0(\bar{c}_-'' - \bar{c}_-')l_-}\ln\left(\frac{\bar{c}_-'' + \frac{\phi X}{2}}{\bar{c}_-' + \frac{\phi X}{2}}\right) \quad (30)$$

At the limit of low concentration of electrolyte, $\Delta\psi$ is given by eq 25 and $P_s$ is expressed by eq 20, from which we can determine $\phi$.

At high concentrations of electrolyte, eq 26 becomes

$$-\Delta\psi\Big/\left(\frac{r-1}{r}\right) = \frac{RT}{F}\left(\frac{\phi X}{2}\right)\frac{1}{c'} \quad (31)$$

except at extremely high concentrations where the water flux $J_0$ is so high that the membrane potential is significantly affected by $J_0$. Equation 31 predicts a linear relationship between $\Delta\psi/[(r-1)/r]$ and $1/c'$, from which we can determine $\phi X$. At high concentrations, the permeation coefficient, eq 19, is given by

$$P_s = \frac{RTfl_-{}^0}{\delta} \quad (32)$$

from which we can determine the tortuosity factor $f$.

## Experimental Section

*Membrane.* The membrane used in this work is an interpolymer membrane of collodion and sulfonated polystyrene, which was reported in a previous paper (membrane C-1).[6]

*Determination of Counterion Concentration in the Membrane.* The membrane was completely converted to the $H^+$ form by treatment with a liberal excess of 1 *N* HCl, until the acid solution was free of metal cation. The membrane was then washed with deionized water to remove the HCl absorbed, until the water was free of $Cl^-$. To determine the acid content of the membrane, the membrane was immersed in a known amount of standard 0.1 *N* NaOH and the excess NaOH was back-titrated with standard HCl using a pH meter. The concentration of counterion in the membrane, $X$, can be calculated from the ion-exchange ca-

pacity and the water content which can be determined from the weights of the membrane in the dry and wet states.

To determine the thermodynamically effective concentration of the membrane charge, $\phi X$, the membrane is equilibrated in an electrolyte solution of concentration c. The electrolyte absorbed in the membrane is washed out with pure water and the amount of the electrolyte is determined by flame photometer and the Mohr method. The $\bar{c}_-$ can be calculated from the amount of absorbed electrolyte and water. Thus, $\phi X$ and, then, $\phi$ can be obtained from eq 8. The values of $\phi$ thus determined can be compared with the values determined from permeation velocity of electrolyte and from membrane potential. The value of $\bar{y}_p$ can be calculated from the value of $\phi$ and the values of $\bar{y}_\pm$ for KCl in aqueous solutions.

*Measurements of Membrane Potential.* The membrane potential cell was constructed with two sections made of poly(methyl methacrylate) resin. A calomel electrode was connected to each section. The solution inlet and outlet were inserted into each half-cell to disturb a diffusion layer on the membrane surface.[39,40] The membrane potentials were measured for KCl, NaCl, and LiCl with the concentration ratios $r$ = 2, 4, and 8 at 25 ± 0.05°.

## Results

*Membrane Potential and Permeation Coefficient.* The data on membrane potentials in KCl solutions at different ratios of electrolyte concentration are summarized in Figure 1, while the data in other electrolyte solutions at a constant ratio $r$ = 4 are summarized in Figure 2. The permeation coefficient $P_s$ for KCl at different ratios $r$ = 2, 4, 8, and 16 are shown in Figure 3 and the data for the other electrolyte solutions at $r$ = 4 are shown in Figure 4. The features in Figures 1–4 are almost the same as those reported by previous authors.[16] The permeation velocity of water at the same experimental conditions is already reported in ref 6.

*Effective Concentration of Counterion in the Membrane.* The ion-exchange capacity was 0.25 mequiv/g of dry $K^+$ form membrane. The water content of the $K^+$ form membrane equilibrated with pure water was 1.96 g/g of dry $K^+$ form membrane. The concentration of counterion in the membrane, $X$, was then found to be 0.13 mol/kg of $H_2O$. The value of $X$ changes with counterion species slightly but may be assumed to be a constant independent of ion species for the present purpose. To discuss the permeation velocity and membrane potential, $X$ should be expressed in mol/cm$^3$. However, since the conversion from mol/kg of $H_2O$ to mol/cm$^3$ is not clear in the membrane because of the volume of fixed charges, we assume $X = 1.00 \times 10^{-4}$ mol/cm$^3$. The ambiguity in $X$ causes an ambiguity in $\phi$, but it is not important for the present purpose.

The values of $\phi$ and $\bar{y}_p$ determined from the Donnan membrane equilibrium in KCl solutions are shown in Figure 5. The values of $\bar{y}_p$ change with KCl concentration, as reported by Kobatake et al.[17,29,30,32,42] and tends to different values at limits of low and high electrolyte concentrations. Both limiting values and the middle value of $\bar{y}_p$ (or $\phi$) in Figure 5 were employed in the following comparison between theory and experiments.

## Comparison between Theory and Experimental Results

*Determination of $\phi$ at the Limits of High and Low Concentrations of Electrolyte.* There are two methods to determine $\phi$ from membrane potential and permeation coefficient: At the limit of high concentration of KCl, eq 31 predicts a linear relation between $\Delta\psi/[(r-1)/r]$ and $1/c'$, from which we can find $\phi X$. At the limit of low concentration of electrolyte, eq 20 predicts a linear relationship between $P_s$ and $c'$ independent of counterion species, from which we can find $\phi X$ if we know the value of $f$. In these two regions,

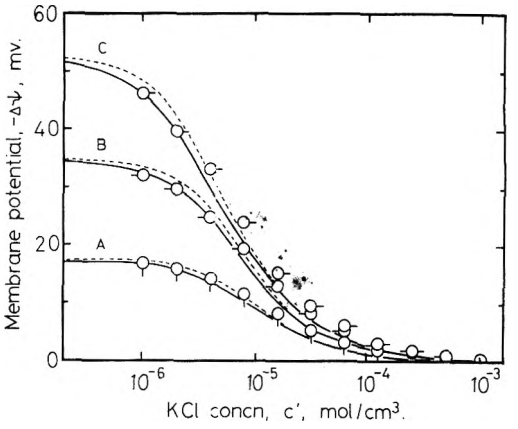


**Figure 1.** Membrane potentials for KCl at various ratios of electrolyte concentrations: A, $r$ = 2; B, $r$ = 4; C, $r$ = 8. Solid and dotted lines are calculated from eq 22 with $\bar{y}_p$ = 0.16 on the assumptions of $J_0 \neq 0$ and $J_0 = 0$, respectively.

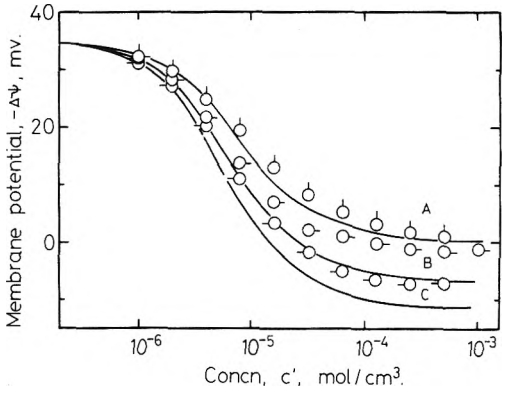


**Figure 2.** Membrane potentials at $r$ = 4: A, KCl; B, NaCl; C, LiCl. Solid lines are calculated from eq 22 with $\bar{y}_p$ = 0.16.

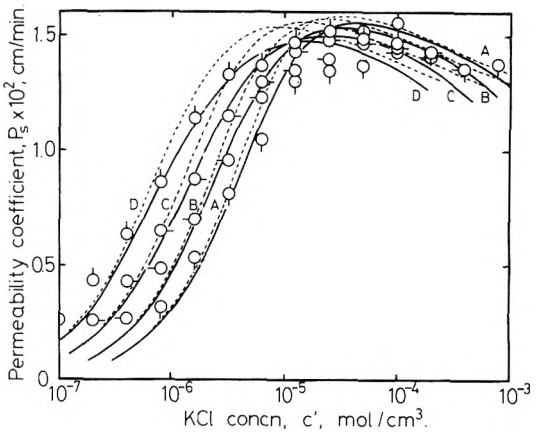


**Figure 3.** Permeability coefficients for KCl at various ratios of electrolyte concentrations: A, $r$ = 2; B, $r$ = 4; C, $r$ = 8; D, $r$ = 16. Solid and dotted lines are calculated from eq 11 with $\bar{y}_p$ = 0.16 on the assumptions of $J_0 \neq 0$ and $J_0 = 0$, respectively.

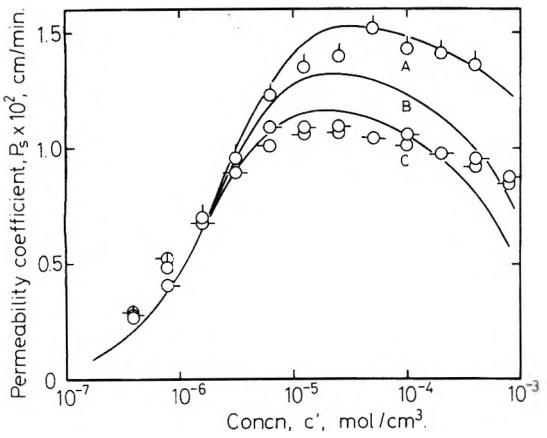


**Figure 4.** Permeability coefficients at $r = 4$: A, KCl; B, NaCl; C, LiCl. Solid lines are calculated from eq 11 with $\bar{y}_p = 0.16$.

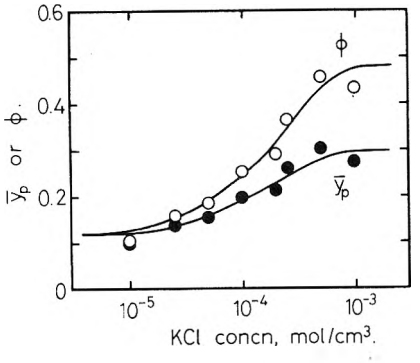


**Figure 5.** Dependence of parameters $\bar{y}_p$ and $\phi$ on concentration of KCl.

$J_0$ was found to be low as reported previously.[6] Therefore, the terms due to $J_0$ are negligible compared with the other terms. The assumption can be supported when the calculated values on $P_s$ and $\Delta\psi$ are compared with experimental values over the entire range of concentration.

Figure 6 shows the linear plot of $\Delta\psi/[(r-1)/r]$ vs. $1/c'$ at high concentrations as predicted. It is found that the data are independent of counterion species, as predicted from eq 31. From the initial slope, we can find $\phi X = 4.8 \times 10^{-5}$ mol/cm$^3$ and then $\phi = 0.48$, which agrees with the value of $\phi$ at the limit of high electrolyte concentration in Figure 5.

Figure 3 shows that $P_s$ tends to an almost constant value $1.36 \times 10^{-2}$ cm/min as the concentration increases, as predicted from eq 32. Using $l_-^0 = 3.6 \times 10^{-14}$ cm$^2$ mol erg$^{-1}$ min$^{-1}$ at $10^{-3}$ mol/cm$^3$ [43] and $\delta = 0.03$ cm, we have $f = 0.46$. The decrease of $P_s$ at higher concentrations is caused by the decrease of $\bar{y}_\pm$ and $l^0$'s.

To compare the experimental data of the permeation coefficient in dilute solutions with eq 20, it is convenient to use $P_s$ at $r = 1$. In Figure 7, the data in Figure 3 are replotted in the form of $P_s/(r+1)$ vs. $c'$ keeping $c''$ constant, as was done by Oda et al.[21] The values of $P_s$ at $r = 1$ can be estimated on the figure and are shown as a function of concentration $c''$ (=c') in Figure 8. The plots for KCl, NaCl, and LiCl are found to be linear with respect to $c$ with a slope of $1.5 \times 10^3$ cm$^4$ mol$^{-1}$ min$^{-1}$ independent of counterion species, as expected from eq 20. Using $f = 0.46$ and $l_-^0 = 4.75 \times 10^{-14}$ cm$^2$ mol erg$^{-1}$ min$^{-1}$,[43] we have $\phi = 0.12$ at the limit of dilute concentration, which agrees with the value in Figure 5.

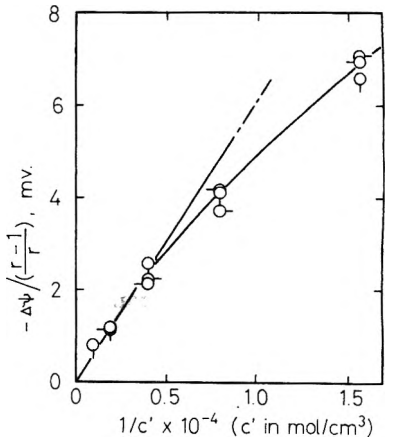


**Figure 6.** Relationship between $\Delta\psi/[(r-1)/r]$ and $1/c'$ for KCl solutions: ○, $r = 2$; ⊖, $r = 4$; ⊖, $r = 8$.

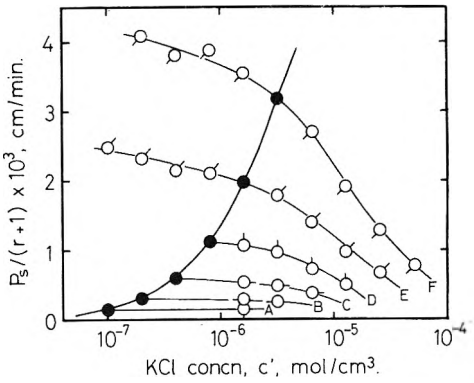


**Figure 7.** Dependence of $P_s/(r+1)$ on concentration of KCl, $c'$, when $c''$ is kept constant. $c''$ (mol/cm$^3$): A, $10^{-7}$; B, $2 \times 10^{-7}$; C, $4 \times 10^{-7}$; D, $8 \times 10^{-7}$; E, $1.6 \times 10^{-6}$; F, $3.2 \times 10^{-6}$.

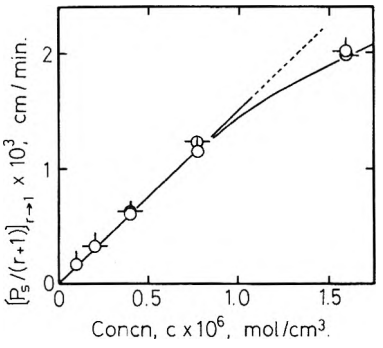


**Figure 8.** Dependence of $P_s/(r+1)$ on concentration of KCl, NaCl, and LiCl at $r = 1$: ○, KCl; ⊖, NaCl; ⊖, LiCl.

*Membrane Potential and Permeation Coefficient over the Entire Range of Concentrations.* Using the values of $\bar{y}_p$ at high and low concentrations (0.3 and 0.12, respectively), the values of $\Delta\psi$ and $P_s$ can be calculated from eq 11 and 22. The value of $J_0$ used for calculation were already reported in ref 6. The value of $y_\pm$ is taken from literature[43] and the value at $(\bar{c}_-' + \bar{c}_-'')/2$ is inserted in both the denominator and numerator of eq 11 and 22. The calculated values are compared with experimental data in Figures 9 and 10. It is found that the experimental values can be well expressed by eq 11 and 22, respectively, in both regions of

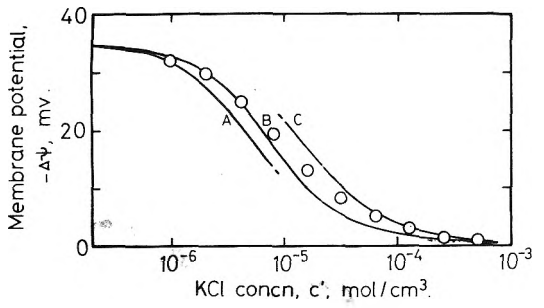


**Figure 9.** Membrane potentials for KCl at $r = 4$ with various values of $\bar{y}_p$: A, $\bar{y}_p = 0.12$ (determined in Figure 8); B, $\bar{y}_p = 0.16$ (middle value in Figure 5); C, $\bar{y}_p = 0.30$ (determined in Figure 6).

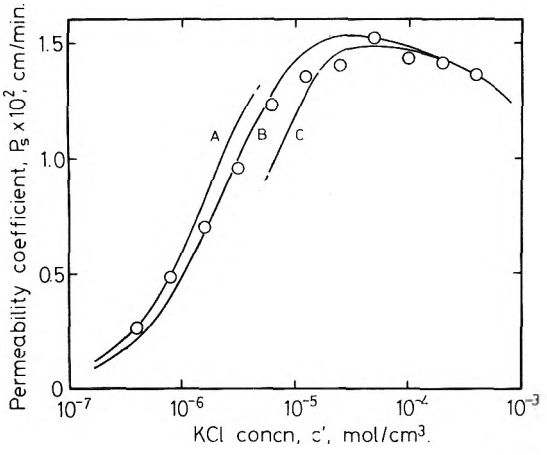


**Figure 10.** Permeability coefficients of KCl at $r = 4$ with various values of $\bar{y}_p$: A, $\bar{y}_p = 0.12$ (determined in Figure 8); B, $\bar{y}_p = 0.16$ (middle value in Figure 5); C, $\bar{y}_p = 0.30$ (determined in Figure 6).

high and low electrolyte concentrations. In the middle range, however, both $\Delta\psi$ and $P_s$ deviate from both calculated lines surely because of the change of $\phi$ with concentration of electrolyte.

The variation of $P_s$ and $\Delta\psi$ with electrolyte concentration in the middle range of concentration is just as predicted from the electrolyte concentration dependence of $\phi$ in Figure 5. However, we cannot use the electrolyte concentration dependence of $\phi$ or $\bar{y}_p$ in Figure 1 to calculate $\Delta\psi$ and $P_s$ from eq 11 and 22, since $\phi$ in eq 11 and 22 is a kind of average value between $c'$ and $c''$, whereas the data of $\phi$ or $\bar{y}_p$ in Figure 5 were obtained at constant concentrations of electrolyte. The nature of the average in eq 11 and 22 is unknown. The best way to compare experimental data with eq 11 and 22, therefore, may be to use a middle value in Figure 5, that is, $\bar{y}_p = 0.16$ for KCl and $\bar{y}_\pm$ as a function of $(\bar{c}_-' + \bar{c}_-'')/2$. The calculated lines with these values are also shown in Figures 9 and 10. The use of the middle value in this paper corresponds to the latest paper of Kamo, Oikawa, and Kobatake.[44]

The calculated values of eq 11 and 22 with $\bar{y}_p = 0.16$ at all experimental conditions are shown by solid lines in Figures 1–4. The disagreement between theory and experiments found in those figures is comparable to those found in Figures 9 and 10.

*Contribution of Water Flow to $P_s$ and $\Delta\psi$.* The contribution of water flow to $P_s$ and $\Delta\psi$ can be estimated from the difference between the calculated values of eq 11 and 22 using the $J_0$ term and those calculated with the assumption of $J_0 = 0$. Examples of the calculated values of $\Delta\psi$ and $P_s$ with the assumption of $J_0 = 0$ are shown by dotted lines in Figures 1 and 3. The contribution of water flow is large in the middle range of electrolyte concentration due to the anomalous osmosis of water and at extremely high concentrations of electrolyte due to the large osmotic flow of water. However, the contribution does not exceed 10% as estimated by Kobatake et al.[40] The effect of water flow on $\Delta\psi$ may be less marked than that on $J_s$ since the effects on both $J_+$ and $J_-$ tend to cancel each other in $\Delta\psi$.

## Discussion

In the study of polyelectrolyte solutions, the physical meaning of $\phi$ or $\bar{y}_p$ is now well clarified if the fixed charges are sulfonate groups and the counterions are alkali metal ions. The use of $\phi$ is supported by the fact that the thermodynamic properties and also transport properties of counterions in polyelectrolyte solutions are approximately given by the sum of contributions of the ions liberated from the polyelectrolyte and from added electrolyte.[34,35,45] That is, the activity, mobility, and other properties of the counterion are approximately additive with respect to the contributions from polyelectrolyte and added electrolyte. Equation 9 is expressed on this assumption, in hope that $\bar{y}_p$ is a constant independent of electrolyte concentration. However, the dependence of $\bar{y}_p$ on the concentration of electrolyte is still as high as a factor of 2, though it is less than that of $\phi$. This variation of $\bar{y}_p$ may arise from the fact that this additivity law, strictly speaking, holds only at the limit of low polyelectrolyte concentration.[38] The value of $\bar{y}_p$ depends on polyelectrolyte concentration slightly and also on electrolyte concentration if the polyelectrolyte concentration is kept constant. The variation in $\bar{y}_p$ is marked as the polyelectrolyte concentration increases. Since the polyelectrolyte concentration is rather high in membrane, it may be reasonable that $\bar{y}_p$ changes with the concentration of KCl.

The values of $\phi$ determined in thermodynamic and transport phenomena do not generally agree with each other. The value of $\phi$ in transport phenomena is generally larger than that in thermodynamic phenomena in dilute polyelectrolyte solutions,[34,35] though Ueda and Kobatake[46] recently reported that $\phi$ values determined thermodynamically and hydrodynamically agree with each other over a wide range of polymer concentration. This is because the nonuniform distribution of counterions around a polyion does not necessarily give the same effect on thermodynamic properties and transport phenomena. In the membrane phenomena, $\phi$ arises in theoretical equations because of both thermodynamic and hydrodynamic reasons. Strictly speaking, moreover, $\phi$ in the $J_0$ term may not necessarily be the same as that in the grad $\bar{\mu}_+$ term of eq 5a. Considering that the use of $\phi$ is based on the assumption that all counterions can be classified into two distinct groups, completely free and completely bound, however, it appears to be beyond the applicability of this ion-binding model to assume two different values for $\phi$ in a phenomenon. Therefore, $\phi$ used in the present theory should be taken as a parameter, based on the assumption that the $(1 - \phi)$ part of the counterions are completely bound on fixed charges and the $\phi$ part behave as if they were in a simple electrolyte solution, both thermodynamically and hydrodynamically. Kobatake and his coworkers have published a series of papers to discuss the features of $\phi$.[29-32,44,46]

Because of these assumptions, we cannot expect perfect agreement between the calculated values of eq 11 and 22

and experimental data if we assume a constant value for $\phi$. The agreement found in Figures 1–4, 9, and 10 may be considered to be satisfactory. Since $\phi$ in eq 9 remains in the limiting eq 20 and 31, it is reasonable to see good agreement between the values of $\phi$ determined in Figures 6 and 8 and the limiting values in Figure 5.

*Acknowledgment.* The authors wish to thank Mrs. C. Wada for her technical assistance in measuring the Donnan membrane equilibrium.

### References and Notes

(1) A. J. Staverman, *Trans. Faraday Soc.*, **48**, 176 (1952).
(2) G. Scatchard, *J. Am. Chem. Soc.*, **75**, 2883 (1953).
(3) K. S. Spiegler, *Trans. Faraday Soc.*, **54**, 1408 (1958).
(4) O. Kedem and A. Katchalsky, *J. Gen. Physiol.*, **45**, 143 (1961).
(5) W. Dorst, A. J. Staverman, and R. Caramazza, *Recl. Trav. Chim. Pays-Bas*, **83**, 1329 (1964).
(6) M. Tasaka, Y. Kondo, and M. Nagasawa, *J. Phys. Chem.*, **73**, 3181 (1969).
(7) N. Lakshminarayanaiah, "Transport Phenomena in Membranes", Academic Press, New York, N.Y., 1969.
(8) E. Riande, *Phys. Electrolytes*, **1**, Chapter 11 (1972).
(9) T. Teorell, *Proc. Soc. Exp. Biol. Med.*, **33**, 282 (1935).
(10) T. Teorell, *Proc. Natl. Acad. Sci. U.S.A.*, **21**, 152 (1935).
(11) K. H. Meyer and J. F. Sievers, *Helv. Chim. Acta*, **19**, 649, 665, 987 (1936).
(12) M. Nagasawa and Y. Kobatake, *J. Phys. Chem.*, **56**, 1017 (1952).
(13) R. Schlögl and F. Helfferich, *Z. Elektrochem.*, **56**, 644 (1952).
(14) J. S. Mackie and P. Meares, *Proc. R. Soc. London, Ser. A*, **232**, 498 (1955).
(15) G. J. Hills, P. W. M. Jacobs, and N. Lakshminarayanaiah, *Proc. R. Soc. London, Ser. A*, **262**, 246 (1961).
(16) Y. Toyoshima, Y. Kobatake, and H. Fujita, *Trans. Faraday Soc.*, **63**, 2814 (1967).
(17) M. Yuasa, Y. Kobatake, and H. Fujita, *J. Phys. Chem.*, **72**, 2871 (1968).
(18) R. Schlögl, *Z. Phys. Chem. (Frankfurt am Main)*, **3**, 73 (1955).
(19) J. S. Mackie and P. Meares, *Proc. R. Soc. London, Ser. A*, **232**, 510 (1955).
(20) P. Meares and H. H. Ussing, *Trans. Faraday Soc.*, **55**, 142 (1959).
(21) Y. Oda and T. Yawataya, *Bull. Chem. Soc. Jpn.*, **29**, 673 (1956).
(22) J. W. Lorimer, E. I. Boterenbrood, and J. J. Hermans, *Discuss. Faraday Soc.*, **21**, 141 (1956).
(23) R. J. Stewart and W. F. Graydon, *J. Phys. Chem.*, **61**, 164 (1957).
(24) A. S. Tombalakian and W. F. Graydon, *J. Phys. Chem.*, **70**, 3711 (1966).
(25) G. J. Hills, P. W. M. Jacobs, and N. Lakshminarayanaiah, *Proc. R. Soc. London, Ser. A*, **262**, 257 (1961).
(26) N. Lakshminarayanaiah and V. Subrahmanyan, *J. Polym. Sci., Part A*, **2**, 4491 (1964).
(27) N. Lakshminarayanaiah, *J. Phys. Chem.*, **70**, 1588 (1966).
(28) N. Lakshminarayanaiah, *J. Phys. Chem.*, **73**, 97 (1969).
(29) N. Kamo, Y. Toyoshima, H. Nozaki, and Y. Kobatake, *Kolloid Z. Z. Polym.*, **248**, 914 (1971).
(30) N. Kamo, Y. Toyoshima, and Y. Kobatake, *Kolloid Z. Z. Polym.*, **249**, 1061 (1971).
(31) N. Kamo and Y. Kobatake, *Kolloid Z. Z. Polym.*, **249**, 1069 (1971).
(32) T. Ueda, N. Kamo, N. Ishida, and Y. Kobatake, *J. Phys. Chem.*, **76**, 2447 (1972).
(33) D. G. Miller, *J. Phys. Chem.*, **70**, 2639 (1966).
(34) S. A. Rice and M. Nagasawa, "Polyelectrolyte Solutions", Academic Press, New York, N.Y., 1961.
(35) A. Katchalsky, *Pure Appl. Chem.*, **26**, 327 (1971).
(36) F. G. Donnan and E. A. Guggenheim, *Z. Phys. Chem., Abt. A*, **162**, 346 (1932).
(37) F. G. Donnan, *Z. Phys. Chem., Abt. A*, **163**, 369 (1934).
(38) M. Nagasawa in "Polyelectrolytes", E. Sélégny, Ed., D. Ridel, Dordrecht, The Netherlands, 1974, p 57.
(39) M. Nagasawa and I. Kagawa, *Discuss. Faraday Soc.*, **21**, 52 (1956).
(40) M. Tasaka, S. Morita, and M. Nagasawa, *J. Phys. Chem.*, **69**, 4191 (1965).
(41) R. Parsons, "Handbook of Electrochemical Constants", Butterworths, New York, N.Y., 1959.
(42) Y. Toyoshima and H. Nozaki, *J. Phys. Chem.*, **73**, 2134 (1969).
(43) "Landolt-Börnstein Tabellen", Vol. II, Part 7, 6th ed, Springer-Verlag, West Berlin, Gottingen, Heidelberg, 1960, pp 51–55.
(44) N. Kamo, M. Oikawa, and Y. Kobatake, *J. Phys. Chem.*, **77**, 92 (1973).
(45) M. Nagasawa, I. Noda, T. Takahashi, and N. Shimamoto, *J. Phys. Chem.*, **76**, 2286 (1972).
(46) T. Ueda and Y. Kobatake, *J. Phys. Chem.*, **77**, 2995 (1973).

# Diffusion in Liquid Systems. II. Computer-Assisted Measurement of Diffusion Coefficients at Various Temperatures

**A. C. Ouano* and J. A. Carothers**

*IBM Research Laboratory, San Jose, California 95193* *(Received September 16, 1974; Revised Manuscript Received March 10, 1975)*

*Publication costs assisted by IBM Corporation*

A physical description of the dispersion of solutes in Poiseuille flow and its analogy to Fickian diffusion is presented. The superior accuracy of the computerized data acquisition and processing technique over the graphical method of obtaining diffusion coefficients from the retention volume distribution (RVD) of solutes in capillaries is demonstrated. The diffusion coefficients of various organic compounds in chloroform at different temperatures were measured and activation energies calculated.

## Introduction

The difficulty of obtaining diffusion coefficients in liquids is well documented.[1-4] This difficulty is very likely the major reason for the meager amount of diffusion coefficient data in the open literature. The introduction of a new technique[4-7] of measuring the diffusion coefficient from the retention volume distribution (RVD) variance of the solute diffusing in a mobile phase, undergoing Poiseuille flow in a long capillary tubing, offers a simpler and faster technique. This technique, which evolved from Taylor's[8] classic paper on the axial dispersion of solutes in Poiseuille flow, is much easier and less time consuming to execute than the classical method of measuring the diffusion coefficient ($D$) using a diaphragm or a Fürth–Nistler type diffusion cell. This technique allows for easier temperature control and hence is suitable for use in obtaining $D$ at various temperatures.

Although the mathematics and formal proof of the underlying principles of axial dispersion in Poiseuille flow

has been fully discussed,[4,8] a physical description of the nature of this phenomenon has not been adequately presented. Thus, it is worthwhile to describe briefly the physical processes which justify the calculation of the diffusion coefficient of a solute from its RVD.

### Physical Description of the Taylor Diffusion Process

Figure 1 illustrates what happens to a pulse of solution which is injected into a solvent undergoing Poiseuille flow in a capillary tubing. Upon injection, the pulse is immediately distorted into a parabolic shape by the streamline velocity of Poiseuille flow. This distortion results in a concentration gradient in the radial direction and the accompanying radial diffusion of the solute.

Let us for the moment assume that the molecular diffusivity is zero. For this case, the solute molecules will remain in their streamline throughout their residence in the tubing, since no radial diffusion took place. Consequently, the solute cloud is dispersed as an ever sharpening and thinning parabola as it moves along the tube. If a concentration detector is placed at the end of the capillary tubing to measure the solute concentration as function of either the time of solute arrival or the retention volume, the shape of the RVD curve will be highly skewed as shown in Figure 1a.

However, this assumption of no molecular mobility in liquids is far from reality and, hence, cannot be verified experimentally. The experimentally observed shape of the RVD in capillary tubing with large length ($l$) to diameter ($d$) ratios, i.e., $l/d > 6000$, is nearly gaussian[4-8] as shown in Figure 1b. To explain this phenomena, let us go back to the introduction of a pulse of solution in the Poiseuille streamline with molecular diffusion. Solute molecules at the tip of the parabola diffuse toward the tube wall into a streamline of lower velocity, while those solute molecules near the wall (tail of the parabola) diffuse into a higher streamline velocity. This phenomenon minimizes the stretching of the parabola through a recirculating or "folding" motion of the solute cloud as if it is being stirred by a molecular stirrer. The speed of circulation depends on the molecular diffusivity, flow rate, and the capillary diameter. If this "mixing" is allowed to continue for a sufficiently long time (very long tubing or very low flow rate), the shape of the dispersed solute cloud will gradually change from that of a parabola to that of a highly diffused pulse which moves along the length of the tubing at the average flow velocity. The rate of mixing of the solute cloud can then be related to the Taylor diffusivity $D_t$ as shown by

$$D_t = R^2U^2/48D \quad (1)$$

where $D$, $R$, and $U$ are the diffusion coefficient, tubing radius, and average velocity, respectively.

It has been shown[4-8] that the solute molecular diffusivity can be expressed in terms of the variance of the retention volume distribution and other easily measurable experimental parameters, i.e.

$$D = (R^2U/24l)(V_t/\sigma)^2 \quad (2)$$

where $V_t$ and $\sigma$ are the peak retention volume and the standard deviation of the retention volume distribution.

In a previous paper,[4] it was shown that $\sigma$ in eq 2 can be approximated by $W/4$ where $W$ is the distance between the two tangents of the RVD at the base line. This graphical method is at best (for gaussian RVD) a rough technique for obtaining $\sigma$ from the RVD. Errors introduced by this approximation are quite large for nongaussian (skewed) RVD,

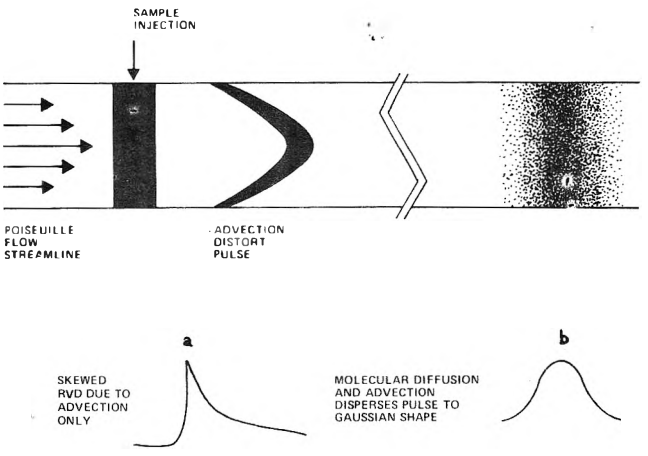


**Figure 1.** Illustration of the dispersion of solutes in a Poiseuille flow. (a) RVD of solutes in Poiseuille flow without molecular diffusion, i.e., dispersion due to a advection only. (b) RVD of solutes in Poiseuille flow with molecular diffusion.

i.e., at a high flow rate or with short tubing. Since the determination of $\sigma$ requires the calculation of the moments of the RVD, it is a tedious and lengthy process. Therefore, the use of computers to reduce the tediousness of calculating $\sigma$ from the RVD becomes a necessity. This work describes the use and application of laboratory automation (application of computers in augmenting the execution of laboratory experiments) for the acquisition and reduction of diffusion measurement data. To illustrate the value of this technique, the diffusion coefficients of various compounds in chloroform at four temperatures were measured. The values of $\sigma$ as calculated by the base line width (graphical method) and by the method of moments were also compared to demonstrate the improved precision obtained with the use of computers. Grushka et al.[10,11] has applied the same technique in moments analysis of gas chromatographic peaks.

### Apparatus Description

The diffusion apparatus used in this work was essentially the same as the one described previously,[4] except for some minor but significant modifications. The alterations were as follows.

The coiled 16,800 cm long capillary tubing was replaced with a shorter but an elongated U-shaped (the bend in the U is only about 60 cm long) 4310 cm long stainless steel tubing with an i.d. of 0.051 cm. This was done to reduce the secondary flow introduced by the circular configuration of the original diffusion capillary tubing.

The temperature of the capillary tubing was maintained constant by incasing it entirely in a ¼-in. i.d. copper tubing through which silicone oil was flowing at ±0.05° of the set temperature. To minimize heat loss or gain through the copper tubing jacket, it was insulated with ⅛ in. thick asbestos tape. Care was taken to minimize bends and "kinks" in the capillary tubing except in the U-bend area. A photograph of the whole diffusion apparatus and injection port is shown in Figure 2.

The third modification made was the addition of the computer interface system to the detector electrical circuit. This modification allows the transmission of the detector concentration analog and volume counter signals to an IBM System/7 sensor-based computer. A sketch of this setup is shown in Figure 3.

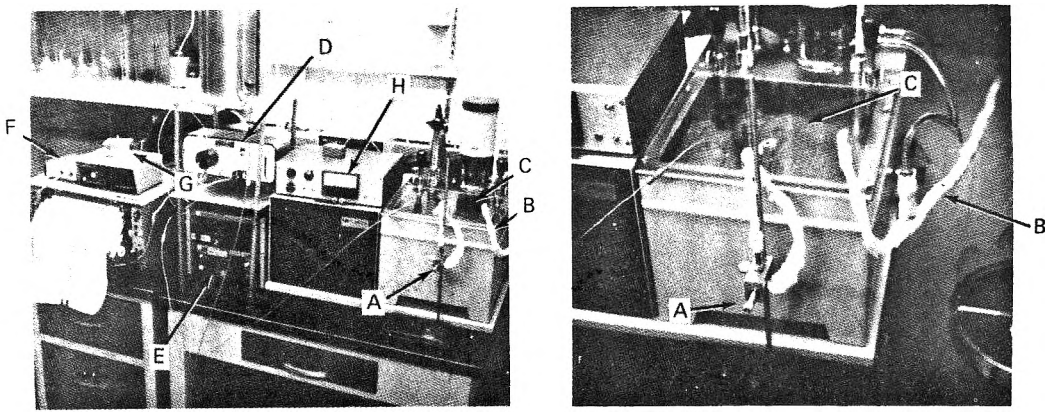


**Figure 2.** Photographs of the diffusion apparatus: (A) septum injection port, (B) diffusion cell, (C) temperature bath, (D) uv concentration detector, (E) diffusion refractometer detector, (F) computer interface, (G) siphon volume counter, (H) temperature controller.

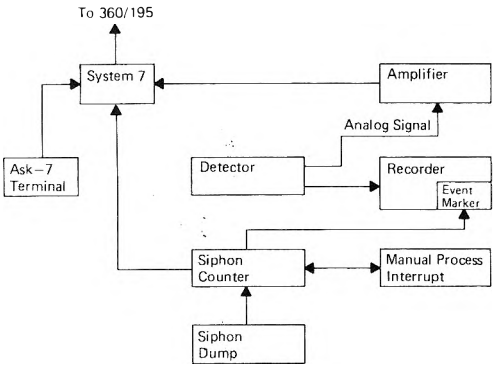


**Figure 3.** Schematic diagram of the computerized data acquisition system of the diffusion apparatus.

## Experimental Procedure

The mobile phase or the diffusion medium used was chloroform (distilled in glass grade, Burdick and Johnson). Chromatographic grade acetone, ethanol, benzene, diethylbenzene, etc., were used as the diffusing solute. The RVD values of each of these samples were measured at different flow rates by injecting it into a capillary diffusion cell via the septum injection port.

The chronological procedure for initiating an experimental run is as follows. (1) Initiate the sensor-based S/7 computer for data acquisition and data reduction through a gas panel (Ask-7) terminal. (2) At the second or third siphon volume counter dump (each dump is occasioned with an event marker "blip"), 5–10 $\mu$l of sample is injected into the diffusion cell via the septum injection port. (3) As soon as the sample is injected, an additional blip is initiated (each sample dump results in an electrical pulse signal which is sensed by the computer and the strip chart recorder) by an external switch. This operation results in a closely spaced blip (double blip), which is usually about 20 sec apart; the normal siphon dump blips at milliliters per minute flow rate are 150 sec apart. This is executed to allow the computer to recognize that a sample has been injected and to record the time when it was introduced into the diffusion cell. (4) After seven to ten siphon dumps, a second sample is injected into the diffusion cell. This event is also signaled with a double blip as above. It is necessary to space the injections of the samples from seven to ten siphon dumps (25 ml) so that the RVD values of the samples do not overlap and have a sufficient straight base line to allow for the precise calculation of the moments of the RVD. (5) After the last sample has been introduced into the diffusion apparatus, the identifications of the samples injected are entered into the IBM 360/195 host computer via an IBM 2741 communication terminal.

At the end of the analytical run in which data for one or more samples (could be as many as desired) have been collected and stored, the data are transmitted to the host computer (360/195) and reduced to the desired form. A flow diagram of the data is shown schematically in Figure 4.

## Data Reduction Program

After the data have been transmitted to the host computer, they are separated into the individual RVD's. These "chopped" data are stored in a data set as an individual RVD with the proper identifications and other computational parameters, i.e., capillary length and volume, siphon volume, etc.

The diffusion coefficient, as well as the flow rate, the Peclect number, and other desired data, is computed from the RVD using the following chronological calculation procedure. (1) Determine the location of the RVD peak and its value. (2) Determine the location and value of the base of the peak (front and back). Draw a base line of the RVD peak by connecting the front and back base points. (3) Compute for the area and the higher moments (first and second) of the RVD using Simpson's rule. The integration intervals are the retention volume intervals between data points. (4) Compute for the variance from the zeroth ($\mu_0$), first ($\mu_1$), and second ($\mu_2$) moments of the RVD using the equation

$$\sigma^2 = (\mu_0\mu_2 - \mu_1^2)/\mu_0^2 \qquad (3)$$

(5) Compute for the flow rate of the mobile phase from the siphon volume counts per unit time

$$Q = V_s N_c \qquad (4)$$

where $Q$, $V_s$, and $N_c$ are the flow rate, siphon volume, and number of siphon dumps per second, respectively. (6) Compute the diffusion coefficient from eq 2 or from

$$D = 0.01326(Q/l)(V_t/\sigma)^2 \qquad (5)$$

The $D$ and $Q/Dl$ values obtained from the computer output are plotted; an example is shown in Figure 5. The diffusion coefficient is obtained from the intercept of the plot.

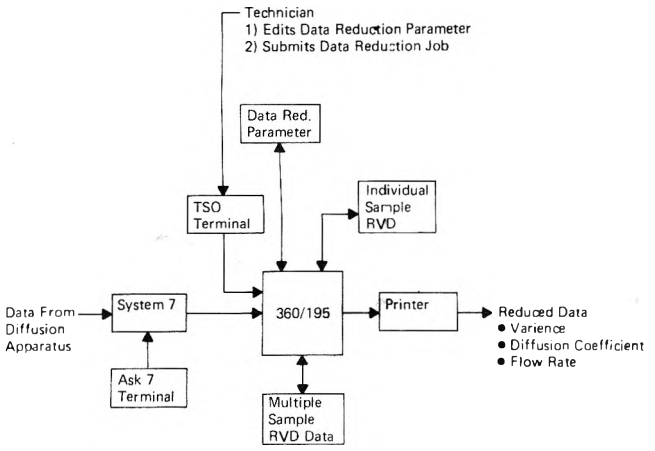


**Figure 4.** Schematic diagram of the computerized data processing system of the diffusion data.

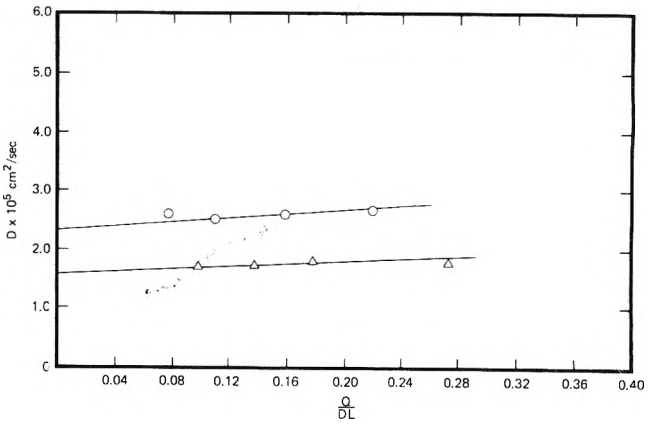


**Figure 5.** Plot of the diffusion coefficient vs. the Peclect number of $C_6H_6$ in $CHCl_3$ at 293°K obtained by computerized (O) and by graphical (Δ) calculation techniques.

**TABLE I: Comparison of Benzene in $CHCl_3$ $D$ Values as Calculated by the Graphical (G) Method and by the Method of Moments (M)**

| Flow rate, ml/min | | Variance, $\sigma^2$, ml$^2$ | | $10^5D$, cm$^2$/sec | | $1/P_e \times 10^2$ | | $10^5D\left(\frac{1}{P_e} \rightarrow 0\right)$,[a] cm$^2$/sec | | Lit. $D$ value, |
|---|---|---|---|---|---|---|---|---|---|---|
| G | M | G | M | G | M | G | M | G | M | cm$^2$/sec |
| 0.43 | 0.52 | 0.10 | 0.08 | 1.7 | 2.58 | 9.8 | 7.8 | 1.8 | 2.39 | 2.30 |
| 0.61 | 0.70 | 0.14 | 0.11 | 1.7 | 2.53 | 14 | 11 | | | |
| 0.86 | 0.97 | 0.19 | 0.15 | 1.8 | 2.57 | 18 | 15 | | | |
| 1.2 | 1.49 | 0.28 | 0.22 | 1.7 | 2.69 | 27 | 21 | | | |

[a] Intercept of Figure 5.

## Discussion of Results

It was mentioned in the preceding section that the approximation of the standard deviation by the graphical method, i.e., $\sigma \approx W/4$, can result in appreciable error in the calculation of the diffusion coefficient. To illustrate this point, the standard deviation and the corresponding diffusion coefficients and $P_e$ of benzene in chloroform at 293°K as calculated both by the graphical method and by the methods of moments (computerized) are compared for the same experimental data in Table I. From Table I and Figure 5, it is obvious that the graphical method tends to overestimate $\sigma$ and, hence, yields a lower $D$ value. In addition to error in the calculation of the variance, the error in calculating the flow rate by graphical means is also apparent in Table I. The graphical method of calculating flow rate is done by dividing the number of siphon dumps with the distance in inches from the point of sample injection to the peak of the RVD and multiplying the quotient with the ratio of the siphon volume to that of the recorder speed in inches per second. The computer method of calculating the flow rate is similar except the total time from the point of injection to the RVD peak is measured directly by the precise "computer clock". Since the diffusion coefficient is proportional to the flow rate and inversely proportional to $\sigma^2$, the errors introduced by the graphical method are compounded.

The dependence of the value of $D$ on the accuracy by which both the flow rate and the $\sigma^2$ can be calculated is further demonstrated by comparing the graphical value of $D$ for benzene in $CHCl_3$ shown in Table I and our previously reported value[4] of 2.01. Since our diffusion measurement system is computerized in both the data acquisition and data reduction, our strip chart recorder output was used only as a visual monitor of the retention volume distribution. We did not rely on it for calculating the diffusion coefficient; consequently we reduced our chart speed (this reduces our paper consumption) to about 4 times less than our previous[4] work. The reduced recorder speed affected directly the accuracy of the graphically determined flow rate (converting linear chart distance to volume via the siphon dump frequency) and $\sigma^2$. This is illustrated in Table I.

It is clear from the above result, that one of the important factors which govern the accuracy of $D$ is the accuracy by which the flow rate and $\sigma^2$ are measured from the linear distances of the strip chart recording. This implies that if the graphical method is used, a high-quality strip chart recorder with accurate chart speed control and variability over a wide speed range is a requisite for precise $D$ measurement. A strip chart recorder with positive chart drive (friction strip chart drive is not recommended), i.e., a stepping motor drive, is highly desirable.

The averages of the replicate runs obtained for the diffusion coefficient $D$ for various compounds at different temperatures are shown in Table II. The variations of $D$ of the replicate runs were found to be less than 1.5%. A comparison with literature data at 293°K[4,9] shown in the last column of Table II shows fairly good agreement with the data obtained in this work.

Figure 6 shows plots of the natural logarithm of the diffusion coefficient vs. temperature. The plots appear to be remarkably parallel except for a slightly higher slope of the acetone and ethanol curves compared to those of the ben-

**TABLE II: Diffusion Coefficient × $10^5$, in $cm^2$/sec at Various Temperatures in $CHCl_3$**

| Compd | 276.5°K | 283°K | 293°K | 313°K | Lit. value at 293°K |
|---|---|---|---|---|---|
| Acetone | 1.97 | 2.17 | 2.41 | 3.20 | 2.39 |
| Ethanol | 1.97 | 2.21 | 2.30 | 3.30 | 1.95 |
| Benzene | 1.87 | 2.30 | 2.39 | 2.90 | 2.30 |
| Butylbenzene | 1.30 | 1.50 | 1.67 | 2.00 | |
| Diethylbenzene | 1.20 | | 1.45 | 1.75 | |
| Xylene | 1.60 | 1.90 | 2.10 | 2.50 | |

**TABLE III: Slopes and Intercept of Figure 6**

| Sample | Slope ($m$) | Intercept ($B$) | Coeff ($A$) × $10^7$ |
|---|---|---|---|
| Acetone | 0.013 | −14 | 5.2 |
| Ethanol | 0.014 | −14 | 4.4 |
| Benzene | 0.010 | −14 | 13.4 |
| Butylbenzene | 0.011 | −14 | 6.2 |
| Diethylbenzene | 0.010 | −14 | 7.5 |
| Xylene | 0.011 | −14 | 7.4 |

**TABLE IV: Activation Energy ($E$) from $D$ vs. $1/T$ Plot**

| Sample | Slope × $10^{-3}$ | $E$, kcal | Intercept (ln $D$ + 12) | Coeff |
|---|---|---|---|---|
| Acetone | −1.2 | 2.5 | 5.6 | $1.7 \times 10^{-3}$ |
| Ethanol | −1.6 | 3.2 | 6.8 | $5.5 \times 10^{-3}$ |
| Benzene | −0.83 | 1.6 | 4.2 | $4.2 \times 10^{-4}$ |
| Butylbenzene | −0.96 | 1.9 | 4.3 | $4.4 \times 10^{-4}$ |
| Diethylbenzene | −0.86 | 1.7 | 3.8 | $2.7 \times 10^{-4}$ |
| Xylene | −0.97 | 1.9 | 4.5 | $5.6 \times 10^{-4}$ |

zene and its derivatives. A linear regression of the data gave slopes and intercepts for the plots of Figure 6. The results, which are presented in Table III, as expected show the ethanol to have the highest slope (0.014) as compared to that of benzene and its derivative (0.010–0.011).

Figure 6 suggests that the relationships between the diffusion coefficients can be expressed as an exponential function

$$D = Ae^{mT} \tag{6}$$

In using the values of $m$ and $A$ listed in Table III it should be remembered that $m$ and $A$ are valid only for the range in temperature of 275°K < $T$ < 313°K. The coefficient $A$ in eq 6 is obtained from the intercept $B$ of Figure 6 through the equation

$$A = e^{B} \tag{7}$$

When the natural logarithm of the diffusion coefficient is plotted against the reciprocal of the absolute temperature, a straight-line relationship is also obtained. If the data are interpreted in this manner, a pseudoactivation energy can be computed from the slope of the ln $D$ vs. $1/T$ plot. A linear regression analysis of this relationship resulted in the data presented in Table IV; again ethanol is shown to have the highest activation energy which is almost twice as high as that of benzene.

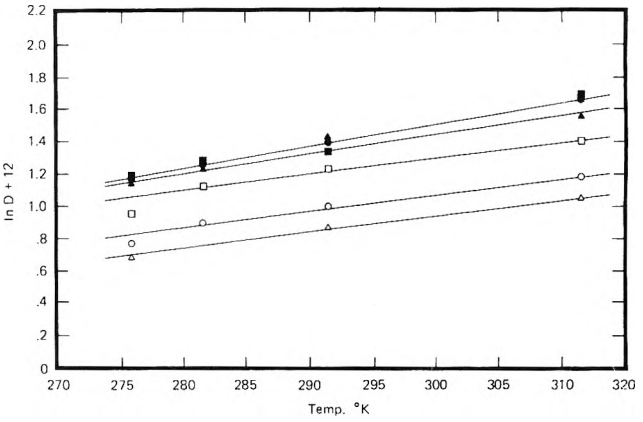


**Figure 6.** Plot of the natural logarithm of the diffusion coefficient vs. the absolute temperature.

## Conclusions

At this point, the ease and flexibility by which the $D$ in liquid can be measured should be apparent. This technique is particularly superior to the classical Fürth–Nistler and diaphragm type cell for measuring diffusion coefficients at various temperatures. Consequently, pseudoactivation energies (enthalpies) associated with the diffusion process can be measured readily.

The graphical method of calculating the variance and the flow rate from the RVD has been shown to be inadequate for the precise calculation of the diffusion coefficient. The more precise and general method of evaluating $\sigma^2$ involves the tedious calculation of the different moments of the RVD. However, this wearisome task can be circumvented by the use of computerized data acquisition and reduction techniques. Moreover, it has been demonstrated that the accuracy of the $D$ value was improved substantially with the use of the method of moments for calculating $\sigma^2$ in lieu of the graphical method.

## References and Notes

(1) T. Graham, *Philos. Trans. R. Soc. London, Ser. A*, **140**, 805 (1950).
(2) H. S. Harned, *Chem. Rev.*, **40**, 461 (1947).
(3) S. A. Sanni and H. P. Hutchison, *J. Sci. Instrum.* **1**, 1101 (1968).
(4) A. C. Ouano, *Ind. Eng. Chem., Fundam.*, **11**, 268 (1972).
(5) K. C. Pratt, D. H. Slater, and W. A. Wakeham, *Chem. Eng. Sci.*, **28**, 1901 (1973).
(6) E. Grushka and E. Kikta, preprint of a paper to be submitted for publication in *J. Phys. Chem.*
(7) K. C. Pratt and W. A. Wakeham, *Proc. R. Soc. London, Ser. A*, **336**, 393 (1974).
(8) G. I. Taylor, *Proc. R. Soc. London, Ser. A*, **219**, 186 (1953).
(9) J. Timmermans, "Physico-chemical Constants of Binary Systems", Vol. 1, 1st ed, Interscience, New York, N.Y., 1959.
(10) E. Grushka, M. Myers, P. Schettler, and J. Giddings, *Anal. Chem.*, **41**, 889 (1969).
(11) E. Grushka and V. Maynard, *J. Phys. Chem.*, **77**, 1437 (1973).

# Isotope Effect in Diffusion of Perdeuteriobenzene and $^{14}C$-Substituted Benzenes in Unlabeled Benzene at 25°

**Ian R. Shankland and Peter J. Dunlop***

*Department of Physical and Inorganic Chemistry, Adelaide University, Adelaide, South Australia* *(Received November 7, 1974)*

Mutual diffusion coefficients, obtained with a Gouy diffusiometer, are reported for the system perdeuteriobenzene–benzene ($C_6D_6$–$C_6H_6$) at 25°. These results are consistent with tracer diffusion coefficients which have previously been obtained in this laboratory for $^{14}C$-substituted benzenes of *varying* molecular weight in benzene. Because of the small difference in refractive index between $C_6D_6$ and $C_6H_6$ only a limited range of concentrations was studied, and thus it was not *meaningful* to extrapolate the mutual data to give tracer diffusion coefficients.

In three previous papers[1-3] tracer diffusion coefficients, $D_T$, were presented for several $^{14}C$-substituted benzenes diffusing in unlabeled benzene. The data in those papers indicated that the tracer diffusion coefficients were a very slight linear function of the molecular weight of the tracer species and were not, as has been sometimes suggested,[4] inversely proportional either to the square root of the mass of the tracer species or to the square root of the reduced mass of the system. The purpose of this article is to present diffusion data for the system perdeuteriobenzene–benzene ($C_6D_6$–$C_6H_6$) which are in agreement with our previous findings.

## Experimental Section and Discussion

The diffusion coefficients for the system $C_6D_6$–$C_6H_6$ were measured with a Gouy diffusiometer[5] and a special diffusion cell which have been previously described,[6,7] as have also the experimental techniques and computations which are used to obtain the mutual diffusion coefficients, $D$. The cell was constructed with a Tiselius-type design but did not have moving surfaces which required lubrication. It is believed that the data for the system $C_6D_6$–$C_6H_6$ are accurate to approximately 0.1–0.2%. The data are summarized in Table I. The $C_6D_6$ and $C_6H_6$ samples were analyzed by gpc and found to contain less than 0.4 and 0.01% of impurity, respectively.

In Figure 1 the data for the system $C_6D_6$–$C_6H_6$ are shown as a function of the mole fraction of $C_6D_6$, $x_2$. The smooth curve has been drawn through the experimental points and the two limiting points derived from the *smoothed* data of Allen and Dunlop.[1] The tracer diffusion coefficient at $x_2 = 0$ corresponds to $^{14}C$-substituted benzene of mol wt 84 diffusing in $C_6H_6$; the tracer diffusion coefficient at $x_2 = 1$ was obtained by assuming the Stokes–Einstein equation[8] could be used to correct the *self*-diffusion coefficient of benzene[1] to the tracer diffusion coefficient of unlabeled benzene in $C_6D_6$. The viscosity of $C_6D_6$ relative to $C_6H_6$ for this calculation was measured with a photoelectric viscometer[9] so constructed that the kinetic energy correction was negligible. The relative viscosity was found to be $1.063_7$ and differed by more than our experimental error from the value of 1.069 reported by Dixon and Schiessler.[10] Also included in Figure 1 are three diffusion coefficients reported by Birkett and Lyons.[11] The two sets of data are in agreement within the error of ±1% claimed by those workers.

Because of the small difference in refractive index between $C_6D_6$ and $C_6H_6$, it was decided not to perform any experiments at concentrations less than $x_2 = 0.18$ since the errors in the diffusion coefficients would be greater than 0.2%. Thus although one cannot say that the *extrapolated* tracer diffusion coefficients agree with the results obtained with $^{14}C$-substituted benzenes, it is quite apparent that the two sets of results do not disagree.

**TABLE I: Mutual Diffusion Coefficients for the System $C_6D_6$–$C_6H_6$ at 25°**

| $\bar{x}_2$[a] | $\Delta x_2$[a] | $J$[b] | $10^5D$ |
|---|---|---|---|
| $0.178_4$ | $0.356_7$ | 44.72 | 2.164 |
| $0.234_2$ | $0.468_4$ | 58.72 | 2.156 |
| $0.350_2$ | $0.700_4$ | 87.80 | 2.141 |
| $0.587_9$ | $0.824_3$ | 103.33 | 2.105 |
| $0.704_7$ | $0.590_5$ | 74.03 | 2.100 |

[a] $\bar{x}_2$ and $\Delta x_2$ are the mean mole fraction and the mole fraction difference, respectively, used in each Gouy experiment. [b] $J$ is the total number of interference fringes obtained in each experiment.

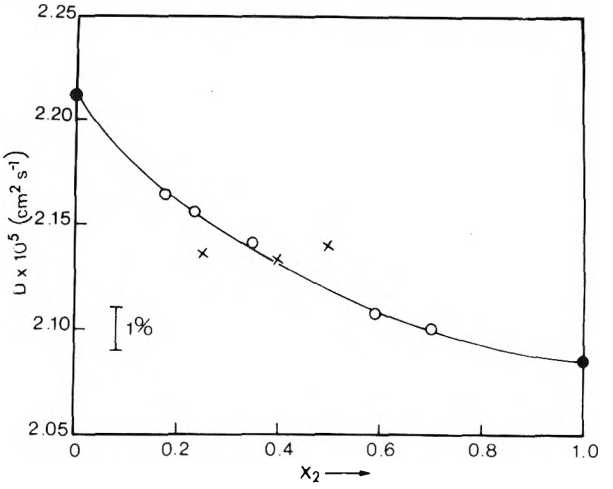


**Figure 1.** Mutual and tracer diffusion coefficients for the system $C_6H_6$–$C_6D_6$ at 25°: O, present results; X, results of Birkett and Lyons;[9] ●, tracer diffusion coefficients from Allen and Dunlop.[1]

*Acknowledgment.* This work was supported in part by a grant from the Australian Research Grants Committee. We wish to thank Dr. B. J. Steel for the use of a photoelectric viscometer.

## References and Notes

(1) G. G. Allen and P. J. Dunlop, *Phys. Rev. Lett.*, **30**, 316 (1973).
(2) S. J. Thornton and P. J. Dunlop, *J. Phys. Chem.*, **78**, 346 (1974).
(3) K. R. Harris, C. K. N. Pua, and P. J. Dunlop, *J. Phys. Chem.*, **74**, 3518 (1970).
(4) L. B. Eppstein and J. G. Albright, *J. Phys. Chem.*, **75**, 1315 (1971).
(5) G. Kegeles and L. J. Gosting, *J. Am. Chem. Soc.*, **69**, 2516 (1947).
(6) H. D. Ellerton, G. Reinfelds, D. E. Mulcahy, and P. J. Dunlop, *J. Phys. Chem.*, **68**, 403 (1964).
(7) G. R. Staker and P. J. Dunlop, *J. Chem. Eng. Data*, **18**, 61 (1973).
(8) H. J. V. Tyrrell, "Diffusion and Heat Flow in Liquids", Butterworths, London, 1961, p 128.
(9) C. James, Ph.D. Thesis, Adelaide University, Adelaide, South Australia, 1971.
(10) J. A. Dixon and W. Schiessler, *J. Phys. Chem.*, **58**, 430 (1954).
(11) J. D. Birkett and P. A. Lyons, *J. Phys. Chem.*, **69**, 2782 (1965).


# COMMUNICATIONS TO THE EDITOR

## Energy Disposal in Unimolecular Reactions. Four-Centered Elimination of HCl

*Publication costs assisted by the National Science Foundation*

*Sir:* The internal energy released to polyatomic products of unimolecular reactions is difficult to measure and, despite several attempts,[1-3] the internal energy of the olefin product from *four*-centered unimolecular HX elimination reactions has not been established. We wish to report definitive results for the vibrational energy released to methylcyclobutene by the HCl elimination reactions from 1-chloro-1-methyl-, 1-chloro-2-methyl-, and 1-chloro-3-methylcyclobutane. The present measurements establish that ~57% of the total available energy (corresponding to ~28% of the potential energy, which is defined as the threshold energy for HX elimination less the endoergicity for final product formation) was retained by the olefin fragment. These conclusions coupled with data from chemiluminescence and chemical laser studies,[4-8] which give the vibrational and rotational energy of the HX product, and the kinetic energy released in the elimination of HCl from polyatomic ions[9] provide a rather complete characterization of energy disposal by this unimolecular reaction system.

Activation of the methylchlorocyclobutane was provided by the C–H insertion reactions of singlet methylene with chlorocyclobutane; experiments consisted of room temperature photolysis of 0.57 $cm^3$ of ketene, 1.7 $cm^3$ of chlorocyclobutane, and 0.25 $cm^3$ of oxygen in vessels of various size to give the desired pressure. The pressure dependence of the relative product yields was measured by dual pass gas chromatographic analysis.

Methylene insertion into the carbon–hydrogen bonds of chlorocyclobutane gave 1-methyl-1-chloro-, 1-methyl-2-chloro-, and 1-methyl-3-chlorocyclobutane with ~109 kcal/mol[3,10] of internal energy (Table I). The vibrationally excited molecules (denoted by an asterisk) are collisionally stabilized or, at reduced pressure, react by ring rupture and HCl elimination to give the products shown in Table I. In this communication we are interested in the energy contents of 1- and 3-methylcyclobutene which were monitored by the rate of their isomerization reactions to give substituted pentadienes.

**TABLE I: Decomposition Products from Methylchlorocyclobutanes**

| | Unimolecular decomposition product | |
|---|---|---|
| Insertion products | HCl elimination[a] | Ring rupture |
| cis- and trans- | | $CH_2{=}CHCl + CH_3CH{=}CH_2$ |
| cis- and trans- | | *cis*- and *trans*-$CH_3CH{=}CHCl + CH_2{=}CH_2$ |
| | | $CH_2{=}CH_2 + CH_2{=}C(Cl)CH_3$ |

[a] The 3-methylcyclobutene product is entered in the table only once, although formed by both 1-methyl-2-chloro- and 1-methyl-3-chlorocyclobutane, because both processes have the same thermochemistry. Conversely the 1-methylcyclobutene is entered for each formation pathway because the associated thermochemistry is different.

Over the experimental pressure range (70–0.4 Torr) the *cis*-pentadiene yield was ~20% of the trans isomer. Although

direct formation of *cis*-1,3-pentadiene from 3-methylcyclobutene as well as isomerization of *trans*-1,3-pentadiene may occur,[11] the mechanism for cis formation is not important for considerations of energy partitioning. The experimental rate constants, $k_a = \omega$[1,3-pentadiene]/[3-methylcyclobutene], for 3-methylcyclobutene are shown in Figure 1. A wide pressure range was examined to obtain the pressure dependence of the rate constants which reflects the breadth of the 3-methylcyclobutene energy distribution.

The critical energy for formation of 3-methylcyclobutene from either 1-methyl-2-chloro- or 1-methyl-3-chlorocyclobutane is ~54 kcal/mol[12] and HCl elimination is ~16 kcal/mol endoergic;[10] therefore, the total available energy is ~93 kcal/mol (~55 and ~38 kcal/mol of excess and potential energy, respectively). Hydrogen chloride elimination reactions from 1-methyl-1-chloro- and 1-methyl-2-chlorocyclobutane have different $E_0$ and $\Delta H_f°$ values[3,10] which complicate the interpretations of the 1-methylcyclobutene channel; however, the magnitude of the experimental rate constants (not shown) support the conclusions based upon the data from 3-methylcyclobutene isomerization shown in Figure 1.

Energy randomization is rapid relative to the time for HX elimination ($10^{-8}$ to $10^{-9}$ sec) from chloro-[3] and fluoroalkanes;[2] thus, the excess energy may be statistically divided among the degrees of freedom of the methylchlorocyclobutane system at the transition state configuration. The calculated statistical distribution function[1,3,13] was combined with a gaussian distribution function, which was chosen to represent the energy released in traversal of the potential energy hypersurface from transition state to products. The solid curve of Figure 1 is the calculated best fit to the experimental rate constants, which was obtained with RRKM $k_E$ values for isomerization and the combined energy distribution that corresponds to retention of ~57% of the total energy by the olefin fragment. This fraction of total energy is ~28% of the *potential* energy, $E_{mp} = 10.5$ and $\sigma = 5.0$ kcal, plus the statistical component which corresponds to 80% of the total excess energy. These results are consistent with conclusions from previous studies[1-3] of four-centered HX eliminations from alkyl halides and this general pattern for release of a relatively small fraction of the *potential* energy to the olefin fragment also may be true for the acyclic halocarbons; however, some of the details may vary.

Previous studies,[14] mainly Dorer and Koob, have used the pressure dependence of consecutive unimolecular rate constants to determine the percentage of *total* available energy partitioned to a polyatomic fragment following photochemical excitation. However, the electronic surfaces on which the photochemically induced reactions proceed are not always well known,[14] thus, the excess and potential energy cannot be easily separated. By contrast the energy disposal from a elementary unimolecular reaction with known input energy can provide information about the dynamics of the reaction on the portion of the surface leading from transition state to products.

Chemiluminescence measurements[4] have shown that HF retains ~13% of the total energy as vibrational energy in the unimolecular elimination from $CH_3CF_3$; similar results are reported[8,15] for photochemically induced HX elimination or from activation of halo olefins by reaction with oxygen atoms. Using the 13% estimate for $\%E_v$(HCl) and our results for $\%E_v$ (olefin), ~30% of the total energy must appear as relative translational or rotational energy of the

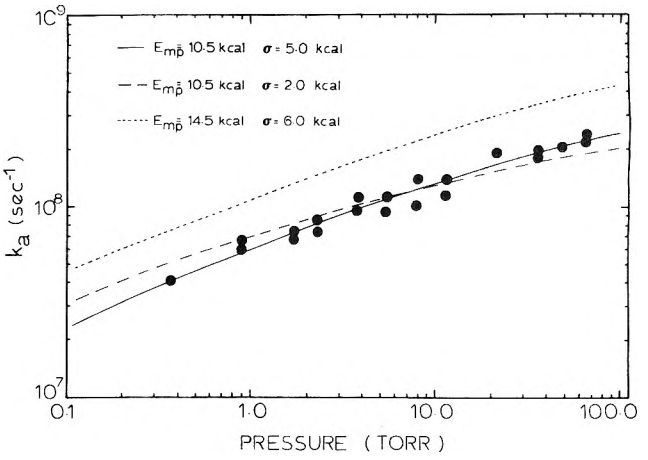


**Figure 1.** The experimental and calculated rate constants for isomerization of 3-methylcyclobutene formed by HCl elimination from 1-methyl-2-chloro- or 1-methyl-3-chlorocyclobutane. The calculated best fit (solid curve) was for a gaussian distribution with $E_{mp} = 10.5$ and $\sigma = 5.0$ kcal which corresponds to a total average energy of 53 kcal mol$^{-1}$ (the available energy is 93 kcal mol$^{-1}$). The high- and low-pressure limits for the best fit were $3.2 \times 10^8$ and $3.5 \times 10^6$ sec$^{-1}$, respectively. The curves labeled (– –) and (- - - -) illustrate the sensitivity of the calculated rate constants to changes in $E_{mp}$ and $\sigma$; the calculated $k_a$ values have a similar dependence to variation in the amount of excess energy. The (- - - -) calculated curve corresponds to 61% of the total energy being released to the olefin, rather than the best fit value of 57%. Since the (- - - -) rate constants are a factor of 2.5 higher than the experimental values, the uncertainty of the total energy assignment is judged to be better than 10%. A change in the threshold energy for isomerization affects the RRKM rate constants for isomerization which influences the energy assignment; for example, calculations using an $E_0$ which was 3.0 kcal higher than the value used in this figure requires $E_{mp} = 19$ kcal (50% of the potential energy) for a good fit to the data points. Since the $E_0$ value should be good to ±1.5 kcal mol$^{-1}$ our estimate of ±10% for the uncertainty in the total energy, assignment should still be valid.

products. Although recent laser results[7] have been interpreted as evidence for the presence of highly rotationally excited HX, most of the remaining energy is likely to be released to translational energy. Since only a small fraction of the statistical energy can be associated with translational energy, the release of the potential energy must favor the translational mode. Ion kinetic energy measurements for decomposition of chloroalkane ions[9] support this conclusion.

We[3] view the dynamics of potential energy release on the hypersurface as a rapid H atom transfer to the Cl atom with release of a portion of the potential energy. This is followed by recoil of Cl–H from the olefin fragment with repulsive release of the remainder of the potential energy, which is partitioned mainly as translational energy and internal energy of the olefin fragment. Our interpretation differs somewhat from the intriguing model advocated by Berry,[8] which implied a major release of energy to HX followed by relaxation of this HX energy because of the time scale for separation of HX and the olefin. A better understanding of the potential energy surface is needed to distinguish between these or other possible models.

*Acknowledgment.* This work was supported by the National Science Foundation, Grants No. 27536X and MPS75-02793. We also are grateful for a fellowship provided to B.E.H. by the Phillips Petroleum Co.

## References and Notes


(1) W. G. Clark, D. W. Setser, and K. Dees, *J. Am. Chem. Soc.*, **93**, 9328 (1971).
(2) K. C. Kim and D. W. Setser, *J. Phys. Chem.*, **77**, 2021 (1973).
(3) K. C. Kim and D. W. Setser, *J. Phys. Chem.*, **78**, 2166 (1974).
(4) P. N. Clough, J. C. Polanyi, and R. T. Taguchi, *Can. J. Chem.*, **48**, 2919 (1970).
(5) H. W. Chang, D. W. Setser, and M. J. Perona, *J. Phys. Chem.*, **75**, 2070 (1971).
(6) M. J. Berry and G. C. Pimentel, *J. Chem. Phys.*, **49**, 5190 (1968).
(7) E. Cuellar, J. H. Parker, and G. C. Pimentel, *J. Chem. Phys.*, **61**, 422 (1974).
(8) The relationship between the energy disposal patterns from chemically vs. photolytically activated HX eliminations has not been established; see M. J. Berry, *J. Chem. Phys.*, **61**, 3114 (1974), for an extensive review of the photolytically initiated elimination studies.
(9) K. C. Kim, J. H. Beynon, and R. G. Cooks, *J. Chem. Phys.*, **61**, 1305 (1974).
(10) Heats of formation of methylchlorocyclobutane and methylcyclobutene were estimated from Benson's group additivity method: S. W. Benson, "Thermochemical Kinetics", Wiley, New York, N.Y., 1968.
(11) C. S. Elliott and H. M. Frey, *Trans. Faraday Soc.*, **64**, 2352 (1968).
(12) The threshold energy for HCl elimination was assumed to be same as for chlorocyclobutane: A. T. Cooks and H. M. Frey, *J. Am. Chem. Soc.*, **91**, 7583 (1969).
(13) Y. H. Lin and B. S. Rabinovitch, *J. Phys. Chem.*, **74**, 1769 (1970).
(14) (a) G. L. Loper and F. H. Dorer, *J. Am. Chem. Soc.*, **95**, 20 (1973), and other papers in the series; (b) K. Dees and R. D. Koob, *J. Phys. Chem.*, **77**, 759 (1973); (c) F. H. Dorer and S. N. Johnson, *ibid.*, **75**, 3651 (1971).
(15) J. T. Gleaves and J. D. McDonald, *J. Chem. Phys.*, **62**, 1582 (1975); these authors report HCl vibrational populations following HCl elimination from addition of oxygen atoms to 3-chlorocyclohexene and 5-chloro-1-pentene. The HCl populations favor higher vibrational states than found in other systems and $N_2/N_1$ is slightly inverted.



*Department of Chemistry*
*Kansas State University*
*Manhattan, Kansas 66506*

**B. E. Holmes**
**D. W. Setser***


*Received February 21, 1975*

## Dependence of the Thermodynamic Stability of the Solvated Electron in Binary Liquid Solutions on Thermodynamic Solution Stability Prior to Electron Injection

*Publication costs assisted by the U.S. Atomic Energy Commission*

*Sir:* Although the physical significance of $E_{\lambda_{max}}$, the photon energy at the wavelength of maximum absorption intensity, has yet to be precisely established, it is a measure of the electron solvation potential well depth in theoretical models which have been developed to date.[1-5] We have examined empirical relationships among $E_{\lambda_{max}}$, composition, and thermodynamic properties of all binary liquid solutions for which requisite data are available. Our purpose is to test the hypothesis that the thermodynamic stability of the solvated electron, as reflected by the magnitude of $E_{\lambda_{max}}$, may be related directly to the thermodynamic stability of the equilibrium binary solution prior to electron injection, i.e., a hypothesis based on the assumption that the solvated electron may fail to equilibrate with respect to the solution created by electron injection during its observable lifetime in solution. Specifically, we have examined relationships between deviations of $E_{\lambda_{max}}$ from the composition weighted average value and corresponding deviations of the enthalpy, entropy, and Gibbs free energy of mixing from those of an ideal binary solution. The fractional deviation of $E_{\lambda_{max}}$ from the composition weighted average value, $\bar{E}_{\lambda_{max},c}$, at composition c (mol %) is given by $\Delta E^{E}_{\lambda_{max},c} = [E_{\lambda_{max},c} - \bar{E}_{\lambda_{max},c}]/[E_{\lambda_{max},2} - E_{\lambda_{max},1}]$, where $E_{\lambda_{max},2}$ is the larger of the observed values in the pure constituents. Figure 1 illustrates the simple relationship which exists between the equimolar excess Gibbs free energy of mixing of the binary solution prior to electron injection and the "excess equimolar shift", $\Delta E^{E}_{\lambda_{max},50}$, for electrons solvated in binary solutions of water, alcohols, amines, ethers, and alkanes selected subject only to existence of reliable optical and thermodynamic data. It is important to point out that no correlation exists between $\Delta G^{E}_{50}$ and $E_{\lambda_{max},2} - E_{\lambda_{max},1}$ for these solutions.

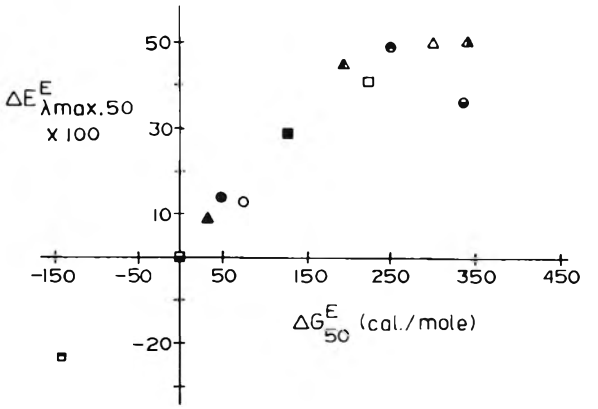


**Figure 1.** Dependence of the excess equimolar shift, $\Delta E^{E}_{\lambda_{max},50}$, on the equimolar excess Gibbs free energy of mixing, $\Delta G^{E}_{50}$, in binary liquid solutions at 298 K: (○) triethylamine–ethanol (ref 10); (●) triethylamine–methanol (ref 10); (□) 2-propanol–water (ref 11); (■) tetrahydrofuran–methanol (ref 12); (⊟) diethylamine–ethanol (ref 13); (▬) ethylenediamine–ethylene glycol (ref 14); (◓) dioxane–water (ref 15); (◒) tetrahydrofuran–water (ref 16); (△) *n*-heptane–ethanol (ref 17); (▲) 2-propanol–*n*-heptane (ref 18); (◭) methanol–diethyl ether (ref 19); (▲) butanol–triethylamine (ref 20).

Observation that an upper limit to the value of $\Delta E^{E}_{\lambda_{max},50}$ is attained at ca. +250 cal/mol is predictable from previous studies of solvated electrons in alcohol–alkane solutions,[6-8] in which it appears that the existence of homopolar domains facilitates electron solvation essentially as in the pure constituent of greater polarity. The dependence of the excess equimolar shift on $\Delta G^{E}_{50}$ below +250 cal/mol implies, however, a correlation of solvated electron stability with equilibrium properties of the binary solution prior to electron injection which is not predictable, if one assumes equilibration of the electron with respect to the solution as a whole. The difference between the interaction potentials of the electron with the pure constituents, as reflected by $E_{\lambda_{max},2} - E_{\lambda_{max},1}$, is typically 2–3 orders of magnitude greater than corresponding excess Gibbs free energies of formation of these solutions. One anticipates, therefore, that following local reorientation of molecules in the immediate vicinity of the electron, the typical system will have a strong thermodynamic tendency to proceed toward complete equilibrium via exchange of molecules between the bulk of the solution and successively closer coordination spheres surrounding the electron. Such equilibration appears not to occur at room temperature. The picture suggested is, rather, one in which the electron accepts a local environment of composition predetermined by the equilibrium structure of the binary solution prior to electron injection and that, following charge-dipole reorientation of its surroundings, no further progress toward minimization

of the solvation potential occurs during its lifetime, i.e., on the microsecond time scale.

No systematic correlations between $\Delta E^{E}_{\lambda_{max},c}$ and the enthalpy or entropy of mixing appear to exist at room temperature. Attempts to correlate observable properties other than $E_{\lambda_{max}}$ with thermodynamic solution properties are in progress. Their results will be reported at a later time.

*Acknowledgment.* The authors are grateful to The U.S. Atomic Energy Commission for partial support of this work under Contract No. AT-(11-1)-1116 and to The Phillips Petroleum Co. for fellowship support of J.B.W.

## References and Notes

(1) A. S. Davydoff, *Zh. Exp. Teor. Fiz.*, **18**, 913 (1948).
(2) J. Jortner, *J. Chem. Phys.*, **27**, 823 (1957); **30**, 839 (1959).
(3) D. A. Copeland, N. R. Kestner, and J. Jortner, *J. Chem. Phys.*, **53**, 1189 (1970).
(4) M. Natori and T. Watanabe, *J. Phys. Soc Jpn.*, **21**, 1578 (1966).
(5) G. Howat and B. C. Webster, *J. Phys. Chem.*, **76**, 3714 (1972).
(6) B. J. Brown, N. T. Barker, and D. F. Sangster, *J. Phys. Chem.*, **75**, 3639 (1971).
(7) R. R. Hentz and G. Kenney-Wallace, *J. Phys. Chem.*, **76**, 2931 (1972); **78**, 514 (1974).
(8) J. R. Brandon and R. F. Firestone, *J. Phys. Chem.*, **78**, 792 (1974).
(9) J. L. Dye, M. G. DeBacker, and L. M. Dorfman, *J. Chem. Phys.*, **52**, 6251 (1970).
(10) Optical data for solutions, this work. $E_{\lambda_{max}}$ in pure triethylamine (0.56 eV) estimated by means of the precise linear dependence of $E_{\lambda_{max}}$ for alkylamines on $D_{st}$ at room temperature. Cf. L. M. Dorfman and F. Y. Jou, "Electrons in Fluids", J. Jortner and N. R. Kestner, Ed., Springer-Verlag, Berlin, 1973; J. F. Gavlas, F. Y. Jou, and L. M. Dorfman, *J. Phys. Chem.*, **78**, 2631 (1974); and ref 9 for pertinent optical data. $E_{\lambda_{max}}$ for ethylamine (0.665 eV) determined in this work. Thermodynamic data are from K. W. Chun and R. Davison, *J. Chem. Eng. Data*, **17**, 310, 307 (1972).
(11) Optical data for solutions from S. Arai and M. Sauer, *J. Chem. Phys.*, **41**, 2297 (1966); thermodynamic data from R. Lama and B. Lu, *J. Chem. Eng. Data*, , **10**, 216 (1965).
(12) Optical data for solutions, this work; thermodynamic data from J. Matous, Z. Živný, and J. Biros, *Collect. Czech. Chem. Commun.*, 37, 3060 (1972).
(13) Optical data for solutions, this work; thermodynamic data from J. L. Copp and D. H. Everett, *Discuss. Faraday Soc.*, **15**, 174 (1953).
(14) Optical data for solutions, this work; thermodynamic data from J. K. Gladden and F. Ghaffair, *J. Chem. Eng. Data*, **17**, 468 (1972).
(15) Optical data for solutions, J. H. Baxencale and M. A. Rodgers, *J. Phys. Chem.*, **72**, 3849 (1968). $E_{\lambda_{max}}$ in pure dioxane estimated to be 0.62 eV, i.e., midway between values exhibited by dimethoxyethane and diglyme (cf., Dorfman and Jou given in ref 10 above).
(16) Optical data for solutions from L. M. Dorfman and F. Y. Jou in "Electrons in Fluids", J. Jortner and N. R. Kestner, Ed., Springer-Verlag, Berlin, 1973. Thermodynamic data from D. Glew and H. Watts, *Can. J. Chem.*, **51**, 1933 (1973); R. Signer, H. Arm, and H. Daeniker, *Helv. Chim. Acta*, **52**, 2347 (1969).
(17) Optical data for solutions, this work; thermodynamic data from H. C. Van Ness, C. A. Soczek, and N. K. Kochar, *J. Chem. Eng. Data*, **12**, 346 (1967).
(18) Optical data for solutions, this work; thermodynamic data from H. C. Van Ness, C. A. Soczek, G. Peloquin, and R. Machado, *J. Chem. Eng. Data*, **12**, 217 (1967).
(19) Optical data for solutions, this work; thermodynamic data from H. Arm and D. Bankay, *Helv. Chim. Acta*, **51**, 1243 (1968).
(20) Optical data for solutions, this work; thermodynamic data from J. L. Copp and T. J. Findlay, *Trans. Faraday Soc.*, **56**, 13 (1960).

*Department of Chemistry*
*The Ohio State University*
*Columbus, Ohio 43210*

**Judith B. Weinstein**
**R. F. Firestone***

*Received January 2, 1975; Revised Manuscript Received April 28, 1975*

## Raman Spectroscopy of Concentrated Calcium Nitrate Solutions at High Pressure

*Sir:* The Raman spectrum of $NO_3^-$ in liquid $Ca(NO_3)_2 \cdot 4H_2O$ has been reported by several groups.[1-4] A free $NO_3^-$ has four fundamental modes: $\nu_1$ a symmetric stretch at 1050 $cm^{-1}$, $\nu_2$ which is Raman inactive at 830 $cm^{-1}$, $\nu_3$ a doubly degenerate mode at 1400 $cm^{-1}$, and $\nu_4$ another doubly degenerate mode at 720 $cm^{-1}$. In dilute solution the $\nu_3$ mode is split into a doublet with further peaks appearing in concentrated solutions, whereas the $\nu_4$ mode exhibits splitting only in concentrated solutions. These splittings have been interpreted as follows. The initial $\nu_3$ splitting in dilute solutions is due to the lifting of the degeneracy by interaction by $NO_3^-$ with water, whereas the new high-frequency component in the region of the $\nu_4$ frequency is regarded as that arising from a new species of nitrate: a bound nitrate ion. In aqueous $Ca(NO_3)_2$ solutions the species has been represented as $[CaNO_3]^+_{aq}$. The concentration of the bound species has been shown to increase with increasing $Ca(NO_3)_2$ concentration and with decreasing temperature between 94 and 26° for a 13.15 *m* $Ca(NO_3)_2$ solution.[4] The ultrasonic absorption spectra of $Ca(NO_3)_2 \cdot RH_2O$ (R = 3,4,6) solutions exhibit dispersion regions which are indicative of a chemical or viscoelastic relaxation.[5-8] It has been postulated that the position of the equilibrium

$$Ca^{2+}_{aq} + NO_3^-{}_{aq} \rightleftharpoons [CaNO_3]^+_{aq}$$

might be sensitive to volume and have a relaxation time corresponding to ultrasonic frequencies. If this were so, then this mechanism might contribute to the phenomena observed above. Raman spectroscopy at high pressures should be of assistance in elucidating these relaxation mechanisms by following the change in the concentration of $[CaNO_3]^+_{aq}$ ion pairs.

$Ca(NO_3)_2$ solutions were prepared from reagent grade $Ca(NO_3)_2 \cdot 4H_2O$ by vacuum filtering a dilute solution. This solution was concentrated by warming gently under vacuum, which also removed air from the system. The samples were contained in a stainless steel pressure vessel fitted with sapphire windows (Figure 1). The sample was pressurized with a standard hydraulic pump, the pressurizing medium being a hydraulic oil not miscible with the $Ca(NO_3)_2$ solution. Care was taken to ensure that hydraulic oil did not enter the sample chamber.

Incident radiation of 488.0 nm from an RCA argon ion laser (Type L.D. 2 140) operating at 200 mW was passed into the bottom aperture and light scattered at 90° was focussed into a SPEX double spectrometer (type 1401). Radiation was detected by an EMI photomultiplier coupled to a Keithly picoammeter, the output of which was recorded on chart paper. Solutions were analyzed by titration with EDTA.

Initially the spectra of a series of $Ca(NO_3)_2$ solutions were recorded as a function of concentration at 298 K and 1 atm pressure. The qualitative results are in accordance with those of Mathieu and Lounsbury.[1] Another preliminary experiment confirmed the results of Hester and Plane[4] for the effect of temperature on the Raman spectrum of concentrated $Ca(NO_3)_2$ solutions.

Two concentrations were studied as a function of pressure: $Ca(NO_3)_2 \cdot 3.24H_2O$ (17.15 *m*) and $Ca(NO_3)_2 \cdot 6H_2O$ (8.82 *m*) at 1 bar and 600 bars at 298 K. There was no observable change in the spectrum of the $Ca(NO_3)_2 \cdot 6H_2O$ solution. A representative spectrum of the $Ca(NO_3)_2 \cdot 3.24H_2O$ sample is shown at 1 and 600 bars in Figure 2. There is a clearly observable change in the 700-$cm^{-1}$ ($\nu_4$) region and a slight change in assymetry of the 1050-$cm^{-1}$ ($\nu_1$) peak. The band arising from the $\nu_3$ mode is not shown, this band becoming only slightly broader at 600 bars. We have computer resolved the peak arising from the $\nu_4$ mode into two

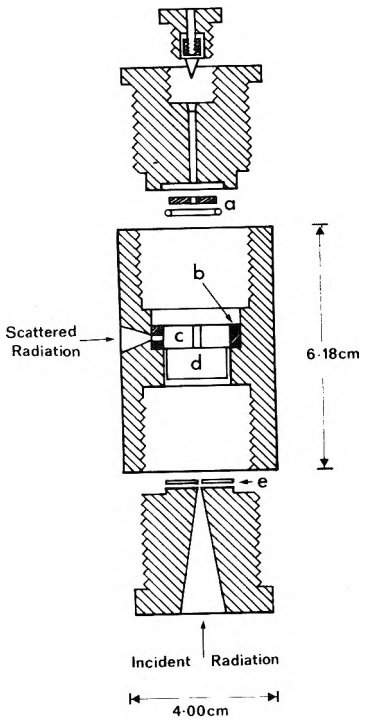


**Figure 1.** High pressure cell for laser Raman studies. Labeled parts are identified as follows: (a) is an O ring which impinges against the sapphire disk (c). This disk also contains the sample in the centrally located hole; (b) is a copper supporting ring; (d) is another sapphire disk; (e) is a thin lead washer which protects the polished face of the sapphire from the end plug.

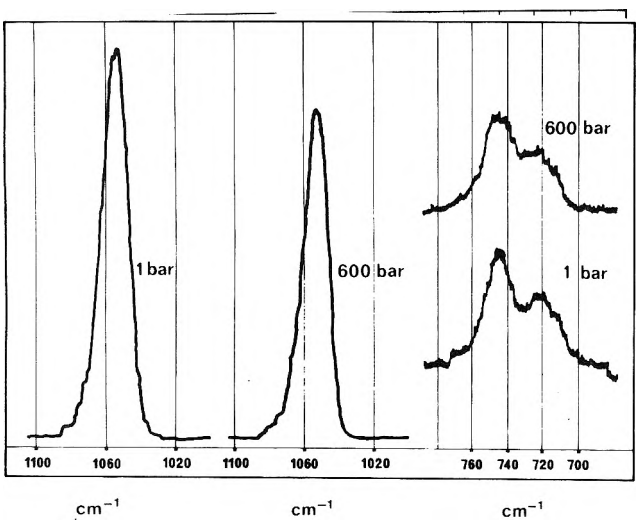


**Figure 2.** Raman spectral peaks of the $Ca(NO_3)_2 \cdot 3.24H_2O$ solution at 1 bar and 600 bars, at 25°.

gaussian components. The spectral resolution is not sufficiently good to warrant a more complex analysis in terms of a Lorentz gaussian product. In agreement with Hester and Plane[4] these are a peak at 719 $cm^{-1}$ due to "free" solvated nitrate and one at 743 $cm^{-1}$, a bound $NO_3^-$ ion. Assuming these assignments to be correct, we calculated that the ratio between the integrated areas of the 743- and the 719-$cm^{-1}$ peaks, $I_{743}/I_{719}$, at 1 bar and 25° is equal to 1.5 ± 0.1 and that at 600 bars is 2.0 ± 0.1. These values represent the average of two curves and the stated errors take into account any deviation of the resolved gaussian curves from experimental spectra. Hester and Plane[4] report that for a 13.15 *m* solution $I_{744}/I_{720} = 1.48$ at 25°. Our value at 1 bar lies within that expected by extrapolating Hester's data. Equation 2 of reference 4 gives

$$\frac{I_{744}}{I_{720}} = \frac{k_b}{k_f}\frac{m_b}{m_f}$$

where $k_b$ and $k_f$ are the intrinsic molal scattering factors for single lines characterizing the bound and free nitrate, respectively. The $m_b$ and $m_f$ are the molal concentrations of bound and free nitrate. A free nitrate ion may be one that is bound only to water molecules and a bound nitrate ion one that is bound to the $Ca^{2+}$ ion in the form of the $[CaNO_3]^+_{aq}$ ion pair.

Using the value of $k_f/k_b = 0.365$ reported by Hester and Plane[4] we calculate that at 1 bar for $Ca(NO_3)_2 \cdot 3.2H_2O$ $(m_b/m_f)_{1\ bar} = 0.55$, and at 600 bars $(m_b/m_f)_{600\ bars} = 0.73$. Thus pressure has caused an increase in the concentration of bound nitrate and hence of $[CaNO_3]^+_{aq}$ ion pairs. This behavior is contrary to what would be expected in general for dilute solutions, where it has been shown by various techniques that pressure causes a decrease in the number of ion pairs.[9] This is because of the volume reduction due to the electrostriction of the solvent by newly formed ions. However, in highly concentrated solutions, although the equilibrium species have "bound" water molecules, there are not enough to produce electrostriction effects since this phenomenon requires several layers of water molecules around the ion. The shift in the equilibrium to favor $[CaNO_3]^+_{aq}$ ions may be the result of a partial covalent bond formation between the $Ca^{2+}$ and the $NO_3^-$ ions. Infrared spectra of $KNO_3$-$Ca(NO_3)_2$ and $NaNO_3$-$Ca(NO_3)_2$ are consistent with the formation of $[CaNO_3]^+_{aq}$ and a partially covalent bond.[10] For aqueous solutions, should this mode exist, it would probably be obscured in the ir spectrum by a water absorption band.

If the equilibrium process involves the reaction of one $Ca^{2+}$ ion with one $NO_3^-$ to form $[CaNO_3]^+_{aq}$, then it can be shown from the above data that the total number of charged species in solution decreases by a factor of 0.9 from 1 bar to 600 bars. Pickston and Smedley[11] have measured the effect of pressure on electrical conductivity of $Ca(NO_3)_2 \cdot 3.6H_2O$ at 25° up to 5 kbars. Their results indicate that a $Ca(NO_3)_2 \cdot 3.2H_2O$ would have an activation volume of 10 $cm^3\ mol^{-1}$ at 1 bar and 25°. This corresponds to a reduction in conductivity by a factor of 0.7 from 1 bar to 600 bars. Thus the reduction in conductivity with increasing pressure can be attributed to at least two effects, the reduction in the concentration of charge carriers and a decrease in the mobility of the ions. It is also possible that the formation of ion pairs may contribute to the viscoelastic relaxation observed in $Ca(NO_3)_2$ solutions of this concentration.

*Acknowledgments.* This paper reports the M.Sc. Thesis work of B.L. Balshaw, submitted to the Victoria University of Wellington, Wellington, New Zealand in 1974. The authors gratefully acknowledge the assistance given by Mr. Gary Dickenson and Dr. G. Wallace of the Department of Scientific and Industrial Research, New Zealand, in curve resolving these experimental spectra.

## References and Notes

(1) J. P. Mathieu and M. Lounsbury, *Discuss. Faraday Soc.*, **9**, 196 (1950).
(2) D. E. Irish and G. E. Walrafen, *J. Chem. Phys.*, **46**, 378 (1967).
(3) D. E. Irish, A. R. Davis, and R. A. Plane, *J. Chem. Phys.*, **50**, 2262 (1969).
(4) R. E. Hester and R. A. Plane, *J. Chem. Phys.*, **40**, 411 (1964).

(5) G. S. Darbari and S. Petrucci, *J. Phys. Chem.*, **73**, 921 (1969).
(6) G. S. Darbari, M. R. Richelson, and S. Petrucci, *J. Chem. Phys.*, **53**, 4351 (1971).
(7) S. Smedley, C. Hall, and E. Yeager, *J. Phys. Chem.*, **76**, 1506 (1972).
(8) J. H. Ambrus, H. Dardy, and C. T. Moynihan, *J. Phys. Chem.*, **76**, 3495 (1972).
(9) S. D. Hamann, "High Pressure Physics and Chemistry", Vol. 2, Academic Press, London, 1963, Chapter 7ii.
(10) R. E. Hester and K. Krishnan, *J. Chem. Phys.*, **46**, 3407 (1967).
(11) L. Pickston and S. I. Smedley, manuscript in preparation. See also C. A. Angell, L. J. Pollard, and W. Strauss, *J. Solution Chem.*, **1**, 517 (1972).

*Chemistry Department* **B. Balshaw**
*Victoria University of Wellington* **S. I. Smedley***
*Wellington, New Zealand*

*Received January 28, 1975*

## Chemiemission from Metal–Oxygen Surface Reactions

*Sir:* Chemiemission (the emission of electrons in vacuo accompanying chemical reactions at a surface) has been observed under ultrahigh vacuum conditions for several metal systems reacting with oxygen, including aluminum,[2] nickel,[3] and magnesium.[4] Emission yields, in terms of electrons emitted per molecule chemisorbed, have in most cases been very small, in the range of $10^{-9}$ to $10^{-5}$, but in the case of cesium reacting with oxygen, Moucharafieh and Olmsted[5] observed yields of the order of $10^{-2}$. In order to test the generality of this higher yield process, we have examined several other metals under the same conditions as those used by Moucharafieh and Olmsted. The results of these experiments are the subject of this communication.

The experimental apparatus used for these studies was the same as that described previously,[5] modified suitably to accommodate different metals. Since the metals studied are all relatively nonvolatile, the gold substrate onto which deposits were made was maintained at room temperature. Lithium, magnesium, and aluminum surfaces were obtained by evaporating the metal from a tantalum wire onto a cylindrical gold sleeve, while potassium was evaporated from a break-seal ampoule which was heated externally by heating tape. Except for potassium, which was purified by vacuum distillation into break-seal ampoules, the metals used were of standard commercial purity.

Four metal–oxygen systems were investigated: lithium, potassium, magnesium, and aluminum. Additionally, some experiments involving cesium metal were carried out in order to delineate further the limits of the chemiemission phenomenon. Within the sensitivity limits of the system, which was of the order of $10^{-13}$ A, no emission was observed for lithium–oxygen, magnesium–oxygen, aluminum–oxygen, cesium–$H_2O$, and cesium–$H_2O$–$O_2$ mixtures. In all cases changes of the photosensitivity of the surface were observed, indicating that reaction of the metal with gas was taking place. Except for cesium, for which pressures used were in the $10^{-8}$ to $10^{-7}$ Torr range, gas pressures were varied from about $10^{-8}$ to $10^{-5}$ Torr.

Potassium metal surfaces also showed no chemiemission in the pressure ranges below $10^{-5}$ Torr. Above $10^{-5}$ Torr oxygen pressure, however, chemiemission was observed with behavior that qualitatively parallels that observed earlier for the cesium–oxygen system.[5] As is shown in Figure 1, at these pressures the emission showed an initial period of development, peaking at about 0.5 min after oxygen admission and followed by either one or two distinctly exponential decay periods. From the sticking probability given in Table I, it can be calculated that the chemiemission peak corresponds roughly to about 50% surface coverage which is qualitatively what one would expect if chemiemission is occurring at a site activated by a previously adsorbed oxygen molecule.[5]

**TABLE I: Chemiemission Parameters for K and Cs Reacting with $O_2$**

| Metal | $s^a$ | $Y_{DM}{}^b$ | $\phi^c$ | $\Delta H^{od}$ |
|---|---|---|---|---|
| K | 0.002 | $5 \times 10^{-5}$ | 51.6 | −68.9 |
| Cs[e] | 0.06 | $4 \times 10^{-2}$ | 41.7 | −63.6 |

[a] Sticking probability. [b] Fraction of adsorptions resulting in electron emission. [c] Photoelectric work function, kcal/mol. Standard literature values for "clean" surfaces (e.g., Handbook of Chemistry and Physics). [d] Heat of formation of superoxide, $MO_2$, kcal/mol. [e] Values are typical ones from ref 5.

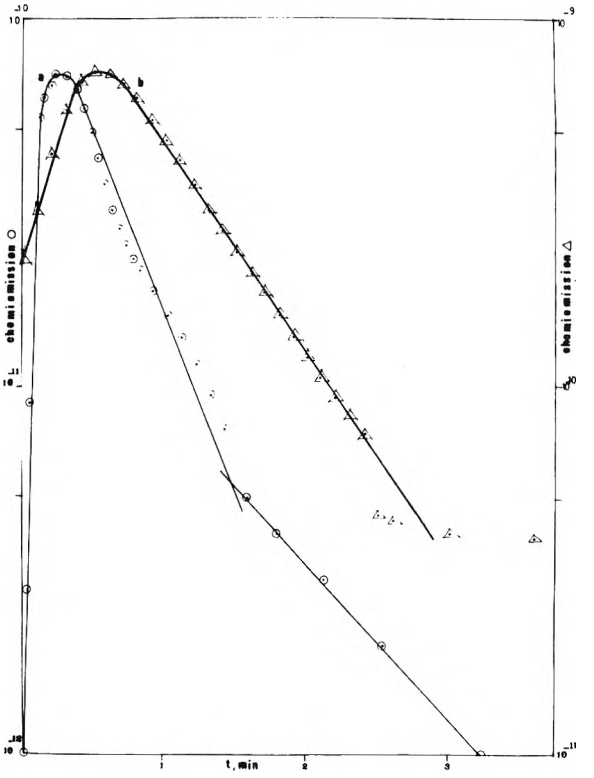


**Figure 1.** Semilog plot of chemiemission development with time for oxygen at constant pressure reacting with annealed potassium films at room temperature. Currents in amperes, curve a, $P_{O_2} = 2.5 \times 10^{-5}$ Torr; curve b, $P_{O_2} = 6 \times 10^{-5}$ Torr.

The major difference between the potassium and cesium results is the three orders of magnitude higher pressures of oxygen required to produce chemiemission, which is coupled with a reduction of the maximum emission current by two to three orders of magnitude. This qualitative indication that the chemiemission efficiency is drastically reduced is verified by computations of the sticking probability(s) from the slope of the exponential decay and the maximum differential yield ($Y_{DM}$), or fraction of adsorptions which results in emission, from the observed maximum in the emission current.[5] A comparison of these values for cesium and potassium is given in Table I, from which it is evi-

dent that oxygen does not chemisorb as readily on potassium as on cesium and that when it does chemisorb, it does so with a significantly reduced likelihood of chemiemission.

Observation of chemiluminescene from other surface–oxygen reaction systems[6] suggested the possibility that the chemiemission observed in alkali metal systems might be photoemission generated by chemiluminescence. To check this possibility, experiments were carried out on the cesium–oxygen system, in total darkness, viewing the reaction site with a photomultiplier tube. No chemiluminescence signals were observed.

The results of these experiments indicate that cesium occupies a unique position with respect to the chemiemission phenomenon, with electron emission yields that are several orders of magnitude higher than even other alkali metals. Energetic considerations alone do not seem sufficient to account for this uniqueness, as the work function and heat of formation values given in Table I indicate. Of course, bulk thermodynamic quantities may not accurately represent what actually happens at the surface, but other estimates of heats of formation including calculations of heats of chemisorption at zero coverage following Hayward and Trapnell[7] also indicate little energetic differences between K and Cs.

One further significant feature of the results is the poisoning effect of $H_2O$ vapor, which not only does not lead to chemiemission but inhibits the $O_2$ chemiemission, as shown by our failure to detect chemiemission from the Cs system when exposed to $O_2$–$H_2O$ vapor mixtures. In our earlier study we suggested a two-step chemisorption process for cesium, with only the second stage capable of yielding chemiemission[5] (SU represents a species present at the surface):

$$O_2 + Cs(SU) \rightarrow O_2{\cdot}Cs(SU)$$

$$O_2 + Cs(SU) + O_2{\cdot}Cs(SU) \rightarrow 2CsO_2 + Ye^-$$

Such a process could easily be inhibited by the presence of $H_2O$ vapor in two ways: by chemisorption of $H_2O$ preferentially to $O_2$ (i.e., with $s = 1$ compared with $s = 0.06$ for $O_2$) thereby hindering the first step, and by $H_2O$ sorption at sites adjacent to the oxygen–surface intermediate, thus blocking the second step.

A possible reason for the unique efficiency of chemiemission from cesium may lie in geometrical requirements for the proposed second, chemiemissive step. The lattice spacing of cesium being larger, owing to its larger atomic number, a second oxygen molecule may be more readily accommodated into a chemiemissive configuration than is the case for the K–$O_2$ system. One would expect, if such is the case, that rubidium would show chemiemission similar to cesium and potassium, with yields of intermediate value, but that since those three are the only metallic elements with atomic radii larger than 2 Å, similar high-yield chemiemission will not otherwise be observed.

## References and Notes

(1) This work is derived from the Master's Thesis of Mr. Saadeh.
(2) J. Wustenhagen, *Z. Naturforsch. A*, **14**, 634 (1959).
(3) T. A. Delchar, *J. Appl. Phys.*, **38**, 2403 (1967).
(4) T. F. Gesell, E. T. Arakawa, and T. A. Callcott, *Surface Sci.*, **20**, 174 (1970).
(5) N. Moucharafieh and J. Olmsted, III, *J. Phys. Chem.*, **75**, 1928 (1971).
(6) B. McCarroll, *J. Chem. Phys.*, **50**, 4758 (1969); L. E. Brus and J. Comas, *ibid.*, **54**, 2771 (1971).
(7) D. O. Hayward and B. M. W. Trapnell, "Chemisorption", Butterworths, London, 1964, pp 202–204.

*Department of Chemistry*
*American University of Beirut*
*Beirut, Lebanon*

**N. K. Saadeh[1]**
**J. Olmsted, III***

*Received December 9, 1974*

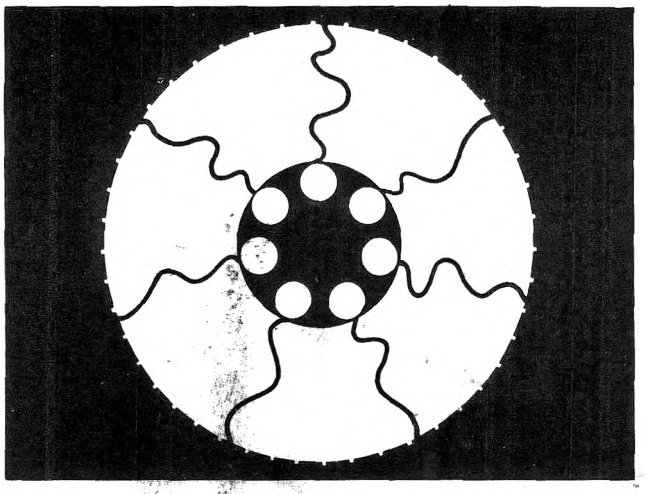

A two-volume symposium honoring Robert D. Vold and Marjorie J. Vold sponsored by the Division of Colloid and Surface Chemistry of the American Chemical Society, edited by K. L. Mittal.

# Adsorption at Interfaces

ACS Symposium Series No. 8

Twenty papers examine thermodynamics of adsorption and interparticle forces; isolated chain molecules; equilibrium film pressure; Gibbs surface excess; water in porous glass; contact angles; nickel hydroxide; adhesion of ice; surface behavior of carbons; olfaction; low interfacial tension; and much more.

290 pages (1975) $12.95 clothbound (ISBN 0-8412-0249-4)

# Colloidal Dispersions and Micellar Behavior

ACS Symposium Series No. 9

Twenty-four papers discuss colloid chemistry history; ultracentrifugal techniques; electric emulsification; macromolecular emulgents; emulsion polymerization; micelles; phase equilibria and structure; water soluble polymers; surfactant-protein interactions; anticoagulant drugs; and other topics.

353 pages (1975) $13.95 clothbound (ISBN 0-8412-0250-8). Nos. 8 & 9 ordered together $25.00. Postpaid in U.S. and Canada, plus 40 cents elsewhere.

Order from:
**Special Issues Sales**
**American Chemical Society**
**1155 Sixteenth St., N.W.**
**Washington, D.C. 20036**

New from Chicago

## SELECTED PAPERS OF ROBERT S. MULLIKEN

***Edited by D. A. Ramsay and J. Hinze***

This book brings together in one volume the most important papers of Robert S. Mulliken, who was awarded the 1966 Nobel Prize in chemistry for his seminal work on chemical bonds and the electronic structures of molecules. The papers collected here range from suggestive to closely detailed analyses of various topics in the theory of spectra and electronic structure of diatomic and polyatomic molecules. Professor Mulliken has written introductory commentaries on each of the volume's seven parts.

*1975 1120 pages Cloth $47.50*

The University of Chicago PRESS

Chicago 60637

# Fate of Organic Pesticides in the Aquatic Environment

**ADVANCES IN CHEMISTRY SERIES No. 111**

*A symposium sponsored by the Division of Pesticide Chemistry of the American Chemical Society with Samuel D. Faust Chairman*

Chemical contamination of the Great Lakes and evidence of DDT in Lake Michigan illustrate the serious problems presented by organic pesticide pollution in aquatic environments today.

This up-to-date collection of thirteen papers gathers together scientific evidence on the distribution and stability of organic pesticides in aqueous systems. These studies report the latest and most challenging research on: occurrence; recovery by liquid-liquid extraction; confirmation by mass spectrometry and NMR techniques; interaction with particulate matter and with natural organic polyelectrolytes; sorption by organic clays; herbicidal residues; photodecomposition of picloram and other pesticides; chemical hydrolysis and oxidation of parathion and paraxon; persistence of carbomate insecticides; and degradation of diazinon chlorinated hydrocarbons.

If you are a pesticide chemist, industrial engineer, or ecology expert, you will find this book invaluable.

280 pages with index. Cloth (1972) $10.50 Postpaid in U.S. and Canada, plus 40 cents elsewhere.

Order from:
Special Issues Sales, American Chemical Society
1155 16th St., N.W., Washington, D.C. 20036